Elucidating the role of manganese-induced IGF signaling and autophagy in Huntington's disease

By

Miles R. Bryan III

Dissertation

Submitted to the Faculty of the

Graduate School of Vanderbilt University

in partial fulfillment of the requirements

for the degree of

DOCTOR OF PHILOSOPHY

In

Neuroscience

December 14th, 2019

Nashville, Tennessee

Approved:

Danny Winder, Ph.D.

Kevin Ess, Ph.D.

Daniel Claassen, M.D.

David Cortez, Ph.D.

Aaron Bowman, Ph.D.

ABSTRACT

Manganese is an essential micronutrient, required for the activity of many enzymes. Our lab has established that cellular and mouse models of Huntington's Disease (HD) exhibit reduced striatal Mn bioavailability. This deficiency manifests as defects in Mn-responsive arginase and ATM/p53 pathways. Here we posit that reduced Mn bioavailability may also incur defects in IGF signaling and autophagy- Mn-responsive processes which are perturbed in HD and have been therapeutically targeted in HD models. Utilizing STHdh, immortalized striatal neuroprogenitors and hiPSC-dervied striatal-like neuroprogenitors, we found that Mn-induced IGF signaling (p-IGFR/IR, p-AKT) and autophagy (LC3-II, p62) are dampened in HD cell models- the former of which is remedied via co-treatment with Mn and IGF. While previous studies have shown Mn can activate tyrosine kinases activity of p-IGFR/IR in biochemical or non-living systems, we have found that biologically relevant concentrations of Mn can increase p-IGFR/IR phosphorylation and maximal downstream phosphorylation of AKT in cells (higher than saturating concentrations of IGF or Mg alone). I have shown previously that the majority of Mn-induced AKT is dependent on PI3K, though it was still unknown which kinase upstream of PI3K was the initial site-of-action of Mn. Utilizing a panel of small molecules inhibitors, we determined that >80% of Mn-induced p-AKT is dependent on direct interactions with the IGFR/IR receptors as opposed to other, upstream activators. While glucose uptake, a downstream process mediated by AKT and perturbed in early HD pathology, is greatly reduced in HD STHdh cells, Mn treatment incurred a significant increase in glucose uptake. Using TEM, we found Mn treatment also ameliorated the previously reported autophagy-dependent cargo recognition failure in HD cells, reducing the number of empty autophagosomes to WT levels. Lastly, in HEK293 cells expressing 72Q-HTT-GFP, Mn treatment alone did not affect the number of mutant HTT aggregates. However, co-treatment with chloroquine, an autophagy inhibitor, and Mn increased the number of mutant HTT aggregates suggesting Mn may increase aggregate-autophagosome association. Together, these data suggest that striatal Mn-deficiency may contribute to defective IGF signaling and autophagy in HD. Additionally, these studies provide proof-of-principle support for increasing bioavailable Mn to restore HD phenotypes and pathology.

DEDICATION

To my wife, Audra, you have been a constant source of peace and sanity amidst all of the chaos. Thank you for all of the love, support, inspiration, and great ideas over the years. This has been a crazy year for us, and I can't wait for many, many more. The greatest scientific mystery of all: how you managed to not let your eyes glaze over once after half a decade of me rambling about manganese.

&

To my parents, Miles Jr. and Kyong- you've always encouraged me find my own way and pursue my own dreams while showering me with unconditional love and support at every stage of my life. I simply wouldn't be here without you.

&

To my brother, Dean, you have always been my role model. You taught me how to persevere and push forward no matter how tough my goals got and how to maintain an edge even when you're an underdog.

&

To my grandfather, the original and best Miles R. Bryan, you're forever my hero. HDD- Hustle, Drive, Desire.

ACKNOWLEDGEMENTS

I would also like to thank my thesis committee- Drs. Danny Winder, Kevin Ess, David Cortez, and Daniel Claassen. You have all showed an incredible amount of support and guidance over the years and your thoughtful insight into my projects is irreplaceable. Most importantly, I cannot be thankful enough for the mentorship of my PI, Dr. Aaron Bowman. Aaron has a rare and infectious curiosity combined with a unique sense of creativity and ingenuity that fuels his mentees. Simply put, the "Boss" has taught me how to approach science with poise, rigor, creativity and enthusiasm. His training has provided me with all the necessary tools and knowledge to be successful during my PhD and further pursue science in post-doc. I am forever thankful for all the effort, brain-power, and countless one-on-one meetings he put towards my thesis work. I also want to thank all of collaborators including the labs of Dr. Michael Aschner and Dr. Vittorio Maglione. This work wouldn't have been possible without the financial support of the Vanderbilt Brain Institute Scholar Award and NIEHS F31 NRSA Pre-doctoral fellowship aware.

And to my wife, Audra, I owe the most gratitude. You have kept me sane, grounded, fed, and happy since the first day and every second since. I don't know how I got so lucky, but I can't imagine going through this whole process of ups and downs with anyone else. You have helped me in countless ways without a second thought and have undoubtedly contributed to the success of this work. I absolutely wouldn't have been able to do it without you. We've had a pretty incredible year, and I can't wait to see what the future holds for us.

To God- thank you for making me who I am and surrounding me with incredible and irreplaceable family, friends, mentors, students, and colleagues who have helped along the way… For guiding my path at every step and providing me with the opportunities to succeed, the courage to face them, the tenacity to push forward, and the wisdom to complete the tasks set before me.

TABLE OF CONTENTS

LIST OF TABLES

LIST OF FIGURES

LIST OF ABBREVIATIONS

HD	Huntington's Disease
PD	Parkinson's Disease
AD	Alzheimer's Disease
NDD	Neurodegenerative disease
Mn	Manganese
Mg	Magnesium
WT	Wild-type
HTT	huntingtin
mutHTT	Mutant huntingtin
CQ	Chloroquine
BafA	Bafilomycin A
3-MA	3-methyladenine
CSF	Cerebral spinal fluid
hiPSC	Human induced pluripotent stem cells
CFMEA	Cellular Fura-2 manganese uptake assay
APV	Autophagic vacuole
GFP	Green fluorescent protein
TEM	Transmission electron microscopy
IGF	Insulin-like growth factor
ROS	Reactive oxygen species
PI3K	Phosphotidyl-3 inositol kinase
IRS	Insulin receptor substrate
GOF	Gain-of-function
LOF	Loss-of-function
MSN	Medium spiny neurons
ICP-MS	Inductively couple plasma mass spectrometry
GFAAS	Graphite furnace atomic absorption spectromety

PREFACE

In Chapter 1 titled "Introduction," I will introduce manganese homeostasis and its potential connections to insulin/IGF signaling. Basic Huntington's disease (HD) pathobiology will also be introduced with an emphasis on how the pathology of this disease is modified separately by Mn or insulin/IGF. Additionally, I will explore yet-to-be substantiated hypotheses linking HD pathobiology to perturbations in manganese-insulin/IGF signaling with a specific focus on autophagy and mitochondrial health. Lastly, I will briefly present previously reported data and hypotheses which may link Mn-insulin/IGF to Mn toxicity, other neurodegenerative diseases aside from HD, and cancer.

In Chapter 2 titled "Phosphatidylinositol 3 kinase (PI3K) modulates manganese homeostasis and manganese-induced cell signaling in a murine striatal cell line," I describe a limited small molecule screen of pharmacological inhibitors to discover a novel role for PI3K in Mn transport in the STHdh, mouse neuroprogenitor cell lines. I will also explore how these small molecules can modulate Mn-induced signaling (p-p53, p-AKT) by directly impinging on net Mn uptake. Additionally, these studies reveal that PI3K is necessary for Mn-induced p-AKT. Interestingly, AKT has been long-known as a Mn-responsive kinase, though the upstream mediators of this response were unknown. These results directly lead to the investigations in Chapter 3, looking upstream of PI3K for the initial site-of-action of Mn on insulin/IGF signaling.

In Chapter 3 titled "Manganese directly activates IGFR/IR-dependent phosphorylation of AKT and glucose uptake in Huntington's Disease cells," I present evidence supporting the hypothesis that reduced Mn bioavailable in HD cell lines contributes to previously described defects in insulin/IGF signaling. Furthermore, these studies elucidate that 1) sub-toxic Mn treatment directly activates the insulin/IGF receptors, 2) Mn treatment increases maximal IGF-induced p-AKT, and 3) Mn-induced p-AKT is almost entirely dependent on the insulin/IGF receptors. Additionally, Mn treatment can slightly restore glucose uptake, a known HD phenotype. Given the large body of evidence supporting a neuroprotective role of AKT in HD, this data warrants additional investigation into how Mn treatment may enhance the efficacy of IGF-based therapeutics in HD.

In Chapter 4 titled "Acute manganese restoration promotes autophagic cargo loading in Huntington's Disease cell lines," I examine the role of Mn homeostasis on autophagic function in HD. A particular focus is describing whether Mn activates or inhibits autophagic processing in neuroprogenitors. Following this, I explore how Mn-induced autophagy can then impinge on mutant HTT aggregate formation and ameliorate previously reported defective autophagic cargo sequestration in HD cells.

In Chapter 5 titled "Future Directions and Global Discussion," I will present unpublished data which could provide the foundation for several future studies examining 1) loss of HTT function on Mn-dependent phenotypes 2) the mechanism of KB-R7943, a Mn-increasing small molecule 3) using patient lymphoblasts as an HD model 4) the effects of IGFR/IR inhibition on Mn neurotoxicity, 5) the effects of Mn on lipophagy and 6) the effects of Mn on autophagy and IGF signaling *in vivo*. I will also discuss global considerations and future directions to follow up the findings described in Chapter 2-4. In particular, I will focus on 1) which experiments are necessary to establish biological validity of my *in vitro* experiments, 2) what new resources/discoveries may allow future researchers to thoroughly examine these questions more clearly, and 3) how these findings may impact the "big-picture" of Mn homeostasis, insulin/IGF signaling, and autophagic function.

CHAPTER 1

INTRODUCTION

Introduction

Between 1-3 out of 100,000 individuals are diagnosed with Huntington's disease (HD) in the U.S. However, given the autosomal dominant etiology and near 100% penetrance of HD, generations of families are devastated by this disease. HD is caused by an expanded tri-nucleotide CAG repeat in the HTT gene. If these repeats surpass 35-40 repeats, there is a near 100% chance that the patient will present with Huntington's disease at some point in their lifetime (usually in middle-late adulthood). While the *HTT* gene was discovered in 1993, there is still no cure for HD though several drugs have been used to treat symptoms (i.e. tetrabenazine for chorea). Furthermore, researchers still do not fully understand 1) the exact function(s) of wild-type HTT is in the human brain 2) how mutant HTT (HTT >35 CAG repeats) causes neurotoxicity and HD. Two of the posited causes for HD are 1) mitochondrial dysfunction 2) autophagic dysfunction and aggregate accumulation. Recently, a series of studies have shown that insulin/insulin-like growth factor (IGF) treatment in HD models can ameliorate both of these pathogenic mechanisms.

Manganese (Mn) has only been recently implicated in HD, and studies have suggested that a Mn deficiency may underlie some of HD pathology. Interestingly, Mn can modulate insulin/IGF homeostasis, shown to be essential for mitochondrial function, and able to stimulate neuroprotective pathways associated with the activation of autophagy, namely insulin/IGF signaling (IIS). **This review explores the functional intersection of these two modifiers of HD, (a) Mn biology and (b) insulin/IGF signaling (IIS)—both have been shown to regulate autophagy and mitochondrial health/function.** Here we will review a role for Mn and IGF joint dysregulation in HD pathology and briefly explore some the implications of this co-regulation in the context of other neurodegenerative diseases and conditions.

While Huntington's disease will be discussed in detail, other neurodegenerative diseases (NDDs) will also be referenced when studies provide mechanistic understanding of the roles of Mn and IGF/insulin given the shared cellular pathologies between NDDs and HD (i.e. aggregate accumulation, reactive oxygen species, mitochondrial dysfunction). It is plausible that the mechanisms of these NDD pathologies might be quite similar to HD.

Insulin/IGF signaling and its role in the brain

Insulin and insulin growth factor (IGF) are homologous growth hormones that classically regulate cellular metabolism. Their role in peripheral tissues has been well elucidated. However, only more recently has their role in brain health and development been studied. In the brain, IIS is necessary for synaptic maintenance and activity, neurogenesis, neurite outgrowth, neuronal survival, mitochondrial function and maintenance as well as upper-level processes including memory and feeding behavior and thus dysregulation in neurotrophic support has long been proposed as a mechanism of neurodegenerative diseases[1-26]. Insulin and IGF are mainly produced in the pancreas and liver, respectively, and transported to the brain from the periphery through the blood brain barrier. Alternatively, IGF and insulin can enter the brain through CSF in the choroid plexus. IGF is also produced locally in all brain regions. Upon binding with their respective ligands, IGF receptors (IGFR) and insulin receptors (IR) undergo autophosphorylation at three tyrosine residues required for activation. Subsequently, the IR kinase domain phosphorylates IR substrates (IRSs) which act as secondary messengers, impinging upon a variety of cell signaling pathways including PI3K/AKT, mTOR, and MAPK/ERK to exert their biological effects (e.g. energy metabolism, cell stress responses)[27]. However, individual receptors can heterodimerize forming hybrid IGF/insulin receptors which can bind either insulin or IGF and activate both the PI3K/AKT and MAPK/ERK pathways S6, a downstream target of mTOR acts as negative feedback, phosphorylating and inactivating IRSs. Six IGF binding proteins exist (IGFBPs) and act to regulate IGF-R binding and modulate signaling. IGFBPs show a selective expression pattern, being in distinct portions of the brain where they presumably act on specific IIS signaling within anatomical subsets of neurons. These proteins have a higher affinity for IGF than do IGF receptors, allowing tight control of IGF bioavailability. The regulation of IGFBPs is still quite unknown but evidence suggests specific mechanisms for each protein including control by epigenetic markers and neuronal activity of specific cell types[28,29].

Most kinases in humans are either magnesium (Mg) or Mn dependent. Though most are Mg dependent, several are preferentially activated by Mn including ATM and mTOR[30,31]. While little research has been done to explore the role of Mn as a signaling molecule its inherent role in kinase activation suggest Mn is essential for cell signaling. Several other proteins are also activated by Mn including Arg, MRE11, Mn-SOD, glutamine synthetase, pyruvate decarboxylase, protein phosphatase 1, and many integrin-related proteins[32-41]. Interestingly Mn has been shown to activate several of the same pathways as IGF/insulin including AKT, mTOR, and ERK/MAPK, and even the insulin/IGF receptor itself— all of which have been found to be neuroprotective in HD[41-51].

Mn and insulin/IGF homeostasis

Mn toxicity has been linked to neuronal cell death and neurodegenerative conditions for several decades— namely Parkinson's disease (PD) and manganism. Though recent studies have yielded greater understanding of toxic effect of Mn on neuronal function, very little is known about basic, neuronal Mn homeostasis. While brain imaging studies have revealed where Mn accumulates within the brain, there is disagreement on what sub-compartment(s) Mn primarily accumulates within a neural cell. The field is in some contention as some studies suggest mitochondria while others suggest within the nucleus[52-54]. Surprisingly few studies have examined whether Mn primarily accumulates in neurons vs glial cells. Lastly, there is poor understanding of how Mn is transported within a cell, primarily due to the high promiscuity of Mn transporters for other metal ions[32,55]. Muddying this understanding, at present there is only one transporter which seems specific for Mn, SCL30A10, an efflux transporter. Interestingly, mutations in this transporter lead to Mn accumulation *in vitro* and *in vivo* and have been linked to increased brain Mn and PD in patients[55-58]. The answers to these basic questions could offer invaluable understanding of Mn biology in the context of both diseased and healthy brains.

Evidence of a role for Mn-dependent regulation of IIS has been steadily amassing since the 1980's. Baly and colleagues showed Mn-deficiency caused glucose intolerance and reduced insulin production in rats, mimicking diabetic-like phenotypes. In addition, rats fed a Mn-deficient exhibited reduced pancreatic insulin output following a glucose stimulus. Furthermore, they and others found Mn to be an insulin-mimetic, promoting insulin excretion and activating insulin-related metabolic kinases[59-64]. Around this same time, another study showed that Mn-deficient rats exhibited decreased circulating IGF-1 and insulin and increased IGFBP3—potentially suggesting Mn might regulate circulating IGF-1 levels via modulating IGFBP3 activity[65]. Later, Lee and colleagues reported that Mn supplementation could protect against diet-induced diabetes in mice via increased insulin excretion, amelioration of glucose intolerance, and increased expression of Mn superoxide dismutase (MnSOD), a Mn-dependent anti-oxidant enzyme in mitochondria[66]. These results were consistent with reports that diabetic patients were responsive to oral Mn treatment as well as reports of reduced blood Mn in diabetic patients[67-69]. Concurrently, other groups established that Mn deficiency was associated with reductions of IGF1 in serum and Mn supplementation could increase IGR-R and IGF1 expression in the hypothalamus of rats[48,49,51,65,70-73] *However, the mechanisms by which Mn increases IGF1 and insulin levels remain unknown.* Together, these findings suggest a functional link between Mn and the regulation of IGF1/insulin levels in both peripheral tissues and brain. While such studies clearly link Mn to diabetes and hypothalamic/pubertal development, the role of this potent regulatory mechanism has never been studied in the context of a neuronal disease or manganese toxicity.

HD pathobiology

HD is an autosomal dominant neurodegenerative disease which results in hyperkinetic movements, behavioral changes in cognition and mood, and ultimately death. An expanded trinucleotide (CAG) repeat in the *Huntingtin* gene (*HTT*) resulting in a mutant HTT protein (mHTT) causes HD. Higher CAG repeats are correlated with increased disease severity and younger age of onset though both are highly variable even between patients with similar repeat size. Usually, the disease manifests in adulthood (though juvenile cases do occur), and gives rise to a combination of motor, cognitive, and psychiatric symptoms which ultimately result in death. A hallmark symptom of HD is chorea, uncontrolled hyperkinetic movements, which has been associated with mHTT-dependent cell death within the striatum. Degeneration in other brain regions (cortex, hypothalamus) usual follows, contributing to the variability in symptoms. As HTT is ubiquitously expressed, the basis for the selective neurotoxicity of mHTT for striatal medium spiny neurons (MSNs) and a handful of other neuronal sub-populations remains a mystery[74-78].

Mn dysregulation in HD

Mn dysregulation has only recently been implicated in HD. In normal brains, Mn accumulation is enriched in the basal ganglia—the part of the brain which most severely degenerates in HD—suggesting Mn serves an important role in this brain region[54,79,80]. Recently a set of studies revealed a Mn transport deficit, **indicative of a brain-specific Mn deficiency**, in an HD immortalized striatal neuroprogenitor cell line (STHdhQ111/Q111), in HD hiPSC-derived striatal NPCs cells, and also in the striata of YAC128Q mouse model of HD[81,82]. The mechanism of this Mn-transport deficit has been difficult to resolve as so little is known about Mn sub-cellular transport. Analysis of Mn homeostasis is complicated by the high promiscuity of proposed Mn transporters for other essential metals[32,55,83,84].

However, Mn is known to activate several of the signaling pathways dysregulated in HD including ATM/p53 and AKT/mTOR[48,49,82,84-86]. STHdh Q111/Q111 and hiPSC-derived striatal neuroprogenitor HD cell models exhibit decreased net Mn uptake leading to diminished ATM activation, a Mn-responsive kinase upstream of p53 and other cellular stress response proteins[82]. Similar to ATM/p53, Mn robustly activates AKT and mTOR, both of which are neuroprotective in HD[87-94]. AKT activation can increase HTT-Ser421 phosphorylation, shown to facilitate axonal transport, restoring mitochondrial and autophagic function in HD models[88,91-93,95-98]. In contrast, Guilarte and colleagues reported decreased HTT-Ser421 phosphorylation by Mn in YAC128 mouse cortical and hippocampal primary cultures, though striatal levels were not assessed[81,99]. Lastly, reinstatement of aberrant mTOR activity in HD

models restores autophagic function, enhances aggregate clearance, and increases MSN health, though some reports have shown mTOR inhibition to be neuroprotective in HD[87,100,101].

IIS dysregulation in HD

Recently, several groups observed impaired IIS in HD. Paradoxically, reduced IGF1 expression has been detected in patient caudate tissue and skin-fibroblasts as well as other non-human HD models, while increased IGF1 has been found peripherally in HD and this has been correlated with cognitive decline[92,102, 103]. Previous studies have shown mutant HTT disrupts intracellular transport and secretion of insulin while others have shown Mn can act as a potent insulin-mimetic *in vivo*[64]. Additionally, several groups reported robust neuroprotective effects of IGF1 treatment in HD cell and mouse models via increased 1) AKT/ERK signaling 2) IRS2/VPS34 signaling and 3) increased HTT Ser421 phosphorylation. Upregulation of these pathways increased autophagic function, aggregate clearance and ameliorated mitochondrial dysfunction[92,93,96,97,104-108]. Administration of IGF and insulin can also rescue microtubule transport, amelioration of motor abnormalities, MSN health, and enhanced survival in cell and rodent models. IGF1 is also neuroprotective in models of other NDDs[109-116].

Autophagy deficits in HD, potential links to Mn and IIS

The inability to clear toxic mHTT aggregates may be a principle mechanism of HD-related cell death though there is contention about which form(s) and fragment(s) are truly toxic and which are a compensatory/protective reaction to cellular toxicity[117-120]. Autophagy, a process by which cells degrade complex organelles and proteins to base nutrients, is also the primary process in clearing mutHTT aggregates[118,120-126]. HTT acts as a scaffold for autophagy and this activity is altered or impaired by mutHTT, potentially exacerbating pathogenesis[123,127-130]. In HD, autophagic impairment causes failure of cargo-recognition and lysosomal function resulting in the accumulation of cellular waste and protein aggregates[131]. This may trigger a feed-forward pathogenic loop with ever increasing mutHTT levels further impairing clearance[123].

IGF treatment incurs robust amelioration of autophagy defects in HD models. Rothman and colleagues observed that IGF1 upregulates autophagy via an IRS2/VPS34-dependent mechanism in HD cells, resulting in a marked increase in aggregate clearance. This is an AKT/mTOR-independent process, though both AKT and mTOR are activated by IGF1[104]. Additionally, other groups have shown that upregulation of mTOR in HD models increases autophagy and aggregate clearance, rescuing HD-related phenotypes even though mTOR canonically acts as a negative regulator of autophagy by inhibiting ULK1[87,132]. Interestingly, published studies indicate Mn both increases and decreases autophagy in neuronal systems in a biphasic, time-dependent manner[50,133]. Given this regulation of

autophagy by Mn and Mn-responsive pathways, it seems plausible that correcting Mn homeostasis in HD models may ameliorate aspects of autophagic dysfunction. To date however, there has been only a handful of studies exploring the role of Mn in autophagy— and the majority have been done in the context of Mn toxicity, instead of Mn essentiality[50,134]. Given clear ties of Mn biology to pathways upstream of autophagy, future studies should interrogate the role of Mn in autophagy during normal neuronal function, in addition to disease states. In particular, we need to establish whether Mn plays a role in basal autophagy or only in the context of Mn toxicity.

Mitochondrial pathology in HD, possible links to Mn and IIS

Mitochondrial dysfunction is another mechanism by which mutHTT may cause selective neurodegeneration in HD. Mitochondrial dysfunction may contribute to neurodegenerative diseases (NDD) for several reasons; 1) High mitochondrial respiration is needed to accommodate high ATP usage in neurons, 2) mitochondria, out of all organelles, produce the highest amount of intracellular reactive oxygen species (ROS), 3) mitochondria are a critical regulator of cell death, a common feature of most NDDs, 4) mitophagy (mitochondrial selective autophagy) is often defective in NDD, and 5) perturbations in various metabolic processes, indicative of mitochondrial dysfunction, are often associated with NDD[135-137]. In HD, specifically, overt metabolic effects such as rapid weight changes and defects in glucose homeostasis have been observed in HD patients and models[138-148]. Also, WT HTT has been shown essential for mitochondrial health[149]. To this end, several basic studies and clinical trials have investigated metabolic targets as potential therapeutics for HD including creatine and Coenzyme Q10, but have found little success[150-156].

Several landmark studies demonstrate IGF1 restores mitochondrial health in HD models[93,96,97]. Given the IIS-mimetic effects of Mn, correcting Mn homeostasis may ameliorate some facets of mitochondrial dysfunction in HD. This hypothesis is consistent with established roles for Mn in mitochondria: 1) Mn accumulates in mitochondria more so than other organelles supporting a functional need in this organelle; 2) Mn has anti-oxidant functions via the Mn-dependent, mitochondrial enzyme, MnSOD; and 3) Mn is essential for the function at least two gluconeogenesis enyzmes[32,52,53,55,84]. Rego and colleagues have reported a series of studies providing a mechanistic understanding of how IGF is capable of such robust amelioration of HD symptoms[96,97,136,150,157-166]. They found HD models exhibit reduced ATP/ADP ratio, decreased oxygen consumption, increased mitochondrial ROS and fragmentation, aberrant lactate/pyruvate levels and decreased mitochondrial membrane potential— all of which indicates mitochondrial dysfunction. Each of these was shown to be ameliorated by IGF treatment via upregulation of PI3K/AKT signaling in cellular and mouse models of HD.

IIS signaling and Mn in other NDDs

Abnormal levels of IGF/insulin and decreased IIS signaling (namely, reduced AKT signaling) have been observed in all neurodegenerative diseases including PD, Alzheimer's disease (AD), amyotrophic lateral sclerosis (ALS), multiple sclerosis (MS), spinocerebellar ataxias (SCA), and other NDD-like conditions such as ataxia telangiectasia (AT). In the case for many models of these diseases, IGF or insulin have been successfully used to ameliorate pathologies *in vitro* and *in vivo;* and they have been used or targeted in clinical trials[111,167-169]. Unfortunately, these clinical trials have reported little success. One possible reason for this is control of IGF-1 bioavailability by IGFBPs. This could be overcome by using a modified IGF-1-like peptide which is unable to bind IGFBPs [170]. Furthermore, although many studies have shown perturbation in metal ion homeostasis in these diseases, few have explored a more specific role for Mn dysregulation. Recent studies elucidating Mn or IGF/Insulin dysregulation in NDDs will be reviewed next, emphasizing developments in recent years.

PD and IIS/Mn

PD is a neurodegenerative disorder resulting in bradykinesia and motor rigidity affecting an estimated 10 million people worldwide. Symptoms of the disease mostly occur in late adulthood as a threshold of dopaminergic neurons in the substantia nigra degenerate. Unlike HD, there is no clear genetic predisposition for most cases of PD, though mutations in some genes are correlated to increased risk for PD. Given this and the late-onset of the disease, many studies have focused on environmental modifiers of the disease[171]. PD has long been associated with perturbations in metal ion homeostasis—particularly iron (Fe) and Mn. Mn toxicity causes parkinsonian-like symptoms and a disease-state known as manganism, but most agree that its pathology is different from that seen in Parkinson's. This is mainly because neurodegeneration in PD occurs primarily in the dopaminergic neurons of the substantia nigra while Mn toxicity manifests within the globus pallidus. Furthermore, at least some patients with Mn induced parkinsonism do not produce Lewy bodies and can be unresponsive to levodopa treatment[172-174]. While these two diseases may be distinct, several lines of evidence support a role for Mn dysregulation in PD. Chronic exposure to Mn is associated with increased risk for PD. Also, Mn toxicity has been linked to reduced trysonine hydroxylase and dopamine levels and DAT cell surface expression but reports regarding impaired neurotransmission and viability in dopaminergic neurons have been inconsistent[32,174-178]. Mn toxicity has also been associated with increased alpha synuclein build-up, but it is unclear if this response is neuroprotective or enhances neurodegeneration[179-181].

IGF has been studied in the context of PD as well. Previous studies have revealed neuroprotective effects of IGF in PD models and associated with increased dopaminergic survival in the substantia nigra[109,179,182-184]. However, the majority of recent studies mainly focus on plasma IGF-1 levels as a biomarker for PD progression. Several groups published studies suggesting IGF-1 levels were increased in the sera of PD patients compared to control[185,186]. Furthermore, studies revealed that increased plasma IGF-1 levels correlate with cognitive decline and motor symptoms[185,187]. While these studies have great utility as a clinical tool and seem to be quite sensitive, they have add minimal mechanistic insight as to if or why IGF-1/insulin and related signaling may be dysregulated or pathogenic consequences. Thus, continued basic and mechanistic experiment to understanding of IGF's role in PD are needed to resolve inconsistencies and provide detail. AKT has received considerable attention in the PD field via its neuroprotective roles in the brain. Aside from reduced p-AKT levels found in post-mortem PD brains, several studies have linked increased AKT and IIS signaling to both reduced dopaminergic cell death, reduced alpha synuclein toxicity and complex interactions with PD-related proteins including PARKIN, PINK1, and DJ1[109,182,188-192].

AD and IIS/Mn

AD results primarily from the degeneration of hippocampal neurons which leads to severe cognitive defects in late-adulthood. Disease is defined by two hallmark pathological features, neurofibrillary tangles (hyperphosphorylated tau) and amyloid beta plaques, two aggregates which incur neurotoxic stress. Heavy metals have also been associated with AD and its aggregate pathology, though few studies have examined Mn levels or dysregulation[193,194]. However, two recent studies investigated plasma Mn levels in AD and reported opposing results. Dehua and colleagues reported elevated Mn levels which were correlated with increased amyloid beta expression and reduced cognition while Bush et al reported reduced Mn levels in sera but no difference in patient erythrocytes[195,196].

AD may have the most significant ties to IGF dysregulation of all NDDs. AD has been heavily correlated to diabetic status and mechanistic understanding of metabolic dysfunction in AD has led to it being referred to as "type 3 diabetes", a form of diabetes that specifically affects the brain[197]. In recent years, studies have focused primarily on the effects of IGF/insulin on amyloid beta accumulation and the use of IGF-1 levels as a biomarker for disease risk and progression. Two studies in 2009 reported that reduced IGF signaling protects against AB accumulation, potentially by acting on the plaques themselves, condensing them to less toxic forms[198-201]. These were contrary to a flurry of studies in the early-mid 2000's revealing IGF resistance and ameliorative effects by IGF treatment on AB

accumulation and cognitive function[112,202-209]. A few years later, insulin resistance and reduced IIS signaling was found in post-mortem AD brain tissue and soon after that, lower serum IGF-1 levels were correlated to an increased risk for AD and dementia while higher levels were associated with greater brain volume[209,210]. Interestingly, increased IGF has been reported in CSF of patients[211,212].Thus, even though conflicting results have been reported, these studies reveal that AD is deeply tied to IGF biology. Contrary to PD, excessive AKT signaling has been observed in AD. Several studies have reduced or inhibited IIS signaling and observed delays in symptoms and reduced AB pathology[203,213,214]. These results, of course, are contrary to aforementioned studies utilizing IGF treatment in AD models. Such conflicting results may be explained by an initial hyperactivation of IIS signaling which desensitizes the pathway. In this way, both IIS inhibition early or IIS treatment late in disease progression may result in ameliorative effects.

ALS and IIS/Mn

ALS is a neurodegenerative disease which affects more than 12,000 people in the U.S. Disease onset is more variable than other diseases and can often occur in younger people. The cause of ALS is unknown but pathology is attributed to loss of motor neurons in the brain and spinal cord resulting in loss of voluntary muscle control and, in late-stage, patients are unable to move or breathe without ventilator support. ALS has also been associated with metal ion dysregulation. Again, few studies focused on Mn levels but a few studies have reported increased Mn in CSF and plasma while the other reports no change in Mn but significant increases in copper and zinc and reduction in selenium[215-218].

IGF dysregulation and insulin resistance has been reported in ALS[219-221]. These data led to a few *in vivo* studies using IGF-1 treatment in ALS models. While subcutaneous injection into the periphery with IGF-1 was largely found to be ineffective, direct intrathecal injections directly into the CSF resulted in some decrease in motor atrophy[167,222]. Given these results, a few clinical trials have been attempted in ALS but have found little success[168,223,224]. One reason may be that these treatments are given peripherally instead of intrathecally[170]. More recently, IGF2 has been found to be neuroprotective in ALS models[110].

Autophagy in other neurodegenerative diseases

Autophagy has been linked to every neurodegenerative disease—namely because most NDDs develop aggregate pathology which is often processed by autophagy. While autophagy is activated as a protective process in order to maintain healthy homeostasis of the cell, if hyperactivated can result in autophagy-mediated cell death. Thus, interactions between aggregates and autophagy play a precarious role in NDDs[225]. Recent studies have begun to explore the affects of metal toxicity on

autophagy as well[50,134]. In PD, autophagy has primarily been investigated in the context of mitophagy (mitochondrial specific autophagy). PD has been linked to mitochondrial toxicity and dysfunction which incurs mitophagy in an attempt to remove unhealthy mitochondria from the neurons to reestablish cellular integrity. PARKIN and PINK1, two proteins associated with familial forms of PD, are essential members of the mitophagy process[226-231]. In AD, autophagy is known to regulate both the secretion and degradation of AB which adds increased complexity to its role in disease pathology. Several studies have revealed increased autophagosome accumulation in AD models, but these results have been inconsistent across disease progression[232-235]. Recently, ALS studies have revealed that two ALS associated proteins, TDP-43 and SOD1, are often dysregulated in ALS patients and models[236-238]. Interestingly, mutations in these proteins (amongst several other observed ALS mutation-associated proteins) cause aberrant autophagic processing in neuronal and spinal cord neurons[239]. Further studies are needed to elucidate mechanistic understanding of these complex relationships to determine whether dysregulated autophagy is a pathogenic mechanism or compensatory "rescue" response. Future investigation must interrogate autophagic flux rather than commonly used end-point measurements as the directionality and capacity of autophagy is necessary for further understanding and therapeutics. The connections that have been drawn between autophagy and Mn or IGF/insulin warrant continued exploration but studies should consider potential co-regulation of Mn and IGF/insulin on autophagy processes and dysregulation.

Manganese toxicity and IGF

Little investigation has been done to examine the role of IGF in manganese toxicity. Tong and colleagues found Mn toxicity caused reduced ATP and insulin/IGF receptor expression. Additionally, as mentioned before, Hiney and colleagues have been revealing a role for Mn-induced toxicity in hypothalamic development via IGF/mTOR related pathways [51,48,49,51,71-73]. It is likely that Mn toxicity in other brain regions are regulated a similar manner. Given that Mn accumulates in the brain primarily in the basal ganglia, not the hypothalamus, it seems likely that and IGF/Mn interaction may play even more crucial roles in other brain regions, particularly in aged model systems. Thus, future studies on Mn toxicity and IGF could be informative on developmental toxicity, chronic environmental exposures, and overall brain health.

The co-regulation of ATM, Mn, and insulin/IGF

Interestingly ATM, a Mn activated kinase, has been linked to both IGF/insulin and Mn signaling. Previous studies have shown that Mn induced p53 activity is regulated by ATM. Furthermore, this Mn-induced activity is blunted in HD due to lack of bioavailable Mn[82]. Separately, low levels of the IGF-1

receptor and loss of IGF-1 sensitivity have been observed in Ataxia Telangiectasia (AT), the disease resulting from loss of function mutations in ATM, and in loss-of-function ATM models[240-243]. Additionally, studies have shown patients with AT have significantly decreased IGF-1 levels[244-247]. Furthermore, others have shown ATM is essential for IGF and IGF-R transcription by phosphorylating and relieving transcription factors and complexes including p53 from their respective promotors, allowing for transcription[240,241,248-251]. Concurrently, downregulation of IGF-R results in increased radiosensitivity and decreased ATM protein levels (mRNA was unchanged) revealing a potential circular regulation between ATM and IGF-R[241,252,253]. Also, given that ATM is required for full activation of AKT, it seems likely that the connections between ATM, Mn, and IGF carry some biological relevance in the context of Mn/IGF co-regulation in NDD[254]. Mn could act as an initiating signaling molecule within this cascade where Mn activates ATM/p53 which results in increased IGF/IGF-R transcription and subsequent activation of the PI3K/AKT pathway. This hypothetical, albeit plausible, interaction could explain how a Mn deficiency in HD might contribute to decreased IIS (AKT/mTOR) and Mn-induced ATM/p53 signaling.

IIS signaling, Mn and cancer

Given the striking parallels and potential co-regulation between Mn and IIS and the pronounced and well-studied roles of IIS in cancer progression, one must wonder if there is role for Mn/IIS co-regulation in cancer etiology. As a pro-growth signaling pathway, IIS is often highly upregulated in cancers particularly during tumor progression[255]. However, most findings suggest Mn is not significantly carcinogenic, even to exposed workers. In fact, Mn deficiency leads to a higher risk. A plethora of studies, namely clinical examination of Mn levels in cancer patients, support the role for Mn deficiency in cancer via reduced MnSOD activity and enhanced ROS accumulation in various cancer types[256-260]. Of note, Mn has been shown to be essential for the activation of ATM and MRE11, two DNA-damage repair proteins, and able to increase phosphorylation of p53, the most-well studied tumor suppressor gene which exerts control on cell cycle supporting a role for Mn deficiency in cancer. In fact, many cancers contain mutations in these same proteins. Somewhat paradoxically, HD is associated with reduced Mn bioavailability and reduced risk for cancers[261]. Accumulating data, studies, and clinical trials support a hypothesis that perturbations in IIS and metal ion homeostasis separately contribute to both NDDs and cancer in somewhat opposite fashions while a dearth of investigation exists to study their potential co-regulation in either disease.

Conclusions

The roles for IGF and Mn separately in HD are far from being fully elucidated. However, the sizeable overlap between their homeostasis and downstream effects supports a need to consider their coregulation in the context of diseased and healthy states. Neuroprotective cell signaling (i.e. AKT, mTOR, ERK/MAPK), mitochondrial health, and autophagic function have been implicated in all NDDs repeatedly by multiple groups. Past and present research has revealed an essential role for IIS in coordinating these cellular processes. However, little attention has been given to Mn role even though distinct lines of evidence substantiate its essentiality in these very same processes and even the upstream regulation of insulin/IGF. There is not enough evidence one way or another to draw a clear conclusion whether Mn may be at the heart of IIS dysregulation in NDDs, but there is certainly enough to warrant serious consideration of its role as a contributing factor.

It is still unclear how Mn is exerting its effects on IGF/insulin levels and signaling. Is Mn acting at the levels of transcription, translation, or post-translationally? The intriguing possibility that Mn might regulate IGF-R transcription through ATM/p53 is one that merits further study as it may have implications in not only NDDs but cancer and diabetes as well. Furthermore, given the widespread transcriptional targets of p53, Mn could be widely essential for the transcription of various proteins. Mn could also be exerting its control post-transcriptionally – potentially at the blood brain barrier or via interactions with IGF binding proteins. Clegg and colleagues reported that Mn deficiency resulted in increased IGF-BP3 which they suspected might reduce IGF bioavailability[65]. However, little investigation has been done to follow up on these findings or explore Mn's role on other IGF-BPs which could offer a clear mechanism of Mn's regulation of IGF.

We discussed here many examples of overlap between HD etiology, IGF/insulin biology, and Mn homeostasis. While these connections have been more fully elucidated in HD, the inherent overlap between NDD pathology suggests similar roles for Mn and IGF/insulin in other NDDs. However, as reviewed here, there is preliminary evidence that these NDDs often exhibit different trends in Mn and/or insulin/IGF homeostasis— for example PD is associated with increased Mn while HD is associated with Mn-deficiency. However, these observations lead to the following additional questions— 1) are we exploring IGF/insulin and Mn dysregulation at the "right" times during disease progression 2) are we inspecting the levels of Mn or IGF/insulin in the correct tissues and 3) is this dysregulation truly a contributor to disease pathology or simply a downstream effect of a higher mechanism? If IGF/insulin and/or Mn are truly dysregulated in NDDs, one would imagine that there are defined stages of disease progression when specific defects can be observed. Mn or insulin/IGF could be affected early on in the

disease prior to symptoms, during early symptom manifestation, or during late-stage progression once significant brain atrophy has occurred (or across the entirety of disease progression). Furthermore, it is likely that this dysregulation may differ in not only magnitude, but directionality, between each stage of the disease as molecular signaling attempts to compensate or desensitize. While serum and plasma levels offer a potential biomarker of brain Mn dysregulation, further studies must examine how these levels correlate to what is seen in actual brain tissue. Studies have found that changes in IGF by age, sex, diet, BMI, and secondary disease status can cause immense variability between patients[115]. Several heavy metals are reported to accumulate in the brain with age and can differ by similar confounds suggesting peripheral Mn may also be an inappropriate measurement for brain Mn. Furthermore, Regulation of IGF/insulin and Mn across the blood brain barrier has been somewhat elucidated, but strict regulation of these molecules is needed to establish brain integrity suggesting that they might be very different from what is seen in serum/plasma or even CSF. Confirming consistencies between serum, plasma, blood, CSF and the brain should be done in rodent models across disease progression to validate IGF/insulin and Mn biomarkers— substantiating their use in clinical studies. For other NDDs, a higher mechanistic understanding of IGF/insulin and Mn biology should be explored at the molecular and cellular levels, similar to what has been done in the HD field. Lastly, given the extended time it takes prior to NDD manifestation, one must ask whether observed defects in IGF/insulin or Mn are either a cause of the disease or instead a consequence of the neurodegeneration. This is a difficult question to answer given the inherent difficulty in working with aged models— namely mouse models which often do not fully recapitulate the pathology observed in humans.

Currently, available methods and technology make it quite difficult to truly investigate these questions in a high-through put manner. Highly sensitive biomarkers for Mn and IGF/insulin levels in the brain are likely required to observe changes across disease progression which are currently unavailable. The high variability and contradictory data of IGF/insulin levels in serum/plasma compared to brain suggest these are not always appropriate measurements for brain levels. While existing techniques can quantify levels of Mn in tissues or cells (ICP-MS, graphite furnace, cellular fura-2 Mn extraction assay (CFMEA)) as well as techniques that allow a cellular/sub-cellar resolution of Mn localization (XANES- X-ray absorption near edge structure), high costs and complexities related to maintaining *in vivo* patterns has limited understanding of Mn brain homeostasis[262]. Thus, creative approaches will be necessary to answer these outstanding questions

CHAPTER 2

PHOSPHATIDYLINOSITOL 3 KINASE (PI3K) MODULATES MANGANESE HOMEOSTASIS AND MANGANESE-INDUCED CELL SIGNALING IN A MURINE STRIATAL CELL LINE

Abstract

In a recent study, we found that blocking the protein kinase ataxia telangiectasia mutated (ATM) with the small molecule inhibitor (SMI) KU-55933 can completely abrogate Mn-induced phosphorylation of p53 at serine 15 (p-p53) in human induced pluripotent stem cell (hiPSC)-differentiated striatal neuroprogenitors. However, in the immortalized mouse striatal progenitor cell line STHdh$^{Q7/Q7}$, a concentration of KU55933 far exceeding its IC$_{50}$ for ATM was required to inhibit Mn-induced p-p53. This suggested an alternative signaling system redundant with ATM kinase for activating p53 in this cell line- one that was altered by KU55933 at these higher concentrations (i.e. mTORC1, DNApk, PI3K). To test the hypothesis that one or more of these signaling pathways contributed to Mn-induced p-p53 we utilized a set of SMIs (e.g. NU7441 and LY294002) known to block DNApk, PI3K, and mTORC1 at distinct concentrations. We found that the SMIs inhibit Mn-induced p-p53 expression near the expected IC$_{50s}$ for PI3K, versus other known targets. We hypothesized that inhibiting PI3K to reduce intracellular Mn and thereby decrease activation of p53 by Mn. Using the cellular fura-2 manganese extraction assay (CFMEA), we determined that KU55933/60019, NU7441, and LY294002 (at concentrations near their IC$_{50s}$ for PI3K) all decrease intracellular Mn (~50%) after a dual, 24-hour Mn and SMI exposure. Many pathways are activated by Mn aside from p-p53, including AKT and mTOR pathways. Thus, we explored the activation of these pathways by Mn in STHdh cells as well as the effects of other pathway inhibitors. p-AKT and p-S6 activation by Mn is almost completely blocked upon addition of NU7441(5μM) or LY294002(7μM), supporting PI3K's upstream role in the AKT/mTOR pathway. We also investigated whether PI3K inhibition blocks Mn uptake in other cell lines. LY294002 exposure did not reduce Mn uptake in ST14A, Neuro2A, HEK293, MEF, or hiPSC-derived neuroprogenitors**.** Next, we sought to determine whether inhibition of PI3K blocked p53 phosphorylation by directly blocking an unknown PI3K/p53 interaction or indirectly reducing intracellular Mn, decreasing p-p53 expression. In-Cell Western and CFMEA experiments using multiple concentrations of Mn exposures demonstrated that intracellular Mn levels directly correlated with p-p53 expression with or without addition of

LY294002. Finally, we examined whether PI3K inhibition was able to block Mn-induced p-p53 activity in hiPSC-derived striatal neuroprogenitors. As expected, LY294002 does not block Mn-induced p-p53 as PI3K inhibition is unable to reduce Mn net uptake in this cell line, suggesting the effect of LY294002 on Mn uptake is relatively specific to the STHdh mouse striatal cell line.

Introduction

The element manganese (Mn) is critical for almost all forms of life, yet in excess can be extremely toxic. In humans and mouse models, Mn toxicity has been linked to Parkinsonian-like neurodegeneration including a condition known as manganism[174,176,194]. This critical axis of essentiality toxicity demands strict regulation of Mn in almost all biological systems. Although some is known about Mn regulation at in the gut, very little is known about its regulation at the neuronal level. Understanding the complexity of this system is caused, in part, by the fact that most metal transporters are highly promiscuous, capable of transporting many different ions. Some of these include transporters divalent metal transporter-1 (DMT-1), transferrin, Ferroportin, Huntingtin interacting protein (HIP)14, PARK9 and calcium channels. In addition, few of these exclusively transport Mn at relevant concentrations aside from some possible exceptions such as SLC30A10[32].

 The STHdh immortalized murine neuroprogenitor cell model is an ideal system to study neuronal Mn biology as the cellular fura 2 manganese extraction assay (CFMEA) was developed and rigorously tested in this system[262]. Cellular Mn uptake in the STHdh cells is robust and can occur at levels which are sub-toxic, yet exhibit sensitive activation of cell signaling pathways which are much less responsive in other neuronal systems. In addition, our previous findings on Mn-induced activation of AKT and ATM/p53 were conducted primarily using in this model system[82,263].

Mn is necessary for the activity of many biologically indispensable enzymes including manganese superoxide dismutase (MnSOD), arginase, and glutamine synthetase and sufficient for the activation of many more including ataxia telangiectasia mutated (ATM) kinase. Both toxic and sub-toxic levels of Mn are known to stimulate several critical cell signaling pathways implicated across a broad variety of biological processes and disease states[41,42,45,48,49,81,82,85,86,264-267]. In this study, we focus particularly on p53 and AKT/mTOR pathways that have not only been studied in the context of Mn toxicity but also extensively implicated in several neurodegenerative diseases including Parkinson's and Huntington's disease[87,88,91,92,96,104,126]. Activation by Mn allows ATM to phosphorylate P53, a tumor suppressor gene[30]. P53 functions most commonly to direct DNA repair, cell cycle arrest, and apoptosis—processes highly implicated in both cancer and neurodegeneration. AKT/mTOR pathways—canonically activated by upstream growth factors—are implicated across a wide variety of

processes spanning glucose metabolism, cell proliferation, autophagy and apoptosis. Presently, the regulation of Mn within neurons is a "black box" with little known about how Mn is transported or sequestered within the brain. Thus, understanding the complete implications of Mn homeostasis on Mn-responsive proteins and processes or even how Mn activates specific proteins has been difficult to study. We sought to study how Mn acts to stimulate the aforementioned cell signaling pathways in a murine striatal neuroprogenitor model and whether these Mn-responsive cell signaling pathways could also modulate Mn levels within these cells.

Results

KU55933 and KU60019 do not completely inhibit p-p53 in wild-type STHdh cells

Recently, our lab has shown that ATM kinase is responsible for the phosphorylation of p53 on serine 15 (p-p53) following exposure to sub-toxic (200µM) concentrations of Mn in human induced pluripotent stem cells (hiPSCs) differentiated into striatal-like neuroprogenitors. We found that 1µM KU55933 completely inhibits phosphorylation of p53 at serine 15 following a 200µM Mn exposure in hiPSC-derived Day 11 striatal neuroprogenitors. However, in E14-derived mouse striatal neuroprogenitors (STHdh), KU55933 does not completely inhibit p-p53 or p-H2AX expression (~50% decrease), two targets of ATM, following a 24 hour, 50µM Mn exposure even at 20µM, a concentration far beyond the reportedIC_{50} for ATM (**Figure 2-1A**). Furthermore, KU60019, a more potent and specific derivative of KU559933, was unable to block Mn-induced p-p53 activity at 10µM as measured by In-cell western (**Figure 2-1B**) [268]. Previous work in this cell model also revealed that 20µM KU55933 was unable to completely block H_2O_2 (1 hour) induced p-p53 activity but could block the DNA mutagen neocarzinostatin (1 hour) induced p-p53 activity, suggesting that other kinases are responsible (at least, in part) for Mn induced p-p53 expression [82].

NU7441 and LY294002 inhibit p-p53 activation and Mn uptake at concentrations which inhibit PI3K.

Given the contradictory results between the hiPSC and STHdh systems, we sought to explore whether alternative kinases act similarly to ATM in the STHdh cells to phosphorylate p53 at serine 15. Additionally, a previous study revealed that KU55933 can inhibit DNApk, mTOR, and PI3K at 2.5µM, 9.3µM and 16.6µM, respectively [269]. In order to determine if any of these kinase signaling pathways are responsible for Mn-induced phosphorylation of p53, we utilized several small molecule inhibitors (SMIs) with overlapping IC_{50}s for DNApk, mTOR, ATM, and PI3K (**Table 1**). As kinase inhibitors are notoriously nonspecific, we used other PIKK inhibitors that also inhibit PI3K at defined IC_{50}s,

Figure 2-1: KU55933 and KU60019 do not completely inhibit Mn-induced p-p53 activity in STHdh cells. A) Two representative blots with identical conditions showing partial inhibition of Mn-induced p-p53 and p-H2AX after treatment with 20M KU55933 in STHdh cells. **B)** Quantified In-Cell Western data showing p-p53 expression after 24-hour Mn and/or KU55933/KU60019 exposure. n=3 with 5 technical replicate wells. Error bars= SEM. ***Work done with the assistance of Michael Uhouse.***

Inhibitor	PI3K	mTOR	ATM	ATR	DNApk
KU-55933	16.6µM[32]	9.3µM[32]	13nM[32]	100µM[32]	2.5µM[32]
KU-60019	Unknown[31]	Unknown[31]	6nM[31]	Unknown[31]	Unknown[31]
NU7441	5µM[33]	1.7µM[33]	100µM[33]	100µM[33]	14nM[33]
Rapamycin	--	.1nM[38,39]	--	--	--
Torin 2	1µM[38,39]	2nM[38,39]	.6µM[38,39]	35nM[38,39]	>1µM[38,39]
LY294002	1-10µM[34]	2.5µM[41]	>20µM[37]	>20µM[37]	1.2µM[40]

Table 1: The literature reveals KU55933 inhibits PI3K at higher concentrations. All inhibitors used in this study are shown below with known, reported IC$_{50s}$ against PI3K, mTOR, ATM, ATR, and DNApk. Note citations in subscript.

providing additional validation of our studies. In this way, we used overlapping, yet specific IC_{50s} to exclude particular protein targets (ie: If KU55933 were to inhibit Mn-induced p-p53 at 2.5 µM, but NU7441 does not inhibit p-p53 at 14nM and LY294002 does not inhibit at 1.2 µM, then DNApk inhibition would likely not be responsible for reduced p-p53– see Table 1). Thus, we first exposed STHdh cells for 24-hours with 50µM Mn and either NU7441 or LY294002. NU7441 is known to inhibit DNApk at 14nM, but also inhibits PI3K at 5 µM.

Given the contradictory results between the hiPSC and STHdh systems, we sought to explore whether alternative kinases act similarly to ATM in the STHdh cells to phosphorylate p53 at serine 15. Additionally, a previous study revealed that KU55933 can inhibit DNApk, mTOR, and PI3K at 2.5µM, 9.3µM and 16.6µM, respectively [269]. In order to determine if any of these kinase signaling pathways are responsible for Mn-induced phosphorylation of p53, we utilized several small molecule inhibitors (SMIs) with overlapping IC_{50s} for DNApk, mTOR, ATM, and PI3K (**Table 1**). As kinase inhibitors are notoriously nonspecific, we used other PIKK inhibitors that also inhibit PI3K at defined IC_{50s}, providing additional validation of our studies. In this way, we used overlapping, yet specific IC_{50s} to exclude particular protein targets (ie: If KU55933 were to inhibit Mn-induced p-p53 at 2.5 µM, but NU7441 does not inhibit p-p53 at 14nM and LY294002 does not inhibit at 1.2 µM, then DNApk inhibition would likely not be responsible for reduced p-p53– see Table 1). Thus, we first exposed STHdh cells for 24-hours with 50µM Mn and either NU7441 or LY294002. NU7441 is known to inhibit DNApk at 14nM, but also inhibits PI3K at 5 µM. LY294002 inhibits PI3K at 7 µM. Upon treatment with Mn and NU7441/LY294002, a ~50% decrease in p-p53 levels was observed with 5µM NU7441 and 7µM LY294002, mirroring the effects of 20µM KU55933 on p-p53 expression (**Figure 2-2A, B**)[270,271]. At these concentrations, NU7441 and LY294002 do not inhibit ATM. Furthermore, NU7441 and LY294002 reduced Mn-induced p-p53 levels in a dose-dependent manner with an approximate IC_{50} near their defined IC_{50} for PI3K (**Figure 2-2C, D**).

LY294002, NU7441, KU55933, and KU60019 can reduce Mn uptake at concentrations near the IC_{50} for PI3K

It was surprising that PI3K inhibition reduced Mn-induced p-p53 expression, as PI3K is not directly linked to the activation of ATM/p53 (though downstream signaling members of PI3K—AKT and mTOR—have been linked to p53 regulation). We hypothesized that these inhibitors (LY294002, NU7441, KU55933, and KU60019) could be acting by reducing Mn uptake itself, thus reducing the intracellular pool of Mn and leading to a decrease in p-p53. Utilizing the cellular fura-2 Mn extraction assay (CFMEA), we examined Mn uptake after a 24-hour dual exposure/treatment with 50µM Mn and
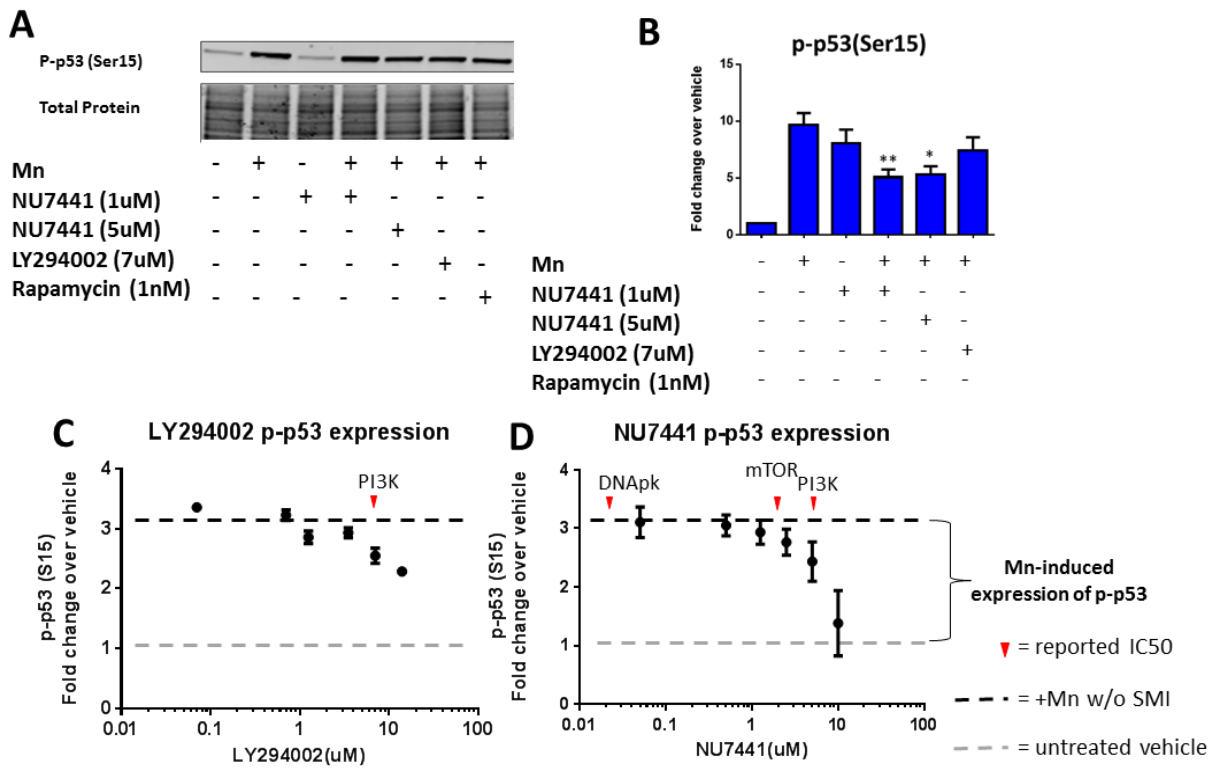
Figure 2-2: NU7441 and LY294002 inhibit phosphorylation of p53 activation and Mn uptake at concentrations that inhibit PI3K. A) Representative western blot showing p-p53 (ser15) expression in STHdh cells with added Mn and/or SMIs. Coomassie stain (total protein, below) was used as a loading control. **B)** Quantification of p-p53 (ser15) from western blots (n=3). Error bars=SEM.). All Mn + SMI values were compared with Mn alone by t-test. *p<0.05, **p<0.01. **C**, **D)** Dose-response curve for Mn-induced p-p53 expression using LiCor In-Cell Western assay with increasing concentrations of LY294002 or NU7441 (n=2 with 5 technical replicate wells, error bars represent SD of all 10 wells). Red arrows denote reported IC$_{50}$ for respective SMI. ***Work done with the assistance of Michael Uhouse.***
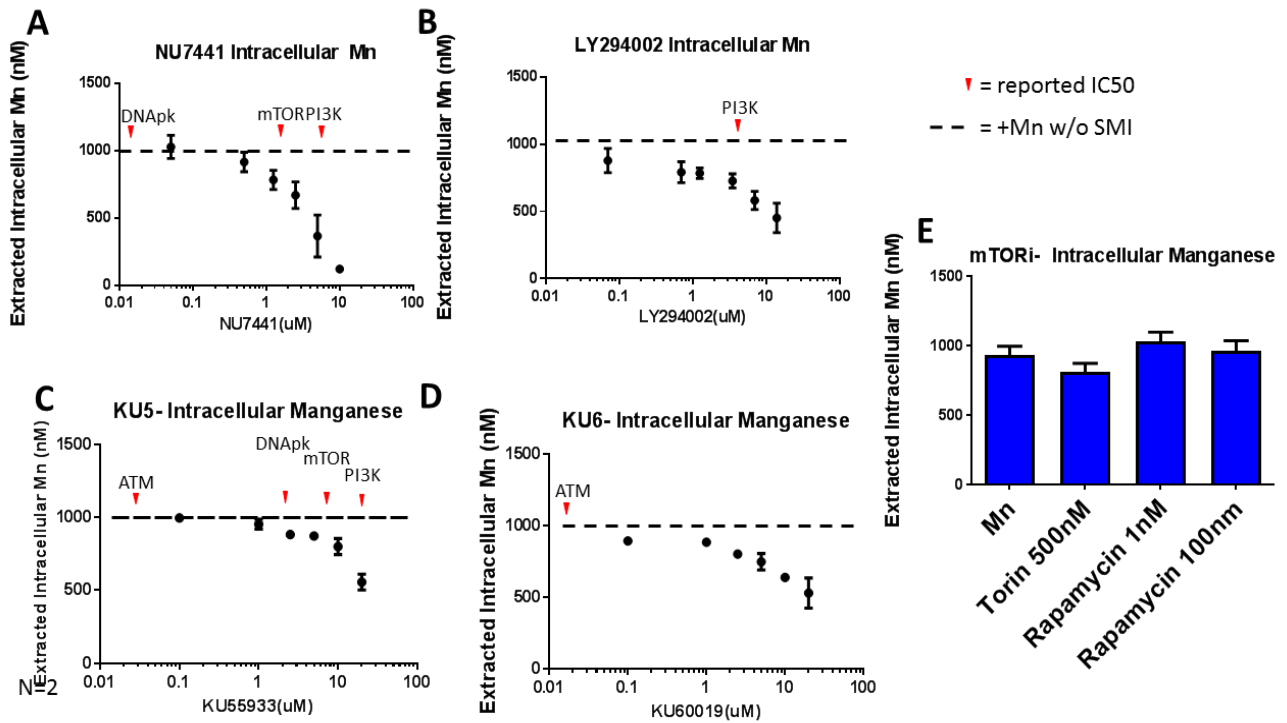
Figure 2-3: LY294002, NU7441, KU55933, and KU60019 can reduce Mn uptake at concentrations near the IC50 for PI3K. A-D) Cellular Fura-2 manganese extraction assay (CFMEA) was used to quantify 24-hour Mn uptake with increasing concentrations of NU7441, LY294002, KU55933, or KU60019. (n=3 with 6 technical replicate wells, error bars represent SD of 3 biological replicates). Red arrows denote reported IC_{50} for respective SMI. **E)** CFMEA after 24-hour Mn and/or mTOR inhibitors "mTORi" (Torin or Rapamycin). ***Work done with the assistance of Michael Uhouse.***

20

an SMI. LY294002, NU7441, KU55933, and KU60019 were able to reduce Mn uptake only at concentrations which neared the IC_{50} for PI3K inhibition (mTOR inhibitors had no effect on Mn uptake even at levels exceeding the IC_{50} for mTOR) (**Figure 2-3**). The two ATM inhibitors (KU55933 and KU60019) were able to inhibit Mn-induced p-p53 expression only at concentrations exceeding the IC_{50} for ATM (**Figure 2-3C, D**). These data suggest that the observed reduction in Mn-induced p-p53 expression by these SMIs is a result of decreased Mn uptake.

LY294002 and NU7441 can reduce Mn-induced p-AKT and p-S6 expression at concentrations near the IC_{50} for PI3K

Mn exposure has been known to activate AKT and mTOR pathways in addition to ATM/p53 [41,42,45,48,49,70,73,81,85,194,264]. STHdh cells were exposed with 50µM Mn and either NU7441, LY294002, or Rapamycin for 24-hours then expression levels of p-AKT(Ser473), and p-S6(Ser235/236) were analyzed by western blot. P-AKT(Ser473) expression levels were greatly reduced after exposure with NU7441 and LY294002 (~3 fold) while Rapamycin was unable to inhibit p-AKT levels (**Figure 2-4A, C**), consistent with mTORC1 signaling being downstream of AKT. p-S6 (Ser235/236) levels, indicative of mTOR activity, were reduced to the greatest magnitude after NU7441 or LY294002 exposure, but also after exposure with 1nM rapamycin (**Figure 2-4B, D).** We examined the effects of LY294002, NU7441, and Rapamycin without Mn (from the same set as data in **Figure 2-4A-D**) which show that mTOR is blocked by LY294002, high concentrations of NU7441 which should inhibit PI3K, and rapamycin. LY294002 and NU7441, but not rapamycin, reduced expression of p-AKT, consistent with their inhibitory cross-reactivity for PI3K. None of the inhibitors blocked basal p-p53 expression (**Figure 2-5**). We observed similar phospho-protein trends after 3 hour exposures but neither LY294002 nor NU7441 could reduce Mn uptake after only 3 hours (**Figure 2-6**). These results confirm that the SMIs are inhibiting the pathways we expected, further confirming a role for PI3K in Mn homeostasis and Mn-dependent cell signaling in this STHdh cell line.

LY294002 is unable to reduce Mn uptake in other cell lines or during shorter exposures

We next investigated whether the inhibition of PI3K also had an effect on Mn uptake in other cell models aside from STHdh. Additionally, given that PI3K is a critical protein involved in both endocytic and exocytic trafficking as well as activation of AKT, we wanted to examine whether the observed effects on Mn uptake are driven by cellular toxicity. We exposed STHdh cells with Mn and/or LY294002, NU7441, KU55933, or KU60019 for 24 hours and used Cell Titer Blue to measure cell viability. Cell viability in the STHdh was relatively unchanged by exposure/treatment with Mn and/or inhibitors (**Figure 2-7B, C**). However, while STHdh cells exhibit robust decreases in net Mn

A — P-AKT (Ser473)

Mn	-	+	-	+	+	+	+
NU7441 (1uM)	-	-	+	+	-	-	-
NU7441 (5uM)	-	-	-	-	+	-	-
LY294002 (7uM)	-	-	-	-	-	+	-
Rapamycin (1nM)	-	-	-	-	-	-	+

B — P-S6 (Ser235/236)

Mn	-	+	-	+	+	+	+	+
KBR (10uM)	-	-	+	+	-	-	-	-
Rapamycin (1nM)	-	-	-	-	+	-	-	-
LY294002 (7uM)	-	-	-	-	-	+	-	-
NU7441 (1uM)	-	-	-	-	-	-	+	-
NU7441 (5uM)	-	-	-	-	-	-	-	+

C — p-AKT(Ser473)

Mn	-	+	+	+	+	+
NU7441 (1uM)	-	-	+	-	-	-
NU7441 (5uM)	-	-	-	+	-	-
LY294002 (7uM)	-	-	-	-	+	-
Rapamycin (1nM)	-	-	-	-	-	+

D — p-S6(Ser235/236)

Mn	-	+	+	+	+	+
NU7441 (1uM)	-	-	+	-	-	-
NU7441 (5uM)	-	-	-	+	-	-
LY294002 (7uM)	-	-	-	-	+	-
Rapamycin (1nM)	-	-	-	-	-	+
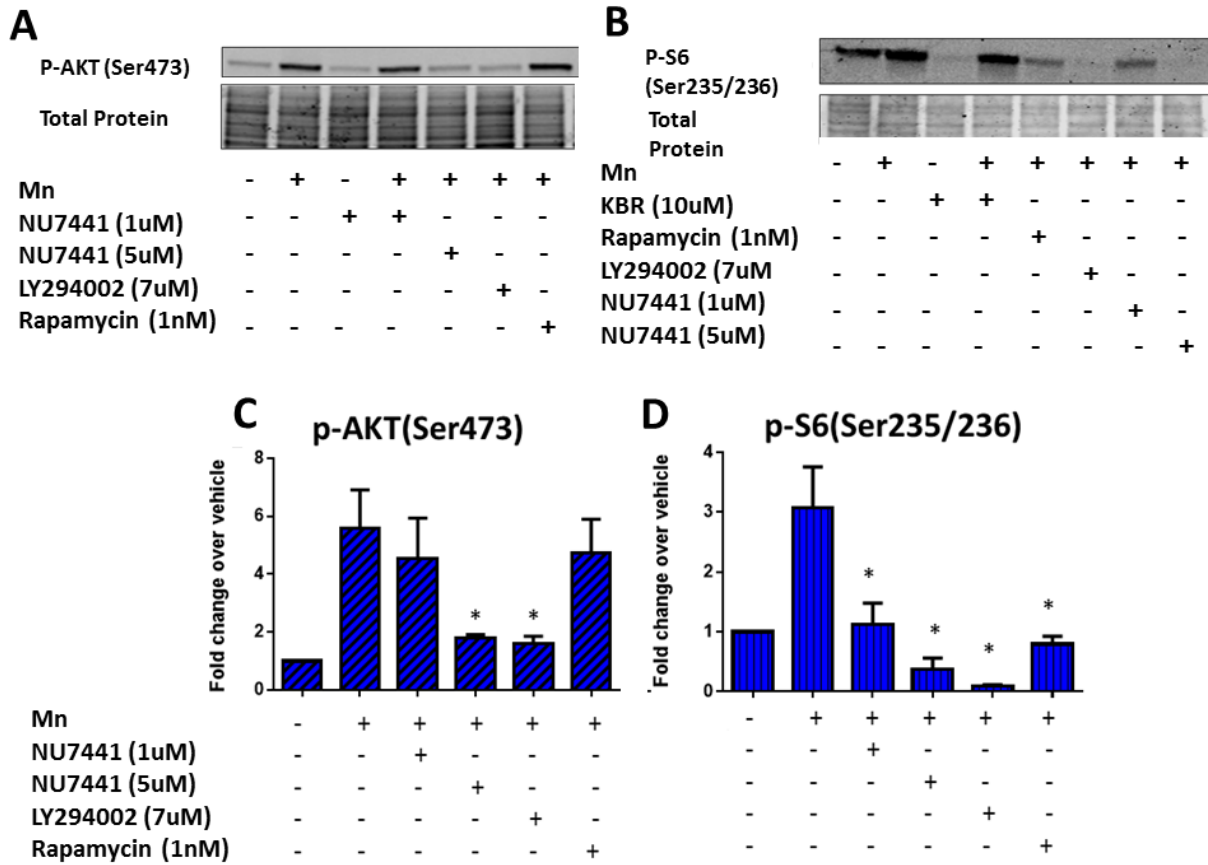
Figure 2-4: LY294002 and NU7441 can reduce Mn-induced p-AKT and p-S6 expression at concentrations near the IC50 for PI3K. A, B) Representative western blots for p-AKT(Ser473) or p-S6(Ser235/236) with Mn and/or SMI for 24 hours. Coomassie stain (total protein, below) was used as a loading control. **C,D)** Quantification of p-AKT(Ser473) or p-S6(Ser235/236) from western blots (n=3). All Mn + SMI values were compared with Mn alone by t-test. *p<0.05, **p<0.01. Error bars =
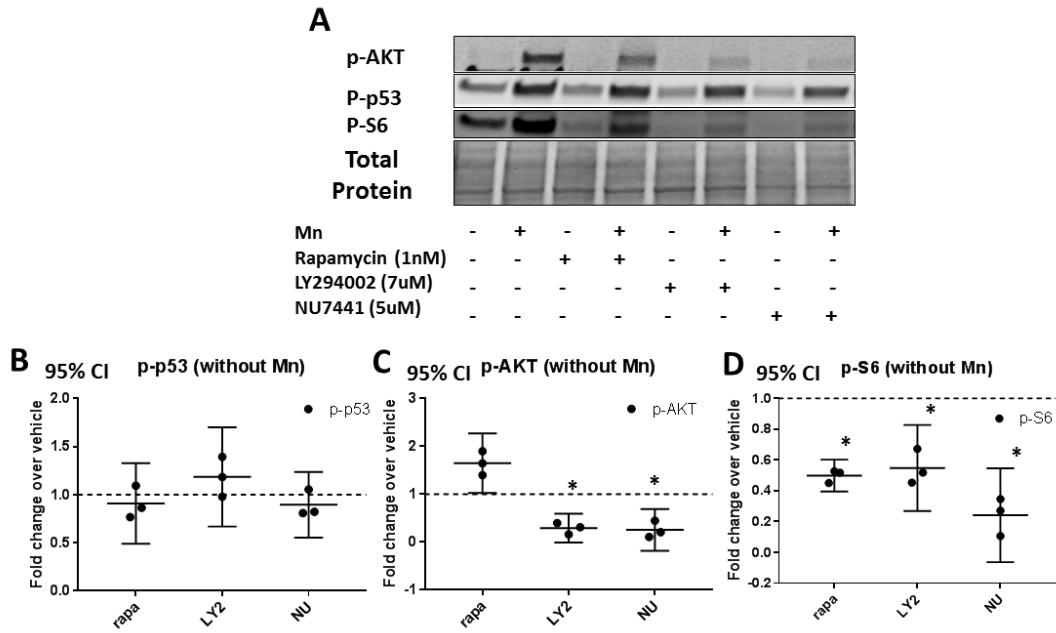
Figure 2-5: LY294002, NU7441, and rapamycin inhibit expected pathways. Western blot analysis on STHdh cells after 24 hour exposure with inhibitors, without Mn. **A)** p-p53 (Ser15), **B)** p-AKT (Ser473), **C)** p-S6 (Ser235/236). n=3. All SMI values were compared to vehicle treated. *p<0.05, **p<0.01. Error bars=95% CI.
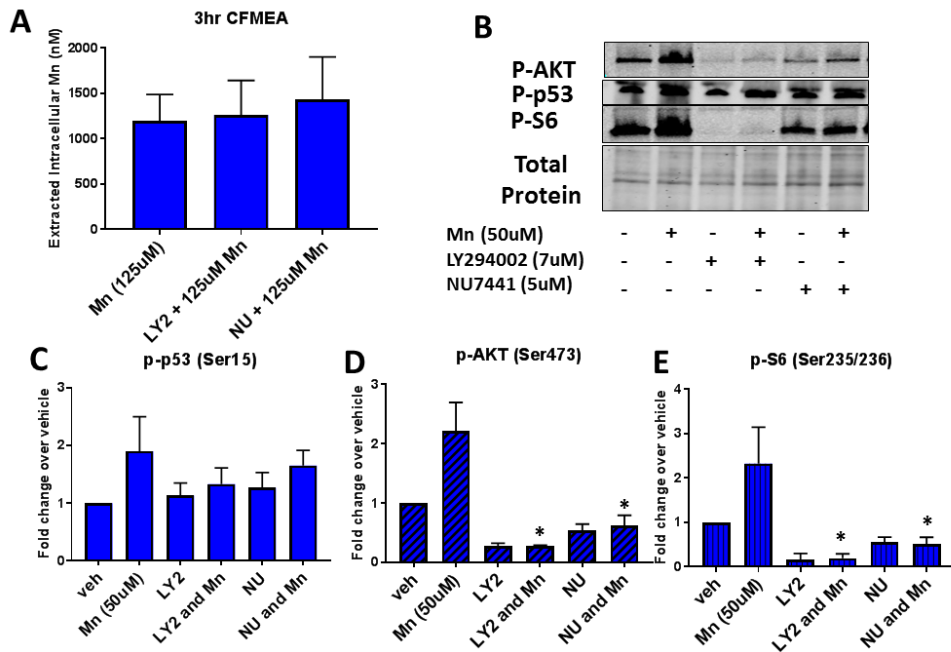
Figure 2-6: LY294002 and NU7441 reduce Mn-induced p-AKT and p-S6, but do not reduce net Mn uptake at concentrations near the IC$_{50}$ for PI3K after 3 hours in STHdh cells. A) CFMEA analysis after 3 hour exposure with Mn and/or LY294002. Western blot analysis for p-p53, p-AKT, and p-S6 after 3 hour exposures (**B-E**). n=3 All Mn + SMI values were compared with 50μM or 100μM Mn alone by t-test. *p<0.05, **p<0.01. Error bars= SEM.
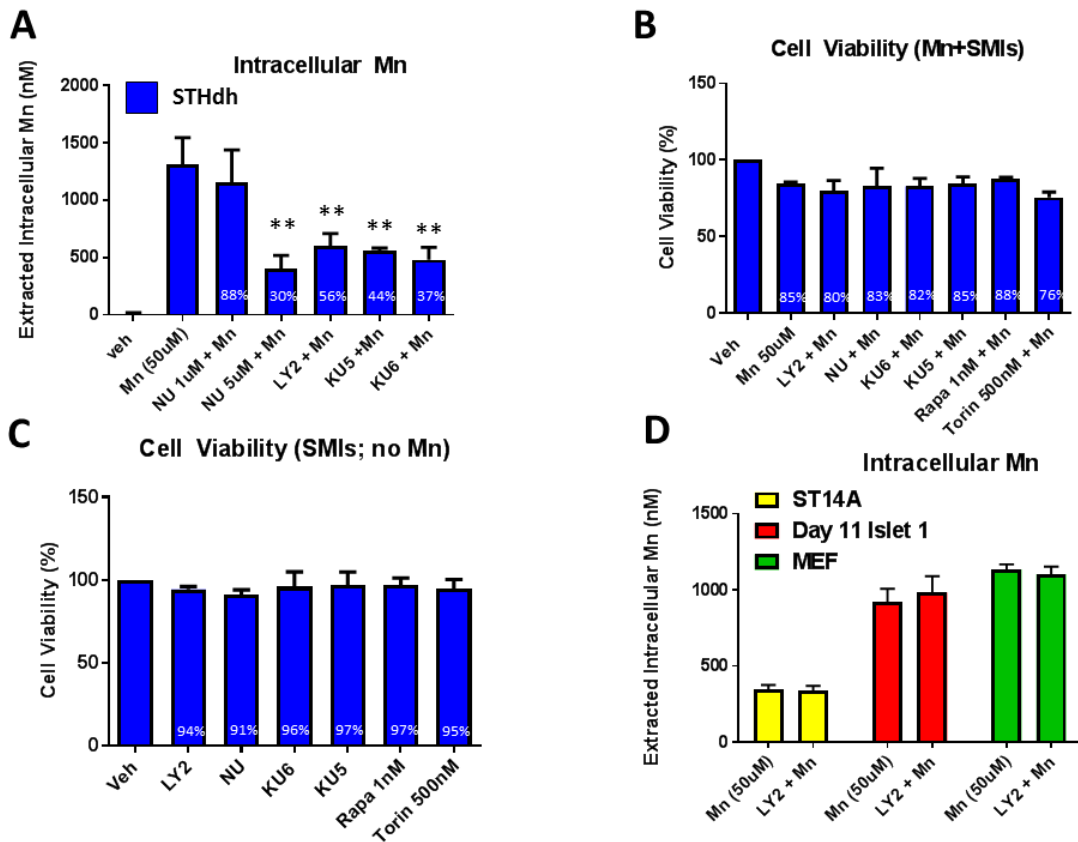
Figure 2-7: LY294002 is unable to reduce Mn uptake in other cell lines. A) CFMEA in STHdh cells after 24 hour exposure with Mn and/or SMIs. **B)** Cell Titer Blue viability assay after 24 hour exposure with Mn and SMIs. **C)** Cell Titer Blue viability assay after 24 hour exposure with SMIs only. **D)** CFMEA on other cell lines after 24 hour exposure with Mn or Mn+LY2. n=3 with 6 technical replicate wells each. All Mn + SMI values were compared with Mn alone by t-test. *p<0.05, **p<0.01. Error bars= SEM.
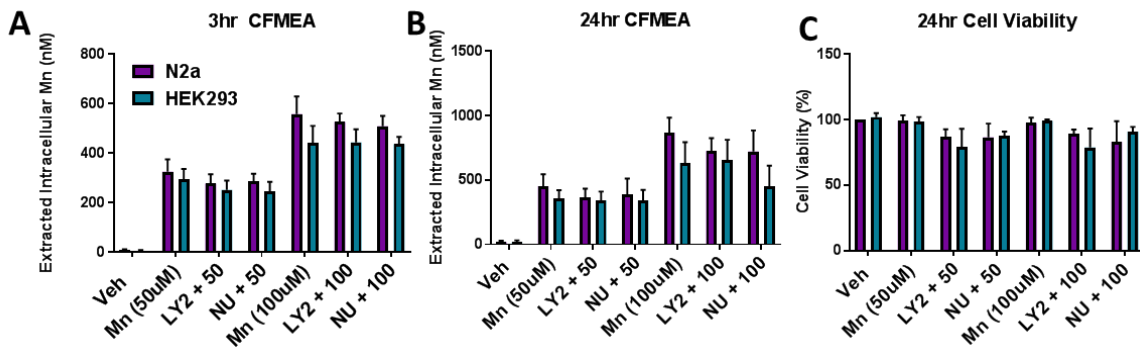
Figure 2-8: LY294002 and NU7441 do not decrease Mn uptake in Neuro2A (N2a) and HEK293 cells. CFMEA analysis after 3hr (**A**) or 24hr (**B**) dual exposure with 50μM or 100 μM Mn and 7μM or 5μM LY294002 or NU7441, respectively. **C)** Cell Titer Blue cell viability analysis after 24 hour exposures. n=3. All Mn + SMI values were compared with 50μM or 100μM Mn alone by t-test. *p<0.05, **p<0.01. Error bars= SEM.

uptake following dual Mn and PI3K inhibitor exposure with limited toxicity, PI3K inhibition was unable to reduce Mn uptake in any of the other cell lines tested (ST14A, Mouse embryonic fibroblasts (MEF), hiPSC differentiated striatal neuroprogenitors) (**Figures 2-7A, D**). We also tested whether LY294002 and NU7441 could inhibit PI3K signaling (p-AKT, p-S6 expression) during 3 or 24 hour exposures in Neuro2A and HEK293 cells. We found that LY294002 blocks basal (~50%) and Mn-induced AKT/mTOR activity in these cell lines after 3 or 24 hours, but both LY294002 and NU7441 do not block Mn uptake (**Figure 2-8, 2-9, 2-10**). These data suggest the mechanism for PI3K inhibition on net Mn uptake is not sufficiently explained by AKT or S6 signaling and is specific to the unique biology of the STHdh cell line.

LY294002 inhibits p-p53 activity in STHdh cells by reducing intracellular Mn

As we observed decreased net Mn uptake with LY294002 and Mn co-exposure, we postulated that the PI3K inhibitor decreases Mn-induced increased p-p53 levels by decreasing intracellular Mn levels. Consequently, we assessed the relationship of intracellular Mn levels and p-p53 levels at a range of Mn exposures (25, 37.5, and 50µM) with and without LY294002 (7µm). LY294002 reduced intracellular Mn and p-p53 expression by 50% at all Mn concentrations. Furthermore, a linear regression of Mn vs. p-p53 activity reveals a high correlation between Mn levels and Mn-induced p-p53 expression (R^2=0.9649, 0.9860, and 0.9775 for Mn, Mn and LY294002, combined Mn and Mn LY294002 values, respectively) **(Figure 2-11A-C)**. In addition, ANCOVA analysis was performed on this data to examine whether these linear regression lines were statistically different from each other. ANCOVA revealed that the slopes of the regression lines were not statistically different and were heavily correlated (R^2=0.98, p=0.218, df=6, F=1.98). These exposures resulted in slight reductions in cell viability, but not enough to account for the observed changes in Mn uptake and p-p53 expression (**Figure 2-11D**). Together these data suggest p-p53 acts as a surrogate rheostat of Mn levels within these cells. Together, these findings confirm our hypothesis that LY294002 reduces intracellular Mn, indirectly reducing activation of p-p53 by Mn, rather than inhibiting direct phosphorylation of p53 by PI3K or a downstream partner.

PI3K inhibition does not block Mn-induced p-p53 in Day 11 Islet 1 hiPSC-derived Neuroprogenitors

Lastly, we sought to test whether LY294002 inhibits Mn-induced increases in p-p53 in a cell line where LY294002 is unable to reduce Mn uptake (day 11 hiPSC-derived Islet-1 striatal neuroprogenitors). Dual LY294002 and 200µM Mn exposure did not block Mn-induced p-p53 activity (p=0.145) in three patient-derived cell lines **(Figure 2-12B, C)**. As a positive control, KU60019 was able to partially reduce Mn-induced p-p53 levels at 1µM (p=0.047), but to a lesser degree than our
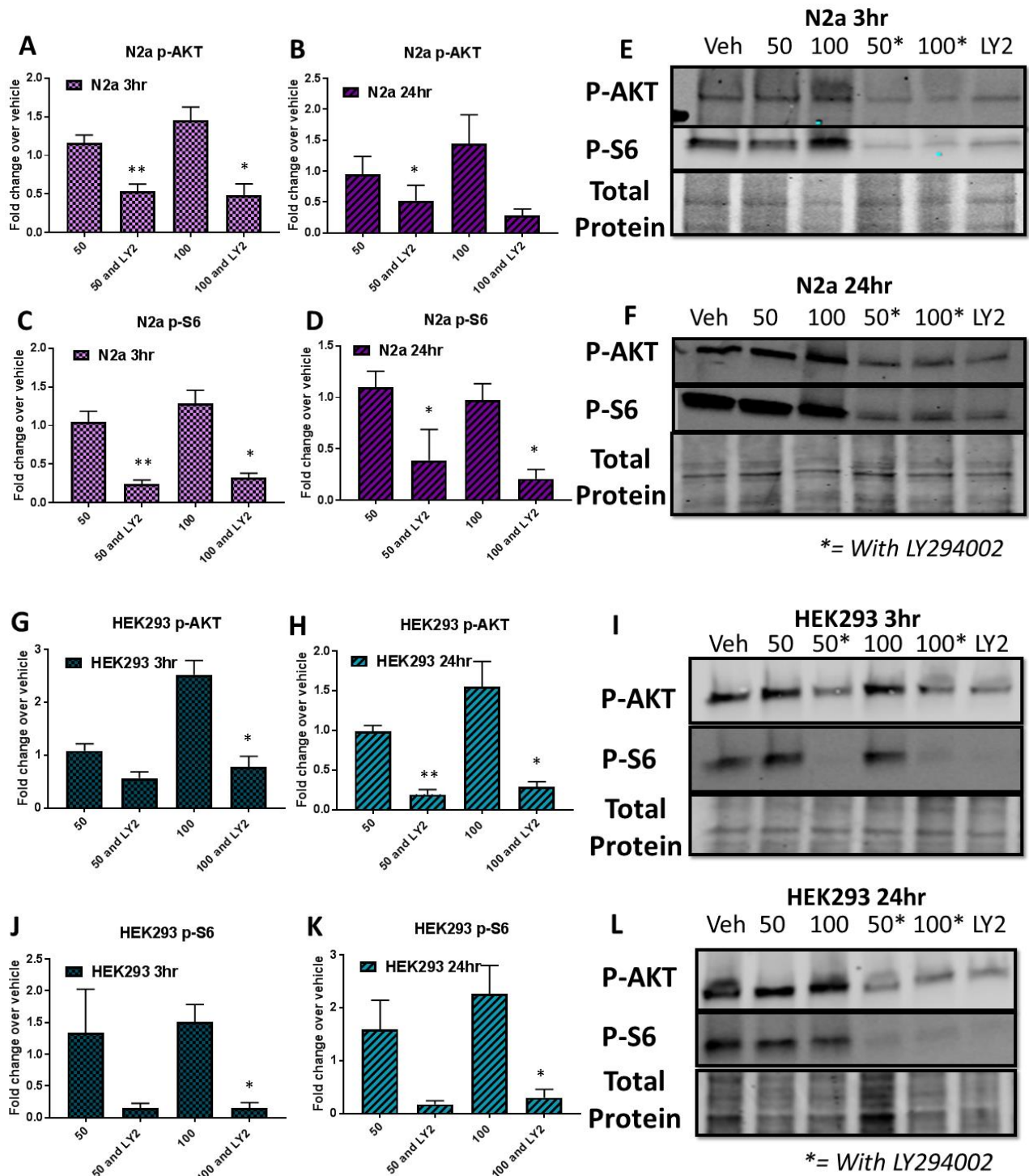
Figure 2-9: LY294002 inhibits Mn-induced p-AKT (Ser473) and p-S6 (Ser235/236) expression in Neuro2A (N2a) and HEK293 cells. Western blot analysis in Neuro2A (**A-F**) and HEK293 (**G-L**) cells after 3 or 24-hour dual exposures (50µM or 100µM Mn and 7µM LY294002). n=3. All Mn + SMI values were compared with 50µM or 100µM Mn alone by t-test. *$p<0.05$, **$p<0.01$. Error bars= SEM. ***Work done with the assistance of Piyush Joshi.***
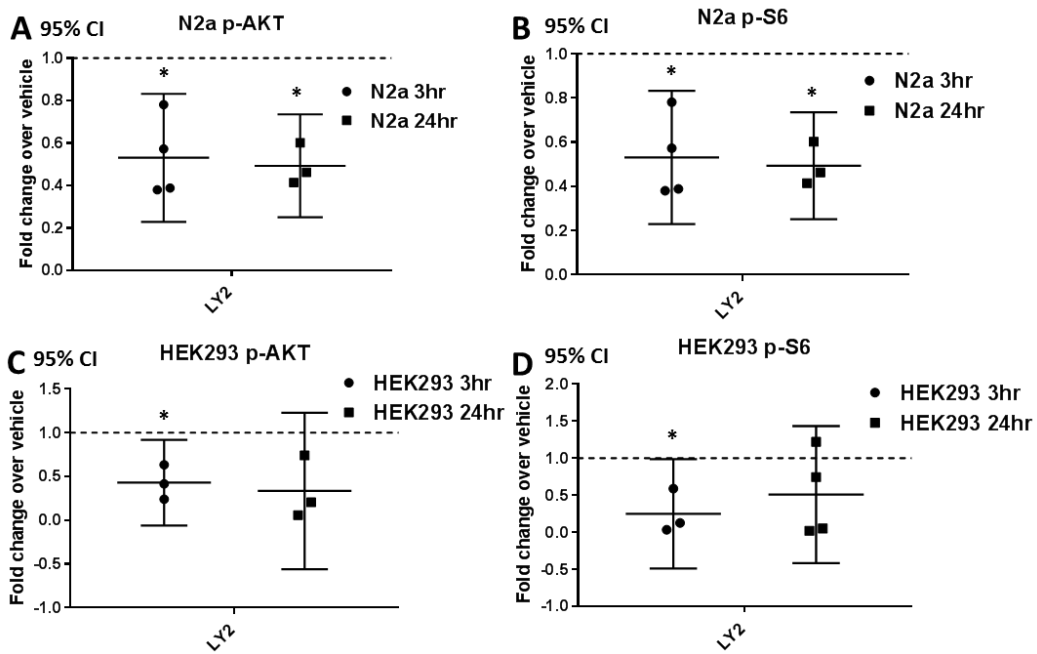
Figure 2-10: LY294002 inhibits basal p-AKT (Ser473) and p-S6 (Ser235/236) in Neuro2A (N2a) and HEK293 cells. Western blot analysis in Neuro2A (**A, B**) and HEK293 (**C, D**) cells after 3 or 24 hour dual exposures (100µM Mn and 7µM LY294002) for p-AKT and p-S6. All SMI values were compared to vehicle treated. n=3. Error bars=95% CI. ***Work done with the assistance of Piyush Joshi.***
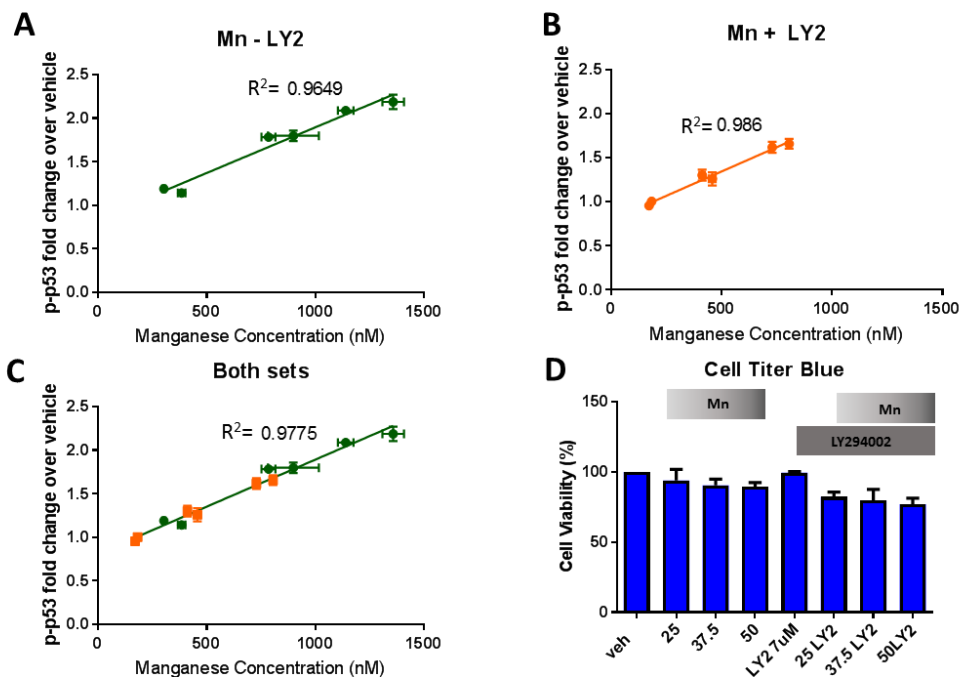
Figure 2-11: LY294002 inhibits p-p53 activity in STHdh cells by reducing intracellular Mn. A-C) Linear regression plots for Mn (X) vs p-p53 (Y) across 25μM , 37.5μM , or 50μM Mn exposures with or without LY2 for 24 hours. Mn **(A),** Mn+LY294002 **(B),** and Mn combined with Mn+LY2 **(C)** are plotted separately (n=2 with 5 replicate wells per condition, error bars are SD for each set of 5 replicate wells). R^2 values are shown next to each line. ANCOVA: R^2=0.98, p=0.218, df=2, F=1.98. **D)** Cell Titer Blue cell viability assay after 25μM , 37.5μM , or 50μM Mn exposure for 24 hours, with and without LY294002. Error bars= SEM.
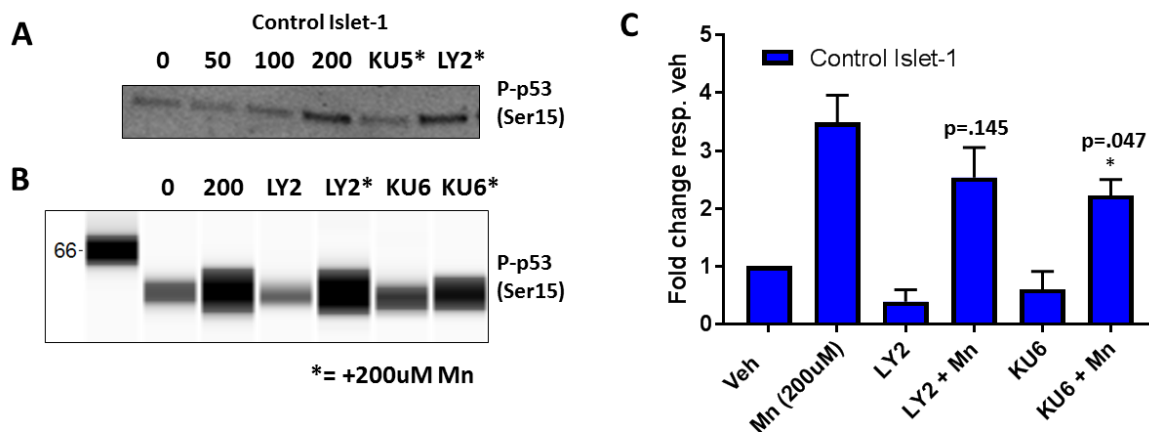
Figure 2-12: PI3K inhibition does not block Mn-induced p-p53 expression in Day 11 Islet 1 hiPSC-derived Neuroprogenitors. A) Representative western blot of confirmed complete inhibition of Mn-induced p-p53 activity after 24 hour treatment with Mn and 1μM KU50019. **B)** Representative Simple Wes "lane view" image of Islet-1 neuroprogenitor lysates – cells were treated with 200uM Mn and 7μM LY294002, or 1μM KU60019 with and without 200μM Mn – probed for p-p53 (Ser15). **C)** Quantification of Simple Wes for p-p53/actin and normalized to respective untreated vehicle. n=3 from three separate control hiPSC cell lines. All Mn + SMI values were compared with 50μM or 100μM Mn alone by t-test. *p<0.05, **p<0.01. Error bars= SEM. ***Work done with the assistance of Kristen Nordham.***

28

previous study (**Figure 2-12A**). Together, these data suggest PI3K plays a unique role in Mn uptake, and thus Mn-induced cell signaling activity, in STHdh cells but not other cell lines— even those of striatal lineage.

Discussion

We have demonstrated that the SMIs KU-55933, NU-7441, and LY294002 can potently inhibit Mn uptake (near ~50% for all three SMIs) in a mouse striatal neuroprogenitor model at concentrations consistent with inhibition of their shared target, PI3K. KU-60019, to the best of our knowledge, has not been reported to inhibit PI3K, though KU55933 is known to inhibit PI3K at concentrations of 16.6uM or higher. Our data suggest that KU-60019 also inhibits PI3K at an approximate IC_{50} of 10μM (**Figure 2-3D**), if it reduces net intracellular Mn uptake in STHdh cells via the same mechanisms the other SMIs used. This conclusion is consistent with the relative inhibition of Mn-uptake for KU-60019 being almost identical (~50%) to the established PI3K inhibitors. Our data suggest KU-55933, NU-7441, LY294002, and KU-60019 do not decrease net Mn levels via reduced cell viability, since effective concentrations only showed about a 15-20% reduction in viability, even in the presence of Mn - this was insufficient to account for the over 50% decrease in Mn uptake seen with these inhibitors. LY294002, a specific inhibitor of PI3K, is effective at reducing net Mn uptake at a concentration consistent with PI3K inhibition from the literature (7μM) (**Figure 2-3**) [272]. Likewise, the concentrations at which NU-7441 and KU-59933 were found to be effective at inhibiting Mn uptake and p-p53 expression (5μM and 20μM, respectively) are also consistent with inhibition of their shared off-target, PI3K (inhibited at 5μM and 16.6μM, respectively) (**Table 1, Figure 2-2**). mTORC1 is also a shared target between all four inhibitors, but use of mTORC1 inhibitors rapamycin or torin at concentrations equal to or surpassing their IC_{50}s for mTORC1 had no effect on Mn uptake (**Figure 2-3E**) [273,274].

As LY294002 could not reduce Mn uptake in the other cell lines tested, the role of PI3K may be uniquely tied to Mn homeostasis in STHdh cells. Perhaps STHdh cells lack a compensatory pathway for PI3K that is preserved in the other cells tested, making STHdh Mn homeostasis exquisitely sensitive to PI3K inhibition. It is also possible the STHdh cell line, because its specific lineage, neuronal maturity, origin, etc. expresses a specific transporter which is PI3K dependent. Alternatively, while LY294002 is reported to be specific to PI3K at the concentrations used, it is possible that LY294002 is also inhibiting another protein, similar to PI3K, in STHdh cells and causal in the observed effects. Reported IC_{50}s of LY294002 for PI3K have been somewhat variable between studies and cell lines (1-10μM). These reports have shown that LY294002 can also inhibit other targets (including mTOR and DNApk) at concentrations lower than 10μM [271,275,276]. However, in this study we utilized more specific inhibitors

(Rapamycin and NU7441) with overlapping IC_{50s}, suggesting that neither mTOR nor DNApk are responsible for the effect. Collectively, available data cannot exclude the possibility that a specific off-target for LY294002, aside from mTOR and DNApk, may be uniquely expressed in STHdh cells and responsible for Mn uptake in these cells and not in other cell lines. However, this specific off-target would have to be coincidentally inhibited by four different inhibitors at all their reported IC_{50s} for PI3K.

While our study does not elucidate the mechanism by which PI3K is modulating Mn uptake, our results do offer some insight. PI3K inhibition only results in reduced Mn uptake in STHdh cells after 24hrs, which could indicate an epigenetic alteration or a transcriptional-to-translational cascade is occurring in these cells after the addition of PI3K inhibitors, reducing Mn uptake (**Figure 2-3, 2-5**). However, these four inhibitors do inhibit basal and Mn-induced p-AKT and p-S6 expression at 3 hours, even in cell lines in which they do not affect Mn uptake (**Figure 2-6, 2-8, 2-9**). Thus, inhibition of AKT and mTOR is not responsible for the reduction in Mn uptake observed upon exposure with PI3K inhibitors. Furthermore, the results suggest that Mn-induced p-AKT and p-S6 signaling are PI3K-dependent.

Our observations reported here raise some very novel and interesting questions. How is PI3K exerting its role on Mn-homeostasis in the STHdh model? What types of transport/transporters is PI3K working through to impinge on Mn homeostasis? Given the inherent difficulty in studying Mn homeostasis due to poorly understood transport and sequestration, understanding how PI3K is capable of such a dramatic effect on Mn uptake could lead to the discovery of other, more commonly shared, pathways of Mn homeostasis. Considering PI3K's downstream role in endocytosis via signaling of PIP2-PIP3, a reasonable hypothesis is that PI3K signaling upregulates endocytosis of a specific, unknown Mn-receptor on the cell surface. This type of transport would mirror clathrin-mediated endocytosis of iron, another biologically indispensable heavy metal. A previous study by our lab has shown that saturating clathrin-mediated uptake with iron, thus blocking transferrin-mediated Mn uptake, only reduces Mn toxicity by ~10% STHdh cells [263]. This suggests clathrin-mediated endocytosis cannot fully explain the effect of PI3K inhibition on Mn uptake. Regardless, Mn uptake has directly been associated with intracellular toxicity via increased generation of reactive oxygen species and mitochondrial dysfunction and has been recognized as a potent neurotoxicant—particularly in dopaminergic neurons [52,177,178,277-283]. This study suggests that PI3K may play a role in neuronal Mn homeostasis, offering a potential target/pathway which can be furthered studied in the context of Mn toxicity. LY294002 causes some toxicity, which is exacerbated by addition of toxic concentrations of Mn and, thus, does not reduce overall intracellular toxicity. In principle, however, using other small molecules to target pathways/proteins (possibly including PI3K) that can reduce Mn uptake in the

context of toxic Mn exposures could be valuable tools for studying future therapeutics.

Similarly, given PI3K is upstream of AKT/mTOR, it is possible that PI3K is responsible for perpetuating an upstream signal leading to the activation of autophagy via the mTOR pathway, which may then act to degrade Mn-laden proteins, releasing Mn into a useable pool for the cell. However, the lack of effect on Mn uptake by rapamycin and Torin, known mTOR inhibitors, do not support this hypothesis. If PI3K does truly exert such potent control on Mn homeostasis, it could also control activation of the wide array of Mn-dependent and Mn-activated enzymes and thus, Mn-dependent cell signaling. In this study, we have shown that p-p53 expression is tightly correlated to Mn status in this cell line and that PI3K can act to modulate this ion-protein interaction (**Figure 2-11**). Furthermore, PI3K's protein-serine kinase activity is Mn-dependent while its lipid activity is inhibited by Mn [284]. Indeed, responding as a Mn "sensor", PI3K could function to regulate not only the ATM/p53 and AKT/mTOR pathways, but many other Mn-responsive processes within the cell, in response to intracellular Mn levels.

Acknowledgements

Materials and Methods

Inhibitors and antibodies

The small molecule inhibitors (KU55933, KU60019, NU7441, and LY294002) were purchased from Tocris, reconstituted in DMSO, and stored at -80 degrees prior to experiments. The rapamycin and Torin 2 were generous gifts from Dr. Kevin Ess. Antibodies were purchased from Cell Signaling Technologies (p-AKT (Ser473) #4060, p-p53 (Ser15) #9286, p-S6 (Ser235/236) #2211, actin #4968S).

Cell culture

The immortalized, wild-type, murine striatal cell line (STHdh$^{Q7/Q7}$) were obtained from Coriell Cell Repository (Cambden, NJ). STHdh$^{Q7/Q7}$ immortalized murine striatal cells were cultured in Dulbecco's Modified Eagle Medium [D6546, Sigma-Aldrich, St. Louis MO] supplemented with 10% FBS [Atlanta Biologicals, Flowery Branch, GA], 2 mM GlutaMAX (Life Technologies, Carlsbad, CA), Penicillin-Streptomycin, 0.5 mg/mL G418 Sulfate (Life Technologies, Carlsbad, CA), MEM non-essential amino acids solution (Life Technologies, Carlsbad, CA), and 14mM HEPES (Life Technologies, Carlsbad, CA). They were incubated at 33°C and 5% CO_2. Cells were passaged before reaching greater than 90% confluency. The cells were split by trypsinization using 0.05% Trypsin-EDTA solution (Life Technologies, Carlsbad, CA) incubated for five minutes. One day prior to exposure, cells were plated in the appropriate cell culture plate type at 8x10^5 cells/mL for STHdh.

Neuro2A, HEK293, ST14A, and mouse embryonic fibroblasts (MEF) were cultured in DMEM with 4.5g/L glucose, L-glutamine, and sodium pyruvate with 10% FBS and penicillin/streptomycin. All cells were grown at 37°C and 5% CO_2. MEF cells were harvested from WT BL6-c57 mice between E12.5-E13.5. For CFMEA experiments, 3 separate MEF lines were used.

Islet-1 striatal neuroprogenitors derived from hiPSCs

Islet-1 hiPSC-derived neuroprogenitor cells were differentiated and harvested for protein exactly as previously described using three separate healthy control patient iPSCs [82]. Protein lysates were frozen prior to BCA protein quantification and preparation for the Simple Wes assay. Additionally, a subset of cells was fixed with ice-cold methanol for 15 minutes at -20 °C and immunocytochemistry was performed to ensure all cultures expressed Islet-1.

Immunoblot analysis

Protein samples were prepared by scraping cells into ice-cold PBS, centrifuging, and adding RIPA buffer containing protease (Sigma-Aldrich, St. Louis, MO) and phosphatase inhibitor cocktails 2

& 3 (Sigma, Sigma-Aldrich, St. Louis, MO) to the pellet. After gentle homogenization, cells were centrifuged at 4°C for 10 minutes at 20,000 g. The resulting DNA containing pellet was removed from the lysate, and the protein concentration was quantified using the BCA assay (Peirce Technologies) with a BSA standard curve. Samples were mixed with 5x SDS loading buffer containing 1% 2-mercaptoethanol and boiled for 5 minutes. 15 µg of protein was loaded for each sample onto a 4-15% pre-cast gel SDS-PAGE gel (BioRad, Hercules, CA) and run at 90V for 120 minutes. The protein bands were then transferred onto nitrocellulose membranes using iBlot Gel Transfer Device (Life Technologies). The remaining gel was stained with IRDye Blue protein stain (LI-COR, Lincoln, NE). Since the gels retained ~1/3 of the original protein after transferring with the iBlot, the stained gels were imaged on the Li-Cor Odyssey Imaging System and the intensity of the entire lane from ~150-20 kDa was quantified. This value was used to normalize the values of immunostained bands. The membrane was blocked in Odyssey Blocking Buffer for one hour prior to the addition of the primary antibodies. The primary antibodies were diluted 1:1000 in Odyssey Blocking Buffer containing 0.1% TWEEN and incubated overnight. After washing 5 times for 5 minutes in TBST, membranes were incubated with secondary antibodies at 1:10,000 (LiCor, Lincoln, NE) for 1 hour. Membranes were imaged using the Li-Cor Odyssey Imaging System, and quantification was performed using Image Studio Lite (LiCOR, Lincoln, NE).

In-Cell Western Assay

Cells were plated in 96-well µClear black-walled plates (Greiner Bio-One, Frickenhausen, Germany) at the appropriate density for the particular line. After exposing cells to toxicants, cells were washed once in room temperature PBS (without calcium and magnesium). The cells were then fixed with 4% paraformaldehyde in PBS for 30 minutes at room temperature, washed 5 times for in PBS with 0.1% Triton-X 100, and blocked for 1.5 hours in 150 µL of Odyssey blocking buffer. Cells were then incubated with primary antibody at 1:400 in Odyssey blocking buffer (LiCor, Lincoln, NE) with 50 µL per well for 2.5 hours. After washing 4 times in PBS with 0.1% Tween-20 for 5 minutes, cells were incubated for 1 hour in the appropriate LiCor IRdye800 secondary antibody at 1:800 dilution in Odyssey blocking buffer along with 1:500 of CellTag normalization dye (LI-COR, Lincoln, NE). An additional round of 5 washes for 5 minutes in PBS with Tween-20 was performed after which all buffer was removed. Plates were imaged with the Li-Cor Odyssey Imaging System and intensities were calculated for each well with Image Studio software. Cultures that were not incubated with primary antibodies served as background. Antibody signals were normalized using the CellTag signal (a measure of total cells).

Cellular Fura-2 Manganese Extraction Assay (CFMEA)

CFMEA was performed as described previously [82].

CellTiterBlue Cytotoxicity Assay

Mouse striatal cells (STHdh$^{Q7/Q7}$) were grown on 96-well plates. The day after replating, the cells were exposed to toxicants in the cell-type appropriate medium. After 22 hours of exposure, 20 µL of CellTiterBlue reagent (Promega, Madison, WI) was added to each well. Prior to this addition, cell lysis buffer was added to several wells to provide an accurate fluorescence background for 0% viable cells. The plates were then incubated for 2 hours at 33° C. Fluorescence was measured using excitation of 570 nm and emission of 600 nm on a microplate reader.

Protein Simple Wes Protein Expression Quantification

The Protein Simple Wes (Protein Simple, San Jose, California) was performed on day 11 Islet-1 striatal neuroprogenitors derived from hiSPCs. The assays were performed following manufacturer's guidelines using the 12-230 kD kit: separation time= 25 min, voltage= 375volts, antibody diluent time= 5min, primary incubation time= 30min, and secondary antibody time= 30min. 5ul of protein lysate at 1ug/uL was used per run, per sample. The p-p53 antibody was diluted 1:50 and actin was diluted 1:200 in 0.1X sample buffer provided by the manufacturer. Expression is given as relative chemiluminescence signal area under the curve at a particular peak.

Graphing and Statistical Analysis

To allow for appropriate post-hoc statistical analysis, western blots comparing SMIs vs Vehicle were normalized to vehicle. For this data, 95% confidence interval testing (GraphPad Prism 7) analysis was performed. Graphs comparing Mn-treated to SMI+Mn were normalized to vehicle. For this data, t-tests were performed using Microsoft Excel. All graphs were made using GraphPad Prism 7.

CHAPTER 3

MANGANESE DIRECTLY ACTIVATES IGFR/IR-DEPENDENT PHOSPHORYLATION OF AKT AND GLUCOSE UPTAKE IN HUNTINGTON'S DISEASE CELLS

*Adapted from: **Miles R. Bryan**, et al. Manganese directly activates IGFR/IR-dependent phosphorylation of AKT and glucose uptake in Huntington's disease cells. Molecular Neurobiology. In Press.*

Abstract

Perturbations in insulin/IGF signaling and manganese (Mn) uptake and signaling have been separately reported in Huntington's disease (HD) models. Insulin/IGF supplementation ameliorates HD phenotypes via upregulation of AKT, a known Mn-responsive kinase. Limited evidence both in vivo and in purified biochemical systems suggest Mn enhances insulin/IGF receptor (IR/IGFR), an upstream tyrosine kinase of AKT. Conversely, Mn deficiency impairs insulin release and associated glucose tolerance in vivo. Here, we test the hypothesis that Mn-dependent AKT signaling is predominantly mediated by direct Mn activation of the insulin/IGF receptors, and HD-related impairments in insulin/IGF signaling are due to HD genotype-associated deficits in Mn bioavailability. We examined the combined effects of IGF-1 and/or Mn treatments on AKT signaling in multiple HD cellular models. Mn treatment potentiates p-IGFR/IR-dependent AKT phosphorylation under physiological (1nM) or saturating (10nM) concentrations of IGF-1 via direct, intracellular activation of IGFR/IR. Using a multi-pharmacological approach, we find that >70-80% of Mn-associated AKT signaling across rodent and human neuronal cell models is specifically dependent on IR/IGFR, versus other signaling pathways upstream of AKT activation. Mn-induced p-IGFR and p-AKT were diminished in HD cell models, and, consistent with our hypothesis, were rescued by co-treatment of Mn and IGF-1. Lastly, Mn-induced IGF signaling is functional as the reduced glucose uptake in HD STHdh cells was partially reversed by Mn supplementation. Our data demonstrate that Mn supplementation increases maximal IGFR/IR-induced p-AKT via direct effects on IGFR/IR and suggests reduced Mn bioavailability contributes to impaired IGF signaling and glucose uptake in HD models.

Introduction

The essentiality of manganese (Mn) is derived from its binding to and activation of several biologically indispensable enzymes, including Mn superoxide dismutase, glutamine synthetase, pyruvate decarboxylase, protein phosphatase 2A (PP2A), and arginase [32]. In addition, Mn is a required cofactor for a variety of kinases, and can often compete with magnesium (Mg) when at sufficiently high concentrations to activate others, including ATM and mTOR [30,31]. As the vast majority of kinases are either Mn- or Mg-dependent, Mn can act as a potent cell signaling modifier. Mn can activate ERK, AKT, mTOR, ATM, and JNK in vitro and in vivo [30,42,44-46,285-290]. As these kinases regulate transcription factors (CREB, p53, NF-kB, FOXO), Mn can also modulate cell function at the transcriptional level [45,82,291,292]. Consequently, the roles of Mn homeostasis and associated signaling in both the essentiality and toxicity of Mn are an important area of investigation. However, it remains uncertain which Mn-dependent enzymes are most sensitive to changes in Mn homeostasis and the relationships between Mn-biology and these signaling cascades.

In contrast, at high concentrations, Mn can be neurotoxic, and this has been associated with risk for idiopathic parkinsonism and the Mn-induced parkinsonian-like disease known as manganism [179,293-295]. High environmental exposure to Mn has been associated with specific occupational settings (welding, mining), exposure to industrial ferroalloy emissions, well water consumption in some regions, or parenteral nutrition [83,194,296-298]. Of particular interest, Mn-induced p-AKT has been observed in a variety of models and in Mn-exposed patient populations [42,85,287,299-301]. However, it is still unclear what the role of this response is or by which upstream signaling mechanism it occurs, though Mn-induced p-AKT is not blocked by the antioxidant Trolox [264]. Thus, the elucidation of the primary signaling mechanism behind Mn-responsive AKT will be informative in the context of both basal Mn homeostasis and Mn neurotoxicity.

Insulin and IGF-1 are highly homologous growth factors which are necessary for a variety of peripheral processes, as well as essential for synaptic maintenance and activity, neurogenesis and neurite outgrowth, and neuronal mitochondrial function [105,302]. Insulin and IGF-1 bind to highly similar cell surface receptors which initiate an autophosphorylation cascade, independent of other kinases, which activates the insulin receptor (IR) and the IGF-1 receptor (IGFR). This causes subsequent activation of phosphatidylinositol-3-kinase (PI3K), insulin receptor substrates (IRSs), and other mediators activating the pro-growth AKT, mTOR, and ERK/MAPK pathways which have widespread roles in multiple biological processes. Dysregulation of these potent neurotrophic growth factors has been associated with neurodegenerative diseases, including HD, PD, and Alzheimer's disease (AD) [109,111,112,115,179,182,183,185,186,201-204,212,303-306]. However, while the vast majority of kinases in the human body are Mg and/or Mn-dependent, few studies have mechanistically elucidated how these metals

maintain kinase signaling cascades in living biological systems or contribute to kinase-dependent pathology of neurodegenerative diseases.

Evidence supporting a role for insulin/IGF-1 synergistic cross talk with Mn has been slowly amassing, but is incompletely understood. Mn deficiency in rodent models reduces insulin production and causes glucose intolerance, while Mn supplementation can protect against diet-induced diabetes rescue glucose intolerance, and increase insulin and IGF-1 ligand levels in rodents [51,59-66,307]. Furthermore, Mn administration stimulates insulin-linked glucose transport and related phosphodiesterase activity in adipocytes, though insulin/IGF receptor activity was not investigated [308]. Two prior studies have examined how supra-physiological Mn (1-10mM) activates insulin receptor activity using non-living, permeabilized rat adipocytes or purified biochemical systems and have shown that Mn directly increases net autophosphorylation of insulin receptors by both enhancing kinase activity and inhibiting receptor dephosphorylation [309,310]. Finally, a previous study reported that JB1, an IGFR1 antagonist, can block Mn-induced IGFR-AKT-mTOR phosphorylation in the preoptic area of prepubertal rats [287]. Together, these data provide a strong premise to examine this signaling pathway at a cellular level and suggest Mn may be a critical mediator of insulin/IGF-1 homeostasis and downstream signaling, including AKT [51,60,64,85,300,301,307,311]. However, the understanding of Mn-IGF synergy lacks mechanistic insight of the direct site-of-action of Mn on IGFR/IR-AKT signaling and requires confirmation of this mechanism in living systems under biologically-relevant, sub-cytotoxic concentrations of Mn (1-500μM). Furthermore, elucidation of an initial site-of-action for Mn may bridge the mechanistic gap between non-living and in vivo systems—directly connecting the role of Mn-induced receptor kinase activity to the changes seen in Mn-responsive metabolism in vivo, such as glucose tolerance.

HD is an autosomal dominant, neurodegenerative disease caused by an expanded CAG repeat within exon 1 of the Huntingtin (HTT) gene. Through a yet unknown pathogenesis, this expanded trinucleotide causes specific cell death in the medium spiny neurons of the striatum, leading to a variety of symptoms—most notably chorea. This disease has variable progression, but is ultimately fatal. There is no cure for HD, but drugs can target symptoms with variable efficacy. Recent research has shown that IGF-1 treatment in HD models results in robust amelioration of a wide-array of phenotypes via AKT signaling-mediated mechanisms. The results of this treatment include: an increase in autophagic function and mutant HTT (mutHTT) aggregate clearance; restoration of mitochondrial function; regularization of energy metabolites; HTT serine 421 phosphorylation; and medium spiny neuron health. Perhaps most importantly, IGF treatment can rescue motor abnormalities and early mortality in HD mouse models [93,96,97,104,105,312]. Furthermore, although HD is primarily a neurological disease, HD

patients develop type 2 diabetes mellitus at a higher incidence than healthy controls and diabetic phenotypes can be rescued via IGF-1 treatment in HD models [105,139,140,142]. These data warrant further investigation into 1) the factors which contribute to dysregulated IGF-AKT signaling in HD and 2) the mechanism through which IGF-1 effectively treats some HD phenotypes.

Here, we assessed whether the synergistic effects of Mn+IGF occur via the ability of Mn to directly act on IR/IGFR to elicit downstream AKT phosphorylation and determined if this mechanism is disrupted in a disease model system (HD) associated with a Mn *deficiency*. Prior studies in our lab have reported reduced Mn uptake in in vitro HD cell models and the striatum of the YAC128 HD mouse model—indicative of a defect in Mn accumulation [262,313,314]. We have shown that Mn treatment rescues deficient arginase activity in HD mice [315] and that in HD cell lines, this reduced Mn uptake manifests as reduced Mn-induced activation of ATM-p53 and AKT cell signaling [81,82]. In contrast, changes in cholesterol metabolism appear unaffected by Mn [316]. Recently, we have established that Mn induced p-AKT is dependent on PI3K, a downstream mediator of IR/IGFR, in STHdh cells [300]. As AKT signaling mediates the restorative effects of IGF-1 administration in HD mouse models, we hypothesize here that Mn promotes AKT signaling through an upstream IGFR-1-dependent mechanism, and that reduced Mn uptake should manifest as impaired Mn→ IR/IGFR→ PI3K→ AKT signaling and contribute to well-established IGF-related deficits in HD. This study aimed to 1) define the synergistic co-regulation between Mn and IGF on AKT signaling in various cellular models, 2) determine the initial, mechanistic target of Mn, which allows for downstream AKT activation, 3) elucidate the effects of Mn+IGF co-treatment on impaired IGFR/IR-AKT signaling in HD cells, and 4) investigate the effects of Mn on glucose uptake, a downstream process of AKT signaling which is perturbed in HD patients and mouse models. These findings provide proof-of-principle evidence that Mn supplementation could improve efficacy of IGF-centric therapies in HD.

Results

Mn and IGF exhibit synergistic regulation of p-AKT expression which is diminished in HD cells

Previous studies suggest that Mn acts as an insulin mimetic, and also increases the kinase activity at the insulin receptor itself; however, these findings were primarily established using recombinant enzymes or permeabilized cellular models [309,310]. Furthermore, Mn has been shown to activate insulin/IGF-responsive kinases and signaling pathways, including AKT. Given these observations, we hypothesized that Mn potentiates IGF-induced p-AKT expression in neuronal cells. We examined p-AKT (Ser^{473}) expression after 1hr serum deprivation in HBSS, followed by 3hr treatment with Mn/IGF in HBSS. For these experiments, we treated STHdh cells with 1nM IGF, which

has been reported to be near physiological concentration [317]. Normal human brain Mn concentrations are estimated to be ~20-55µM [318]. Mn begins to induce in vitro cytotoxicity after 24hr, 100-200µM Mn exposures, depending on cell type [81,82]. Across short exposures (3hrs), we did not observe any decrease in cell viability following 500µM Mn in any cell type (**data not shown**). Thus, for our experiments, we utilize sub-cytotoxic 50-500µM Mn exposures based on cell type and exposure duration. Mn/IGF co-exposure induced a nearly 30-fold increase in p-AKT, ~15 times higher than 500µM Mn alone, and ~3 times higher than IGF alone (**Fig 3-1A**). This confirms a synergistic regulation of AKT signaling by Mn and IGF in living cells. Furthermore, treatment with Mn alone resulted in an insignificant increase in p-AKT, suggesting that Mn-induced p-AKT is dependent on the presence of an upstream ligand, such as IGF or insulin. To examine this further, we treated WT Q7/Q7 STHdh cells with 50 or 500µM Mn in normal serum-containing media or in serum-free HBSS following 1hr serum deprivation. Consistent with previous results, 3hr treatment with Mn (50 or 500µM) did not cause a significant increase in p-AKT in serum-free HBSS (though 500µM trended towards increase p-AKT in HBSS), but did significantly increase p-AKT in serum-containing media at both concentrations. *This suggested that a potential interaction with a serum component, such as insulin or IGF, is essential for Mn-induced p-AKT* (**Fig 3-1B**).

The STHdh Q111/Q111 HD cell model exhibits both a basal Mn uptake deficit as well as a reduced net Mn accumulation after an exogenous exposure, making it an ideal model to study Mn-induced IGF signaling and the consequences of perturbations to this system [81,82]. Thus, we hypothesized that this cell model would also exhibit reduced Mn/IGF-induced p-AKT expression. This would be consistent with other studies demonstrating defects in AKT signaling in HD [92,93,95,96,319]. Indeed, the Q111 HD cell model exhibited reduced Mn/IGF-induced p-AKT expression following a 3hr Mn exposure in serum-free media (**Fig 3-1C**). However, treatment with IGF+500µM Mn in the Q111 HD cells restored p-AKT expression to levels seen with IGF+200µM Mn in the Q7 WT model. Total AKT levels were unchanged by Mn after 3hrs in media or HBSS (**Fig 3-2A**). *This confirms reduced Mn-induced p-AKT in this HD cell model, and demonstrates that the Mn-uptake defect can be attenuated via higher doses of Mn treatment, compensating for the uptake deficit.*

We reasoned that if Mn acts as an insulin/IGF "mimetic" by increasing ligand concentration or ligand-receptor occupancy, Mn should be unable to further activate p-AKT in the presence of saturating concentrations of insulin/IGF. We determined that the saturating concentration of IGF-1 in
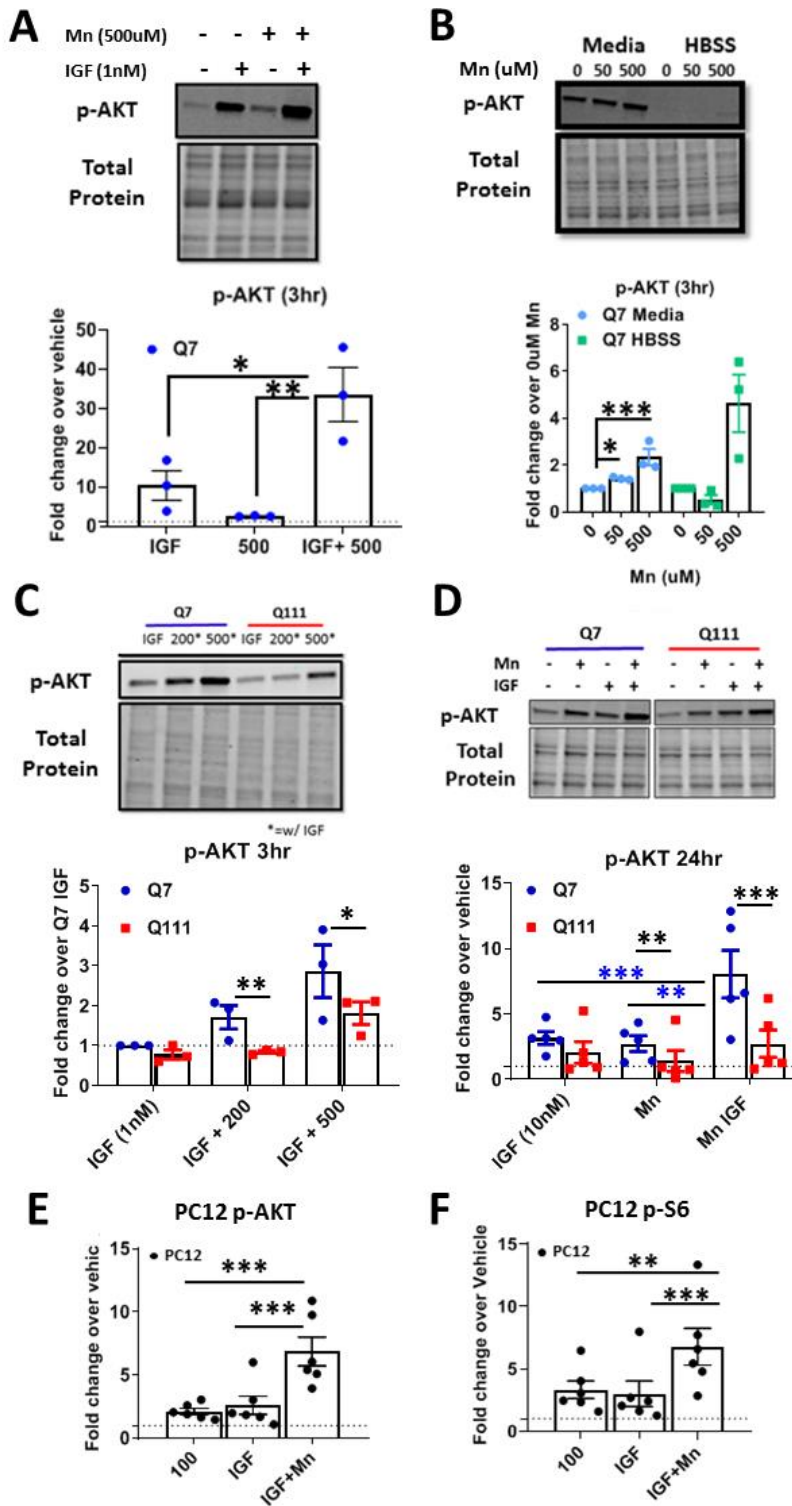
Figure 3-1: Mn can potentiate IGF-1 induced p-AKT and Mn-induced p-AKT is reduced in HD cells. A) p-AKT expression in STHdh Q7/Q7 following a 1hr serum deprivation, then 3hr exposure in HBSS with 1nM IGF-1 and/or 500µM Mn. Vehicle=dotted line. One-way ANOVA; treatment= $F_{(2,6)}$= 20.12; p=0.0022. **B)** Quantification of p-AKT after 3hr, 50/500µM Mn exposure in serum free HBSS (following 1hr serum deprivation) or media containing 10% FBS. Two-way ANOVA; treatment= $F_{(2,6)}$=40.84; p=0.0003; media/HBSS= $F_{(1,3)}$= 671.6; p=0.0001; treatment-media interaction= $F_{(2,6)}$= 24,37; p=0.0013. **C)** p-AKT expression in STHdh WT and HD cells following 1hr serum deprivation then 3hr Mn (0/200/500µM) + IGF (1nM) exposure in HBSS. Two-way ANOVA; treatment= $F_{(2, 4)}$= 10.29; p=0.0265. **D)** p-AKT expression after 24hrs treatment with 10nM IGF-1, 50µM Mn, or both in STHdh Q7/Q7 and Q111/Q111. Two-way ANOVA; treatment= $F_{(2,10)}$=40.84; p=0.0064; genotype= $F_{(1,5)}$= 671.6; p=0.0163; treatment-genotype interaction= $F_{(2,10)}$= 1.587; p=0.2515. **E,F)** p-AKT (Ser) and p-S6 (235/236) in uninduced PC12 cells following treatment with 100µM Mn, 10nM IGF-1, or both. For these PC12 experiments, all uninduced (i.e. were only expressing WT rat HTT) samples from the 23Q, 74Q, and 140Q (3 biological replicates each) were used. Representative blot in figure 3-2C. One-way ANOVA; p-AKT treatment= $F_{(2,10)}$=36.71; p=<0.0001; One-way ANOVA; p-S6 treatment= $F_{(2,10)}$=20.57; p=<0.0003; Error bars= SEM. Dotted line= vehicle (=1). N=3 for Panel A-C; N=4 for panel D; N=5 for panel E; N=6 for panels F and G. *= significant by Tukey's (A, F, G), Dunnet (B), and Sidak multiple comparison (D-E). *P<.05, **P<.01, ***P<.001. ***Work done with the assistance of Kristen Nordham.***

40
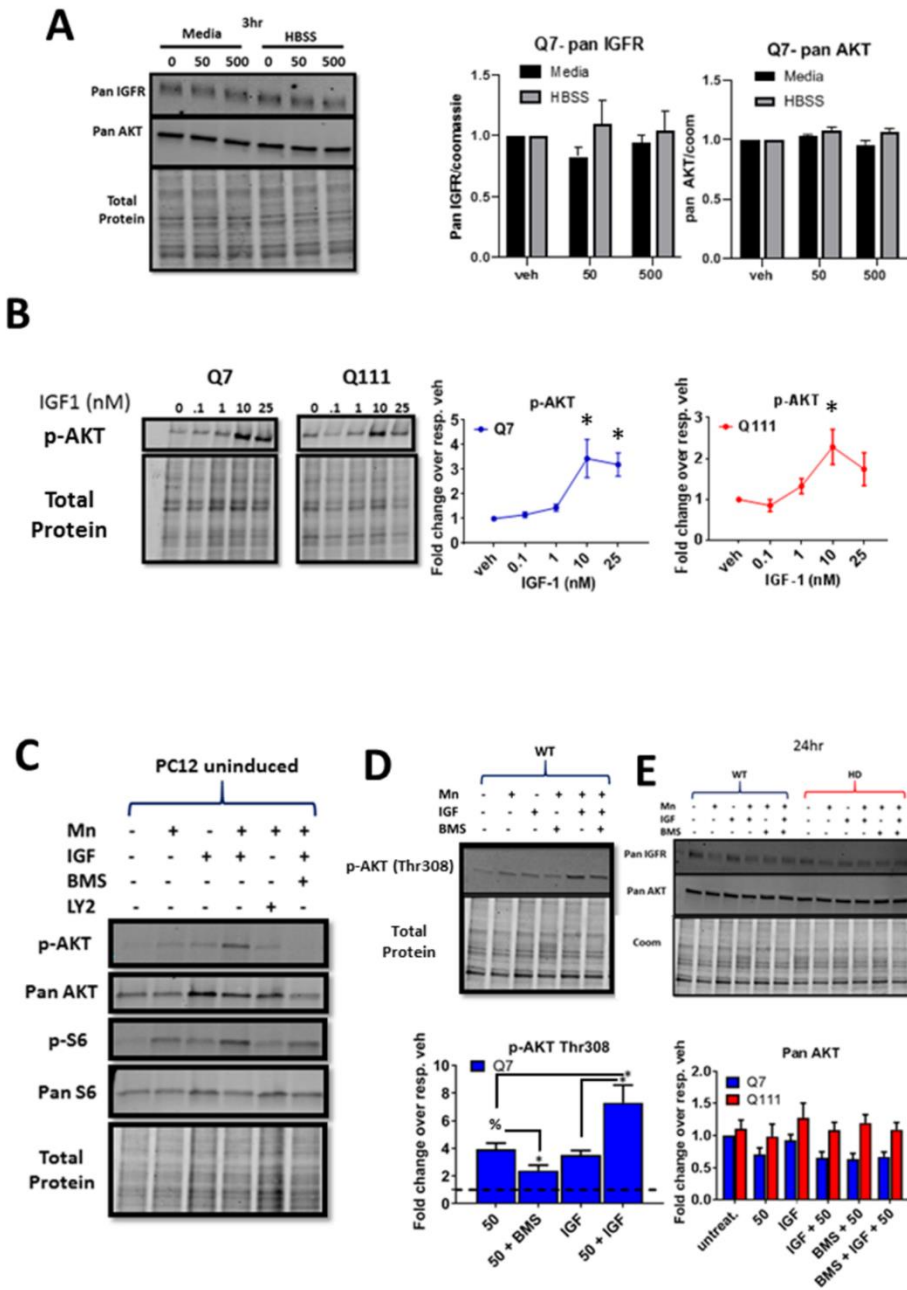
Figure 3-2: IGF-1 saturation curves and expression of pan AKT, S6, IGFR in STHdh and PC12 cells. A) Representative blot and quantification of p-AKT following 24hr exposure with .1-25nM IGF-1 in STHDh Q7/Q7 and Q111/Q111. B) Representative western blot of p-AKT, pan AKT, p-S6, and pan S6 in non-HTT induced PC12 cells following 24hr exposures with Mn (100uM), IGF (10nM), BMS-536924 (1uM), LY294002 (7uM). C) Representative western blot and quantification of p-AKT (Thr308) following 24hr exposure with Mn (50uM), IGF (10nM), and BMS-536924 (1uM) in STHdh Q7/Q7. D) Representative western blot of pan IGFR and pan AKT and quantification of pan AKT in STHdh cells following 24hr exposure with Mn (50uM), IGF (10nM), and BMS-536924 (1uM). E) Representative western blot and quantification of pan IGFR and pan AKT in STHdh Q7/Q7 cells after 3hr, 50,500uM Mn exposure in Media or HBSS.

serum-containing media for p-AKT after 24hrs is approximately 10nM (**Fig 3-2B**). Co-treatment with 10 nM IGF-1 and 50 μM Mn for 24hrs in normal (serum-containing) media resulted in supra-additive p-AKT responses (>2fold compared to IGF or Mn alone) in STHdh and p-AKT and p-S6 in uninduced, differentiated PC12 cells mirroring the effects seen in the 3hr exposures above (**Fig 3-1D-F, Fig 3-2C**). P-p53, another Mn-responsive pathway in these cells, was indistinguishable between Mn and Mn+IGF exposed conditions, demonstrating that this is not a broad effect across all Mn-responsive pathways (**data not shown**). As expected, Mn-induced p-AKT was blunted in HD cells following 24hr exposure. Furthermore, Mn/IGF co-treatment significantly increased p-AKT activation compared to the effects of Mn or IGF alone in the Q111 HD cells (**Fig 3-1D**), similar to **Fig 3-1C**. Total AKT levels (Pan-AKT) were not significantly different in any of the conditions and p-AKT (Thr^{308}) showed a highly similar trend to Ser^{473}; thus, going forward, we only quantified p-AKT (Ser^{473}) (**Fig 3-2D**). *Together, these data suggest that Mn synergistically increases the maximal activity of the AKT pathway, even under saturating concentrations of ligand, but expression of mutHTT dampens this effect.*

Phosphorylation of AKT is specific to Mn and not shared by other cation exposures

We hypothesized that Mn-induced p-AKT is a consequence of a Mn-responsive kinase upstream of AKT rather than a broad effect of heavy metal exposure, such as reactive oxygen species (ROS) accumulation. In other words, if Mn is acting as a cofactor for an upstream kinase, then its activity on downstream proteins should be unique to Mn vs other metal cations not capable of serving as kinase cofactors. Thus, we determined 1) whether other metal cations are capable of increasing p-AKT similarly to Mn and 2) if HD genotype cells exhibit reduced p-AKT in response to other metal cations. We tested a battery of cations (Fe, Cu, Mg, Zn, Cd, Ni, and Co) and examined p-AKT expression after 24hrs. For these experiments, we used concentrations which are near the toxic threshold in these cells after 24hr exposures as shown in our previous work [81] and found that Mn was the only cation which elicited a significant p-AKT response, and thus, the only metal which exhibited an HD phenotype. Cu trended towards an increase in p-AKT but this was not significant (**Fig 3-3A-C**). As Mn and Mg often act as cofactors with the same enzymes, we supplemented the media for these cells with an additional 50μM Mg or Mn (though DMEM contains high physiological concentrations of Mg) increasing the available combined pool of Mg/Mn, and did not observe Mg-induced p-AKT (**Fig 3-3C**). *This supports the hypothesis where the role of Mn to increase p-AKT expression is metal ion-specific, and furthermore, that Mn is able to do this under saturating concentrations of Mg (a known, competing cofactor for many kinases).*
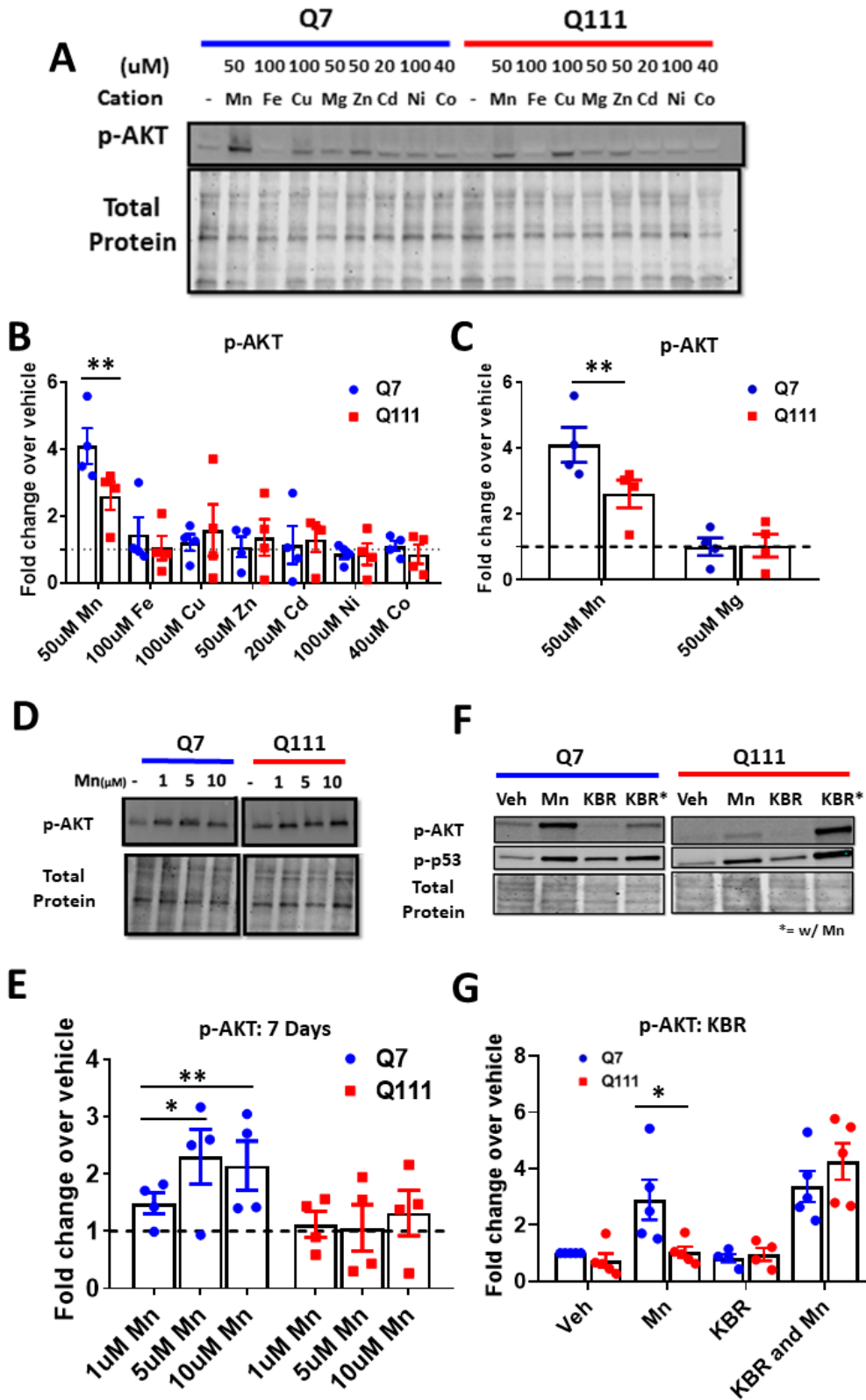
Figure 3-3: **Assessing the specificity and dynamics of the Mn-AKT interaction. A**) Representative blot for p-AKT expression in STHdh Q7/Q7 and Q111/Q111 cells following 24hr exposures with Mn, Fe, Cu, Mg, Zn, Cd, Ni, or Co. **B**) Quantification of p-AKT expression, blot shown in panel A. **C**) Quantification of only Mn and Mg-induced p-AKT after 24hrs, blot shown in panel A. Two-way ANOVA; treatment= $F_{(8, 24)}$=2.509; p=<0.0388. N=4; Error bars= SEM; Normalized to respective vehicle. **D**) Representative blot for p-AKT expression in STHdh Q7/Q7 and Q111/Q111 cells following 7-day exposure with Mn (1/5/10µM). **E**) Quantification of p-AKT expression, blot shown in panel D. Normalized to respective vehicle. N=4. Error=SEM. Two-way ANOVA; treatment= $F_{(3,9)}$=.5284; p=0.6738; genotype= $F_{(1,3)}$= 33.39; p=0.0103; treatment-genotype interaction= $F_{(3,9)}$= 4.912; p=0.0273. **F**) Representative blot for p-AKT and p-p53 expression following 24hr exposure with 50µM Mn, 10µM KB-R7943, or both. **G**) Quantification of p-AKT expression, blot shown in panel H (p-p53 quantification not shown). Two-way ANOVA; treatment= $F_{(3,12)}$=24.91; p=<0.0001; genotype= $F_{(1,4)}$= 2.840 p=0.1672; treatment-genotype interaction= $F_{(3,12)}$= 4.761; p=0.0207. N=4; Error bars= SEM. *= significant by Dunnet (B, C, E), and Sidak multiple comparison tests (G,H). *P<.05, **P<.01, ***P<.001. ***Work done with the assistance of Kristen Nordham.***

43

Reduced Mn-induced p-AKT in HD cells persists under prolonged physiologically-relevant Mn exposures

While we observed reduced Mn-induced p-AKT in HD cells after high dose, acute Mn exposure, we wanted to assess whether this phenotype would persist under lower dose, subacute, week-long exposures. Thus, we treated STHdh cells for 1 week with 1, 5, or 10 µM Mn. In Q7/Q7 cells, Mn-induced p-AKT was observed after a 7-day exposure, with 5 and 10 µM eliciting the highest effect (**Fig 3-4D, E**). *Phosphorylation of AKT was almost completely unresponsive in Q111/Q111 HD cells to low-dose Mn exposure, confirming that the HD genotype perturbation persisted under these subacute treatments. Additionally, this suggests Mn-induced p-AKT occurs with changes in Mn homeostasis well below the toxic threshold.*

Normalization of net Mn uptake ameliorates Mn-induced p-AKT defect in HD cells

The Q111/Q111 HD STHdh cells exhibit reduced Mn-induced p-AKT across several treatment paradigms (**Fig 3-1C,D, 3-3D,E**). If reduced Mn-induced p-AKT in HD cells is dependent on intracellular Mn levels, normalization of intracellular Mn uptake in the HD cells to match WT levels would be predicted to ameliorate Mn-induced p-AKT differences between the genotypes. KB-R7943 is a drug which inhibits the sodium-calcium uniporter (NCX1/3) and normalizes Mn uptake in these HD cells by an unknown mechanism. This drug was previously used to normalize Mn uptake and Mn-induced p-p53, concurrently. When HD cells were exposed to KB-R7943 and 50 µM Mn, Mn-induced p-AKT was restored to levels observed in WT cells treated with Mn alone (**Fig 3-3F, G**). *This suggests reduced Mn-induced cell signaling levels are driven by the decreased intracellular Mn in this model. Although the mechanism by which KB-R7943 restores Mn uptake is unknown, these data also demonstrate that the drug can increase the bioavailable pool of Mn, as opposed to merely sequestering Mn in metabolically inaccessible regions of the cell.*

Expression of mutHTT is sufficient to reduce Mn-induced p-AKT in differentiated PC12 cells

Next, we sought to confirm if other HD model cells lines exhibit reduced Mn-induced p-AKT. First, we utilized differentiated PC12 cells which express WT HTT but are capable of additional ponasterone A-induced HTT expression (23, 74, 145 CAG or CAA). These cells were differentiated into a neuronal phenotype by treatment with nerve growth factor (NGF) over the course of a week and expressed tyrosine hydroxylase, indicating a catecholaminergic population (**data not shown**). After 7 days of differentiation with NGF and mutHTT induction with ponasterone A, 145 CAG-expressing PC12 cells exhibited reduced Mn-induced p-AKT compared to uninduced counterparts
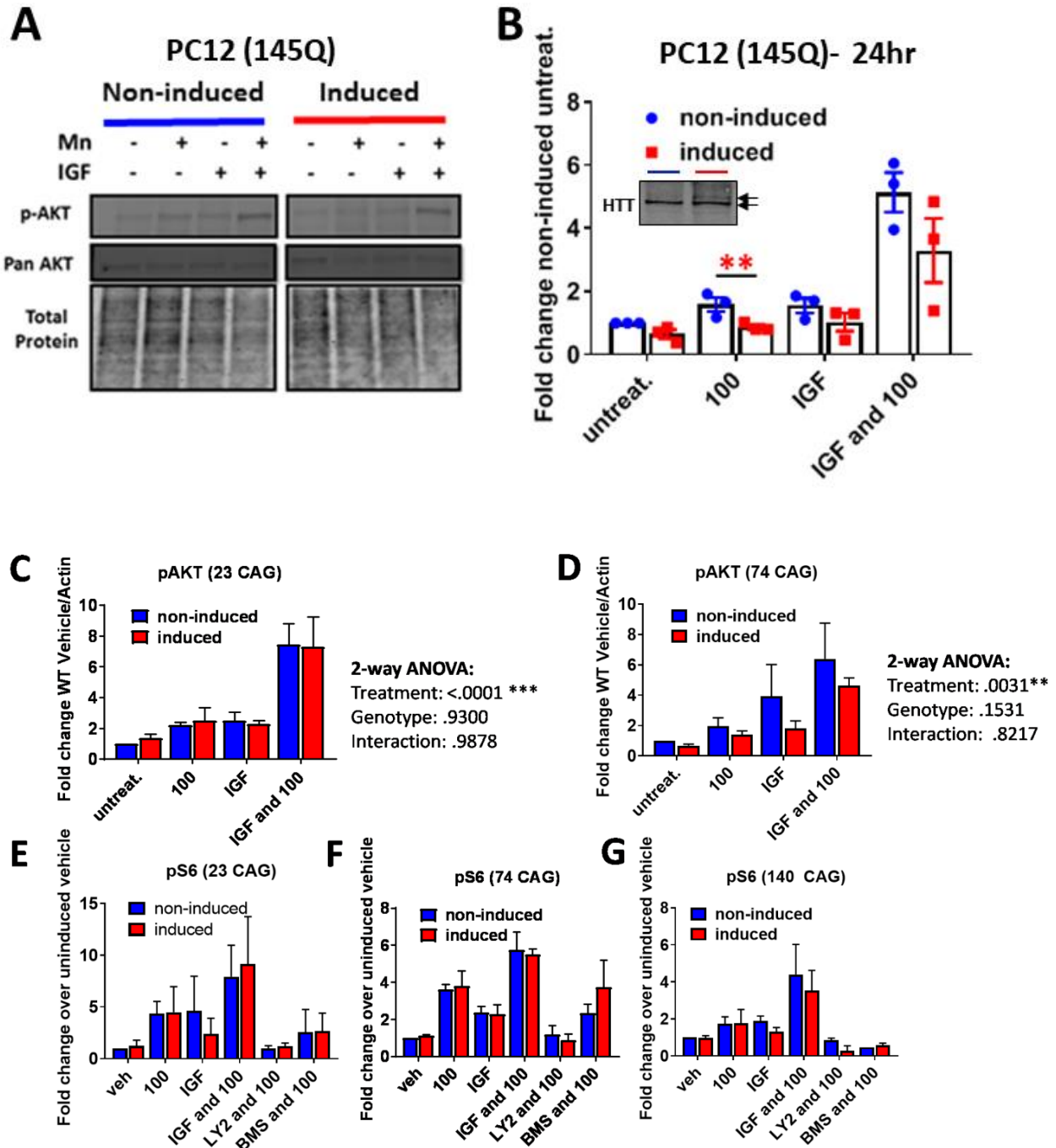
Figure 3-4: **Assessing the effects of WT and mutant HTT in Mn-induced p-AKT. A)** Representative western blot of PC12 cells in differentiated and 145Q HTT-induced PC12 cells following 24hr exposure with 100µM Mn and/or IGF (10nM) **B**) Quantification of p-AKT expression. 145Q induced HTT cells (red) are compared to uninduced counterparts (blue). Image of WT HTT (bottom arrow) and 145Q HTT (top arrow) expression using mAb 2166 inset within graph. **C, D)** p-AKT expression in 23CAG and 74CAG expressing PC12 cells (paired with 140CAG cells in A, B). Two-way ANOVA stats listed next to each. **E-G)** p-S6 expression in 23, 74, and 140Q expressing PC12- cells. blue= non-induced, red= induced. N=3; Error bars= SEM, *= significance genotype difference by student's t-test. *P<.05, **P<.01, ***P<.001.

(**Fig 3-4A,B**). Induction of 74CAG mutHTT resulted in a modest, but insignificant, reduction in Mn-induced p-AKT, and, as expected, induction of 23 CAG HTT had no effect, suggesting this is a CAG-repeat dependent defect (**Fig 3-4C, D**). Pan AKT and pan S6 were unaffected in all conditions, similar to STHdh cells (**Fig 3-4A, Fig 3-1C**). Mn induced p-S6 was unaffected by mutHTT expression (**Fig 3-4E-F**). *Together, these data demonstrate impairments in Mn homeostasis and signaling are present in a variety of HD cell lines and occur within days of mutHTT expression.*

Mn potentiates IGF-induced p-IR/IGFR expression which is blunted in HD cells

We established a specific, synergistic effect on p-AKT signaling by Mn/IGF co-treatment which was diminished in several HD cell lines. We sought to elucidate the mechanistic target of Mn which allows for the synergistic effect on p-AKT. This target is likely responsible for driving the reduced Mn-induced p-AKT in HD models. As Mn is a known cofactor for a variety of kinases, we hypothesized that Mn may be directly interacting with IR/IGFR. To our knowledge, phospho-specific antibodies do not exist which distinguish between p-IR or p-IGFR, as they are phosphorylated at highly similar residues [320,321]. Thus, to examine this, we co-treated Q7 WT and Q111 HD STHdh cells with Mn/IGF for 3hrs following a 1hr serum deprivation and assessed p-IR/IGFR levels. We found that Mn potentiated IGF-induced IR/IGFR phosphorylation. Further, Mn-induced p-IR/IGFR levels were blunted in HD cells but co-treatment with IGF+500µM in HD cells elicited similar p-IR/IGFR expression as IGF+200µM Mn in WT cells (**Fig 3-5A,B**). These observations mirror the effects of Mn on p-AKT expression in **Fig 3-1C**. *Altogether, these data support a role for Mn directly increasing IR/IGFR activity, thereby activating downstream signaling including AKT.*

Mn reduces total IGFR protein expression and IGFR mRNA expression

Our data suggest that Mn can increase maximal IGF-induced p-AKT activity. Thus, we wanted to assess whether this leads to negative feedback on total IGFR expression. We hypothesized that Mn (in conjunction with IGF) exposure *reduces* total IGFR expression after 24hrs to reduce overall activity of the AKT pathway. Indeed, 50µM Mn treatment, similarly to IGF treatment, decreased total IGFR expression by ~50%—perhaps acting through a negative feedback mechanism to prevent overactivation of the pathway (**Fig 3-5C,D**). Unlike IGFR, Mn did not reduce total IR expression in WT or HD cells, but IGF treatment alone decreased total IR expression specifically in HD cells (**Fig 3-5E,F**). Mn exposure for only 3hrs in media or HBSS left total IGFR unchanged (**Fig 3-2A**).

To determine whether the Mn-induced reduction in total IR/IGFR expression is mediated, at least in part, by a transcriptional mechanism, we assessed the effects of Mn on IR/IGFR mRNA
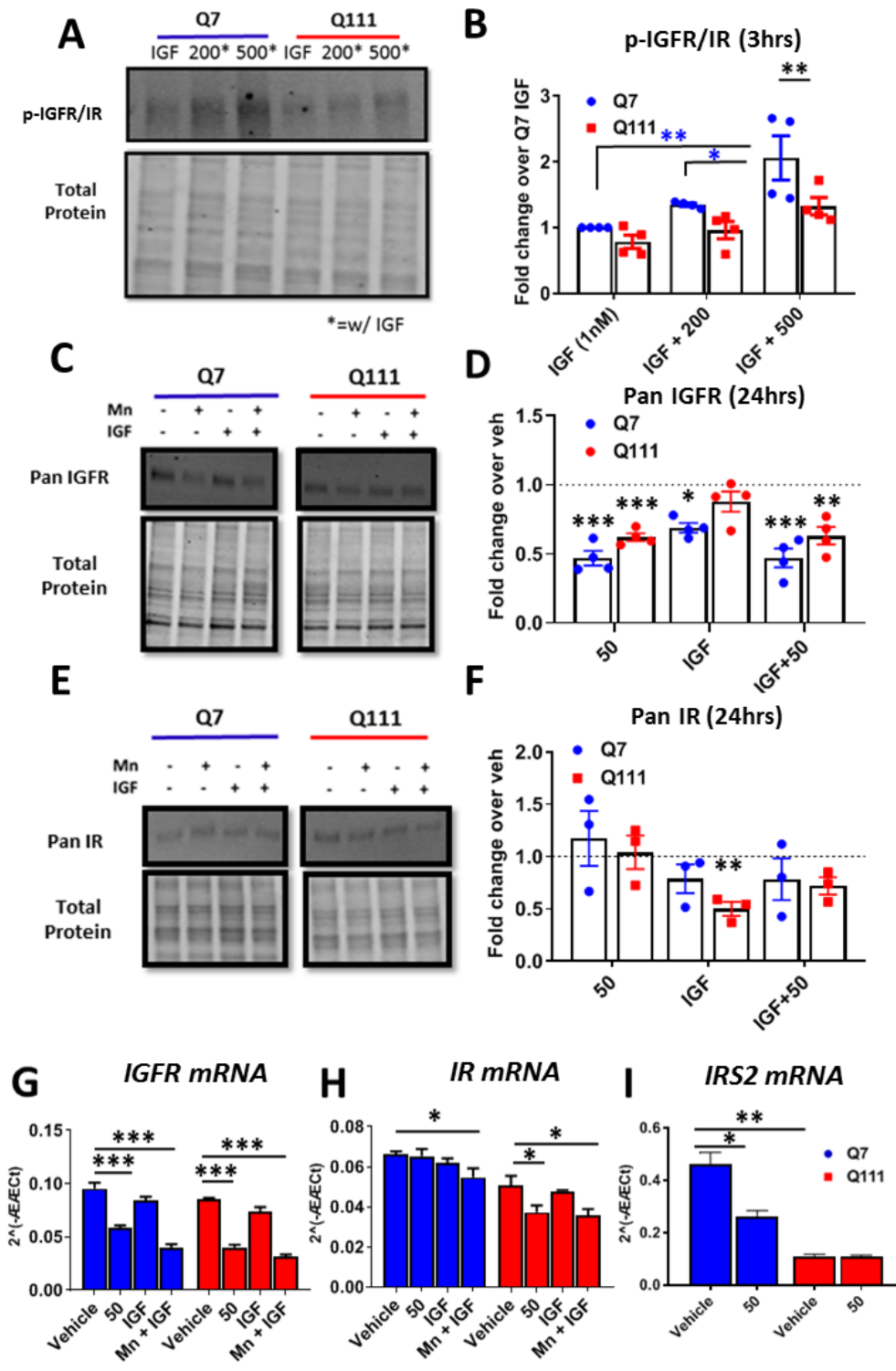
Figure 3-5: **Mn increases phosphorylation of IR/IGFR and decreases total protein and mRNA expression. A,B**) Representative western blot and quantification of p-IGFR expression in STHdh cells following 1hr serum deprivation and 3hr Mn (200/500µM) + IGF(1nM) exposures. Note representative blot is the same samples/run as Figure 1C. Two-way ANOVA; treatment= $F_{(2,6)}=5.461$; p=<0.0446; genotype= $F_{(1,3)}= 30.98$; p=0.0114; treatment-genotype interaction= $F_{(2,6)}= 3.275$; p=0.1093. N=4. **C,D**) Representative western blot and quantification of pan IGFR protein expression in STHdh cells following 24hr exposure with Mn (50µM) and/or IGF (10nM). Dotted line= respective vehicle (=1). Two-way ANOVA for IGFR; treatment= $F_{(3,9)}=16.71$; p=<0.0005. N=4. **E,F**) Representative western blot and quantification of pan IR protein expression in STHdh cells following 24hr exposure with Mn (50µM) and/or IGF (10nM). Dotted line= Vehicle (=1). Two-way ANOVA for IR; treatment= $F_{(3,6)}=20.59$; p=0.0015. N=3. **G-I**) mRNA expression of IGFR (**G**), IR (**H**), and IRS2 (**I**) after 24hr Mn (50µM) and/or IGF (10nM) exposure. Two-way ANOVA treatment for IGFR: $F_{(3,6)}=85.01$; p=<0.0001. For IR: $F_{(3,6)}=7.204$; p=<0.0205. For IRS2: $F_{(1,3)}=213.8$; p=<0.0007. Error bars= SEM; N=4 for panels A-D, G-I; N=3 for E,F. P<.05, **P<.01, ***P<.001. *= significant by Tukey's (B) or Dunnet's (D, F, G, H, I) multiple comparison tests. ***Work done with the assistance of Audra Foshage.***

47

expression. We found that 24hr Mn (or Mn+IGF) treatment reduced IGFR mRNA expression and Mn+IGF co-treatment modestly reduced expression of IR mRNA expression in both genotypes, suggesting that Mn may have a more specific effect on IGFR signaling than that of IR (**Fig 3-5G,H**). Mn specifically reduced IR mRNA expression in HD cells only. The HD genotype did not affect basal IGFR or IR mRNA expression. Additionally, we assessed mRNA expression of IRS2, a downstream partner in insulin/IGF signaling. IRS2 mRNA was greatly reduced in HD cells and Mn exposure reduced IRS2 mRNA in Q7 cells only (**Fig 3-5I**). *Together these data demonstrate that Mn also modulates total IR/IGFR protein expression via transcriptional downregulation.*

Mn-induced p-AKT is completely abrogated by pharmacological IR/IGFR inhibition

After observing that Mn and IGF exert synergistic effects on p-AKT and p-IR/IGFR, we hypothesized that IGF and Mn may be cooperatively activating on the same upstream kinase to increase AKT phosphorylation. Previously, we found that Mn-induced p-AKT is dependent on PI3K in these cells, as LY294002, a PI3K inhibitor, can completely abrogate Mn-induced p-AKT [300]. This narrows down the possible targets to upstream activators of PI3K including IR/IGFR. Given these data and the prior evidence of a role for IR/IGFR signaling, we hypothesized some or all of Mn-induced p-AKT is IR/IGFR-dependent. IR/IGFR are essential to neuronal differentiation, development, and homeostasis which complicates the generation and use of knockout cell lines, and less-than-complete efficiency of siRNAs would allow for remaining receptors to compensate [105,302]. Thus, we turned to pharmacological modulation of IR/IGFR. While small molecules allow dosing to achieve near-complete inhibition, they are prone to off-target effects. Thus, to increase the rigor of our findings we employed a battery of four ATP-competitive IR/IGFR inhibitors (BMS-536924, BMS-754807, Linsitinib (OSI-906), and NVP-AEW541) so that multiple inhibitors could be used across each cell line. Additionally, these inhibitors have different known off-target proteins (**Fig 3-6A**), so any shared effects by the inhibitors are likely via IR/IGFR only [322-325].

Using these various inhibitors across STHdh and PC12 cells, we found 1) Mn-induced p-AKT was inhibited in STHdh cells with 100nM BMS-536924 (**Fig 3-6B, C**), 0.1-1µM Linsitinib (**Fig 3-6D,E**), or 0.1-1µM NVP-AEW541 (**Fig 3-6D,F**) and 2) Mn-induced p-AKT and p-S6 was blocked with 100nM BMS-536924 in PC12 cells (**Fig 3-6G-H,Fig 3-2C**). In PC12 cells, >100% of Mn-induced p-AKT (below vehicle levels) and 59% of Mn-induced p-S6 was inhibited using 100nM BMS-536924 (near the estimated IC50 concentration) (**Fig 3-6G-H, Fig 3-7B)**. BMS-536924 inhibited 46% of Mn-

A

Inhibitor Reference	IC50 nM	Known Off-targets	Concentrations Used
BMS-536924 [86]	100 (IGFR), 73 (IR)	FAK, MEK, LCK	100nM, 1uM
BMS-754807 [87]	1.8 (IGFR), 1.7 (IR)	Trk, Met, Ron, Aurora	2nM, 10nM
NVP-AEW541 [89]	150 (IGFR), 140 (IR)	FLT1/3, TEK	100nM, 1uM
Linsitinib (OSI-906) [88]	35 (IGFR), 75 (IR)	IRR	100nM, 1uM
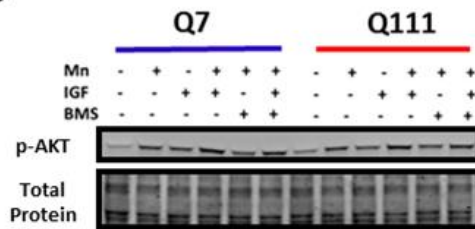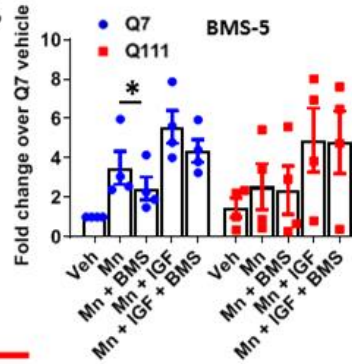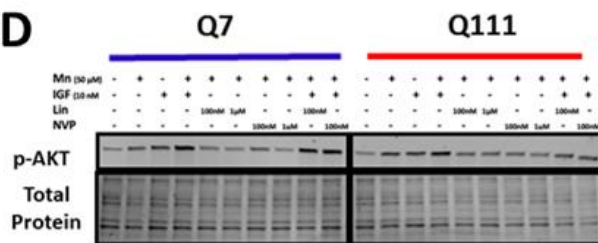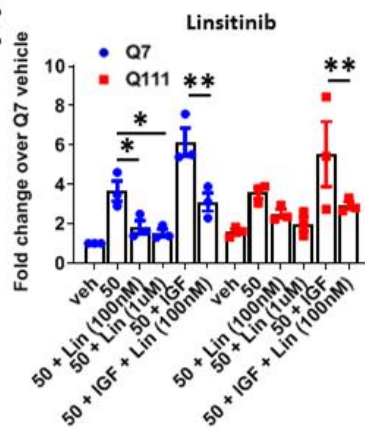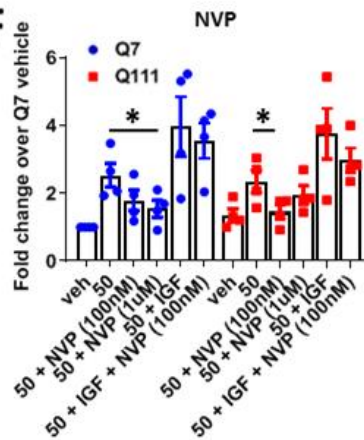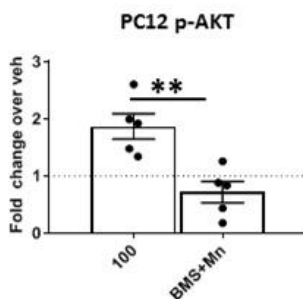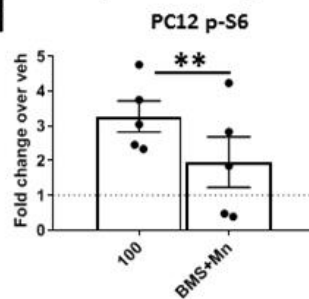
Figure 3-6: IR/IGFR inhibitors block Mn-induced p-AKT. A) List of IR/IGFR inhibitor names, IC50s for IR/IGFR, off-targets, and concentrations used here. **B**) Representative western blot of pAKT expression STHdh Q7/Q7 and Q111/Q111 after 24hr treatment with Mn (50µM), IGF (10nM), and/or BMS-536924 (100nM).**C**) Quantification of Mn/IGF induced p-AKT expression with BMS536924 (100nM). Two-way ANOVA for BMS5 treatment; $F_{(1.610, 4.831)}=20.03$; $p=.0039$. N=4. **D**) Representative western blot of p-AKT expression in STHdh Q7/Q7 and Q111/Q111 after 24hr treatment with Mn (50µM), Linsitinib (100nM/1µM), NVP-AEW541-AEW541 (100nM/1µM) and Mn+IGF(10nM). **E, F**) Quantification of Mn/IGF-induced p-AKT expression with Linsitinib (**E**) or NVP-AEW541 (**F**) Two-way ANOVA for Linsitinib treatment; $F_{(4,8)}=8.414$; $p=.0182$; Two-way ANOVA for NVP treatment; $F_{(4,8)}=10.68$; $p=.0027$. N=3-4. **G, H**) Quantification of p-AKT (**G**) and p-S6 (**H**) expression in uninduced PC12 cells treated with 100µM Mn or Mn (100µM) + BMS536924 (100nM) after 24hr exposures. Representative blot Supp Fig 1C. *= significance by student's t-test. For these PC12 experiments, uninduced samples from the 23Q, 74Q, and 140Q (total N=5) were used. Note representative blot Fig 3-2. Error bars= SEM. Dotted line= Vehicle (=1). *P<.05, **P<.01, ***P<.001. ***Work done with the assistance of Kristen Nordham.***

49

A STHdh Q7/Q7 (Fig. 3-6)

Inhibitor	Reported IC50 (nM)	Mn-induced pAKT inhibited (Mn)(%)	Mn-induced AKT inhibited (Mn+IGF)(%)
BMS-536924 (100nM)	100 (IGFR), 73 (IR)	45.5±12.9	24.1±20.3
Linsitinib (100nM)	35 (IGFR), 75 (IR)	71.1±10.9	60.0±9.2
Linsitinib (1uM)	35 (IGFR), 75 (IR)	80.7±6.6	N/A
NVP-AEW541 (100nM)	150 (IGFR), 140 (IR)	54.2±19.5	1.8±28.57
NVP-AEW541 (1uM)	150 (IGFR), 140 (IR)	65.4±32.7	N/A

B Non-striatal cells (3T3, HEK293- Fig. 3-8; PC12- Fig 3-6)

Linsitinib (1uM) IC50- 35, 75nM (IGFR, IR)	Mn-induced pIGFR/IR inhibited (%)	Mn-induced pAKT inhibited (%)	Mn-induced pS6 inhibited (%)	AKT:IGFR/IR Correlation Score*	S6:IGFR/IR Correlation Score*
3T3	98.3±2.51	97.2±0.56	60.6±32.48	98.8	61.7
HEK293	98.3±1.80	40.5±22.1	19.1±60.1	41.1	19.4
PC12	N/A	128.2±42.0	58.7±36.6	N/A	N/A

*Inhibition correlation score= (%pAKT or pS6 inhibition) / (%pIGFR/IR inhibition)

C hiPSC-derived neuroprogenitors (Control- Fig. 3-13)

Inhibitor	Reported IC50 (nM)	Mn-induced pIGFR/IR inhibited (%)	Mn-induced pAKT inhibited (%)	Mn-induced pS6 inhibited (%)	AKT:IGFR/IR Correlation Score*	S6:IGFR/IR Correlation Score*
BMS-536924 (100nM)	100 (IGFR), 73 (IR)	59.9±8.9	47.6±17.1	8.6±37.4	79.5	14.4
BMS-536924 (1uM)	100 (IGFR), 73 (IR)	96.8±1.3	71.5±18.0	64.5±33.5	73.9	66.6
BMS-754807 (2nM)	1.8 (IGFR), 1.7 (IR)	84.2±12.7	57.0±24.4	37.8±37.7	67.7	44.9

*Inhibition correlation score= (%pAKT or pS6 inhibition) / (%pIGFR/IR inhibition)

Figure 3-7: **Quantification of degree of Mn-induced p-AKT, p-IGFR, and p-S6 inhibition using IGFR/IR inhibitors** in WT STHdh (**A**), non-neuronal cells (**B**), and hiPSC-derived striatal-like neuroprogenitors (**C**)- quantified from data in Figures 3-6, 3—8, 3-13 respectively. The name, concentration, and IC50 of inhibitors used is listed followed by the inhibited % of Mn-induced p-AKT, p-IGFR, and p-S6 expression after inhibitor treatment (Mean±Stdev). For B,C an inhibition correlation score is also calculated (%pAKT or p-S6 inhibition)/(%pIGFR/IR inhibition).

induced p-AKT at this approximate IC50 in SThdh cells (**Fig 3-6B, C, Fig 3-7A**). 100nM linsitinib (approximately the IC50 for IR, 3X IC50 for IGFR) inhibited 71% of Mn-induced p-AKT (**Fig 3-6D, E, Fig 3-7A)**. 100nM NVP-AEW541 (approximately 65-70% the IC50 for IR and IGFR) inhibited 54% of Mn-induced p-AKT **(Fig 3-6D, F, Fig 3-7A)**. At 1µM (10-fold higher), Linsitinib and NVP-AEW541 inhibited 81% and 65% of Mn-induced p-AKT. Additionally, Linsitinib, the most specific of the inhibitors, was able to inhibit 60% of Mn+IGF induced p-AKT in STHdh cells at 100nM (**Fig 3-6D, E, Fig 3-7A**). We confirmed that these inhibitors blocked IGF-induced p-IR/IGFR in the STHdh cells (**data not shown**). *The high degree of dose-dependent inhibition by multiple IGFR inhibitors suggests that the vast majority of Mn-induced IGFR/AKT signaling is IR/IGFR-dependent.* IR/IGFR exhibit autophosphorylation upon binding to insulin/IGF (and necessary co-factors) and do not require the kinase activity of other upstream kinases for activation. *With this in mind, this data in addition to our observed Mn-induced p-IGFR/IR (***Fig 3-5A,B***) also suggest Mn is directly activating IR/IGFR (or affecting extracellular insulin/IGF production or binding) as opposed to another kinase upstream of these tyrosine kinases receptors.*

Non-neuronal cell types also exhibit IR/IGFR-dependent, Mn-induced p-IGFR/p-AKT

We hypothesized Mn-induced p-AKT was not specific to NPCs and would be present in other cell types. To investigate this, we exposed isolated primary rat astrocytes to 500µM Mn, 1nM IGF, or both for 3hrs following a 1hr serum deprivation. As in neuroprogenitors, addition of Mn+IGF increased p-AKT significantly more than either Mn or IGF alone **(Fig 3-8A, B)**. Additionally, we tested whether Mn-potentiated p-IGFR/p-AKT occurred in other non-neuronal, peripheral cell types— immortalized 3T3 fibroblasts and HEK293 kidney cells. Similar to what we observed in STHdh cells, a 3hr 500µM Mn exposure did not activate p-IGFR, p-AKT, or p-S6 in the absence of IGF-1 in these cells **(Fig 3-8C-E, Fig 3-9)**. This confirms that Mn-induced IGFR/AKT signaling requires the presence of ligand (IGF-1 or insulin) across a variety of cell types. In NIH3T3 and HEK293 fibroblasts, Mn+IGF increased p-AKT and p-IGFR expression more than IGF or Mn alone after 1hr serum deprivation **(Fig 3-8C, E, Fig 3-9)**. This corroborates the finding that the synergistic effects between Mn and IGF are not restricted to neuronal cells. Additionally, Linsitinib (1µM) completely inhibited p-IGFR/IR (>98%) in 3T3 cells and the vast majority of Mn+IGF-induced p-AKT (≥80%) could also be blocked by Linsitinib or LY294002 (PI3K inhibitor). In HEK293 cells, the vast majority of p-IGFR (≥98%) was inhibited with Linsitinib, but only 40% of Mn-induced p-AKT was blocked, suggesting Mn-induced p-AKT is less dependent on IGFR/IR in HEK293 cells than in 3T3 cells. **(Fig 3-8F,H, 3-7B)**. Furthermore, by comparing the degree of p-IGFR/IR inhibition to p-AKT inhibition by Linsitinib, we can estimate the
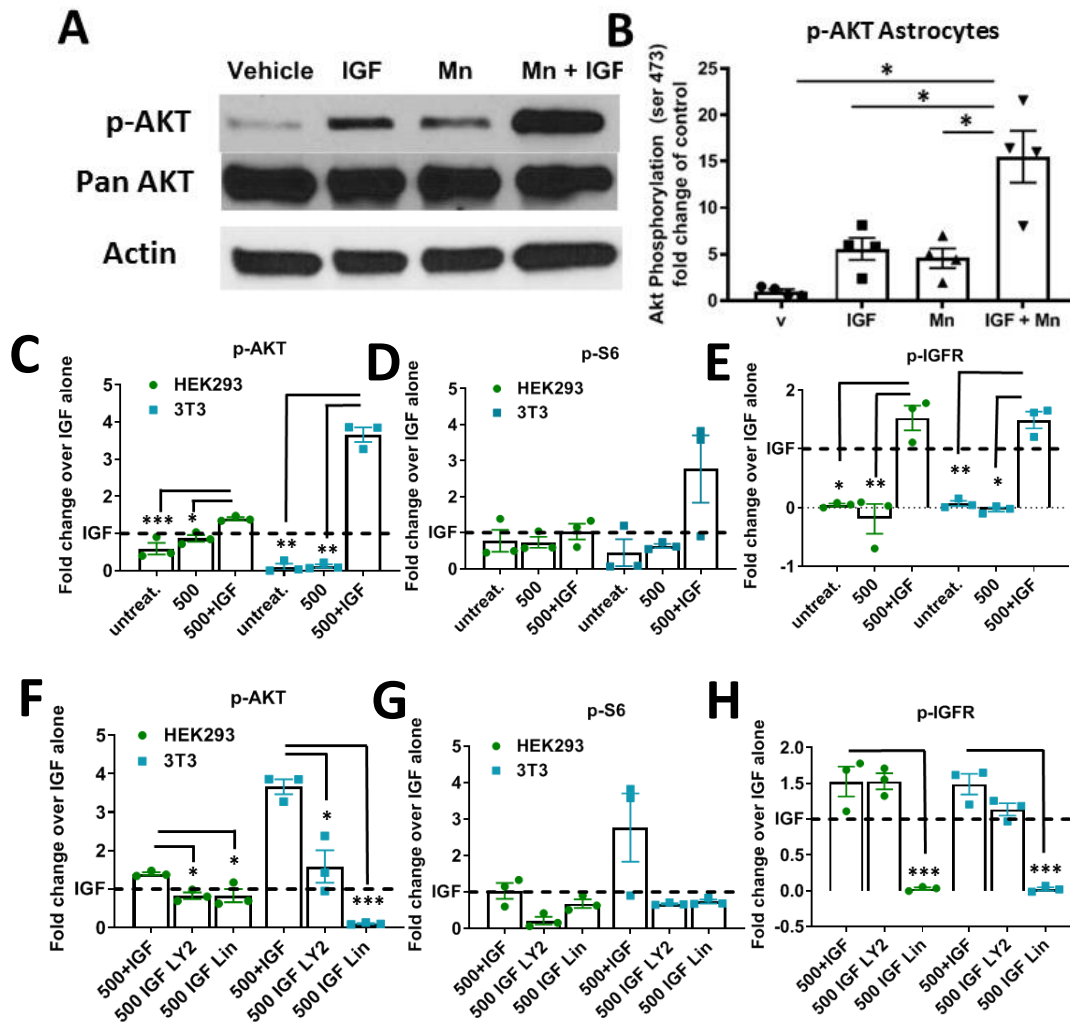
Figure 3-8: **Mn increases p-AKT and p-IGFR expression in the presence of IGF-1 in astrocytes and non-neuronal cell lines. A, B)** Representative western blot and quantification of p-AKT in astrocytes after 1hr serum deprivation followed by 3hr exposure with Mn (500µM), IGF (1nM), or both. One-way ANOVA; treatment= $F_{(1.167, 3.501)}$=24.37; p=<0.0104. N=4. Error= SEM. **C-E)** Quantifications of western blots of 3T3 and HEK293 p-AKT (**C**) p-S6 (**D**), p-IGFR (**E**) expression after 1hr serum deprivation followed by 3hr exposure in HBSS with Mn (100µM), IGF (1nM), or both. **F-H)** Quantifications of western blots of 3T3 and HEK293 p-AKT (**F**), p-S6 (**G**), p-IGFR (**H**) expression after 1hr serum deprivation followed by 3hr exposure in HBSS with Mn (100µM) + IGF (1nM) with LY294002 (7µM), and/or Linsitinib (1µM). Representative blot in Figure 3-9. N=3; Error bars= SEM; Dotted line= IGF alone (=1). One-way ANOVA for p-IGFR; HEK: $F_{(1.284, 2.568)}$= 38.12; p=.0129; 3T3: $F_{(1.221, 2.442)}$=99.63; p=.0048. One-way ANOVA for p-AKT; HEK: $F_{(4,8)}$= 9.391; p=.0041; 3T3: $F_{(4,8)}$=8.544; p=.0055. One-way ANOVA for p-S6; HEK: $F_{(1.274, 2.548)}$= 5.081; p=.1270; 3T3: $F_{(1.014, 2.028)}$=3.123; p=.2180 *= significance by Dunnet's multiple comparison test.*P<.05, **P<.01, ***P<.001. ***Work done with the assistance of Filipe Gonclaves.***

Figure 3-9: **Western blot for Mn-induced signaling 3T3 and HEK293 cells.** A) Representative western blot of p-IGFR, p-AKT, and p-S6 for 3T3 and HEK293 cells following 3hr exposure with Mn (100uM), IGF-1 (1nM), LY294002 (7uM), and linsitinib (1uM) in HBSS (after 3hr serum deprivation).
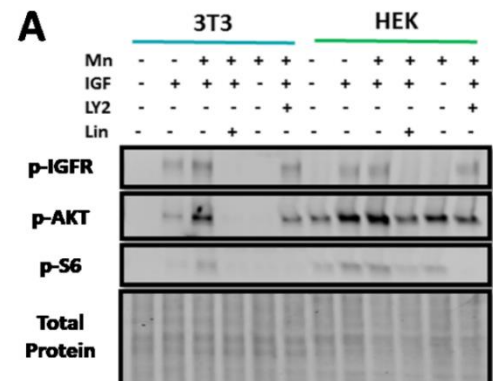
percentage of Mn-induced p-AKT which is dependent on p-IGFR/IR [(% of p-AKT inhibition) / (% of p-IGFR/IR inhibition)]. Using this calculation, we estimate that 99% of Mn-induced p-AKT in 3T3 cells and 41% in HEK293 cells is dependent on p-IGFR (**Fig 3-7B**). This confirms that Mn-induced p-AKT is IR/IGFR-dependent in these non-neuronal cell types as well, particularly 3T3 cells. P-S6 also trended with p-AKT across conditions in 3T3 cells, but due to the variability in Mn+IGF treatment, this trend was not significant (**Fig 3-8D,G**). Additionally, we found that there was only a 62% correlation between p-S6:p-IGFR/IR inhibition in 3T3 cells and 19% correlation in HEK293 cells, suggesting Mn-induced p-S6 is much less dependent on IGFR/IR than p-AKT (**Fig 3-7B**). *These data provide strong evidence that Mn-induced p-IGFR and p-AKT are not restricted to specific neuronal lineages.*

Mn-induced IGF signaling is dampened in human induced pluripotent stem cells (hiPSC)-derived striatal neuroprogenitors and is blocked by IGFR inhibition

We wanted test whether the HD-dependent IGF signaling defect observed in cell line models of HD would also be seen in a non-transformed human neuronal model. We chose to utilize the hiPSC-derived Islet-1-expressing striatal neuroprogenitor cells (NPCs) which are derived via a protocol designed in our lab [82]. After a 24hr exposure, Mn-induced p-AKT in Islet-1+ hiPSC-derived striatal-like NPCs from HD patients was not significantly different than control cells; also, p-IGFR and p-S6 (often used as a readout for mTOR activity) were both induced by Mn, but neither was differentially affected in HD cells (**data not shown**). However, in striatal NPCs, we observed that under these conditions, IGF-1 was unable to activate p-AKT, likely because their normal NPC media conditions contain saturating insulin (**Fig 3-10**). Thus, this standard striatal NPC media conditions are not a biologically-relevant setting to study IGF signaling or disease-relevant IGF/AKT-centric phenotypes. However, the data do suggest that Mn can upregulate maximal AKT phosphorylation even under insulin-saturating concentrations.

To circumvent this issue of saturating insulin in the media, we found that growth factor/insulin deprivation prior to exposure allowed detection of p-IGFR in these NPCs and decreased variability in downstream p-AKT/p-S6 signaling. Thus, we used a 3hr growth factor deprivation followed by 3hr exposure with Mn and/or IGF, and then assessed p-AKT, p-S6, and p-IGFR expression. Cells were treated under insulin/IGF-deprived conditions (though there are likely trace amounts of insulin/IGF left behind or produced by the cells themselves) and in the presence of 1 nM IGF. IGF, as expected, stimulated p-IGFR and p-AKT expression, though there were no apparent differences in magnitude between control and HD patient cells. Surprisingly, IGF did not significantly increase p-S6 expression in control or HD cells (**Fig 3-11C**).
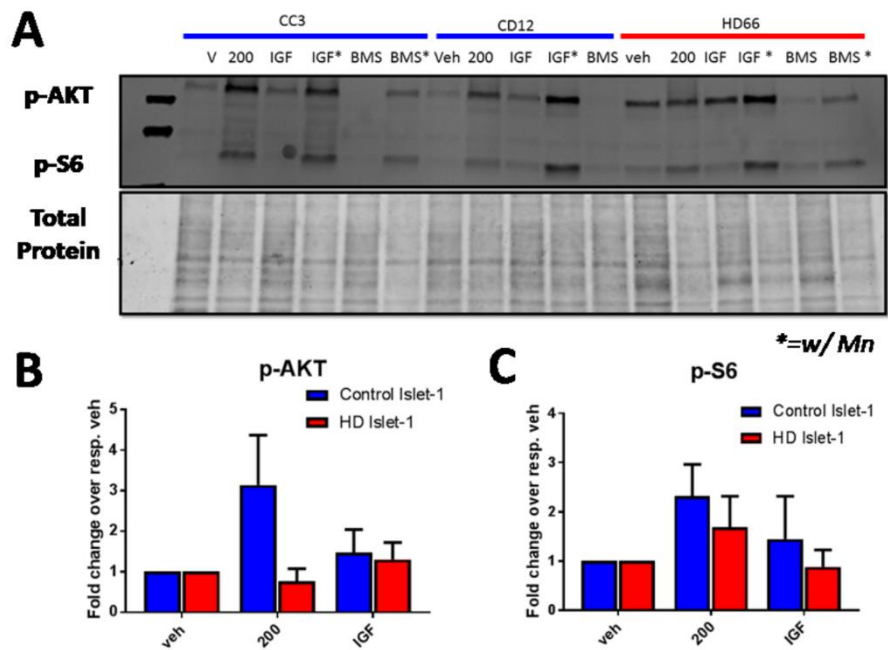
Figure 3-10: IGF-1 cannot stimulate pAKT expression in hiPSC-derived neuroprogenitors after 24hr exposure in conventional growth-factor (N2) containing media. **A**) Representative western blot of p-AKT and p-S6 treated with Mn (200uM), IGF (10nM), and/or BMS-536924 (100nM) under normal +N2 containing (insulin saturating) media in two control and one HD patient-iPSC-derived neuroprogenitors following 24hr treatment. **B, C**) Quantification of p-AKT (**B**) and p-S6 (**C**). Error bars= SEM; N=4 control; N=3 HD. **D)** from Fig 7.

Figure 3-11: **Mn-induced p-AKT, IGFR is reduced in HD hiPSC-derived neuroprogenitors. A-C**) Western blot quantification of hiPSC-derived neuroprogenitors from three control patients and three HD patients (CAG repeat 58, 66, 70) for p-AKT (**A**), p-IGFR (**B**), and p-S6 (**C**), following treatment 3hr treatment with Mn (200/500µM) or Mn+IGF (1nM) in growth factor/insulin free media, after 3hr serum deprivation. N=8-12 for control from three separate patients, N=7-9 for HD including three separate patients; Error bars= SEM. All data normalized to respective control or HD treated IGF-1 alone. Representative blot in Figure 3-12. **D**) One-way ANOVA statistics *= significance from vehicle by Dunnet's multiple comparison test. *P<.05, **P<.01, ***P<.001.
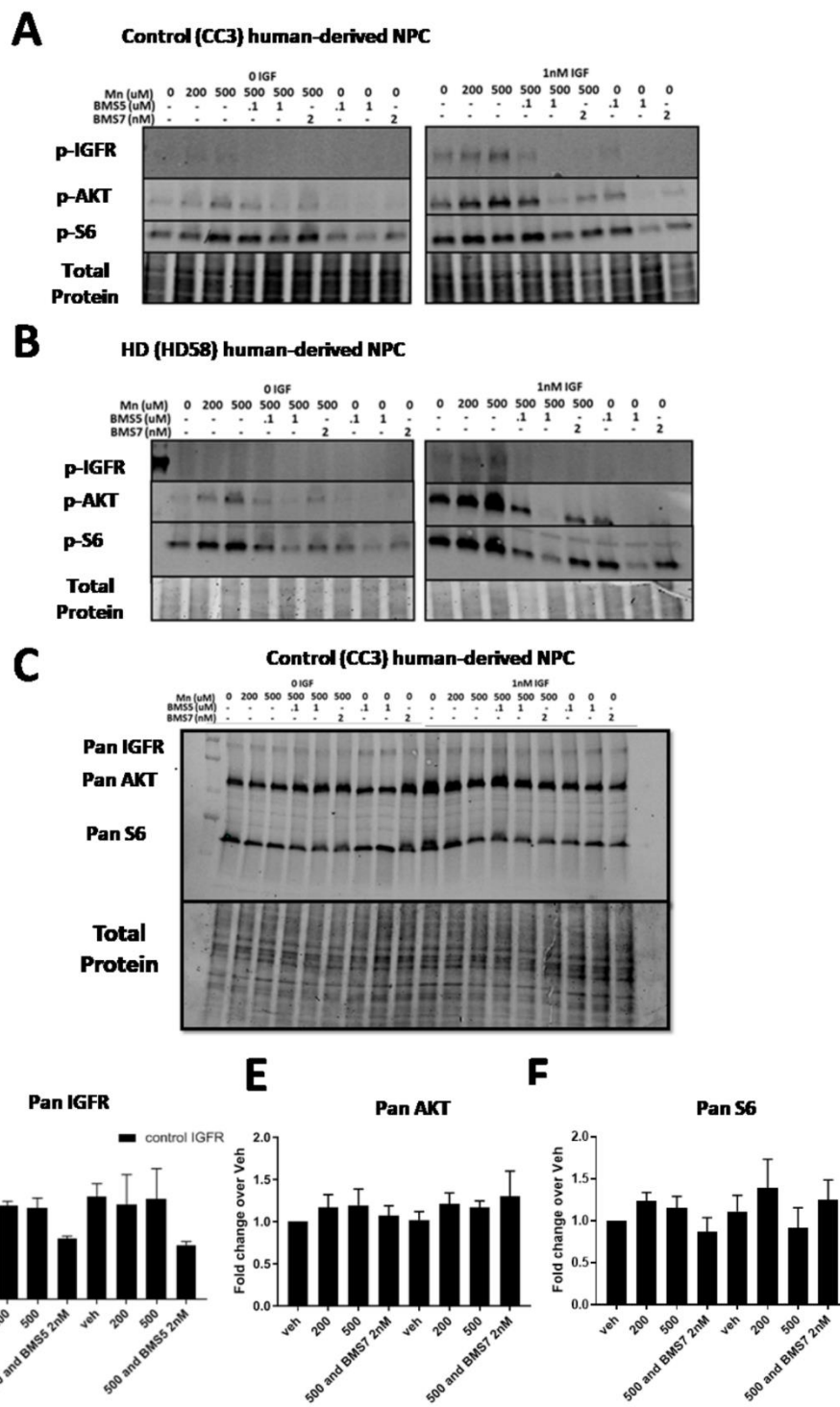
Figure 3-12: Representative western blots for hiPSC-derived neuroprogenitors. A, B) Representative western blot of of hiPSC-derived neuroprogenitors from a control patient (CC3, **A**) and an HD patient (HD58, **B**) for p-IGFR, p-AKT, p-S6 following 3hr treatment with Mn (200/500uM) or Mn+IGF (1nM) and BMS-536924 (100nM, 1uM) BMS-754807 (2nm) in serum free media, after 3hr serum withdrawal. **C)** Representative western blot for pan IGFR, pan AKT, and pan S6. Same blot as Panel A. **D-F)** Quantification of pan IGFR (**D**), pan AKT (**E**), and pan S6 (**F**). Left set of conditions (veh, 200, 500, BMS754807+500) is with no IGF, right side is with 1nM IGF.-N=4; 2 control patients from 2 separate differentiations.

A 200-500µM Mn treatment for 3hrs increased p-AKT and 500µM treatment increased p-IGFR and p-S6 in control cells (**Fig 3-11A-C, 3-12**). p-AKT and p-IGFR responses to Mn were greater in conditions with IGF, suggesting a synergistic relationship similar to the one observed in STHdh cells (**Fig 3-11A,B, 3-12**). Mn was able to significantly increase p-IGFR, p-AKT, and p-S6 in the absence of added IGF (**Fig 3-11A-C, 3-12**). This may be a result of trace IGF left behind in the media or generation of IGF by the cells themselves. In HD cells, Mn induced p-AKT was only significant after 500µM Mn treatment, and neither p-IGFR or p-S6 were significantly impacted (**Fig 3-11A, B, 3-12**). Mn-induced p-S6 is completely diminished without the addition of IGF-1 to HD cells (**Fig 3-11C, 3-12**). We found that total levels of IGFR, AKT, and S6 did not change with Mn or IGF exposures, and thus we only quantified p-IGFR, p-AKT, and p-S6 (**Fig 3-12C-F**). *These results confirm that Mn-induced IGF signaling is diminished in HD patient-derived striatal-like NPCs.*

We then assessed whether BMS-536924 and/or BMS-754807 could block Mn-induced IGF signaling in these cells, to validate that IR/IGFR signaling was required for the effects on p-IGFR, p-AKT and/or p-S6 effects. Similar to other cells tested, with some trending exceptions, both inhibitors blocked a portion of Mn-induced p-IGFR, p-AKT, and p-S6 in both control (**Fig 3-13A,B**) and HD (**Fig 3-13C,D**) cells at ~IC50 concentrations (100nM for BMS-536924 and 2nM for BMS-754807). 100nM BMS-536924 inhibited 48% of Mn-induced p-AKT, but at higher concentrations (1µM) could inhibit Mn-induced p-AKT even further, achieving >71% inhibition (**Fig 3-13A**). BMS-754807 inhibited 57% of Mn-induced p-AKT at its ~IC50 concentration (100nM) (**Fig 3-13B**). We estimate ≥68% of Mn-induced p-AKT is dependent on p-IGFR/IR across both inhibitors (74-80% with BMS-536924, 68% with BMS-754807) in Mn+IGF treated control cells. These inhibitors were less effective at inhibiting Mn-induced p-S6, similar to 3T3 and HEK293 cells (**Fig 3-7C**). These two inhibitors also inhibited basal p-IGFR, p-AKT, and p-S6 (**Fig 3-14C,D**). *Together, these results suggest that, similar to STHdh and PC12 cells, in human derived NPCs: 1) Mn-induced IGF signaling is dampened in HD cells, and 2) Mn-induced p-AKT is dependent on IR/IGFR.*

IGFR inhibition does not impinge on EGF-induced p-AKT/S6

We were surprised that Mn-induced p-AKT was almost entirely blocked by IGFR inhibition as AKT signaling can be induced via a variety of mechanisms, including cytokines, integrins, GPCRs, and several distinct families of receptor tyrosine kinases (RTKs) including IGFR/IR [326]. As even the most specific of inhibitors have off-target effects, we wanted to ensure our IGFR inhibitors weren't broadly inhibiting other RTKs. Epidermal growth factor (EGF) receptors are highly similar to IGF
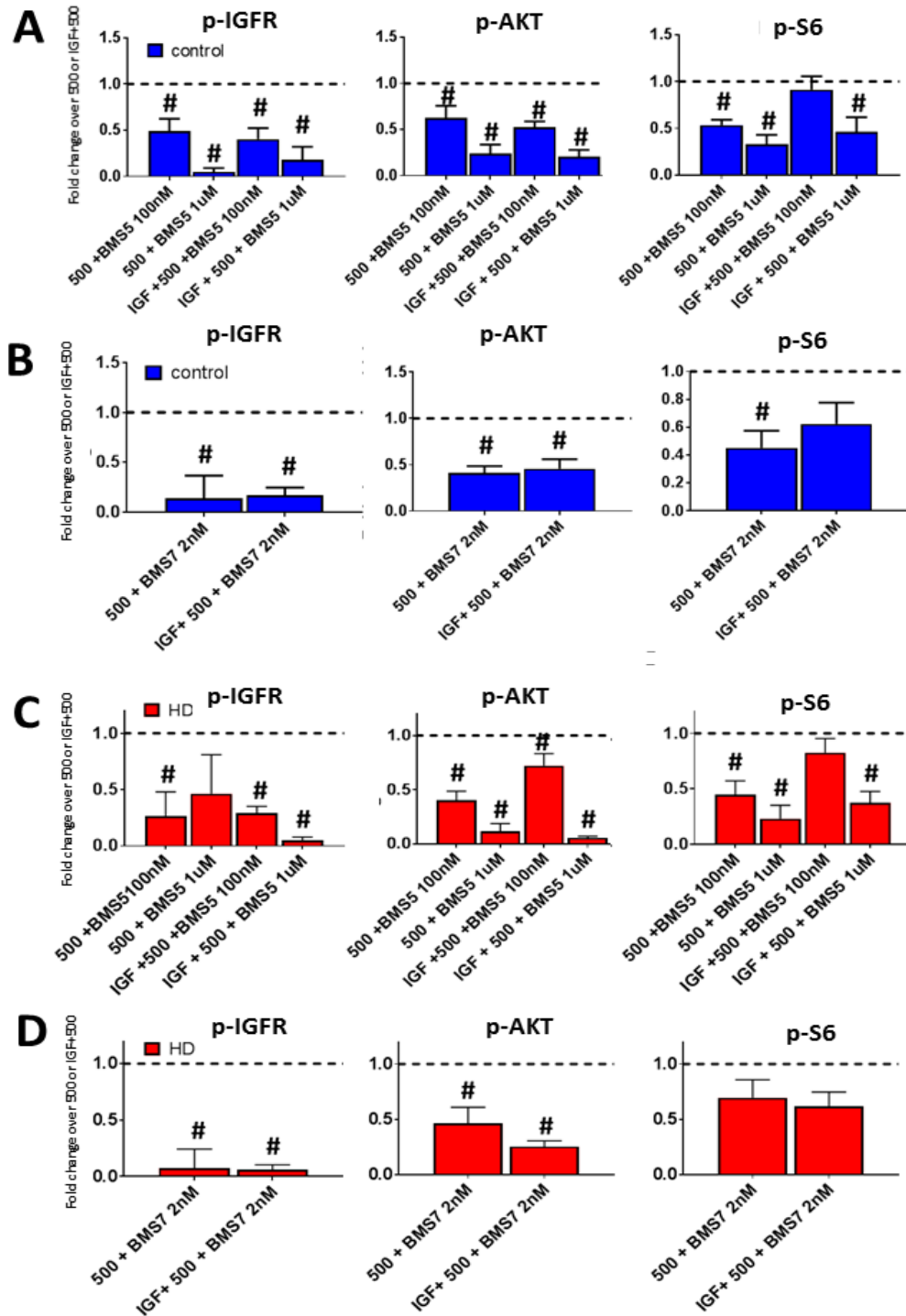
Figure 3-13: Mn-induced p-AKT, IGFR is blocked by IR/IGFR inhibition in HD hiPSC-derived neuroprogenitors. Western blot quantification of control and HD patient iPSC-derived neuroprogenitors following treatment 3hr treatment with Mn (500μM) or Mn+IGF (1nM) in growth factor/insulin-free media, after 3hr N2 supplement (insulin/growth factor) withdrawal. **A-D)** Quantification of p-IGFR, p-AKT, and p-S6 in control (Blue, **A**,**B**) or HD (Red, **C**,**D**) after treatment with BMS-536924 (100nM/1μM; **A**,**C**) or BMS-754807 (2nM; **B**,**D**). All data is represented as fold change compared to Mn alone or Mn+IGF (both normalized=1). Samples were from the exact same patient cell lines and differentiations as Figure 7. N=4-6 per condition across three control and three HD patients. Representative blot in Fig 3-12. #= significant difference to Veh (dotted line=1 for -IGF conditions) or IGF alone (dotted line=1 for +IGF conditions) by 95% CI.
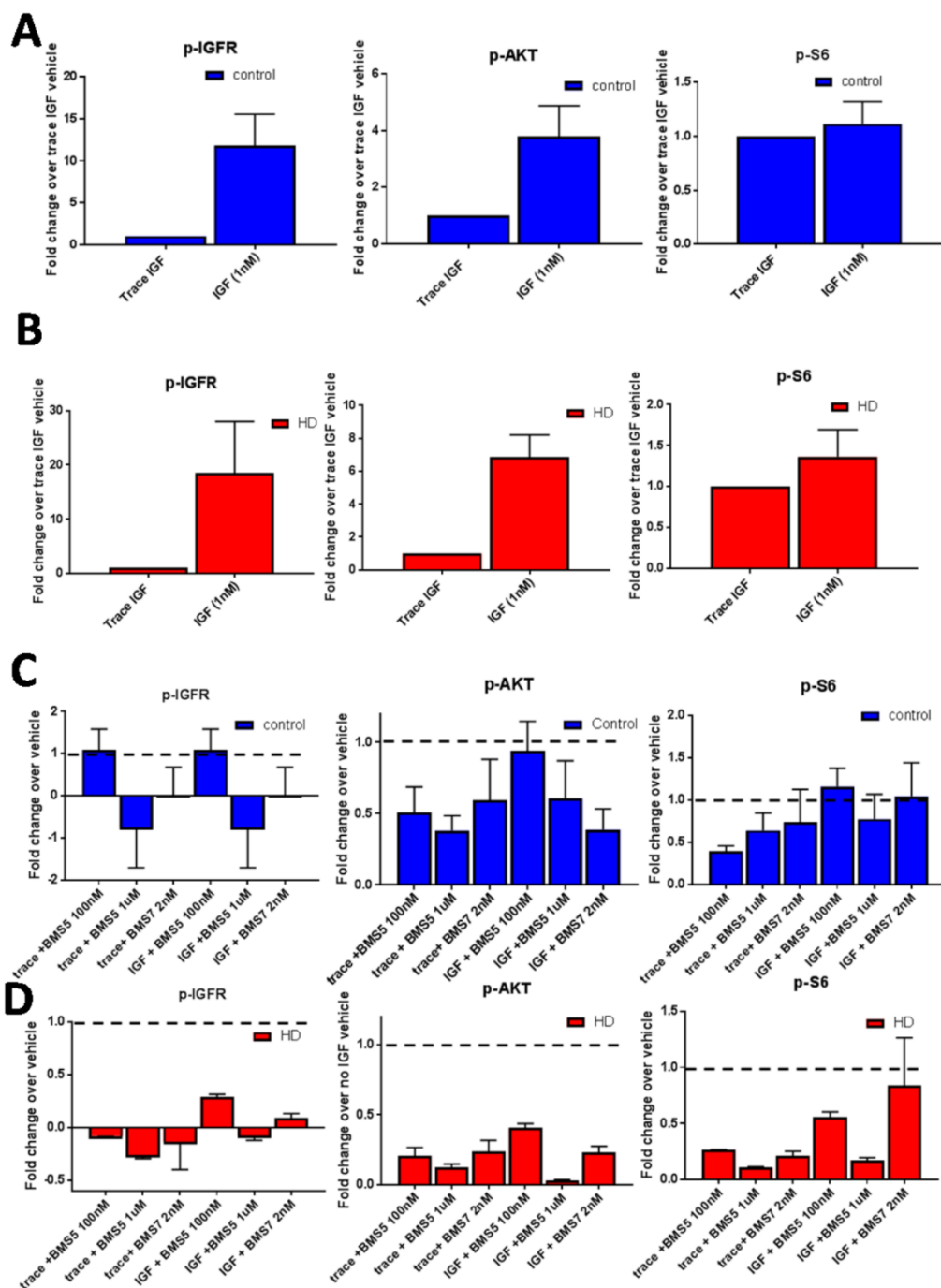
Figure 3-14: Western blot quantification for hiPSC-derived neuroprogenitors. A, B) Quantification of p-IGFR, p-AKT, and p-S6 in control **(A)** or HD **(B)** hiPSC-derived neuroprogenitors after no treatment (trace IGF) or stimulation with IGF-1 alone (1nM) for 3hrs, following 3hr serum deprivation. **C, D**) Quantification of p-IGFR, p-AKT, and p-S6 in control **(C)** or HD **(D)** hiPSC-derived neuroprogenitors after treatment with BMS-536924 (100nM, 1uM) or BMS-754807 (2nM) alone for 3hrs, following 3hr serum deprivation in either trace IGF or 1nM IGF only containing conditions (no Mn).
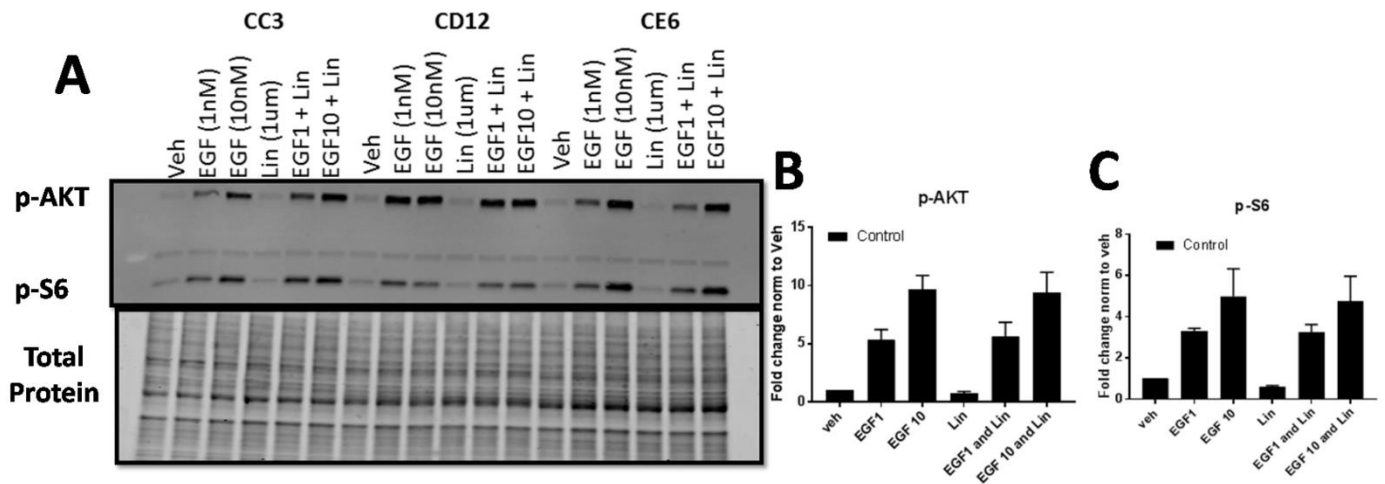
Figure 3-15: **EGF-induced p-AKT/S6 are not blocked by IGFR inhibition.** A) Representative western blot for p-AKT and p-S6 expression in control hiPSC-derived striatal neuroprogenitors after 3hr serum deprivation followed by 3hr treatment with EGF (1/10nM) and Linsitinib (1uM). Quantification of p-AKT (B) and p-S6 (C). N=3; Error bars= SEM

receptors and share many of the same downstream partners, including AKT. For these experiments, we exposed three control-patient hiPSC-derived striatal-like neuroprogenitors to 1 or 10 nM EGF with or without Linsitinib (1µM) for 30 minutes following a 3hr serum withdrawal. EGF-induced p-AKT and p-S6 were completely untouched by IGFR inhibition, indicating Linsitinib does not inhibit the EGF family of RTKs (**Fig 3-15**). This adds additional confidence that Mn activates the AKT pathway via specific interactions with IR/IGFR.

Mn promotes IGF receptor phosphorylation via intracellular interactions

Since the vast majority of Mn-induced p-AKT was dependent on IR/IGFR (**Fig 3-5, 3-13)** which autophosphorylate and do not require the presence of upstream kinases, our data suggest that Mn is either 1) directly impinging on IGFR/IR activity intracellularly (kinase domain) or 2) affecting insulin/IGFR production or receptor binding, extracellularly. To test this, we exposed hiPSC-derived NPCs to Mn for 3hrs, followed by a thorough set of media washes. After washing off the exogenous Mn, we added Mn-free HBSS with or without 1nM IGF-1 to the cells. We reasoned that if Mn activates IGFR/AKT extracellularly, pre-exposure with Mn should not potentiate IGF-induced IGFR/AKT/S6 phosphorylation, as extracellular Mn would be negligible in the presence of IGF. However, if Mn acts intracellularly to promote IGFR activity, pre-exposure with Mn will lead to a lasting increase of intracellular Mn and should still cause additive increases to IGF-1-induced signaling. Consistent with an intracellular action of Mn, we found that pre-exposure with Mn was able to increase p-IGFR and p-AKT expression (**Fig 3-16A-C**). Similar to WT cells in Fig 7C, Mn only increased p-S6 in conditions when IGF was absent (**Fig 3-16D**), suggesting the synergy between Mn+IGF co-treatment on p-S6 signaling may be quite different from that of p-AKT and p-IGFR in these cells. *Together, these data support our hypothesis that Mn acts on IGFR via intracellular interactions.*

Acute Mn exposure increases glucose uptake in HD cells only

To determine whether Mn-associated IGF/AKT signaling is associated with the decreased IR/IGFR-related functional processes in HD cells, we examined glucose uptake. IGF/AKT signaling has been associated with energy and glucose homeostasis, both of which are perturbed in HD and even precede onset of primary symptoms in HD mice [147,160,165,327-330]. Accordingly, we observed that HD STHdh cells exhibit ~60% reduction in glucose uptake compared WT, consistent with published reports in HD patients [331]. We then measured glucose uptake in STHdh cells after a 24hr Mn exposure. Consistent with an insulin-mimetic role of Mn, 100 µM Mn was able to modestly, but significantly, increase glucose uptake in HD cells, but not WT cells—although glucose levels in HD cells did not reach WT levels (**Fig 3-17)**. We did not observe any effect at 50 µM (data not shown). *This HD-specific*
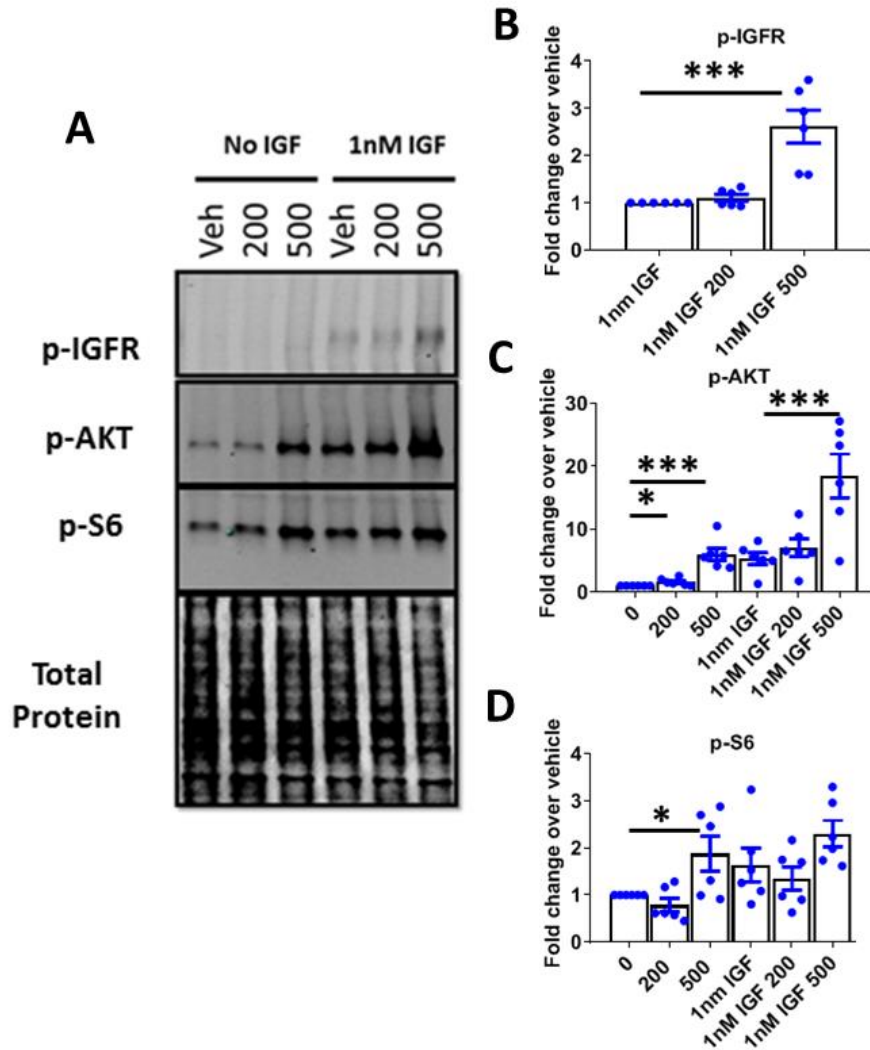
Figure 3-16: Mn-induced p-IGFR/AKT is due to intracellular, not extracellular Mn. A) Representative western blot of control hiPSC-derived neuroprogenitors for p-IGFR, p-AKT, and p-S6 following 3hr Mn exposure with 200/500µM Mn in HBSS, 3X HBSS washes, then exposure with 1nM IGF (without Mn) or HBSS (no IGF or Mn) for another 3hrs. **B-D)** Quantifications of p-IGFR **(B)** One-way ANOVA for treatment $F_{(2,6)}= 116.5$; $p<.0001$, p-AKT **(C)** One-way ANOVA for treatment $F_{(5,15)}= 107.2$; $p<.0001$, and p-S6 (**D**) One-way ANOVA for treatment $F_{(5,15)}= 14.12$; $p<.0001$. N=6 (two differentiations of three separate control patients); Error bars= SEM. *= significance by Tukey multiple comparison test.
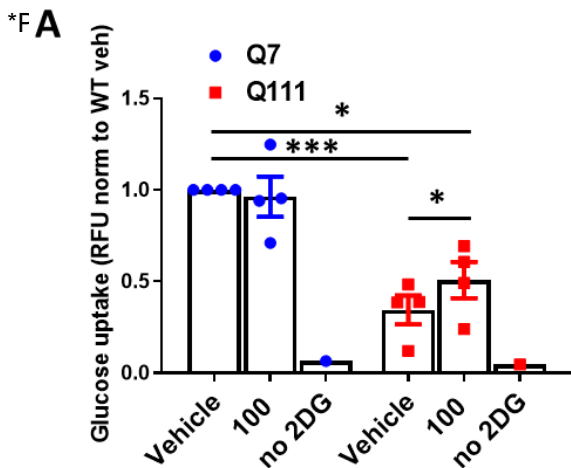
Figure 3-17: Mn increases glucose uptake in Q111 cells. A) Quantification of glucose uptake in STHdh Q7/Q7 and Q111/Q111 following 24hr exposure with 50/100µM Mn. "no 2DG" is a negative control in which no glucose was added to cells. N=4; Error bars= SEM. Two-way ANOVA; treatment= $F_{(2,6)}=1.443$ $p=<0.3079$; genotype= $F_{(1,3)}= 5.585$ $p=0.0991$; treatment-genotype interaction= $F_{(2,6)}= 5.939$ $p=.0370$. *= significance by Tukey's multiple comparison test. *$P<.05$, **$P<.01$, ***$P<.001$. ***Work done with the assistance of Kristen Nordham.***

effect provides evidence that homeostatic Mn levels play a role in maintaining glucose homeostasis, and suggests that reductions in bioavailable Mn (such is the case is with Q111/Q111 cells) contribute to perturbations in glucose uptake, a known phenotype in HD patients.

Discussion

Several laboratories have observed Mn-induced insulin/IGF-related signaling (primarily AKT) in cell and rodent models, but the direct mechanism by which Mn stimulates these pathways was unclear [85,287,300,301]. Here, we sought to define the ambiguous relationship between Mn and insulin/IGF signaling, and how this interaction mediates Mn-induced signaling—namely AKT. We also wanted to investigate how perturbations in this relationship may manifest in HD—as models of HD exhibit reduced Mn uptake and defective insulin/IGF signaling.

Here, we observed that IGF and Mn work synergistically to regulate insulin/IGF activity. In the presence of IGF, Mn was able to increase maximal AKT signaling more than near-physiological (1nM) or saturating (10nM) concentrations of IGF alone (**Fig 3-1C, D**) [332]. Furthermore, Mn was able to increase phosphorylation of IR/IGFR, in the presence of physiological levels of IGF (1nM) (**Fig 3-5A, 6, 7B**). Additionally, after 24hr exposure, Mn decreased total IGFR protein expression and IGFR mRNA expression (**Fig 3-5C-E**). We propose that sustained exposure with Mn causes a negative feedback loop to reduce total IGFR protein by decreasing IGFR mRNA, thus dampening total IGF signaling activity. These findings are consistent with a previous study showing that Mn inhibits insulin receptor dephosphorylation, in addition to increasing kinase activity [309]. This sustained activity would likely require a negative feedback loop to prevent continuous stimulation of the pathway, facilitating restoration of homeostasis. Together, our data demonstrate that Mn is able to modulate insulin/IGF signaling via multiple avenues directly related to the IR and IGFR, and thereby impacts downstream p-AKT levels (**Fig 3-18**). Furthermore, it is possible that cellular Mn levels could be further regulating this signaling via means which we have not examined in this study, such as receptor internalization, Mn-induced phosphatase activity, or interactions with autophagy or the proteasome. Thus, to fully understand the complete coordination between Mn homeostasis and IGF signaling, all of these distinct modalities of IGF signaling regulation must be assessed in the future.

Mn-induced AKT signaling was first reported years ago, specifically in the context of toxic exposures, but the mechanism of this effect remained unknown [42]. Our recent study demonstrates that the majority of Mn-induced AKT is dependent on PI3K [300] (which also uses Mn as a cofactor), however, PI3K and AKT can be activated via dozens of routes including receptor tyrosine kinases,
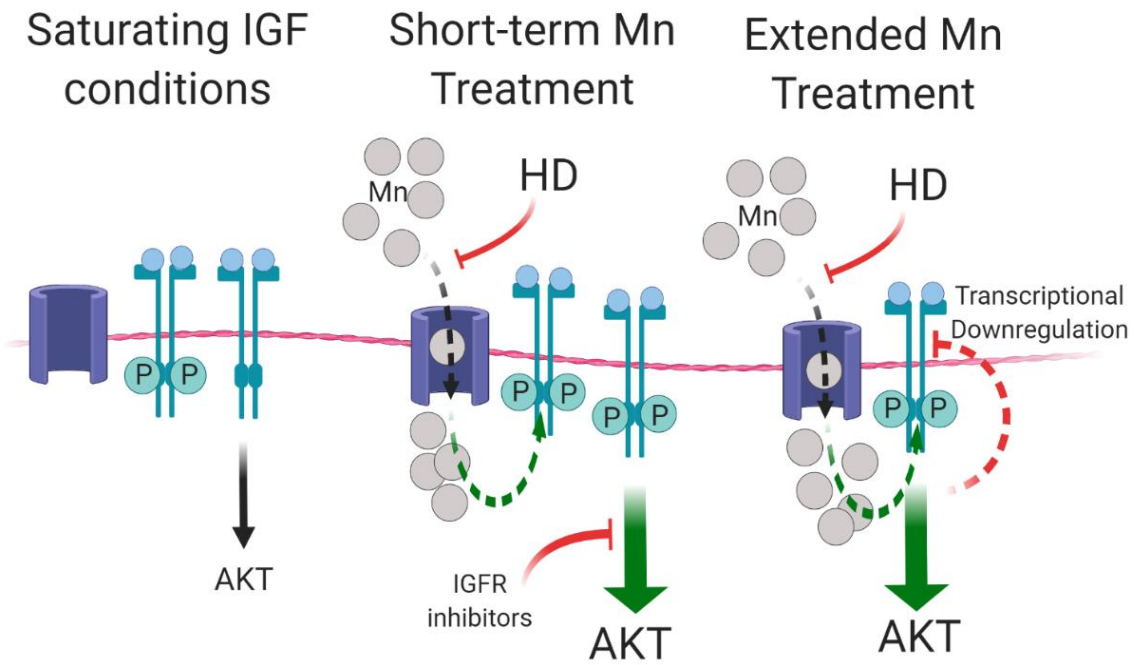
Figure 3-18: Mn modulates IGF signaling via increased phosphorylation of IGFR/IR in short-term treatments but decreases total IGFR/IR expression after extended treatments.

integrins, cytokines, and G protein-coupled receptors [284,326]. Given the extensive crosstalk between Mn and IGF observed in this study, we posited that Mn-induced AKT signaling is mediated by IR/IGFR. We found that several IR/IGFR inhibitors with non-overlapping off-target kinases (**Fig 3-6A**) could inhibit the vast majority of Mn-induced p-IGFR and p-AKT across every cell model tested (with the exception of HEK293 cells)— achieving ~50% inhibition of Mn-induced p-AKT at approximate IC50 concentrations and >70% inhibition at higher concentrations (**Fig 3-6, 3-8, 3-13, 3-7A-C**). By correlating the degree of p-IGFR inhibition to p-AKT inhibition [(% of p-AKT inhibition) / (% of p-IGFR/IR inhibition)], we estimate that >70-80% of Mn-induced p-AKT is dependent on p-IGFR in most cell lines (**Fig 3-8B-C**). Our observations strongly suggest that the vast majority of Mn-induced AKT signaling in many cell types is mediated via interactions between Mn and the insulin/IGF receptors themselves, rather than other upstream or downstream effectors.

Our data show that Mn synergistically works with IR/IGFR to promote downstream AKT signaling, and that this is most likely due to the effects of intracellular, not extracellular, Mn (**Fig 3-16**). Together, with the previously discussed inhibitor data (**Fig 3-6, 3-13**), we can narrow the initial site of action to the intracellular kinase domains of IGFR/IR (as these receptor-kinases do not require an upstream kinase for activation). As Mn is a known cofactor for several other kinases, we postulated that Mn is binding the kinase domain of IR/IGFR to stimulate receptor autophosphorylation and propagate signaling downstream. Our results are consistent with cell free in vitro experiments demonstrating the ability of Mn to increase kinase activity in a defined biochemical system [309,310]. Future studies using structural crystallography or computational assessments could be performed to confirm that Mn binds this intracellular region, but this will be challenging given the limited utility of available methods to detect Mn-binding of proteins in living systems. Previous studies have shown that Mn can stimulate insulin production itself to promote IGF signaling [59,66]. This study does not directly assess whether Mn can increase insulin/IGF production, though our data suggest the mechanism of the Mn-induced effect on IR/IGFR is derived from intracellular interactions, not interactions with the extracellular, ligand-binding, regions of the receptor (**Fig 3-16**). As the vast majority of Mn-induced p-AKT is regulated by IR/IGFR, and Mn is able to increase maximal AKT activity even under saturating concentrations of IGF, this also supports the hypothesis that Mn is not acting at the ligand-binding domain or increasing the ligands themselves in our conditions/cell lines. However, we cannot exclude that Mn may be able to promote insulin/IGF production or extracellular binding *in addition* to intracellular stimulation of the receptor itself.

Heavy metals, including Mn, have specific proteins to which they bind, leading to activation of specific biological responses. However, excessive accumulation of cations can incur broad, non-

specific activation of specific signaling cascades due to dyshomeostasis and toxicity. For instance, accumulation of many heavy metals will promote ROS production, broadly activating several signaling cascades [333,334]. In this study, we provide evidence that Mn-induced IGF signaling is due to a highly specific interaction between Mn and insulin/IGF receptors themselves, not merely a shared effect, such as ROS, by other cations (**Fig 3-3A-C**). This is supported by a previous study in which Mn-induced p-AKT in the striatum was not blocked by antioxidant treatment, consistent with a ROS-independent mechanism [264]. The concentrations we chose are the highest concentrations that these cells can be exposed to these cells for 24hrs without incurring detectable cell death [81]. While Mn can clearly activate p-AKT at sub-cytotoxic concentrations at 24hrs or during sub-acute, 7-day exposures (**Fig 3-3A-F**), it is possible that other metals could activate p-AKT at supra-toxic concentrations due to non-specific toxicity. A previous study in our lab observed that Cd could induce p-AKT at 50µM, which is a cytotoxic concentration of Cd [81]. In this study, we used 20µM Cd which did not induce p-AKT. We posit that cytotoxic levels of Cu, Ni, Zn and other metals may also promote AKT signaling as this has been previously shown, though we did not detect any increase p-AKT induction by sub-toxic concentration of these metals [335-339].

Mn and Mg can compete for binding and activation of the same protein kinases. In fact, the vast majority of kinases in the human body are Mn- and/or Mg-dependent, though more often Mg-dependent [340]. Since DMEM-based media contains high physiological concentrations of Mg to sustain enzymatic activity, we could not directly test whether Mg could stimulate p-AKT alone. However, even in the presence of apparent saturating concentrations of Mg, Mn was still able to incur a ~3-4 fold increase in p-AKT after 24hrs in WT cells (**Fig 3-1D, 3-3B**). Previous studies in a biochemically defined system reported the activation of the insulin receptor in the presence of Mg or Mn+Mg. Consistent with our results in living cells, these studies observed that the combination of Mn+Mg evoked higher insulin receptor activity [309,310]. Our data demonstrate that Mn can increase the maximal activity of the insulin/IGF receptors compared to Mg alone in a living biological system as well. In this way, intracellular Mn could modulate maximal IGF signaling in a biological setting, even when sufficient Mg is present in the cell. In the case of HD, reduced intracellular Mn may cripple maximal IGF signaling and contribute to the AKT-related defects observed in HD, discussed more below.

Mn is an essential cofactor for a variety of enzymes[32]. Other studies, including our own, show that Mn can incur activity of specific kinases and pathways that are not broadly shared by other metals[30,31,39,82,284,307,309,311,341] (**Fig 3-3A-C**). However, Mn is not broadly recognized as a signaling molecule itself. We know that Mn binds to and promotes activity of specific kinase pathways, but few studies have examined how biologically-relevant intracellular Mn may help regulate cellular kinase

activities, facilitating signaling cascades within the cell. Additionally, most studies have only examined the effect of Mn-induced signaling at toxic concentrations of Mn—here we demonstrate that Mn-induced signaling can also occur at sub-cytotoxic concentrations. This suggests biologically-relevant concentrations of intracellular Mn play a role in the normal signaling homeostasis of dozens of pathways. The discovery of a Mn-specific chelator or small molecules that could manipulate intracellular Mn could be incredibly beneficial in further elucidating the necessity of Mn in cell signaling.

The AKT response to Mn has also been associated with neuroprotection, as a way to stimulate pro-growth pathways [88,89,109,182,342-344]. Here we observed that Mn increased glucose uptake in STHdh HD cells only (**Fig 3-17**). While this increase was modest, it was also genotype-dependent, occurring only in a model of HD which exhibits reduced Mn uptake. This increase in glucose uptake is consistent with a role for AKT in promoting PFK1 phosphorylation and GLUT4 translocation to stimulate glucose uptake [326,345]. This suggests that Mn, particularly in cases of reduced Mn bioavailability, can stimulate neuroprotective processes, such as glucose uptake, which are impeded in neurodegenerative diseases like HD. This also demonstrates that Mn-induced IGF signaling serves a role in mediating responsive, downstream biological processes, not merely just a broad response to higher intracellular Mn.

Humbert and colleagues discovered that mutant HTT can be phosphorylated at Ser[421] specifically by AKT, and this results in robust amelioration of cellular pathology, increasing cell survival and reducing aggregate accumulation [88,91]. Since then, other studies have examined the neuroprotective capacity of AKT stimulation more closely [95,98,107]. Ahmed et al found that loss of IMPK, a mediator of PI3K and AKT activity, is disrupted in models of HD. However, overexpression of IMPK stimulated AKT activity and rescued cellular pathology and motor abnormalities in HD models, consistent with the neuroprotective potential of AKT. Similarly, we hypothesized, that in the context of reduced Mn bioavailability [81,82], suboptimal Mn levels impair activation of IR/IGFR, reducing activity of AKT downstream and concurrently reducing the neuroprotective, pro-growth signaling that AKT provides to combat disease pathology. Of particular interest, Rego and colleagues have elucidated the neuroprotective effects of IGF treatment in cell and mouse models of HD, including upregulation of HTT Ser[421] phosphorylation [92,93,96,97,163,346]. Additionally, Hiney and colleagues have shown that Mn administration upregulates IGFR/AKT/Rheb/mTOR in vivo, which have been targeted to combat HD pathology in separate studies, providing a proof-of-principle that in vivo Mn administration alone can potentiate IGF signaling in the brain [87,287]. Our study suggests Mn can increase the maximal activity of the IGF signaling axis in living cells, even under saturating concentrations of IGF and Mg (**Fig 3-1D, 3-3A-C**). Given the synergistic co-regulation of IGF and Mn presented in this study, we hypothesize that

co-treatment of HD models with Mn+IGF may incur the greatest AKT stimulation and thus, increase the neuroprotective potential and therapeutic benefit of IGF-1 treatment alone.

Author contributions

MRB and ABB designed all experiments. MRB performed most data analyses on all data. MRB, KN, DR, MO, RN, and MU carried out cell culture and experiments for all figures. PJ carried out hiPSC-derived cell culture and differentiations. AMF performed all qRT-PCR. FG performed all experiments and analysis in primary astrocytes. MA assisted in experimental design and interpretation. All authors read and approved the final manuscript.

Materials and Methods

Immortalized cell culture

The immortalized, murine striatal cell lines (STHdh$^{Q7/Q7}$ and STHdh $^{Q111/Q111}$ were obtained from Coriell Cell Repository (Cambden, NJ). STHdh striatal cells were cultured in Dulbecco's Modified Eagle Medium [D6546, Sigma-Aldrich, St. Louis MO] supplemented with 10% FBS [Atlanta Biologicals, Flowery Branch, GA], 2 mM GlutaMAX (Life Technologies, Carlsbad, CA), Penicillin-Streptomycin, 0.5 mg/mL G418 Sulfate (Life Technologies, Carlsbad, CA), MEM non-essential amino acids solution (Life Technologies, Carlsbad, CA), and 14mM HEPES (Life Technologies, Carlsbad, CA). They were incubated at 33°C and 5% CO_2. Cells were passaged before reaching greater than 90% confluency, and were never passaged past the recommended 14th passage. The cells were split by trypsinization using 0.05% Trypsin-EDTA solution (Life Technologies, Carlsbad, CA) incubated for five minutes. One day prior to exposure, cells were plated in the appropriate cell culture plate type at 8×10^4 cells/mL for WT and 1×10^5 cell/mL for HD (as these HD cells grow slightly slower than WT counterparts). For some experiments, STHdh cells underwent serum deprivation in HBSS prior to exposures. For these, STHdh cells were plated the same as above. The day after, cells were wash 3X with HBSS and incubated for one hour in HBSS. After this, treatments were added to the cells in HBSS for another 3 hours before lysates were collected for western blot.

For 1 week, low-dose Mn exposures, STHdh cells were exposed to 0, 1, 5, or 10µM Mn, 10 or 100nM IGF 24 hours after plating. The cells were split once, 1:4, midway through the week once they were near confluency. Exposure was continued with fresh media. Cells were harvested on day 7 at the same time of day as the original exposure day. Because of the original plating density difference, the density of Q7 and Q111 cells at the end of the 7 days was approximately equal.

NIH-3T3 and HEK293 cells were a generous gift from the Tansey lab. Cells were maintained and plated

with high-glucose DMEM (Corning 0013CV) with penicillin-streptomycin. For experiments, they were plated at 100,000 cells/mL. After 48 hours, cell media was aspirated, cells were washed 1X with HBSS, and then fresh HBSS (without growth factors) was added for another hour to begin growth factor deprivation. After 1 hour of deprivation, media with IGF and/or Mn and inhibitors was added to the cells for an additional 3 hours before protein lysates were collected.

Primary Rat Astrocyte cell culture

Primary cortical astrocytes were obtained according previous published protocols. Briefly, cortices of newborn Sprague-Dawley rats were carefully dissected and the meninges were removed[347,348]. Next, the cells were dissociated with a multi extraction protocol using dispase and DNAse and plated at 10,000 cells/cm^2 on poly-l-lysine coated dishes. The cells were maintained in minimum essential medium (MEM) supplemented with 10% horse serum, 100 U/ml penicillin and 100 µg/ml streptomycin. The first media exchanged occurred 24 hours after plating the cells, and after that once every 3-4 days. After 7-8 days in culture, the cells reached confluence and the astrocytes were used for the respective experiments.

hiPSC cell culture

Three control and HD-patient derived hiPSC-lines were differentiated into striatal islet-1-positive neuroprogenitor cells as previously described [82]. HD patient mutant alleles were 58, 66, and 70 CAG repeats. All hiPSC lines were confirmed to be pluripotent (PluriTest- Expression Analysis, Durham, NC) and to have normal karyotypes (Genetics Associates, Nashville, TN). Additionally, a subset of cells was fixed with 4% paraformaldehyde for 15 minutes and immunocytochemistry was performed to ensure all cultures expressed the striatal marker Islet-1.

For experiments, striatal neurprogenitor cells were plated at 300,000 cells/mL at day 10 of differentiation. At day 11, purmorphamine and rock inhibitor-containing media was replaced with fresh media containing purmorphamine (.65µM) for 24hrs. For 3-hour exposures, cells were washed with HBSS 3X and then cells underwent growth factor/insulin deprivation in media without N2 supplement (which contains the insulin for the differentiation media) for 3 hours. This was followed by exposing the cells in N2supplement-free media with Mn, inhibitors, and IGF-1 for another 3 hours prior to protein collection. Other N2 components include human transferrin, progesterone, putrescine, and selenite.

In order to test the effects of intracellular vs extracellular Mn, cells were exposed to 200 or 500 µM Mn for 3hrs in -N2 media 24hrs after removing rock inhibitor containing media. After, cells were washed 3

times with HBSS and then replaced with IGF-containing -N2 media for another 3 hours prior to protein collection. -N2 media without IGF was added to half the wells to ascertain the effect of IGF alone.

Inhibitors/growth factors/metals

Inhibitors/growth factors were used at the following concentrations: recombinant human IGF-1 (R+D systems Cat# 291-G1)= .1-10µM, recombinant human EGF protein (R+D systems Cat# 236-EG), BMS-53692436924 (SelleckChem)= 100nM-1µM, BMS-7548075480754807 (SelleckChem)= 2nM, Linsitinib (SelleckChem)= 100nm-1µM, NVP-AEW541 (SellekChem)= 100nM-1µM, and LY294002 (Tocris)= 7µM.

The following metallic compounds were used as sources for the metal exposures: $MnCl_2$ for $MnCl_2 \cdot 4H_2O$ (Sigma Aldrich, St. Louis, MO) for Mn, $FeCl_3$ (Sigma Aldrich, St. Louis, MO) as Fe, : $CuCl_2 \cdot 2H_2O$ (Alfa Aesar, Ward Hill, MA) for Cu, $MgCl_2 \cdot 6H_2O$ (Alfa Aesar, Ward Hill, MA) for Mg, $ZnCl_2$ (Acros Organics, Morris, NJ) for Zn, $CdCl_2 \cdot H_2O$ (for Cd, $NiCl_2 \cdot 6H_2O$ (Alfa Aesar, Ward Hill, MA) for Ni, and $CoCl_2 \cdot 6H_2O$ (MP Biomedicals, Solon, OH) for Co exposures.

Western blot

Cells were washed once with ice cold PBS and then scraped from wells of a 6-well plate directly into 100ul, ice-cold RIPA buffer containing protease inhibitor (Sigma-Aldrich, St. Louis, MO) and phosphatase inhibitor cocktails 2 & 3 (Sigma, Sigma-Aldrich, St. Louis, MO). Cell lysates were centrifuged at 4°C for 10 minutes at 20,000 *g*. Protein concentration was quantified using the BCA assay (Peirce Technologies). Samples were mixed with 5x SDS loading buffer containing 1% 2-mercaptoethanol and boiled for 5 minutes. Fifteen µg of protein was loaded for each sample onto a 4-20% pre-cast gel SDS-PAGE gel (BioRad, Hercules, CA) and run at 90V for 120 minutes. The protein bands were then transferred onto nitrocellulose membranes using iBlot Gel Transfer Device (Life Technologies). The remaining gel was stained with Coomassie Blue stain (Biorad, Hercules, CA). Since the gels retained ~1/3 of the original protein after transferring with the iBlot, we imaged the stained gel on the Li-Cor Odyssey Imaging System and quantified the intensity entire lane from ~150-20 kDa. This value was used to normalize the quantification of the immunostained bands. The membrane was blocked in Odyssey Blocking Buffer for one hour prior to the addition of the primary antibodies. The primary antibodies were diluted 1:1000 in Odyssey Blocking Buffer containing 0.1% TWEEN and incubated overnight. After washing three times for 5 minutes in TBST, membranes were incubated with secondary antibodies at 1:10,000 (LiCor, Lincoln, NE) for 1 hour. Following three, 5-minute washes in TBST, membranes were imaged using the Li-Cor Odyssey Imaging System, and quantification was

performed using Image Studio Lite (LiCOR, Lincoln, NE). In Figure 6A, membranes were visualized using CL-XPosure film (Thermo Scientific, #34090) and quantified via ImageJ.

pIR/IGFR Tyr[1135] (3918), pan IR/IGFR (9750), p-AKT Ser[473] (4060), p-AKT Thr[308] (2965), pan AKT (2920), and pan S6 (2317), p-S6 Ser[235/236] (2211) antibodies were purchased from cell signaling technologies and used at 1:1000 dilution except pIR/IGFR was used at 1:500. Note: Unless stated, all western blots examined p-AKT at the Ser[473] residue. All blots aside from Figure 6A were normalized by total protein (Coomassie). Figure 6A was quantified at p-AKT over actin. Pan was quantified separately in the supplement as it did not significantly change under our exposure paradigms.

Note: Many of our experiments were performed to maximize the number of conditions/genotypes/cell lines/exposure time and, thus most replicates of western blots included conditions that were not relevant for specific figure panels. Thus, some western blot images were cut to exclude these non-relevant conditions. However, any western blots that are grouped together for any specific figure panel come from a single blot and are only cut/copied to exclude unneeded conditions/replicates for simplicity and space.

PC12 cell HTT induction and differentiation

HTT PC12 cells were purchased from Coriell Repositories (CH00285, CH00287, CH00289). Undifferentiated cells were plated at 75,000 cell/mL in DMEM F12 media with 4.5 g/L glucose, L-glutamine, and sodium pyruvate with 10% fetal bovine serum, 5% horse serum, 250ug/mL zeocin (Invitrogen), 100ug/mL G418, and 1% penstrep. Cells were plated on collagen-coated plates at 75,000 cells/mL. Cells were induced with 5µM ponasterone A (Invitrogen) and differentiated with 50ng/uL neural growth factor (NGF- Cell signaling technologies) for 6 days prior to exposures. On the 6th day, exposures were added for an additional 24 hours with ponasterone A. Cells were imaged by microscopy for neurite outgrowth and expression of RFP-HTT, assuring induction and differentiation of cultures.

qRT-PCR for IR/IGFR/IRS2

STHdh Q7/Q7 and Q111/Q111 cells were plated in 6-well plates and treated with Mn and/or IGF-1. After 24 hours, cells were lysed in 1mL of TRIzol® Reagent (CatNo. 15596) and stored at -80°C until use. Total RNA was extracted using TRIzol® Reagent, according to the manufacturer's User Guide (Invitrogen, Carlsbad, CA). RNA was DNAse I treated, following the NEB DNase I Reaction Protocol (M0303) (New England BioLabs® Inc, Ipswich, MA). cDNA was generated on Bio-Rad Laboratories' S1000™ Thermal Cycler, using 50µM Random Hexamers (P/N 100026484, Invitrogen, Carlsbad, CA), 50U MuLV Reverse Transcriptase (P/N 100023379, Applied Biosystems, Foster City, CA), 10mM

dNTPs (CatNo. N0446S, NEB, Ipswich, MA), 20U RNAse, Inhibitor (CatNo. N8080119, Applied Biosystems, Foster City, CA), 25mM $MgCl_2$ (P/N100020476, Applied Biosystems, Foster City, CA), 10x PCR Buffer II (RefNo. 4486220 Applied Biosystems by Life Technologies, Austin, TX), and 1ug of extracted RNA, and using the following cycling times: 25°C for 10 min, 42°C for 60 min, 99°C for 5 min, 5°C for 5 min, 4°C forever. Q-RT-PCR was performed on Eppendorf's Mastercycler® epGradientS Realplex[2], using KAPA SYBR® FAST qPCR Master Mix (2X) Universal according to the manufacturer's recommendations (KM4101, KAPA Biosystems, Wilmington, MA). Sequences of primers used are as follows: *mpgk1*_R2 AAAGGCCATTCCACCACCAA, *mpgk1*_F2 GCTATCTTGGGAGGCCTAA, *Irs2* forward, GTCCAGGCACTGGAGCTTT, *Irs2* reverse, GCTGGTAGCGCTTCACTCTT, IGFR For Primer GCTTCTGTGAACCCCGAGTATTT, IGFR Rev Primer TGGTGATCTTCTCTCGAGCTACCT, IR For Primer TTTGTCATGGATGGAGGCTA, IR Rev Primer CCTCATCTTGGGGTTGAACT.

Glucose uptake assay

Glucose Uptake-Glo Assay was conducted per manufacturer instructions (Promega, Madison, WI). Q7 and Q111 cells were cultured after plating for 16-24 hours in 96-well tissue plates. 24 hours prior to the Glucose Uptake-Glo Assay, the media was removed and replaced with media containing 0, 50, or 100µM Mn. The, the media was removed and the wells washed with 100µl PBS. 50µl of prepared 1mM 2DG was added per well, plates were briefly shaken, and incubated for 10 minutes at room temperature. The, 25µl of Stop Buffer was added and the plate briefly shaken again. Thereafter, 25µl of Neutralization Buffer was added to each well and the plate shaken briefly. This was followed by addition of 100µl of 2DG6P Detection Reagent to each well, the plate was briefly shaken and then incubated for 30 minutes at 33 degrees (the normal temperature for these cell lines). Luminescence was recorded using a 0.3–1 second integration on a microplate reader (BioTek Synergy H1, Winooski, VT).

Statistical analysis

GraphPad Prism version 8.0.2 was used. Most data are shown by fold change to increase clarity for the reader. However, all data that was analyzed by one-way or two-way ANOVA was converted to log values to allow for a normal distribution for the statistical analysis. For any data comparing values versus a unitary value (=1) on a graph- raw, unnormalized data was converted to log values and underwent ANOVA analysis. If data sets were significant by ANOVA, post-hoc multiple comparisons tests were used to determine specific differences within data sets. For analyses across all possible treatments/genotypes, Tukey's test was performed. For analyses comparing data back to a specific condition only, Dunnet's or Sidak's tests were performed. For the majority of data sets, paired analyses

were used as all samples were collected as full sets. For the data sets which compared two points specifically, a paired student's t-test was used as indicated.

CHAPTER 4

ACUTE MANGANESE RESTORATION PROMOTES AUTOPHAGIC CARGO LOADING IN HUNTINGTON'S DISEASE CELL LINES

Abstract

The molecular etiology linking the pathogenic mutations in the Huntingtin (*Htt*) gene with Huntington's Disease (HD) is unknown. Prior work suggests a role for *Htt* in neuronal autophagic function and mutant HTT protein disrupts autophagic cargo loading. Reductions in the bioavailability of the essential metal manganese (Mn) are seen in models of HD. Excess cellular Mn impacts autophagic function, but the target and molecular basis of these changes are unknown. Thus, we sought to determine if changes in cellular Mn status impact autophagic processes in a wild-type or mutant *Htt* dependent manner. We report that the HD genotype is associated with reduced Mn-induced autophagy, and that acute Mn exposure increases autophagosome induction/formation. To determine if a deficit in bioavailable Mn is mechanistically linked to the autophagy related HD cellular phenotypes, we examined autophagosomes by electron microscopy. We observed that a 24hr 100uM Mn restoration treatment protocol attenuated an established HD "cargo-recognition failure" in the STHdh HD model cells by increasing the percentage of filled autophagosomes. Mn restoration had no effect on HTT aggregate number, but a 72-hour co-treatment with CQ in GFP-72Q-expressing HEK293 cells increased the number of visible aggregates in a dose-dependent manner. As CQ prevents autophagic degradation this indicates that Mn restoration in HD cell models facilitates incorporation of aggregates into autophagosomes. Together, these findings suggest that defective Mn homeostasis in HD models is upstream of the impaired autophagic flux and provide proof-of-principle support for increasing bioavailable Mn in HD to restore autophagic function and promote aggregate clearance.

Introduction

Huntington's disease (HD) is an age-progressive neurodegenerative disease characterized by the primary symptom, chorea, uncontrolled motor behavior. However, symptoms and progression are highly variable between patients. There is no cure and few symptomatic treatments for this fatal disease. An expanded CAG repeat within exon 1 of the HTT gene produces the mutated protein. While age of onset is inversely correlated with CAG repeat, it is still unclear how mutant HTT (mutHTT) causes specific cell death in the medium spiny neurons of the striatum[76,119,349]. Variability in age of onset, which can be up to ±30 years for identical CAG repeats, has been mostly attributed to environmental factors. Though debated, it has been shown that mutHTT aggregates (or at least some forms of mutHTT aggregates) contribute to eventual cell death[117,118,124,125]. Autophagy is the primary process by which mutHTT aggregates can be degraded. However, it is thought that loss-of-function of WT HTT, via the HD mutation, disrupts autophagy-mediated aggregate clearance. In fact, WT HTT has binding motifs for both p62 and ULK-1/LC3, critical proteins for labeling and incorporation of autophagic cargo, respectively. Acting as an autophagy scaffold, WT HTT promotes proximal localization of autophagic cargo and the autophagosome itself[127-129]. Recent evidence shows that HD cells exhibit autophagy "cargo recognition failure": autophagosomes are ineffectively loaded with cargo, resulting in reduced rates of macroautophagy and an accumulation of lipids and mitochondria within the cells[131]. This deficit is suspected to impede aggregate clearance and thought to be caused by an abnormal association between mutHTT and the ubiquitin-binding protein, p62, a proposed "linker" protein between autophagosomes and their respective cargo[131]. Upregulation of autophagy via both mTOR-dependent and independent mechanisms can facilitate mutHTT aggregate clearance and rescue HD phenotypes. Genetic and pharmacological manipulation of autophagy via mTOR-dependent and independent mechanisms have been shown to promote mutHTT aggregate clearance, rescue medium spiny neuron health, and normalize motor behavior in flies and mice[87,101,104,124,126,350-354]. Given this evidence, there has been a large impetus in the field to 1) understand how mutHTT dysregulates autophagy and 2) how to manipulate autophagy pathways to promote autophagic function in HD and potentially target this process pharmacologically.

Manganese (Mn) is an essential metal, a cofactor for a variety of enzymatic processes and potent modulator of cell signaling, but in excess is neurotoxic. The highest levels of Mn in the brain normally are found in the striatum, the region of the brain most vulnerable in HD, suggesting Mn plays a particularly important, yet poorly understood, role in this brain region[32,84]. HD models exhibit striatal-specific reduced Mn uptake suggestive of a HD-dependent, brain-specific Mn deficiency[81,262,263,314]. This deficit in net Mn uptake confers increased resistance to Mn cytotoxicity in HD cells. This also

manifests as dysregulation in the Mn-dependent arginase-citrulline pathway and ATM, p53, and AKT signaling in these models, though we posit that many other Mn-responsive pathways and processes are also affected[82,315]. Recently, groups have shown that Mn exposure causes rapid, yet temporally bi-phasic, increases in common autophagy markers (p62, LC3, Beclin) in a variety of cell types and mouse models, which have been associated with both activation and inhibition of autophagy by Mn.[50,133,134,290,355-358]. Mn also is known to activate ERK, AKT, ATM, AMPK, mTOR and various transcription factors (TFEB, CREB, p53, FOXOs, etc.) all of which regulate autophagy[42,45,48,49,81,85,288,299-301,359]. Evidence supports a neuroprotective role for autophagy in the context of Mn neurotoxicity. However, given the intricacies of interpreting autophagy data, the mechanism by which Mn impinges on autophagic function, particularly in the context of HD is unknown. Given the role of Mn-responsive cell signaling proteins in the regulation of autophagy and a potentially striatal-specific Mn deficiency in HD models, we hypothesized that elevating extracellular Mn levels to restore subcellular Mn homeostasis would promote autophagic functions in HD cells via normalization of "Mn-starved" cell signaling processes. In this study, we set out to 1) employ a battery of autophagy methodologies to rigorously assess the effects of Mn on autophagy, and 2) evaluate the effects of Mn on autophagic flux and cargo sequestration in HD cells.

Results

Mn increases p62 and LC3-II/I expression after 24hrs in WT cells, presence of HD mutation suppresses this effect

Previous reports have demonstrated that Mn exposure increases expression of common autophagy proteins—namely Beclin, LC3-II and p62 [50,133,134,355,357]. However, elevated expression of these proteins can be a result of either increased autophagic flux or decreased autophagic clearance. Thus, it is still unclear whether upregulation of these proteins by Mn is indicative of inhibition or activation of autophagy. Here, we defined how Mn impinges on autophagy, particularly in the STHdh striatal neuroprogenitor cell model (Q7 and Q111, wild-type and HD models respectively), which is a widely used mouse striatal cell line model of HD. LC3 and p62 expression was measured, as a marker of autophagy. To assess LC3 turnover, we calculated an LC3-II/I ratio, as LC3II is the lipidated form of LC3I and runs faster on SDS-PAGE[360]. A 24hr Mn exposure caused significant increases in both p62 and the LC3-II/I ratio in WT cells, the increase in p62 being greater in magnitude (**Fig 4-1A,C,E**). The increase in LC3-II/I ratio was driven primarily by a decrease in LC3I rather than an increase in LC3II, consistent with the lipidation of LC3I to LC3II during the synthesis/incorporation of autophagy (**Fig 4-1A**). Mn-induced p62 and LC3-II/I was significantly blunted in HD cells. This finding is consistent with
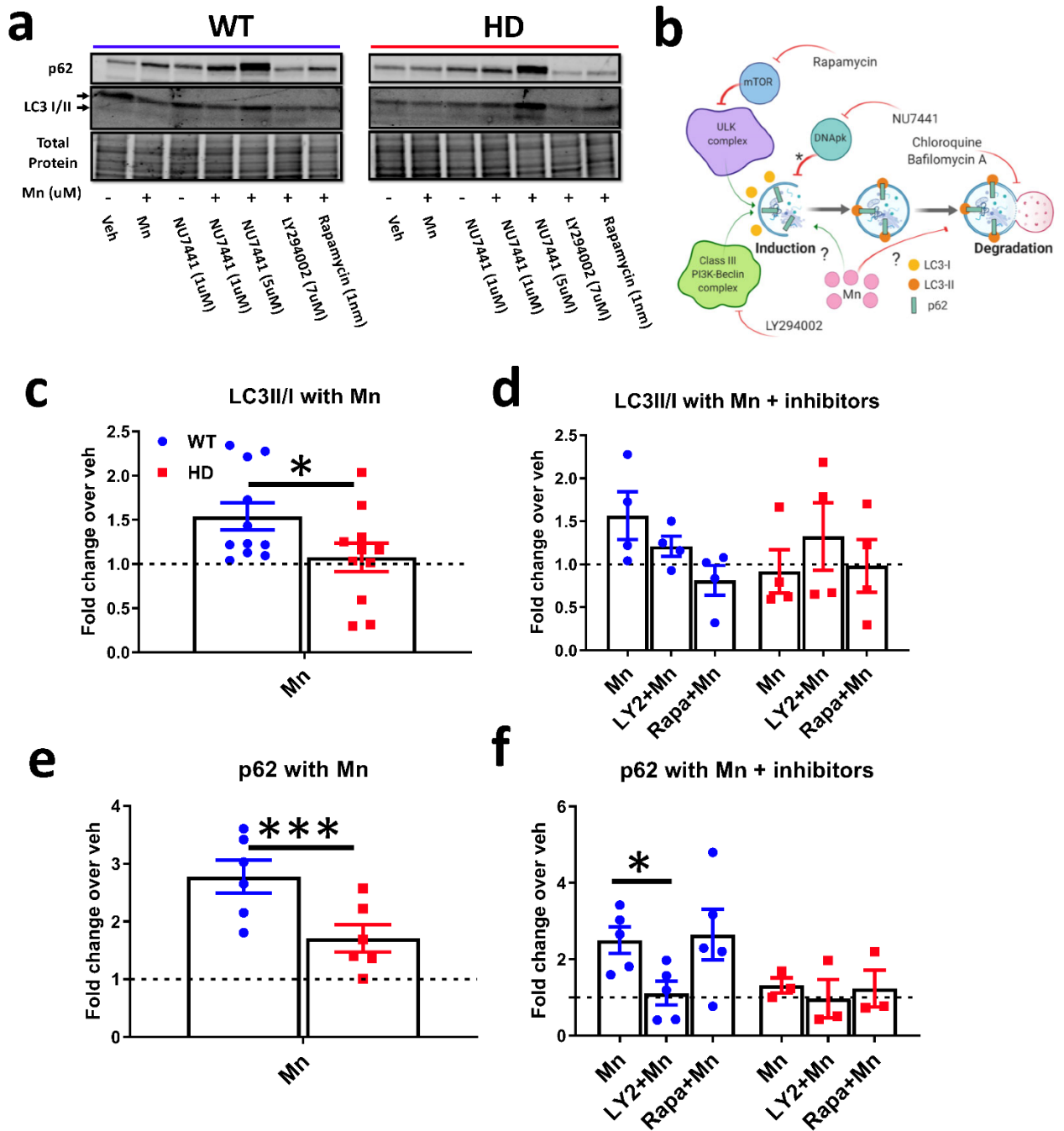
Figure 4-1: Mn increases expression of LC3-II/I and p62 which is reduced in Q111 cells. A)
representative western blot of STHdh Q7/Q7 and Q111/Q111 after 24hr exposure with Mn (50uM), NU7441
(1/5uM), LY294002 (7uM), or Rapamycin (1nM). LC3-I= top arrow, LC3-II= bottom arrow. **B**) Quantification
of LC3-II/I in cells treated with Mn only. *= significant by paired t-test. N=11. **C**) Quantification of LC3-II/I in
cells treated with Mn and LY294002 or Rapamycin. Two-way ANOVA; treatment= F(2,6)= 2.665; p=0.1485.
N=4 **D**) Quantification of p62 in cells treated with Mn only. *= significant by paired t-test. N=6. **E**)
Quantification of p62 in cells treated with Mn and LY294002 or Rapamycin. Two-way ANOVA; treatment=
F(2,6)= 5.579; p=0.0428. N=3. For Panels **B-E**, each cell line's vehicle is normalized to 1. NU7441 was
used as a control for **Fig 1A** blot but were not quantified. Blue= WT; Red= HD. Error bars= SEM. *=
significant by Dunnet's post-hoc test was used to compare back to Mn treated in Fig c, e. *P<.05, **P<.01,
***P<.001.

77

the reduced net Mn uptake phenotype observed in these cells[81,82]. To assess whether Mn-induced p62/LC3 were dependent on Mn-dependent kinases (PI3K and mTOR)[48,49] we exposed STHdh cells to a series of small molecule inhibitors to see if they modulated Mn-induced autophagy (**Fig 4-2B**). NU7441, a DNApk inhibitor known to activate autophagy[361] induced p62 expression, similar to Mn, and also exhibited synergistic, additive effects when co-exposed with Mn (**Fig 4-1A,B, 4-2A**). Co-exposure with NU7441 did not ameliorate impaired Mn-induced p62 or LC3II/I in Q111 cells **(Fig 4-2A,B)** (NU7441 inhibits mTOR and PI3K at 5uM, thus only NU7441 (1uM) was quantified and more specific inhibitors of PI3K and mTOR were used [300,362]. Interestingly, Mn-induced p62 was completely abrogated by PI3K inhibition (LY294002) but not affected by mTOR inhibition (Rapamycin), suggesting Mn-induced p62 is PI3K, but not mTOR, dependent (**Fig 4-1A,E**). LY294002 and rapamycin did not have a significant effect on Mn-induced LC3-II/I, though both inhibitors were trending to block Mn-induced LC3-II/I (**Fig 4-1A,C**). LY294002 and Rapamycin were validated to inhibit basal and Mn-induced p-AKT and p-S6, respectively, in these cells, at the same concentrations, in a previous study in our lab[300].

Mn induces autophagy by increasing autophagosome induction and formation

To determine whether Mn activates autophagic synthesis/incorporation or inhibits autophagic degradation we assessed autophagic flux via lysosomal autophagy inhibitors (chloroquine, bafilomycin A) to block autophagosome degradation, thus allowing for assessment of autophagosome induction and formation only (i.e. autophagy activators, but not inhibitors, will induce autophagic protein expression if the degradation of autophagosome is blocked) (**Fig 4-2C-F**). We first determined concentrations of inhibitors that completely inhibit autophagosome degradation. To determine the effective saturating concentrations for chloroquine (CQ) and bafilomycin A (BafA), we utilized stable, dsRed-LC3-II expressing WT and HD STHdh cells. We found that 10uM CQ and 10nM BafA caused maximal accumulation of LC3II puncta without incurring cell death or morphological changes, while super-saturating 20μM CQ caused extensive, "swiss-cheese-like" vacuolization in WT STHdh, and 20nM BafA reduced cell size and caused cell death **(Fig 4-3, 4-4).** Thus, we exposed STHdh cells to Mn and 10 uM CQ or 10 nM BafA for 24hrs and monitored p62 and LC3II/I expression. Mn increased p62 and LC3-II/I in WT and HD cells and LC3-II/I in WT cells, even in the presence of saturating concentrations of CQ (**Fig 4-5A,B,C)** or BafA (**Fig 4-5A,D,E**). This supports our hypothesis that Mn increases autophagic induction/formation. We observed similar increases in magnitude of p62 and LC3-II/I in HD cells compared to WT cells with BafA and slightly blunted responses with CQ. However, Mn did not significantly increase LC3II/I in HD cells. The observed p62 doublet in BafA-treated conditions is consistent with reports in mouse brain and liver, however we only quantified the bottom band as this was not observed in every condition[363].
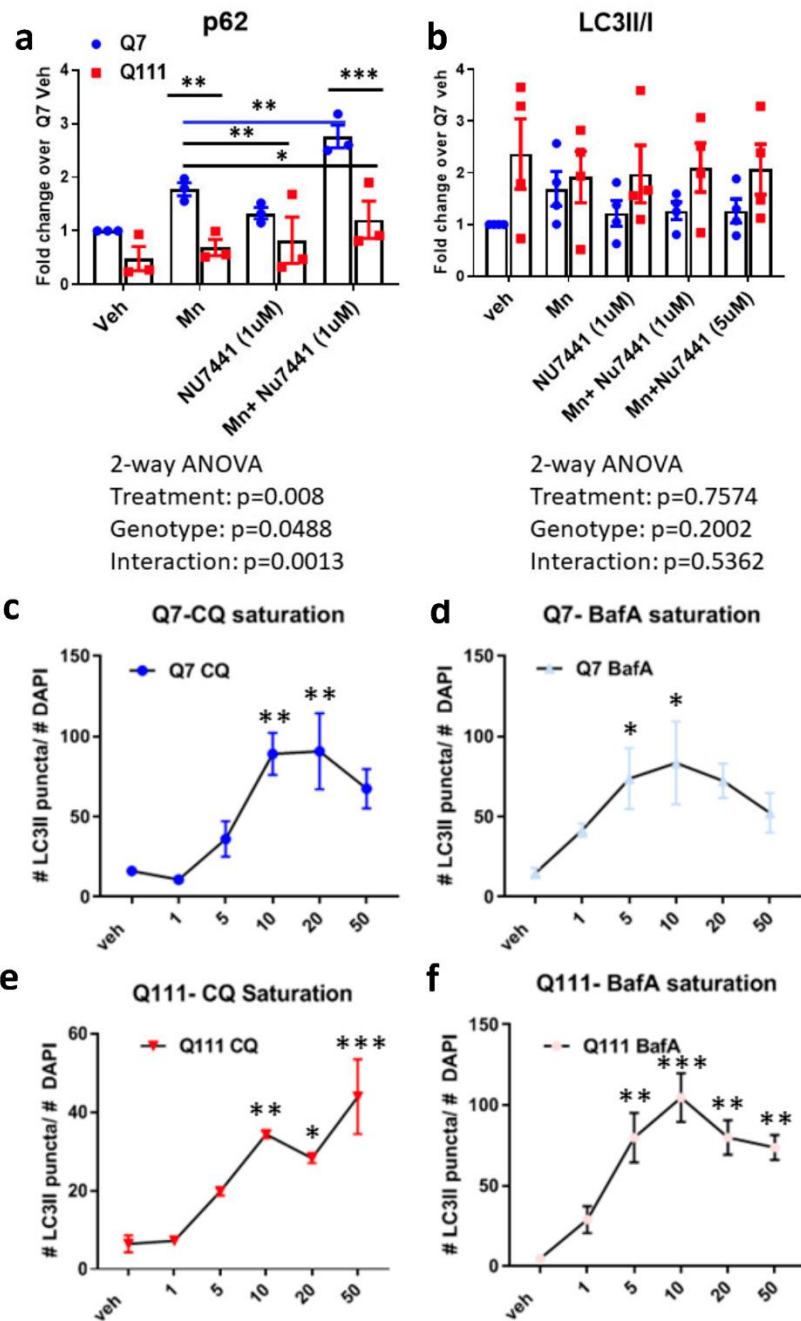
Figure 4-2: **Assessing saturating concentrations of Chloroquine and Bafilomycin A. A-B**) Quantification of p62 (**A**) and LC3II/I (**B**) from Figure 1a after exposure with Mn(50uM) and/or Mn+NU7441(1/5uM) for 24hrs. n=4. #= significant genotype difference by student t-test. **C-F**) Number of LC3-II puncta over number of DAPI puncta for STHDh Q7/Q7 cells treated with Chloroquine: Univariate ANOVA; $F_{(5,12)}= 7.540$; $p=0.0021$. (**C**) or Bafilomycin A: Univariate ANOVA; $F_{(5,12)}= 3.141$; $p=0.0484$. (**D**), and STHdh Q111/Q111 cells treated with Chloroquine: Univariate ANOVA; $F_{(5,12)}= 13.68$; $p=0.0001$. (**E**) or Bafilomycin: A Univariate ANOVA; $F_{(5,12)}= 11.86$; $p=0.00003$. (**F**) Cells were exposed for 24hrs with chloroquine (1-50uM) or Bafilomycin A (1-50nM). Quantified as (#LC3-II puncta)/(# of DAPI) per image. N= 10 images per condition, with ~5-10 cells per image; Error bars= SEM. *= significant difference by post-hoc Sidak test comparing back to vehicle for each concentration, per inhibitor. *P<.05, **P<.01, ***P<.001.

CQ Q7

BafA Q7
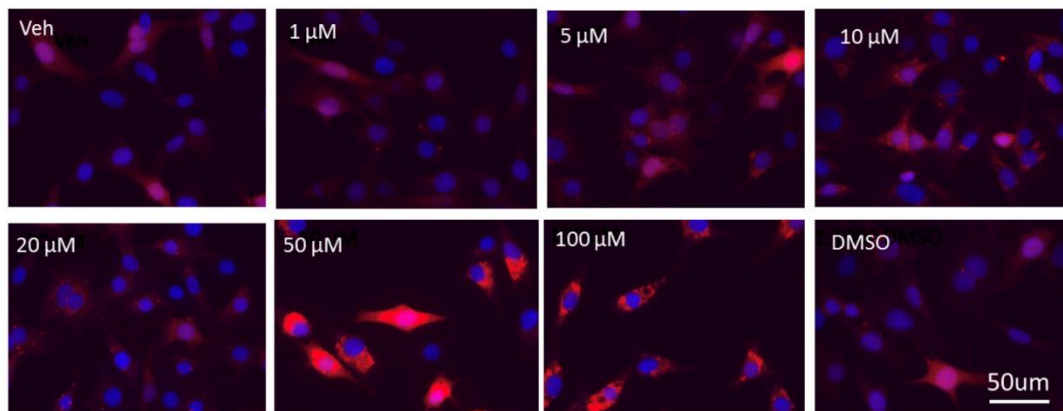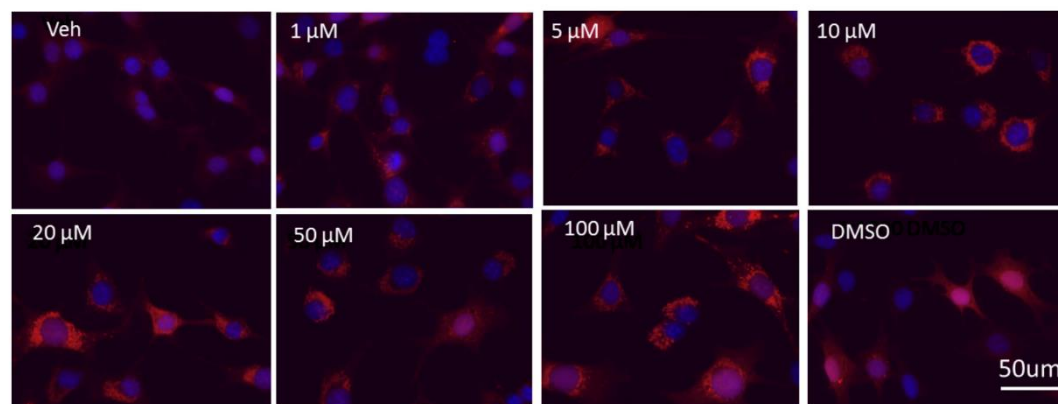
Figure 4-3: **Representative LC3-II images Q7/Q7.** Representative images (40X, Zeiss fluorescent light microscope) for lysosomal autophagy inhibitors (CQ-top, BafA-bottom) saturation curves after 24hrs in Q7/Q7 cells. Quantification in Fig 4-2.

CQ Q111

BafA Q111

Figure 4-4: **Representative LC3-II images Q111/Q111.** Representative images (40X, Zeiss fluorescent light microscope) for lysosomal autophagy inhibitors (CQ-top, BafA-bottom) saturation curves after 24hrs in Q111/Q111 cells. Quantification in Fig 4-2.
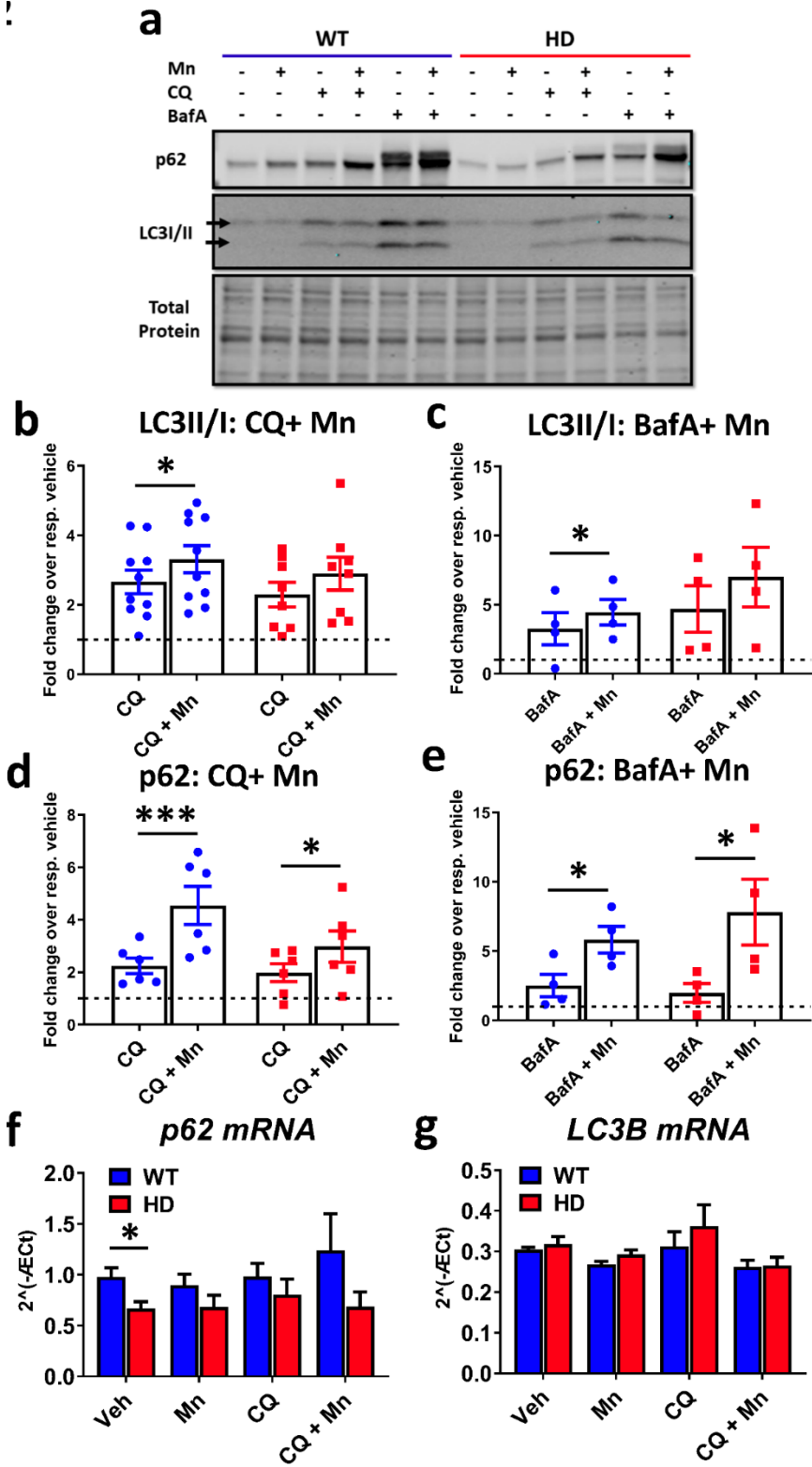
Figure 4-5: Mn increases LC3-II/I and p62 expression in the presence of Chloroquine and Bafilomycin A. A) Representative western blot of p62 and LC3-II/I in SThdh Q7/Q7 and Q111/Q111 after 24hr exposure with Mn (50uM), CQ (10uM), BafA (10nM). LC3-I= top arrow, LC3-II= bottom arrow. **B**) Quantification of LC3-II/I in cells treated with CQ+Mn. Two-way ANOVA; treatment= F(1,10)= 18.08; p=0.0017. N=8. **C**) Quantification of LC3-II/I in cells after treatment with BafA+Mn. Two-way ANOVA; treatment= F(1,3)= 2.374; p=0.2211. N=6. **D**) Quantification of p62 in cells after treatment with Mn+CQ. Two-way ANOVA; treatment= F(1,3)= 229.2; p=0.006. N=4. **E**) Quantification of p62 in cells after treatment with BafA+Mn. N=4. Two-way ANOVA; treatment= F(1,3)= 10.13; p=0.0500. In BafA-treated conditions, only the bottom band of p62 was quantified in order to compare to CQ-treated conditions where only one band was present. **F,G**) qRT-PCR analysis for p62 (**F**) and LC3B (**G**) in SThdh Q7/Q7 and Q111/Q111 after 24hr hour treatment with Mn (50uM) and/or CQ (10uM). N=4 for qRT-PCR results. Two-way ANOVA for p62; treatment= F(1.296,3.887)= 0.7953; p=0.4590, Two-way ANOVA; genotype= F(1,3)= 17.63; p=0.0247; Two-way ANOVA for LC3B; treatment= F(1.296,3.887)= 0.7953; p=0.4590, Two-way ANOVA; genotype= F(1,3)= 17.63; p=0.0247. Blue= WT; Red= HD. Error bars= SEM.*= significant difference from vehicle by post-hoc comparisons. *P<.05, **P<.01, ***P<.001. For Fig b-e, Sidak's multiple comparison test compared CQ/BafA and Mn+CQ/BafA for each genotype. For Fig f,g; Dunnet's multiple comparison test compared all treatments back to vehicle for each genotype.

Mn-induced LC3 and p62 protein expression is not due to an increase in mRNA expression

We tested the hypothesis that Mn upregulates p62 and LC3B expression by increasing their mRNA expression. Mn and/or CQ exposure did not significantly change p62 or LC3B mRNA expression in either genotype (**Fig 4-5F,G**). We did not observe a difference in basal LC3B mRNA between Q7 and Q111 cells, but observed a genotype difference in basal p62 mRNA. However, as no large increases in mRNA expression were observed, the Mn-induced modulation of protein markers of autophagy is not consistent with a transcriptional mechanism in these cells.

Mn increases free ATG5, but not ATG5-12 complex, and decreases p-ERK expression

The ATG5-12 complex facilitates lipidation and conversion of LC3I to LC3II[364]. Mn increased free ATG5 expression in WT but not HD cells, but it did not increase expression of the ATG5-12 complex. Interestingly, CQ had no effect on free ATG5 or ATG5-12 (**Fig 4-6A-C**). This difference between Mn and CQ, a known autophagy inhibitor, further supports the hypothesis that Mn activates autophagy. Furthermore, Beclin expression was unchanged by Mn or CQ/BafA (**Fig 4-6A**). All together, these observed increases in autophagy-related proteins after Mn treatment, under saturating concentrations of CQ/BafA suggest Mn promotes autophagic synthesis/incorporation. Additionally, other groups have found that Mn increases p-ERK in astrocytes which regulates lysosomal activity. However, we found that Mn exposure in WT STHdh cells actually decreased p-ERK expression. HD cells exhibited reduced basal p-ERK and were unresponsive to Mn treatment (**Fig 4-6D,E)**.

Mn-induced autophagy increases autophagic vacuole area

An increase in autophagic markers (LC3/p62) can be indicative of 1) increased number of autophagosomes or 2) increased area and content of autophagosomes. To explore whether Mn-induced autophagy resulted in increased autophagic vacuole (APV) area, we utilized electron microscopy, the gold-standard method to assess autophagy. Because of the density of APVs in some conditions, number of APVs could not be assessed. We observed a slight increase in APV area with Mn alone in both WT and HD cells, this was only significant in Q111 cells treated with 50 µM Mn (**Fig 4-7C**). This discrepancy was not surprising, as autophagy is in flux without addition of lysosomal autophagy inhibitors, so detecting small changes in active autophagy by EM would likely need a much higher sample size. However, CQ+50 µM Mn significantly increased APV area over CQ alone in Q7 cells only and BafA+50 µM Mn was also trending but not significantly (**Fig 4-7D**). We also observed increased presence of larger, multi-vesicular bodies with treatment of Mn with CQ or BafA
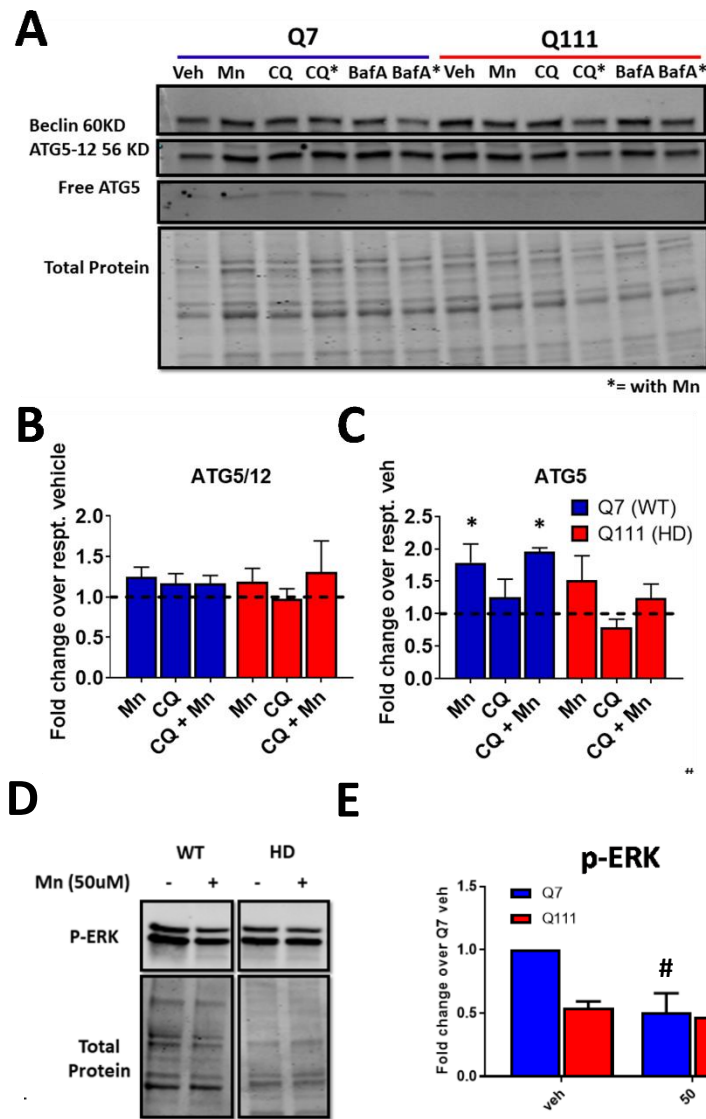
Figure 4-6: Mn increases free ATG5 expression. A) Representative western blot for Beclin, free ATG5, ATG5-12 complex of STHdh Q7/Q7 and Q111/Q11 treated with Mn (50uM), CQ (10uM), and BafA (10nM). **B)** Quantification of ATG5 complex **C)** Quantification of free ATG5-12. Veh, Mn, CQ, CQ+Mn conditions quantified. Beclin was unchanged and not quantified. **D)** Representative blot of p-ERK after 24-hr Mn treatment. **E)** Quantification of p-ERK.N=3; Error bars= SEM; *= significant difference by student t-test; #= significant difference by 95% CI.
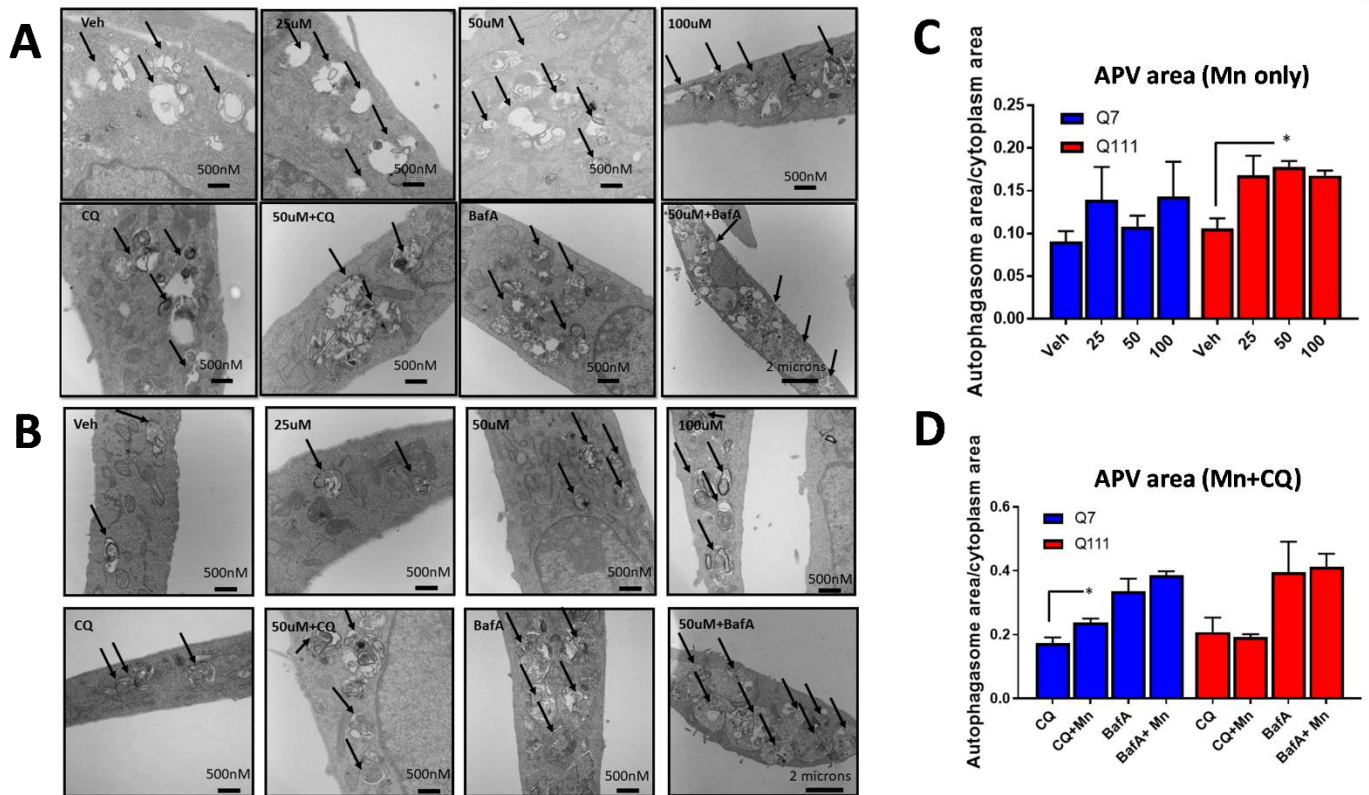
Figure 4-7: Mn increases autophagic vacuoles area. A) Representative EM images from WT Q7/Q7 cells. **B**) Representative EM images from HD Q111/Q111 cells. Assessment of relative autophagasomal vacuole area over cytoplasm area per image in STHdh Q7/Q7 and Q111/Q111 after 24hr treatment. **C**) APV area after treatment with Mn alone **D**) APV area after treatment with Mn+CQ. Quantification of 8-20 images per condition for two separate TEM sections from each of two biological replicates. Error bars= SEM *= significance by student t-test. ***Work done with the assistance of Michael O'Brien.***

(Fig 4-7A,B). Contrary to our western blot findings, we did not observe significant increases in APV area in the Q111 cells when co-exposed with Mn and CQ/BafA (**Fig 4-7D**). We also did not observe a basal difference in APV area between WT and HD cells. These differences may be a result of the fact that autophagosome area was measured instead of autophagosome number or because we cannot easily distinguish between an autophagosome and an autophagolysosome by EM. Both of these factors should be taken into consideration while comparing results from various autophagy methods.

Mn induces LC3II/I, but not p62, expression in non-neuronal cell lines

We hypothesized that Mn induced autophagy may be specific to neuronal cell types, as the vast majority of studies investigating Mn and autophagy have examined neuronal regions/cells, and the brain is a primary source for Mn toxicity (citations). To test this, we used immortalized neuronal (Neuro2A) and non -neuronal (HEK293, human lymphoblasts) and exposed them to Mn and/or CQ. For this set of experiments, we also utilized a second autophagy inhibitor, KB-R7943 (KBR), as a secondary confirmation for our results with CQ (Long et al., 2016). 100 µM Mn+CQ/KBR was able to increase p62 and LC3II/I expression over CQ/KBR alone in Neuro2A and LC3II/I only in HEK293 cells (**Fig 4-8A-F**). KBR was able to recapitulate the effects of CQ in the N2A cells. In human lymphoblasts, LC3 was hard to detect under Mn-alone treated conditions and p62 did not exhibit a stable trend (**Fig 4-8G**). However, 100 µM Mn+CQ increased LC3II/I more than CQ alone (**Fig 4-8G**). Together, these findings suggest that Mn-induced LC3II/I is shared by other cells lines, both neuronal and non-neuronal. As all neuronal lines tested exhibited Mn-sensitive p62 expression and all non-neuronal lines exhibited lack of Mn-induced p62, this brings up the interesting possibility that Mn-induced p62 expression is specific to neurons. However, overall, this data suggest Mn-induced autophagy is not specific to these cells."

Exposure with chloroquine/bafilomycin A increases net Mn uptake in Q111 cells, attenuating defective Mn-induced autophagy

To gain mechanistic insight into why Mn exposure, under conditions where autophagy degradation is inhibited, induces LC3-II/I and p62 in HD cells to the same magnitude as WT cells (despite established reductions in net Mn accumulation in HD cells; (**Fig 4-4A-E**), we tested the hypothesis that CQ and BafA are capable of normalizing Mn uptake in HD cells. Using the cellular fura-2 Mn uptake assay (CFMEA) developed in our lab[262], we assessed net Mn uptake after 24hr exposure with Mn and CQ/BafA. Interestingly, CQ and BafA increased net Mn uptake in both Q7 and Q111 cell lines exposed to 25 µM Mn (**Fig 4-9A-B**). The lower 25 µM Mn concentration was used to test for the
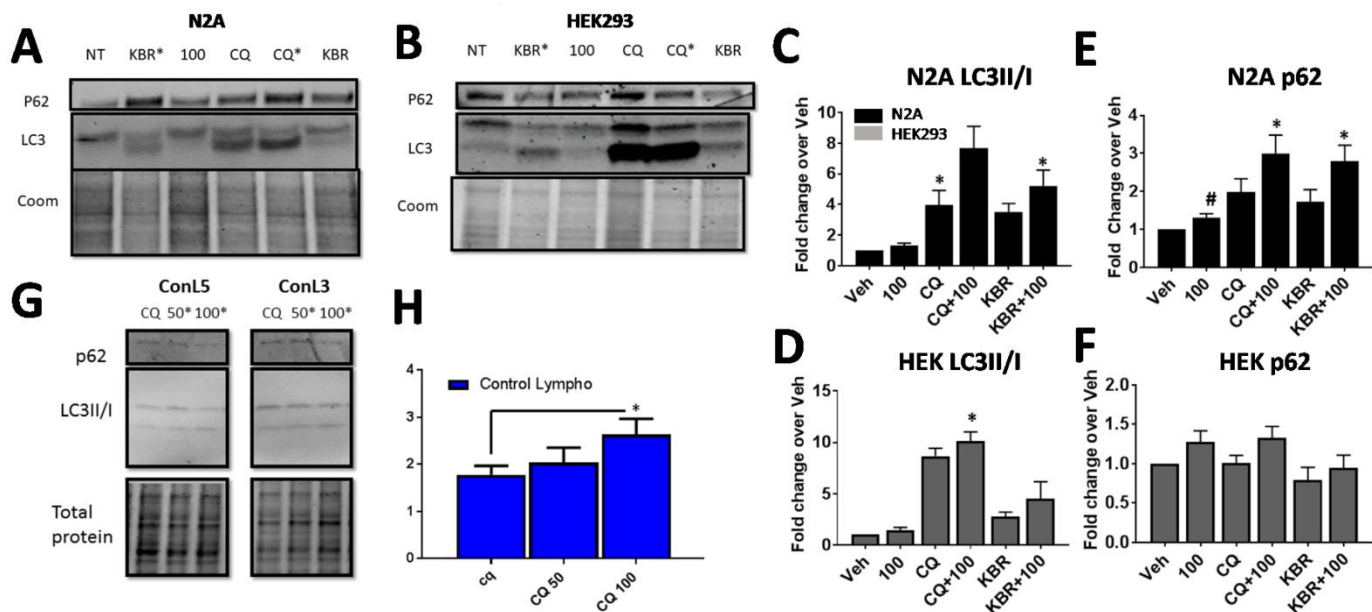
Figure 4-8: Mn induces autophagy in other neuronal and non-neuronal cell lines. Representative western blot for Neuro2A (**A**) and HEK293 (**B**) cells after 24hr Mn or CQ treatment. KB-R7943 is another inhibitor that was used but not quantified. Quantification of LC3II/I for N2A(**C**) and HEK293 (**D**). Quantification of p62 for N2A(**D**) and HEK293 (**F**) (**G, H**) Representative western blot and LC3II/I quantification in human-derived lymphoblasts after 24hr Mn+CQ treatment. P62 not quantified. N=3 or more for all experiments. Error bars= SEM; #= significance difference from veh by 95%CI to vehicle (=1); *= significant difference by student t-test
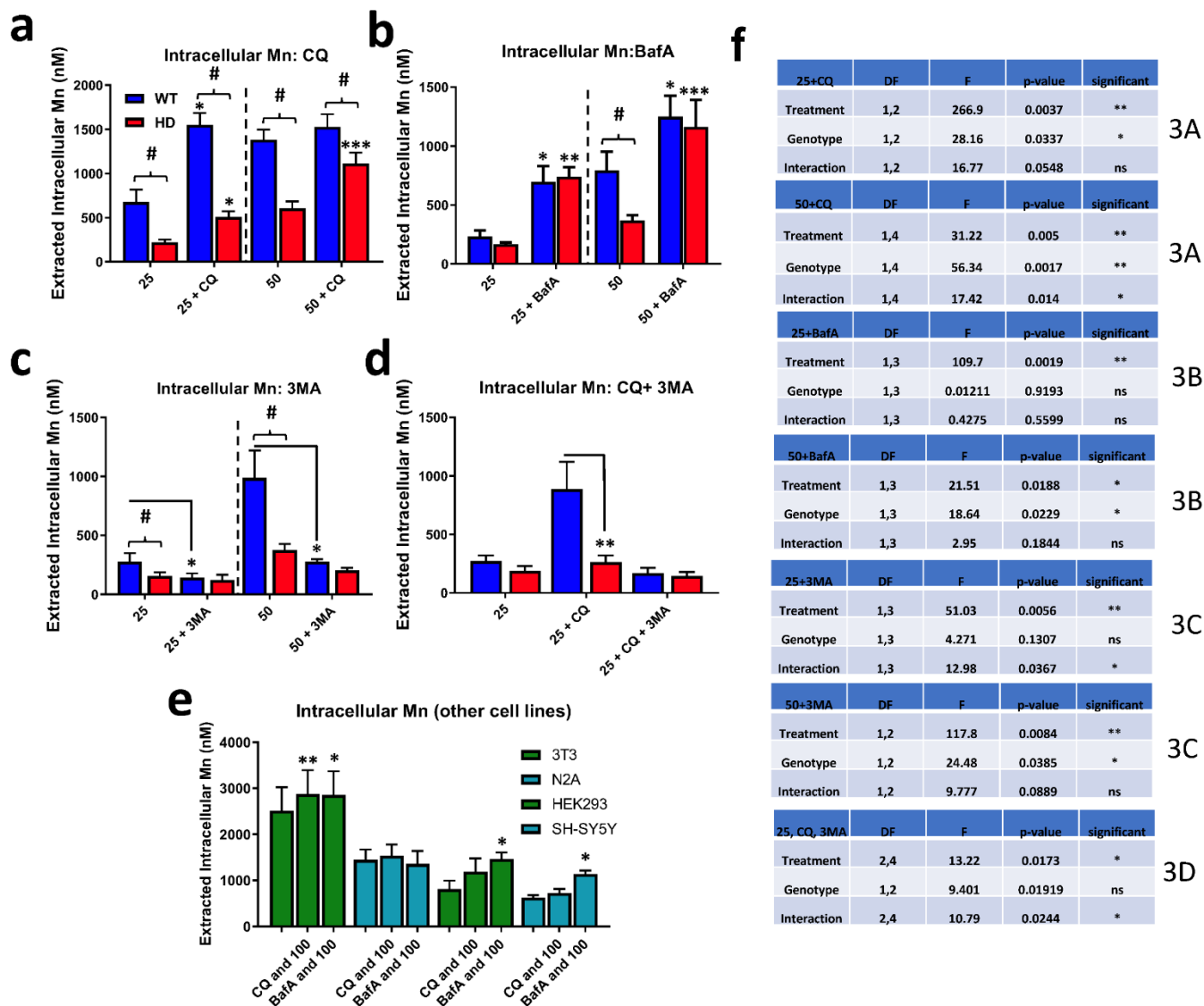
Figure 4-9: Chloroquine and Bafilomycin A increase net Mn uptake which is blocked by 3-methyladenine. Assessment of intracellular Mn by CFMEA in STHdh Q7/Q7 and Q111/Q111 cells after 24hr exposure with **A**) Mn (25/50uM) and CQ (10uM) **B**) Mn (25/50uM) and BafA (10nM), **C**) Mn (25/50uM) and 3MA (5mM), and **D**) Mn (25uM), CQ (10uM), and 3MA (5mM). Note: dashed lines separate experiments where 25uM or 50uM Mn was used. N=3 for all experiments; Error bars= SEM. Blue= WT; Red= HD. #=significant genotype difference; *= significance by Sidak multiple comparison test. Two-way ANOVA analysis in Supp Fig 4. **E**) CFMEA measuring intracellular Mn levels in NIH3T3, Neuro2A, HEK293, and SH-SY5Y cells after 24hr exposure with Mn (100uM), CQ (10uM), and BafA (10nM). **F**) Two-way ANOVA statistics. *= significance by paired student's t-test compared to Mn alone at same concentration. *P<.05, **P<.01, ***P<.001. ***Work done with the assistance of Michael O'Brien.***

possibility of a Mn-uptake ceiling effect in Q7 cells at the higher concentration. After exposure to 50 µM Mn, (the same concentration used in previous experiments) we found CQ and BafA normalized net Mn uptake between the control and HD cell lines (**Fig 4-9A,B**)**.** Furthermore, these increases were completely blocked with addition of 5mM 3-methyladenine (3MA), an autophagy inhibitor that blocks activation of autophagy by inhibiting class III PI3K (**Fig 4-9D**). Additionally, 3MA alone was able to reduce net Mn uptake in these cells. 3MA reduction of Mn uptake could be due to inhibition of class III PI3K, or possibly through off-target inhibition of class I PI3K (**Fig 4-9C**), consistent with our recent report that inhibition of class I PI3K in these cells reduces net Mn uptake[300]. We found that CQ and BafA increased net Mn uptake in other cell lines (3T3, HEK293, SH-SY5Y), though to a lesser extent than seen for STHdh cells (**Fig 4-9E**). These data, 1) explain why Mn-induced autophagy is similarly affected in WT and HD STHdh cells that are co-exposed with Mn+CQ, despite the reduce Mn accumulation usually seen in the HD STHdh cells; and 2) suggest that autophagy plays a novel role in Mn homeostasis which contributes to the impaired Mn uptake in HD cells.

HD genotype suppression of Mn-induced autophagy markers is also observed in human patient-derived striatal neuroprogenitors

We investigated whether Mn-induced autophagy was also a phenotype in non-transformed neural precursor cells derived from HD patient derived-induced pluripotent stem cells. Utilizing a differentiation protocol developed in our lab, we differentiated three control and three HD patient-derived cell lines to 11-day old Islet-1 expressing striatal-like neuroprogenitors[82]. These cells were exposed to 200 µM Mn with or without CQ/BafA for 24hrs. Previous reports from our lab show 200uM Mn exposures in these human cells results in nearly the same amount of intracellular Mn (nm/ug DNA) as STHdh cells after 50uM[82]. Mn induced LC3-II/I expression (with BafA) was similar between control and HD cells (**Fig 4-10A,B**). However, Mn-induced p62 was severely blunted in all Mn-exposed conditions in HD patient-derived cells (**Fig 4-10A,C,D**). We did not detect a difference in basal p62 expression. We also noted that CQ had little effect on LC3 or p62 expression in these cells; in a separate experiment, we used CQ at twice the concentration (20uM) and still observed no change in the expression of LC3 or p62 (**data not shown**). The lack of an observable LC3-II band in most conditions may reflect highly-efficient autophagy processing in these cells. As CQ and BafA inhibit autophagic degradation somewhat differently (CQ inhibits lysosome-autophagosome binding, BafA primarily prevents acidification of lysosomes[365-367]), this may explain why BafA, but not CQ, resulted in a prominent LC3-II band. These data suggest Mn can activate autophagy in hiPSC-derived neuroprogenitors, and that defects in Mn-induced autophagy, particularly Mn-induced p62, are present in both HD mouse and human striatal neuroprogenitors.
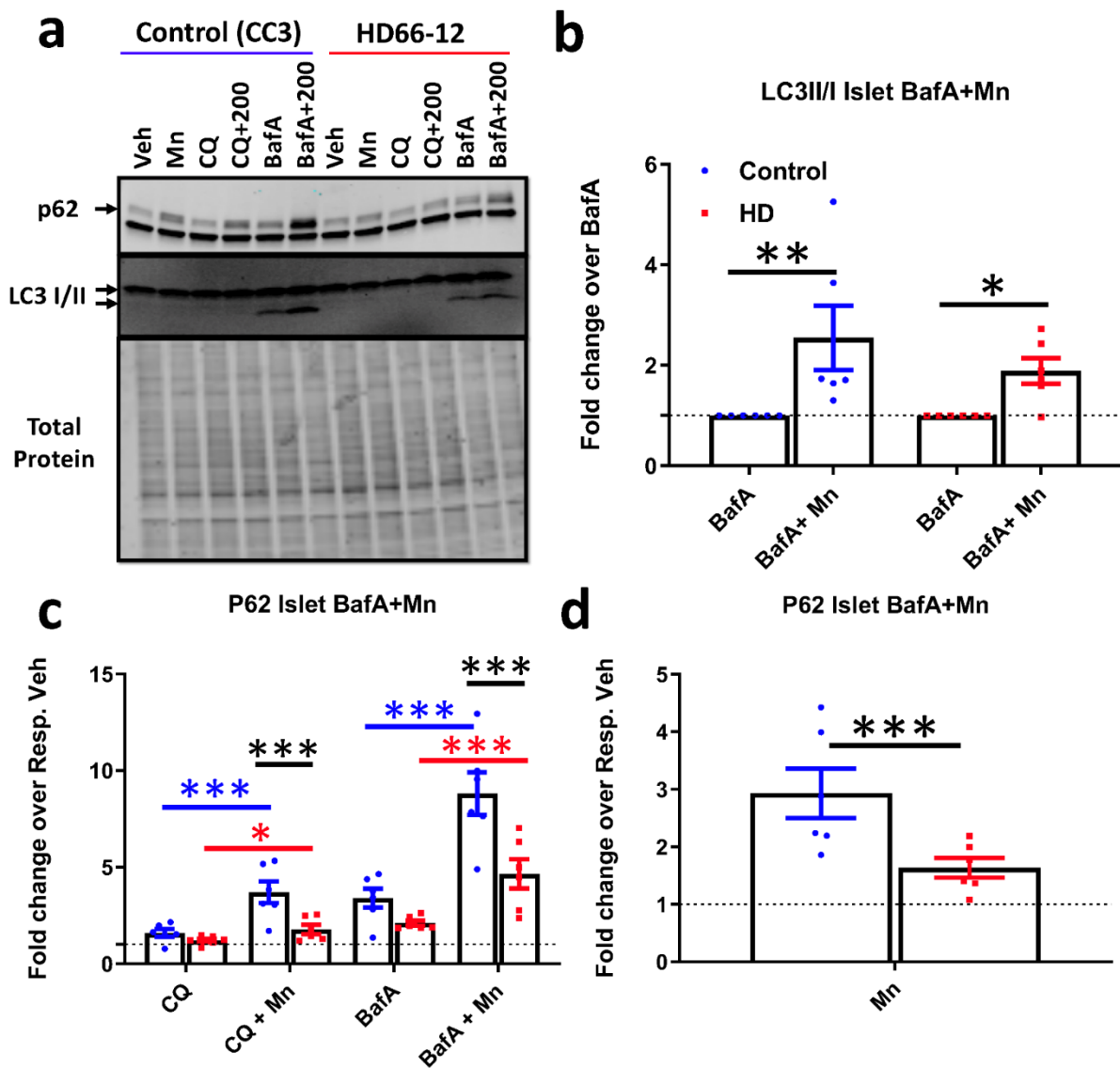
Figure 4-10: HD patient iPSC-derived neuroprogenitors exhibit defects in Mn-induced autophagy A)
Representative western blot of p62 and LC3-II/I in hiPSC-derived neuroprogenitors (CC3=control cells; HD66-12
= HD cells) after 24hr exposure with Mn (200uM), CQ (10uM), and BafA (10nM). p62= top arrow, (non-specific
LC3 band below p62); LC3-I= top arrow, LC3-II= bottom arrow. **B**) Quantification of LC3-II/I in cells treated with
BafA and BafA+Mn. N=5. Dotted line: BafA=1. Two-way ANOVA; $F(1,4)= 20.38$; $p=.0107$. **C**) Quantification of
p62 after treatment with Mn and CQ, and BafA. **D**) Quantification of p62 after treatment with Mn alone. Error
bars= SEM. Blue= WT; Red= HD. N=6. Dotted line: vehicle=1. Two-way ANOVA; treatment= $F(4,20)= 65.73$;
$p=0.0001$; genotype=$F(1,5)= 13.40$; $p=.0146$; treatment-genotype interaction= $F(4,20)=3.730$; $p=.0200$. *=
significant by Sidak (b) Tukey's (c) multiple comparison test. Blue *= WT treatment difference; red*= HD
treatment difference; black *= genotypes difference. *P<.05, **P<.01, ***P<.001.

89

HD-dependent defects in Mn-induced autophagy are corroborated by reduced LC3-II puncta

In order to confirm our western blot findings, we also performed LC3-II fluorescent microscopic analyses. To quantify specifically LC3-II we utilized dsRED-LC3-II expressing STHdh cells. Q7 and Q111 cells exhibit similar levels of basal LC3-II puncta (**Fig 4-11A**). CQ induced LC3 puncta in both cell lines, though to a lesser magnitude in HD cells (**Fig 4-11C, 4-12B, 7A,B**). Mn alone increased LC3-II puncta significantly in both cell lines, though this occurred at significantly lower concentrations in WT cells and this genotype and genotype x Mn difference was significant by two-way ANOVA (**Fig 4-11B, 4-12A, 7A,B**). Contrarily, Mn-induced autophagic flux (i.e. with CQ) was similar, if not more sensitive, in HD cells (**Fig 4-11D, 4-12A,B**), similar to our western blot results, and is likely due to the normalization of net Mn uptake after CQ exposure in STHdh cells. In addition, we measured autophagic severity in Q7 cells via a 4-point, blinded assessment and observed similar results (**Fig 4-12C**). Mn induced p62 puncta similarly to LC3-II puncta, even in presence of CQ (**Fig 4-14A-C),** however, we did not detect a genotype difference between Q7 and Q111 cells (**data not shown)** likely due to limited sensitivity of this assay and analysis**.** Mn did not increase co-localization between LC3-II and p62 (**data not shown**). Taken together, these results strongly support the conclusion that reduced Mn-induced autophagy in HD can be attenuated by restoring Mn levels to a non-deficient condition.

Lysosomes are necessary for the proper degradation of autophagosomes and, thus, modulation of lysosomal processing can be reflected in autophagic measures. Previous reports found Mn decreased lysosome number and increased lysosome size[133]. We quantified the number of lysosomes via Lysotracker in dsRED-LC3-II-expressing STHdh cells. As predicted, CQ increased Lysotracker puncta in Q7 and Q111 cells. Mn did not affect the number of lysosomal puncta in WT cells, but reduced puncta slightly in HD cells at 50uM (**Fig 4-11E, 4-15, 4-16**). This suggests Mn-induced autophagy with these cells/conditions is not a secondary effect of a Mn-lysosome interaction.

Mn induced autophagy is cation-specific and occurs in a dose-dependent manner

Up to this point our data supported the hypothesis that increasing cellular Mn levels activates autophagy, but it has been unclear whether this effect was specific for Mn. Many other metals are capable of modulating autophagy, however, it is unknown whether this is through activation or inhibition of autophagic flux, or whether this can occur at sub-toxic concentrations[368-371]. To assess whether other metal cations activate autophagy similarly to Mn at similar concentrations we measured LC3-II puncta in dsRed-LC3-II-expressing Q7 cells after 24hr exposures with Mn, Mg, Fe, Cu, Zn, Ni, and Co with
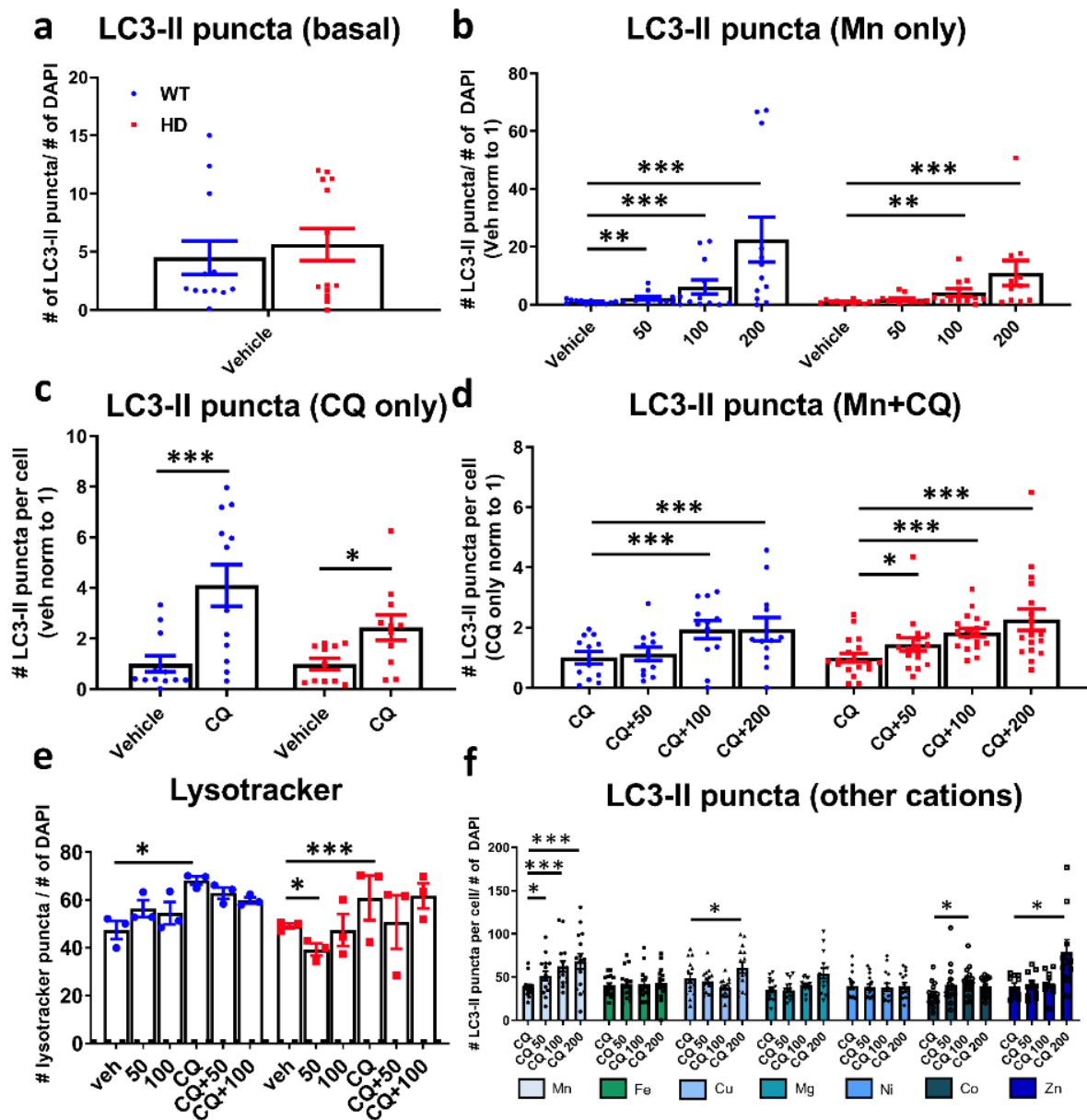
Figure 4-11: Mn increases LC3-II puncta. Quantification of number of LC3-II puncta over number of DAPI in STHdh Q7/Q7 and Q111/Q111 after 24hr exposures with: **A**) Untreated (basal), **B**) Mn (50/100/200uM), **C**) CQ (10uM), or **D**) Mn (50/100/200uM) + CQ (10uM). Quantified as (# of LC3-II puncta)/(# of DAPI) per image. N=3-4 biological replicates; each with 5 images per condition. Images of the vehicle treatment (or CQ in panel f) per biological set were all averaged and this value was set to 1. All other data points in each biological set were normalized respective to this value. Error bars= SEM. Two-way ANOVA statistics for panel b-d shown in Supp Fig 5. **E**) Quantification of number of lysotracker puncta per number of DAPI puncta after 24hr treatment with Mn (25/50/100uM) and/or CQ (10uM) in STHdh Q7/Q7 and Q111/Q111. Quantified as (# lysotracker puncta)/(# of DAPI) per image. Two way ANOVA; treatment= $F_{(5,70)}$= 9.456; p=<0.0001. N=3 biological replicates with 5 images per set. Error=SEM. Blue= WT; Red= HD. **F**) Quantification of LC3-II puncta after 24hr treatment with Cu, Fe, Mn, Mg, Ni, Co, or Zn (0/50/100/200uM) with CQ (10uM) for 24hrs. Two way ANOVA; treatment= $F_{(31,34)}$= 15.43; p=<0.0001. N=3 biological replicates, each with 5 images per condition. Quantified as (# puncta)/(# of DAPI) per image. Error bars= SEM. *= significant difference from Veh (b,c,e) or CQ (d,f) by Dunnet's multiple comparison test. *P<.05, **P<.01, ***P<.001. ***Work done with the assistance of Michael O'Brien and Audra Foshage.***

91
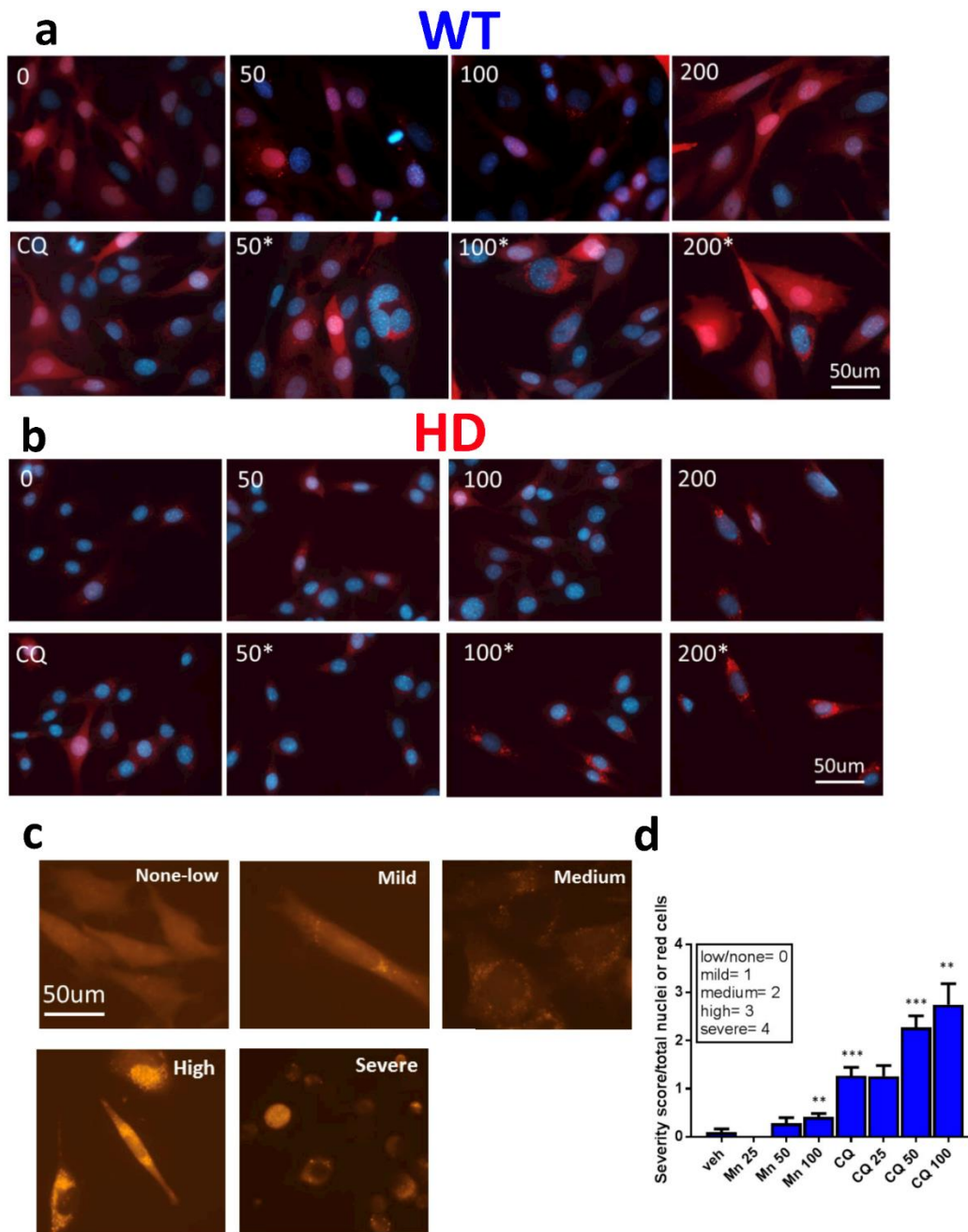
Figure 4-12: **Mn increases LC3-II puncta- representative images. A, B**) Representative images (40X, Zeiss fluorescent light microscope) of WT Q7/Q7 (**A**) and HD Q111/Q111 (**B**) cells after 24hr exposure with Mn (50/100/200uM) and/or CQ (10uM). *= indicated Mn concentration also exposed with 10uM CQ. Quantification in Figure 5a-d. **C,D**) Qualitative scoring of LC3-II puncta severity following 24hr Mn (25/50/100uM) and/or CQ (10uM) exposure in WT Q7/Q7 cells. Images were taken by one individual, randomized by a second individual, and graded 0-4 by a third individual. (**C**) Representative images for scoring. (**D**) Quantification of scoring. Error= SEM; N=3 with 3 images per condition, per set. Mn alone and CQ alone were compared against vehicle, CQ+Mn were compared to CQ alone. *= significant by student's t-test compared back to Mn (25-100uM) or CQ alone (CQ+25-100uM). *P<.05, **P<.01, ***P<.001.

a

Fig 5B	DF	F	p-value	Significant
Mn x HD interaction	3	F (3, 86)= 2.819	.0437	*
Mn	3	F (3, 86)= 8.109	<0.0001	***
HD	1	F (1, 86)= 4.357	0.0398	*

b

Fig 5C	DF	F	p-value	Significant
Mn x HD interaction	3	F (1,42)= 2.454	0.1247	ns
CQ	1	F (1, 42)= 18.20	0.0001	***
HD	1	F (1, 42)= 2.454	0.1247	ns

c

Fig 5D	DF	F	p-value	Significant
Mn x HD interaction	3	F (3, 86)= 0.4435	0.7225	ns
Mn	3	F (3, 86)= 7.284	0.0002	***
HD	1	F (1, 86)= 0.6728	0.4143	ns

Figure 4-13: Mn increases LC3-II puncta-two-way ANOVA. A-C) Two-way ANOVA results for LC3-II immunofluorescence quantification in Figure 5: A Mn alone, **B**) CQ alone, and **C**) Mn+CQ.
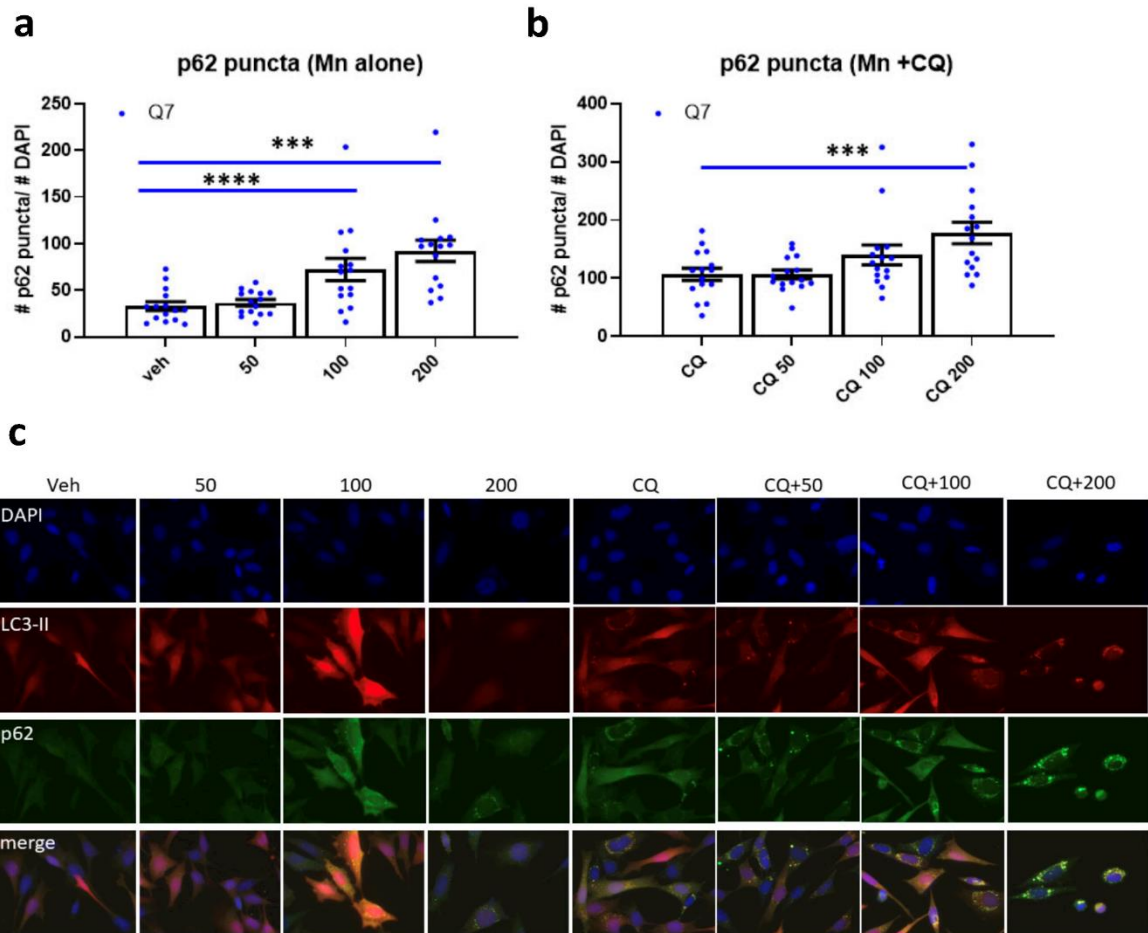
Figure 4-14: Mn induces p62 puncta. Quantification of number of p62 puncta over number of DAPI in STHdh Q7/Q7 and Q111/Q111 after 24hr exposures with: **A**) Mn (50/100/200uM) or **B**) Mn (50/100/200uM) + CQ (10uM). Quantified as (# of p62 puncta)/(# of DAPI) per image. N=3 biological replicates; each with 5 images per condition. Error bars= SEM. Two way ANOVA; treatment= F(7,223)= 34.24; p=<0.0001. genotype= F(71,223)=4.719; p=.0309. *= significant difference within genotype by Tukey's post-hoc analysis. p=<0.0001. P<.05, **P<.01, ***P<.001. **C**) Representative images of p62 and LC3-II puncta after 24hr treatment. p62= green; LC3-II= red; DAPI= blue.

Q7/Q7 Lysotracker

a

Q111/Q111 Lysotracker

a

b

b
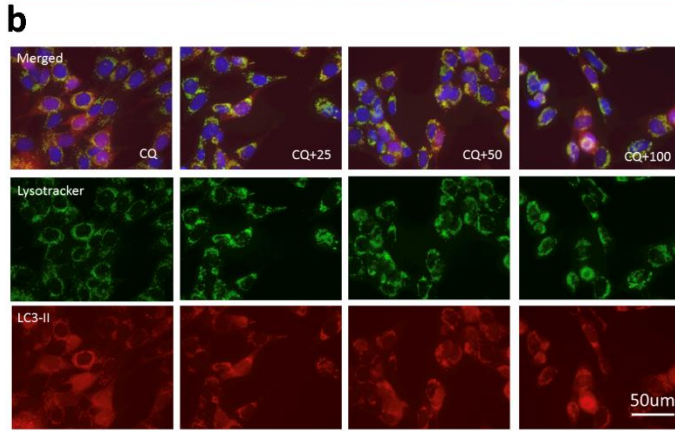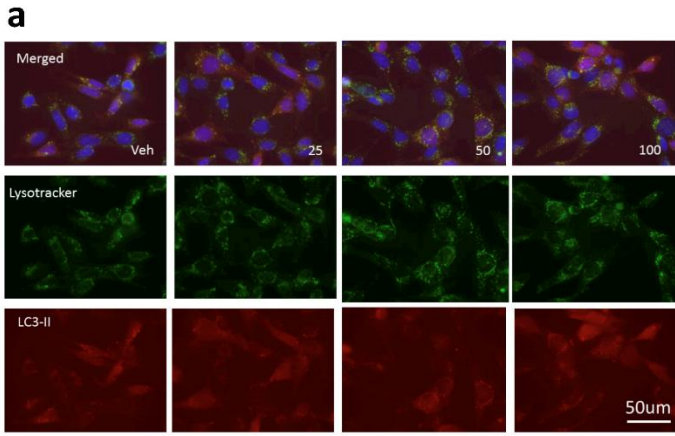
Figure 4-15: **Representative Lysotracker images Q7/Q7.** Representative fluorescent microscopy (40X, Zeiss fluorescent light microscope) images of dsRED-LC3-II (Red), lysotracker (Green), and both merged with DAPI (Blue) for Q7/Q7 cells treated with Mn alone (25/50/100uM) (**A**) or CQ (10uM) + Mn (25/50/100uM) (**B**). Quantification in Figure 4-11E. *Work done with the assistance of Michael O'Brien.*
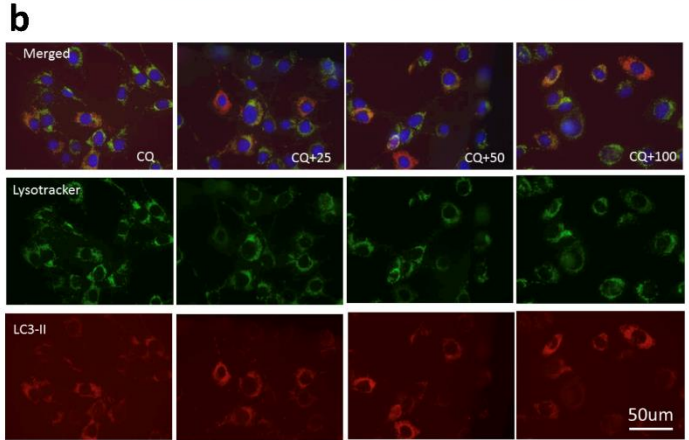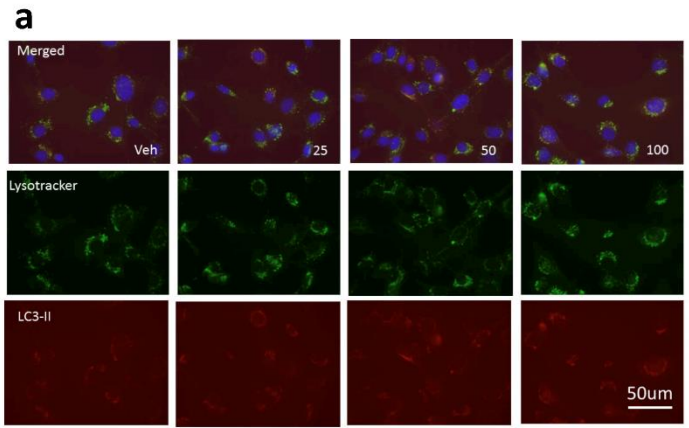
Figure 4-16: **Representative Lysotracker images Q111/Q111.** Representative fluorescent microscopy images (40X, Zeiss fluorescent light microscope) of dsRED-LC3-II (Red), lysotracker (Green), and both merged with DAPI (Blue) for Q111/Q111 cells treated with Mn alone (25/50/100uM) (**A**) or CQ (10uM) + Mn (25/50/100uM) (**B**). Quantification in Figure 4-11E. *Work done with the assistance of Michael O'Brien.*
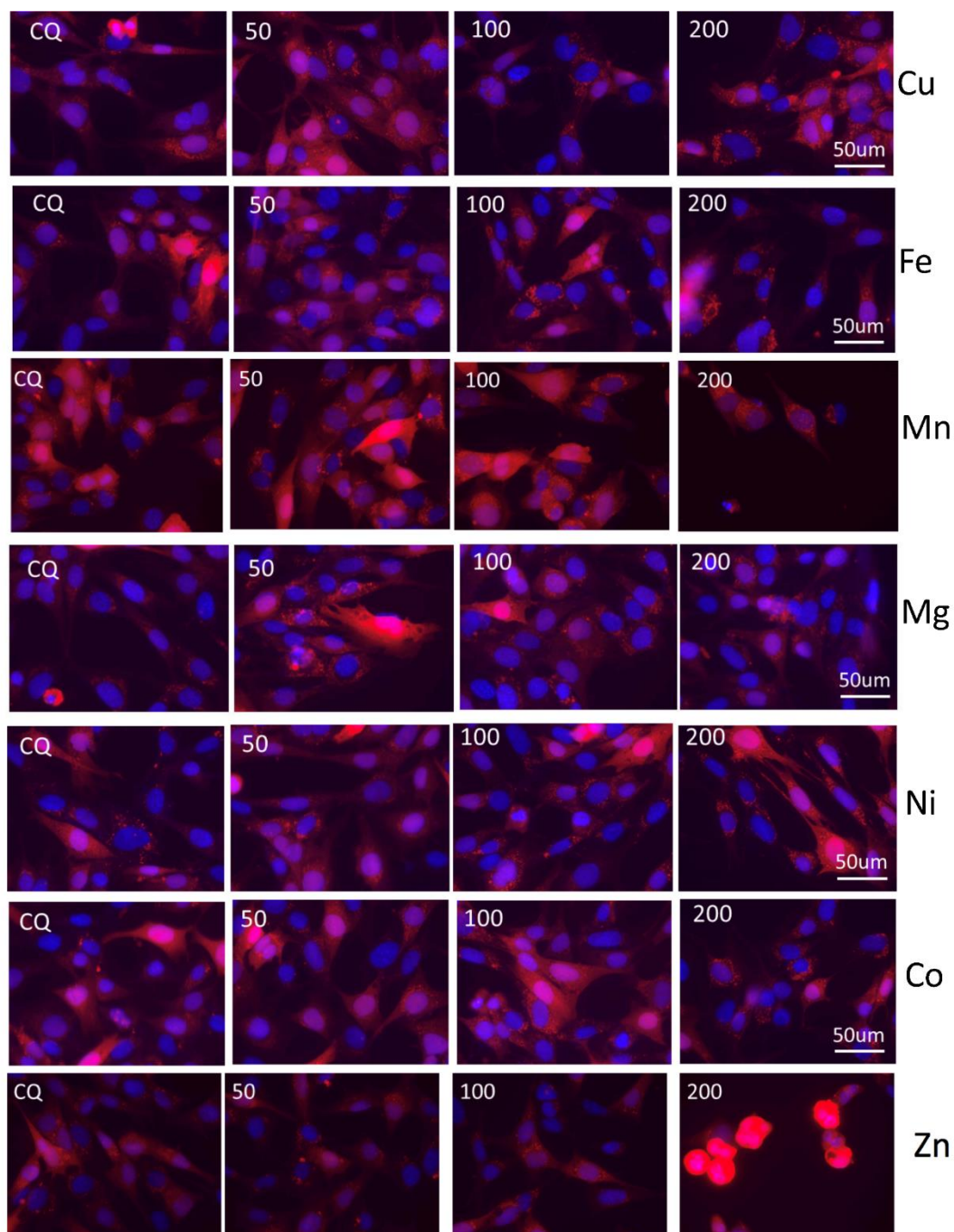
Figure 4-17: **Other cations do not increase LC3-II puncta- representative images.**
Representative images (40X, Zeiss fluorescent light microscope) for ds-RED LC3-II (Red) and
DAPI (Blue) in Q7/Q7 STHdh after 24hr exposures with 10uM CQ and 50/100/200uM Cu, Fe,
Mn, Mg, Ni, Co, and Zn. Quantification in Figure 4-11F. *Work done with the assistance of
Michael O'Brien.*

cells. LC3-II puncta induced by other metals (Cu, Co, Zn) trended upward only with higher doses and this was associated with increased cell death in Zn-treated cells (**Fig 4-11F, 4-17**). Together, these data suggest that the ability of Mn to modulate autophagy in these cells is cation-specific, and occurs in a dose-dependent manner (**Fig 4-11F**). This specificity further supports the hypothesis that reduced bioavailable Mn (but not other essential or heavy metals) in HD cells contributes to the observed autophagic defects.

Mn increases mutHTT aggregate-autophagosome association in 72Q-expressing HEK293 cells in a dose-dependent manner

Poly-Q aggregates are primarily degraded by autophagy. We hypothesized that Mn treatment facilitates mutHTT aggregate association into autophagosomes. Our data suggest Mn can activate autophagy, thus, we posited that Mn promotes mutHTT aggrephagy (autophagy of protein aggregates) via activation of autophagic flux, possibly via upregulation of p62 (as perturbations in p62 cargo recognition have been proposed to underlie autophagy-related HD defects). However, Q111 cells do not produce quantifiable HTT aggregates, thus mutHTT-transfected cell lines are often used[131]. In order to examine the effect of Mn on mutHTT aggregate loading into autophagosomes, we utilized HEK293 cells which were transfected to express GFP-72Q-mutHTT. These cells produce robust amounts of aggregates immediately after transfection, which can be easily assessed by fluorescent microscopy. We quantified the degree to which mutHTT aggregates were proximately located with autophagic markers, based upon the expectation from previous work by others that LC3 puncta would be associated with, but not co-localized with, mutHTT aggregates[372,373]. We found some mutHTT aggregates associated closely, but not precisely co-localized, with LC3 puncta after Mn+CQ exposure (**Fig 4-18A**). Because autophagy is a process in flux and HTT aggregates are continuously produced, we utilized CQ to inhibit autophagosome degradation to ascertain whether mutHTT aggregate clearance was autophagy-dependent in these cells. Consistent with previous reports, 10uM CQ increased the number of aggregates by ~75% (higher concentrations were cytotoxic) (**Fig 4-18B, 4-19**). These data suggest mutHTT clearance is, at least, partially autophagy-dependent in 72Q cells. We further investigated whether elevated cellular Mn levels increase aggregate-autophagosome association. We found that a 72-hour exposure to 50 to 100uM Mn treatment in the presence of CQ significantly increased the number of visible HTT aggregates compared to CQ alone (up to ~2 fold) (**Fig 4-18C, 4-19A**). Whereas shorter exposures of 24 hours had no effect, with an intermediate effect being seen after 48 hours (**data not shown**). We observed no effect with Mn alone, even at the highest concentrations tested, suggesting Mn is 1) not inhibiting autophagic degradation similar to CQ 2) not promoting aggregation by itself to increase visible aggregate number and 3) the effect of Mn on
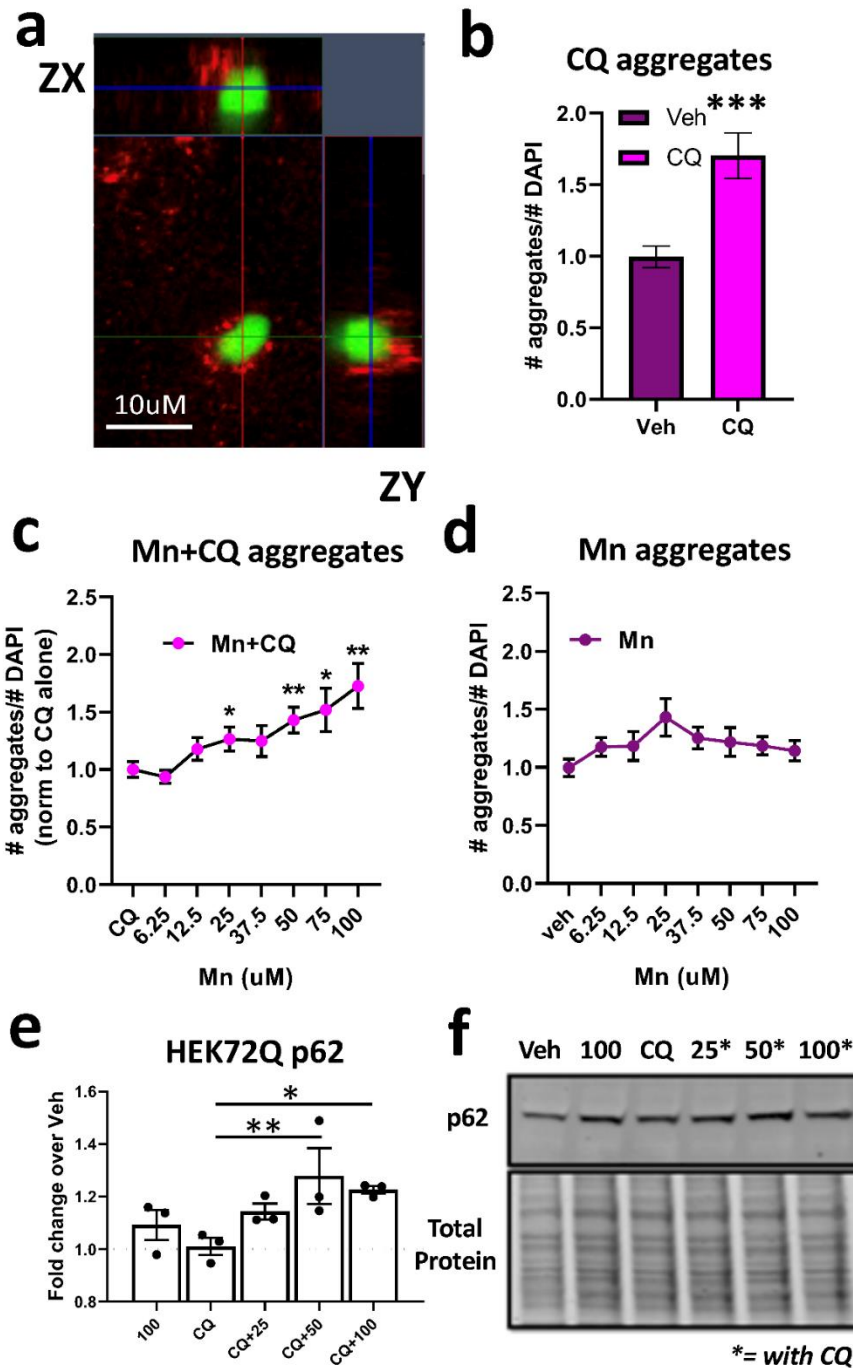
Figure 4-18: Mn+ CQ but not Mn alone increases the number of HTT aggregates. **A**) Representative 63X confocal image of GFP-HTT-72Q aggregates (green) near LC3-II puncta (red) in transfected HEK293 cells after treatment with 75uM Mn + 10uM CQ. Includes ZX and ZY view. **B**) Quantification of relative number of aggregates after CQ (10uM) treatment for 72hrs. *= significant difference by student's t-test. **C**) Quantification of number of aggregates after 72hr treatment with increasing amounts of Mn + 10uM CQ. Univariate ANOVA; $F_{(4.085, 98.04)}= 5.552$; $p=0.0004$. **D**) Quantification of number of aggregates after 72hr treatment with increasing amounts of Mn alone. Univariate ANOVA; $F_{(4.046, 89.02)}= 1.369$; $p=0.2907$. Quantification of (**C**) is normalized to CQ alone and quantification of (**D**) is normalized to no treatment. N=3 biological replicates, each with 10 images. **E**) Quantification of p62 after 72hr treatment with Mn (25/50/100uM) and/or CQ (10uM), in 72Q-GFP HEK293 cells. N=3. Univariate ANOVA; $F_{(4,8)}= 5.743$; $p=0.0177$. **F**) Representative western blot for HEK72Q p62. *= exposed with 10uM CQ. Error bars= SEM; *$P<.05$, **$P<.01$, ***$P<.001$. *= significance difference by Dunnet's multiple comparison tests. ***Work done with the assistance of Michael O'Brien and the use of HTT plasmid by the lab of Dr. Vittorio Maglione.***
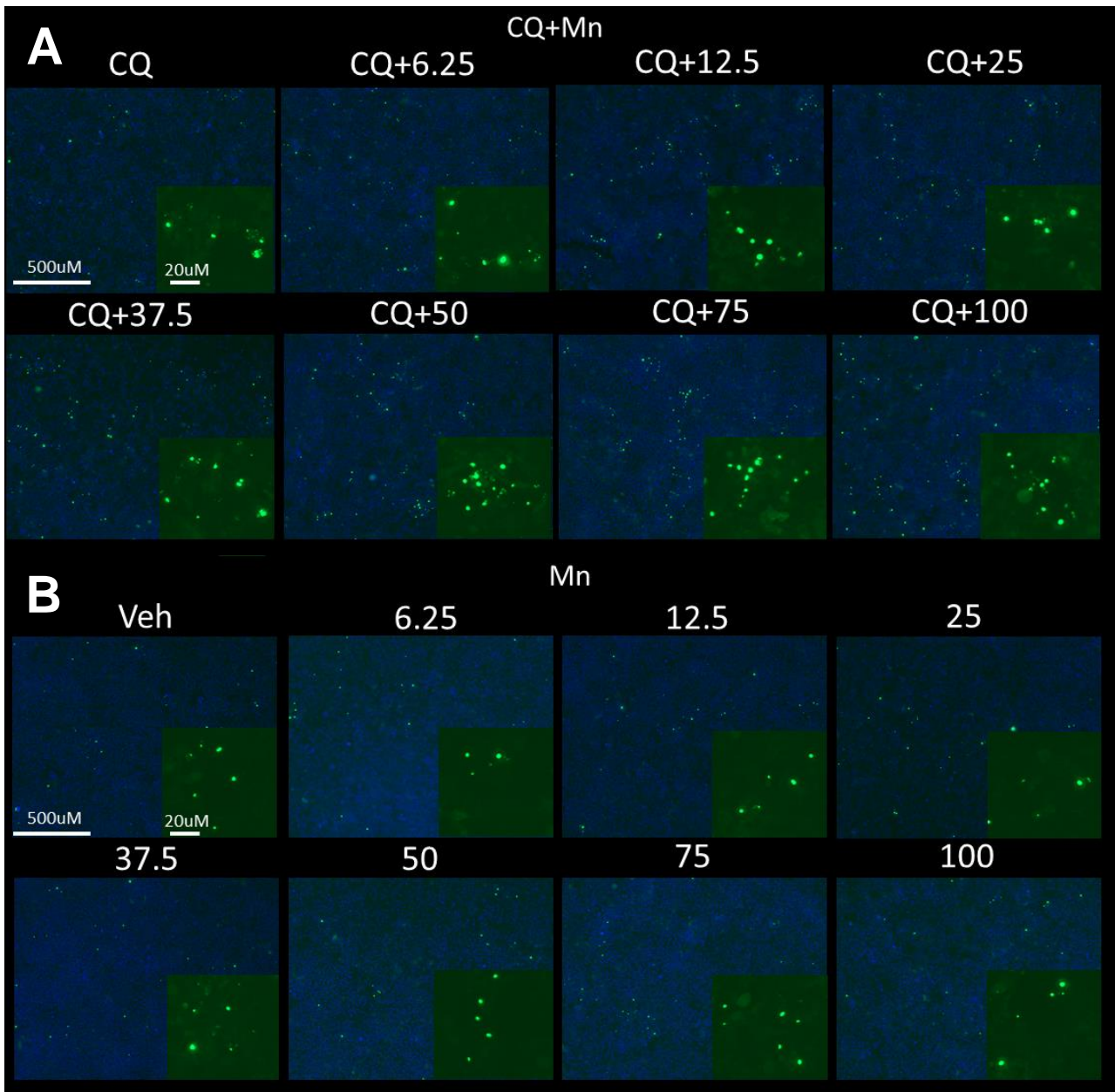
Figure 4-19: Mn increases the association of autophagosomes with mutant HTT aggregates. a,b)
Representative images in GFP-HTT-72Q transfected HEK293 cells taken at 5X on a Zeiss Fluorescent light
microscope of Mn+CQ (**A**) and Mn alone (**B**) with GFP-HTT-72Q aggregates (green). 10uM CQ;
6.25/12.5/25/37.5/50/75/100uM Mn used. DAPI is cropped and inset within each panel at same magnification.
N=3 biological replicates, each with 10 images. *Work done with the assistance of Michael O'Brien and
the use of HTT plasmid by the lab of Dr. Vittorio Maglione.*

aggregate number is autophagy-dependent (**Fig 4-18D, 4-19B**). Furthermore, p62 expression was significantly upregulated in the presence of Mn+CQ compared to CQ alone, mirroring the effects seen on mutHTT aggregate number (**Fig 4-18E,F**). Total LC3 or the LC3-II/I ratio was unaffected by CQ or Mn in 72Q cells (**data not shown**). Together these data suggest Mn can increase aggregate-autophagosome association in a dose-dependent and time-dependent manner.

Acute Mn treatment ameliorates cargo-recognition failure in Q111 cells

Given our evidence that Mn exposure can activate autophagy and promote aggregate-autophagosome association, we posited that Mn exposure also promotes proper autophagic function, particularly in HD cells which exhibit reduced Mn bioavailability. The presence of empty autophagic vacuoles (APVs), lacking osmiophilic, visible cargo, is one of the most striking cellular phenotypes in STHdh Q111 cells. This has been attributed to failed interactions between p62 and mutHTT during autophagosome scaffolding and formation, leading to autophagic "cargo recognition failure"[131]. Since Mn-induced p62 is robust in these cell lines, we hypothesized that our acute Mn treatment protocol, which causes the upregulation of autophagic flux, could increase autophagosome recognition and loading. Similar to previous reports by other investigators, we independently confirmed that STHdh Q111 cells exhibit 2-3 fold more empty/partially full APVs than the WT control STHdh Q7 cells[131]. Consistent with our hypothesis, 100 µM Mn restoration treatment rescued the number of full APVs to WT levels after 24hrs (**Fig 4-20A,C**). This suggests acute, sub-toxic, Mn exposure ameliorates the autophagy cargo sequestration defect in Mn-deficient HD cells. This suggests Mn upregulates the amount of osmophilic cellular constituents incorporated into autophagosomes such as endosomes, ER, and mitochondria. We also found that 100 µM Mn decreased the number of empty APVs in WT cells to <5% of total autophagosomes, suggesting that this Mn-induced effect is not necessarily HD-specific (**Fig 4-20B**).

Discussion

Numerous studies have observed Mn-induced autophagy but most of these studies based their findings on "snapshot" assessments of autophagy and utilized limited methodology, without pharmacologically manipulating autophagic degradation[50,133,290,356,357]. Autophagy is a complex biological process which is constantly in flux (autophagosome synthesis vs. degradation). Thus, to properly study the effects of Mn on autophagic flux, we inhibited autophagosome degradation with CQ and BafA, known lysosomal inhibitors. We found that Mn upregulates expression of two key autophagy
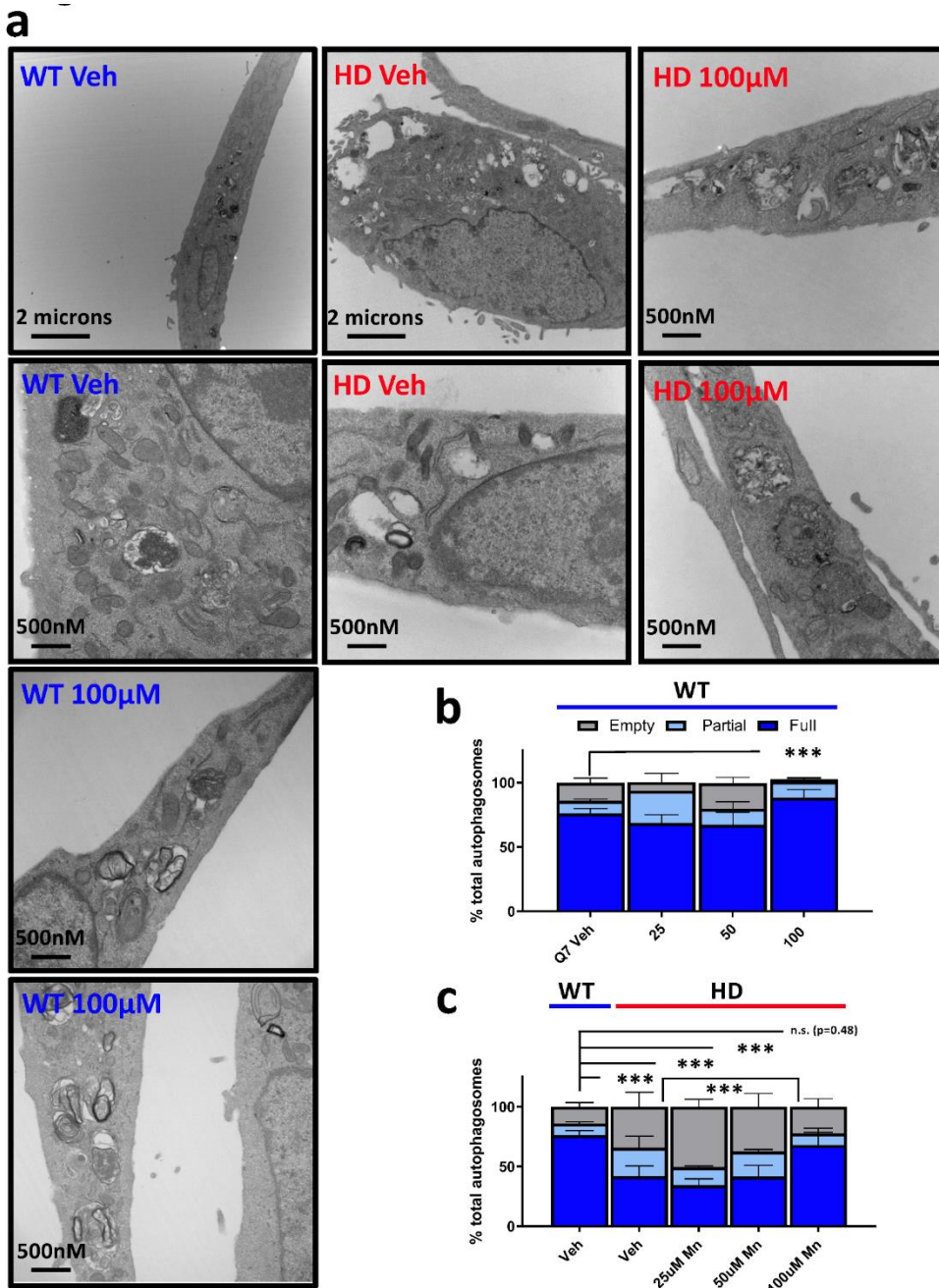
Figure 4-20: Acute Mn exposure attenuates empty autophagic vacuole phenotype in Q111 STHdh cells. A) Representative Transmission Electron Microscopy (TEM) images of STHdh WT Q7/Q7 (blue) and HD Q111/Q111 (red) cells with no treatment (Veh) or 100uM Mn for 24hrs. Some autophagosomesmarked with black arrows in HD cells. **B,C**) Quantification of empty, partial, or full autophagosomes after 24hr treatment with 25/50/100uM Mn in STHdh WT Q7/Q7 (**B**) and HD Q111/Q111 (**C**) cells. Note: For panel C, vehicle-treated WT is re-plotted on the left for comparison. 15-20 images per condition were analyzed across two independent TEM sections from two independent biologically experimental sets giving a technical n= ~30-40 per condition. Error bars= SEM; *= significant difference by chi-square analysis. *P<.05, **P<.01, ***P<.001. ***Work done with the assistance of Michael O'Brien.***

proteins—LC3-II/I and p62—in the absence or presence of saturating concentrations of CQ or BafA. Given our current understanding of autophagy, our data thus demonstrate that Mn increases autophagosomes induction/formation in neuroprogenitor-like cells types **(Fig 4-1, 4-3)**. Induction of autophagy appears to be specific to Mn, since eight other metals tested did not increase LC3-II puncta (in the presence of CQ) when applied at sub-cytotoxic concentrations **(Fig 4-11F)**. The mechanism by which Mn increases the LC3-II/I and p62 expression does not involve the upregulation mRNA expression **(Fig 4-5F)**. Given the results of our study, future studies should determine whether basal levels of Mn play a role in modulating normal autophagic function, or whether this effect only occurs under high, exogenous concentrations of Mn.

While our study provides strong evidence that increasing cellular Mn levels can activate autophagy, future studies are needed to explore the mechanism by which Mn activates autophagy and if Mn also plays a role in modulating autophagic function at basal levels. Our study does offer some clues. First, we show that Mn-induced p62 is PI3K-dependent, as LY294002 completely abrogates Mn-induced p62 in STHdh cells **(Fig 4-1F)**. These results are consistent with other published work suggesting LY294002 actively inhibits p62 synthesis and autophagy[374]. This has been hypothesized to occur via inhibition on Class III PI3K (VPS34), an early autophagy protein which interacts with Beclin, rather than Class I PI3K which canonically acts upstream of the AKT pathway[374-376]. Furthermore, rapamycin had no effect (**Fig 4-1D,F**), suggesting Mn induced autophagy is independent of mTOR, despite of its involvement in the regulating of autophagy[124]. Additionally, we observed increased p62 and LC3II/I expression after exposure with NU7441, a DNApk inhibitor which is consistent with previous reports suggesting NU7441 can activate autophagy (though the mechanism is unclear) and causes radiosensitization in cancer cells leading to selective autophagic cell death. When cells were co-treated with Mn, this caused additive increases in p62 and LC3II/I expression, providing additional proof-of-principle that Mn can activate autophagy. Interestingly, addition of NU7441+Mn normalized Mn-induced autophagy in the Q111 cells **(Fig 4-2A,B)**. However, this interaction between NU7441, Mn, and autophagy remains unclear because 1) the mechanism by which NU7441 and DNApk inhibition increase autophagy is unknown 2) NU7441 inhibits PI3K at concentrations of 5uM or higher[300,361,362], yet exhibits the opposite trend on autophagy as LY294002, a specific PI3K inhibitor and 3) NU7441 can actually decrease Mn uptake in STHdh cell at concentrations of 5uM or higher because it inhibits PI3K[70]. Thus, while this interaction is interesting, specific complexities prevented fruitful follow-up studies.

Secondly, previous reports suggest that in microglial cells Mn-induced autophagy is dependent on ATG5[356]. We found that Mn-induced autophagy is unaffected by ATG5 siRNA-mediated knock-

down, a protein heavily involved in the formation of autophagosomes, suggesting Mn-induced autophagy is not ATG5-dependent (**Figure 4-21**). However, this knockdown was only partially effective (~40-50% free ATG5 knockdown, no knockdown of ATG5-12 complex), so it is unclear whether the remaining pool of ATG5 could compensate for the knockdown. Ma et al. recently demonstrated Mn-induced iNOS increased s-nitrosylation of JNK and Bcl-2, which affects interactions between Bcl-2 and Beclin-1[358]. In our study, we found that a 24hr exposure to 50 um Mn (or CQ/BafA) did not affect Beclin-1 expression (**Fig 4-6A**), thus we don't believe this mechanism is driving Mn-induced autophagy in our cells. As Mn is a known co-factor for many kinases (PI3K, insulin/IGF receptor, ATM) which are implicated in autophagy, it is possible that Mn activates autophagy via a specific set of these kinases[284,377,378]. Additionally, while Mn does not seem to greatly affect mRNA expression of autophagy proteins, Mn could help stabilize p62 or LC3 protein expression via interactions with the proteasome[379]. Nrf2 and KEAP1 signaling have also been heavily implicated in Mn exposure and are known to be activated by p62[380,381]. Given these results, future studies should investigate whether Mn-induced Nrf2 signaling is mediated via Mn associated p62 expression. Lastly, Mn is a co-factor for PP2A phosphatase which has been proposed to regulate axonal transport of autophagosomes[203,382]. Furthermore, PP2A also complexes with MID1, a ubiquitin ligase, and can regulate translation of mut*htt* mRNA[383]. Together, these may provide a mechanism by which Mn regulates autophagy and mutHTT protein expression.

This study is the first, to our knowledge, to provide evidence that inhibiting autophagy can increase net Mn uptake **(Fig 4-9)**. While we cannot distinguish whether CQ and BafA (lysosomal autophagy inhibitors) increase intracellular Mn by upregulating influx or decreasing efflux, the data are consistent with previous reports suggesting lysosomes are a common storage organelle for intracellular Mn[384-386]. The mechanism(s) underlying neuronal Mn homeostasis and transport have long been a "black-box," and few Mn-specific transport routes have been elucidated[32]. Our study suggests that autophagy is a novel and poorly understood mechanism of neuronal Mn transport (and possibly responsible for the Mn-uptake defect in HD cells), though further studies assessing basal neuronal Mn levels in different autophagy models are needed.

We set out to explore the impact of reduced bioavailable Mn on autophagic function in HD. We found that Mn-induced autophagy is blunted in cellular models which exhibit reduced Mn uptake[81,82]. Furthermore, we found that lysosomal autophagy inhibitors (CQ and BafA) increase net Mn uptake. In Q111/Q111 HD cells, these inhibitors normalize Mn uptake, thereby ameliorating the defects in Mn-induced autophagy **(Fig 4-5, 4-9)**. This demonstrates that reduced Mn bioavailability in these cells hampers activation of Mn-induced autophagy, and that normalizing intracellular Mn can effectively
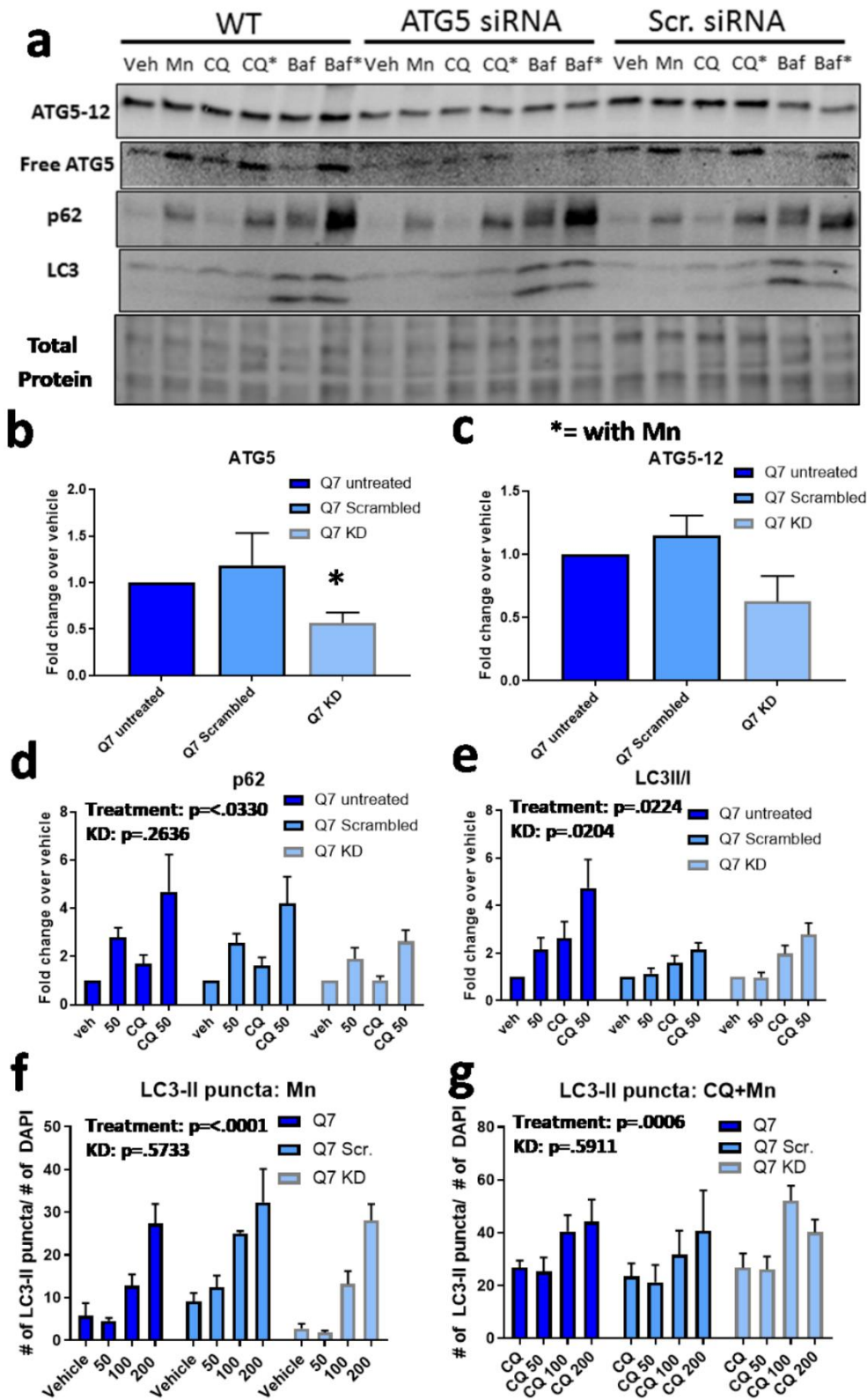
Figure 4-21: **ATG5 siRNA knockdown in STHdh cells does not inhibit Mn-induced expression of LC3 and p62.** **A**) Representative western blot for WT (non-siRNA treated), ATG5 siRNA-treated, and scrambled siRNA-treated Q7/Q7 STHdh cells for ATG5-12 complex, free ATG5, p62, and LC3. Cells were treated with Mn, CQ, BafA for combination for 24hrs, 48hrs post-transfection with siRNA. **B**) Quantification of free ATG5 (from vehicle lane) for each treatment. **C**) Quantification of ATG5-12 complex (from vehicle lane) for each treatment. **D-E**) Quantification of p62 (**D**) and LC3II/I (**E**) after treatment with Mn, CQ, or CQ+Mn for 24hrs. **F-G**) Quantification of LC3-II puncta after treatment with Mn (0-200μM) or (**G**) CQ+Mn (10μM; 0-200μM). For LC3-II puncta, 10 images per condition were taken for three individual biological replicates (separate siRNA knockdown experiments) were quantifed. Error bars= SEM; *= significant by 95%CI in **B-C**. Two-way ANOVA was performed on data for **D-G** and statistical significance of treatment or siRNA KD are listed in top left of graphs. ***Work done with the assistance of Michael O'Brien.***

attenuate this defect. Perhaps the most notably autophagy-related defect in HD is the presence of empty autophagic vacuoles, devoid of osmophilic cargo, due to "cargo-recognition failure"[131]. In this study, we have recapitulated this phenotype in Q111 cells (~50% empty or partially full APVs). Further, we found that rescue of a Mn deficit condition by restorative treatment with 100uM Mn for 24hr eliminated this defect **(Fig 4-20)**. Lastly, positing that Mn is facilitating cargo-loading in HD cells, we wanted to know whether Mn also facilitates the packaging of mutHTT aggregates into autophagosomes. As Q111 cells do not produce HTT aggregates, we utilized transiently transfected HEK293 cells with GFP-tagged, 72Q mutHTT. While these results do not confirm whether Mn can increase aggregate clearance itself, as we did not observe an effect on aggregate number by Mn alone, we found that treatment with CQ and Mn caused a significant (~2-fold) increase in the number of aggregates compared to CQ alone **(Fig 4-18, 4-90)**. Our current understanding of autophagic processing and the effects of CQ lead us to hypothesize that Mn facilitates cargo loading and mutHTT aggregate packaging into autophagosomes in HD cells. At present, it is unclear why Mn+CQ exposure is able to increase the total number of visible aggregates. Mn alone does not change aggregate number suggesting that Mn does not promote aggregation. If Mn exposure increases aggregate packing into autophagosomes, Mn+CQ should only change the localization of aggregates (outside autophagosomes to inside autophagosomes) since autophagy-mediated clearance is blocked, but this treatment should not increase the total number of visible aggregates. However, we suggest two possible ways Mn+CQ may result in increased number of visible aggregates: either 1) Mn inhibits the proteasome and shunts aggregates to autophagy, allowing aggregates that would have previously been degraded by the proteasome to be visualized; or 2) Mn helps package small mutHTT "seeds," precursors to mutHTT aggregates, into autophagosomes (perhaps by stalling autophagic processing), thus increasing GFP signal and concurrently, the visible number of aggregates. Further studies manipulating the proteasome (i.e. using MG132) or investigating aggregates at a higher resolution (which can detect mutHTT seeds), are needed to confirm either of these hypotheses. These studies are needed to address whether elevating cellular Mn levels would increase mutHTT aggregate clearance, or merely increase the association between autophagosomes and mutHTT aggregates. An inducible mutHTT system would provide the ideal model to test whether Mn-induced autophagy truly increases aggregate clearance.

Martinez-Vicente and colleagues posit that the cargo recognition failures in HD may be due to an abnormal association between mutHTT and p62, a key protein for recognizing autophagosomes with polyubiquinated aggregates and organelles[131]. Given the robust increase in p62 expression after Mn treatment (even under saturating CQ conditions), we hypothesize Mn-induced p62 expression may promote cargo recognition. Additionally, p62 directly associates with the adapter protein ALFY, which

also facilitates autophagic degradation of protein aggregates. Of particular interest, overexpression of ALFY has led to significant reduction in HTT aggregates in *Drosophila* HD models[387,388]. Further research should investigate whether Mn also increases expression of ALFY, in addition to p62, which may further explain its effects on cargo sequestration.

At first glance, our results are quite contrary to the recent findings of *Harischandra et al.,* which describe the ability of Mn to promote exosome transmission of alpha synuclein aggregation-inducing miRNAs[389]. There could be several reasons for the discrepancy between our findings and *Harischandra et al*'s. First, the mechanisms of PD and alpha synuclein pathology compared to HD/mutHTT are similar, but distinct. Mn could have entirely different effects on alpha synuclein aggregation than mutHTT aggregation, particularly in HD cells which exhibit reduced, brain-bioavailable Mn. Second, these findings were observed under toxic Mn concentrations while ours have focused on high, yet sub-cytotoxic exposures. Third, it is quite possible Mn could have both positive and negative effects on aggregation. Though our results pinpoint a therapeutic facet of Mn replacement therapy, this treatment could very well have off target effects (potentially through exosome-mediated miRNA transmission) which could promote aggregation. Altogether, these data warrant further investigation into the differential effects of Mn on autophagy/proteasome function and PD/HD.

Although our data strongly suggest that Mn activates autophagic vesicle formation, it does not exclude the possibility that Mn could *both* activate autophagic flux by elevating autophagosome formation while inhibiting the processing of autophagosome maturation and fusion with lysosomes. If this is the case, it is possible that the effect Mn has on filling autophagosomes is actually driven by the slowing of autophagosome processing. As seen in **Fig 4-22** exposure with CQ or BafA alone in Q7, or BafA alone in Q111, significantly increases the number of full autophagosomes by EM, similar to Mn exposure. We hypothesize that Mn, CQ, and BafA are inhibiting autophagosome degradation, stalling autophagosome processing long enough for HD cells to package more cargo into them. This may explain why Mn+CQ exposure increases the number of mutHTT aggregates, by slowing down autophagy processing and allowing for greater accumulation of mutHTT aggregates into autophagosomes.

Autophagy activators have long been studied in the context of HD as a potential therapy for the disease—primarily via upregulation of autophagy-mediated degradation of mutHTT aggregates. Fasting, IGF-treatment, upregulation of AMPK, and most commonly, modulation of mTOR, have all been investigated as potential HD therapies with promising results on a variety of cellular and *in vivo*
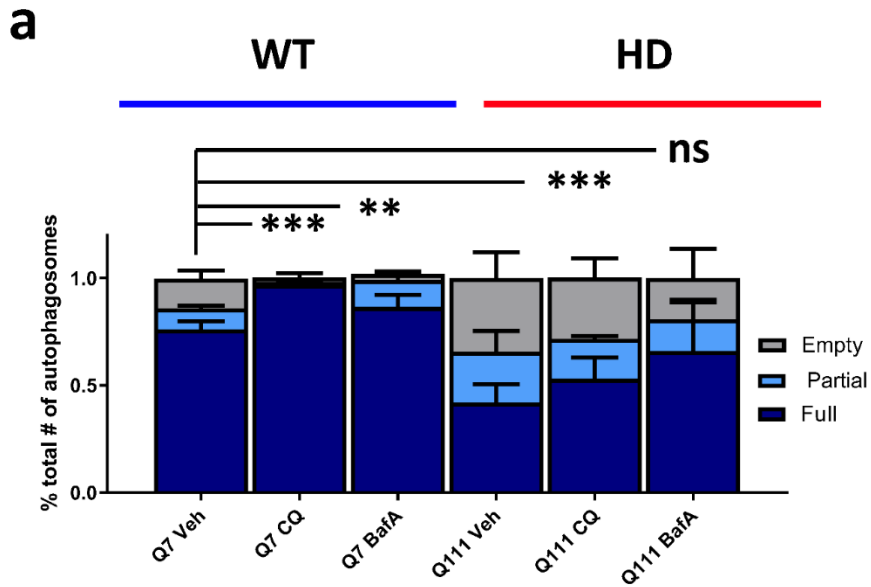
Figure 4-22: **Lysosomal autophagy inhibitors increase the percentage of full autophagosomes in HD cells. A**) Quantification of empty, partial, or full autophagosomes as graded by electron microscopy images in STHdh WT Q7/Q7 and HD Q111/Q111 cells following 24hr exposure with CQ (10uM) or BafA (10nM). These images were taken from the exact same samples as Figure 8 and judged during the same process by the same individual. *= significance by chi-square analysis. *P<.05, **P<.01, ***P<.001. ***Work done with the assistance of Michael O'Brien.***

pathologies[87,101,104,125,126,350,351,390-393]. Our study suggests that Mn treatment may also be a viable therapy by modulation of autophagy and autophagy-related HD pathologies. Furthermore, as our lab has shown, there is reduced bioavailable Mn in HD models, and Mn treatment could target a contributing cause of defective autophagy (reduced net Mn uptake), rather than merely upregulating the autophagy process, to combat disease pathology and at the same time benefit other Mn enzymatic pathways affect by HD, such as arginase in the urea cycle[315].

Conclusions

We demonstrate that the essential metal, Mn, is capable of activating autophagy in mouse and human-derived neuroprogenitors at sub-toxic concentrations via the use of pharmacological inhibitors and complementary autophagy methodologies. Furthermore, Mn treatment attenuates the well-characterized autophagic cargo recognition failure phenotype in HD cells and can increase autophagosome-aggregate association, suggesting Mn can facilitate cargo sequestration, including autophagic sequestration of HTT aggregates. Together these findings provide novel evidence that Mn-centric therapies could remedy autophagy-related phenotypes in HD and warrant further investigation.

Materials and Methods

Immortalized cell culture

The immortalized, murine striatal cell lines (STHdh$^{Q7/Q7}$ and STHdh $^{Q111/Q111}$) were obtained from Coriell Cell Repository (Cambden, NJ). Cells were cultured in Dulbecco's Modified Eagle Medium [D6546, Sigma-Aldrich, St. Louis MO] supplemented with 10% FBS [Atlanta Biologicals, Flowery Branch, GA], 2 mM GlutaMAX (Life Technologies, Carlsbad, CA), Penicillin-Streptomycin, 0.5 mg/mL G418 Sulfate (Life Technologies, Carlsbad, CA), MEM non-essential amino acids solution (Life Technologies, Carlsbad, CA), and 14mM HEPES (Life Technologies, Carlsbad, CA). They were incubated at 33°C and 5% CO$_2$. Cells were passaged before reaching greater than 90% confluency and were never passaged past the recommended 14th passage. The cells were split by trypsinization using 0.05% Trypsin-EDTA solution (Life Technologies, Carlsbad, CA) incubated for five minutes. One day prior to exposure, cells were plated in the appropriate cell culture plate type at 8x10^4 cells/mL for WT and 1x10^5 cells/mL for HD. HEK293 cells were a generous gift from William Tansey. HEK293, 3T3, SH-SY5Y, and Neuro2A cells were maintained at 37°C and treated in high glucose DMEM with L-glutamine and (Corning CV-0013) and Penicillin/Streptomycin, and cells plated at 100,000 cells/mL for experiments.

hiPSC cell culture

Islet-1 positive hiPSC-derived neuroprogenitor cells were differentiated as previously described using iPSCs from three separate control and HD patients[27]. HD patient mutant alleles were 58, 66, and 70 CAG repeats. All hiPSC lines were confirmed to be pluripotent (PluriTest- Expression Analysis, Durham, NC) have normal karyotypes (Genetics Associates, Nashville, TN). Additionally, a subset of cells was fixed with 4% paraformaldehyde for 15 minutes and immunocytochemistry was performed to ensure all cultures expressed Islet-1. For experiments, differentiated cells from the Islet-1 positive cells were plated at 300,000 cells/mL at day 10 of differentiation. At day 11, rock inhibitor containing media was taken off of cells are replaced with fresh media containing purmorphamine (.65uM). For 24hr exposures, cells were exposed to Mn and/or small molecules in day 11 differentiation media containing purmorphamine.

Inhibitors/metals

Chloroquine diphosphate, bafilomycin A, KB-R7943, 3 methyladenine, and LY294002 were purchased from Tocris Biologicals. Inhibitors were used at following concentrations unless otherwise stated: Chloroquine diphosphate= 10uM, Bafilomycin A= 10nM, KB-R7943= 10uM, 3 methyladenine= 5mM, LY294002= 7uM. The following metallic compounds were used as sources for the metal exposures: Mn= $MnCl_2$-$4H_2O$ (Sigma Aldrich, St. Louis, MO), Fe=$FeCl_3$ (Sigma Aldrich, St. Louis, MO), Cu=$CuCl_2$-$2H_2O$ (Alfa Aesar, Ward Hill, MA), Mg=$MgCl_2$-$6H_2O$ (Alfa Aesar, Ward Hill, MA), Ni=$NiCl_2$-$6H_2O$ (Alfa Aesar, Ward Hill, MA), Co=$CoCl_2$-$6H_2O$ (MP Biomedicals, Solon, OH), Zn=$ZnCl_2$ (Acros Organics, Morris, NJ).

Cellular Fura-2 Manganese Uptake Assay (CFMEA) was performed as described previously[262].

Western blot

Protein samples were prepared by scraping cells into ice-cold PBS, centrifuging, and adding RIPA buffer containing protease (Sigma-Aldrich, St. Louis, MO) and phosphatase inhibitor cocktails 2 & 3 (Sigma, Sigma-Aldrich, St. Louis, MO) to the pellet. After gentle homogenization, cells were centrifuged at 4°C for 10 minutes at 20,000 g. Protein concentration was quantified using the BCA assay (Peirce Technologies) with a BSA standard curve. Samples were mixed with 5x SDS loading buffer containing 1% 2-mercaptoethanol and boiled for 5 minutes. 15 µg of protein was loaded for each sample onto a 4-15% pre-cast gel SDS-PAGE gel (BioRad, Hercules, CA) and run at 90V for 120 minutes. The protein bands were then transferred onto nitrocellulose membranes using iBlot Gel Transfer Device (Life Technologies). The remaining gel was stained with IRDye Blue protein stain (LI-

COR, Lincoln, NE). Since the gels retained ~1/3 of the original protein after transferring with the iBlot, we imaged the stained gel on the Li-Cor Odyssey Imaging System and quantified the intensity entire lane from ~150-20 kDa. This value was used to normalize the values of immunostained bands. The membrane was blocked in Odyssey Blocking Buffer for one hour prior to the addition of the primary antibodies. The primary antibodies were diluted 1:1000 in Odyssey Blocking Buffer containing 0.1% TWEEN and incubated overnight. After washing 5 times for 5 minutes in TBST, membranes were incubated with secondary antibodies at 1:10,000 (LiCor, Lincoln, NE) for 1 hour. Membranes were imaged using the Li-Cor Odyssey Imaging System, and quantification was performed using Image Studio Lite (LiCOR, Lincoln, NE). LC3A/B (4108), p62 (5114) antibodies were purchased from cell signaling technologies and used at 1:1000 dilution except LC3A/B was used at 1:500. LC3 was quantified at the ratio of LC3-II divided LC3-I. Note that the doublet for p62 in Figure 2A is consistent with previous reports in neuronal cell types[363], but this is different from the non-specific band near p62 in Figure 4A which appears after probing for LC3 in the hiPSC-derived neuroprogenitors.

Gene expression analysis

STHDH Q7/Q7 (referred to as Q7) and Q111/Q111 (referred to as Q111) cells were plated in 6-well plates and treated with Mn and/or lysosomal autophagy inhibitors. After 24 hours, cells were lysed in 1mL of TRIzol® Reagent (CatNo. 15596) and stored at -80°C until use. Total RNA was extracted using TRIzol® Reagent, according to the maunfacturer's User Guide (Invitrogen, Carlsbad, CA). RNA was DNAse I treated, following the NEB DNase I Reaction Protocol (M0303) (New England BioLabs® Inc, Ipswich, MA). cDNA was generated on Bio-Rad Laboratories' S1000™ Thermal Cycler, using 50uM Random Hexamers (P/N 100026484, Invitrogen, Carlsbad, CA), 50U MuLV Reverse Transcriptase (P/N 100023379, Applied Biosystems, Foster City, CA), 10mM dNTPs (CatNo. N0446S, NEB, Ipswich, MA), 20U RNAse, Inhibitor (CatNo. N8080119, Applied Biosystems, Foster City, CA), 25mM MgCl$_2$ (P/N100020476, Applied Biosystems, Foster City, CA), 10x PCR Buffer II (RefNo. 4486220 Applied Biosystems by Life Technologies, Austin, TX), and 1ug of extracted RNA, and using the following cycling times: 25°C for 10 min, 42°C for 60 min, 99°C for5 min, 5°C for 5 min, 4°C forever. Q-RT-PCR was performed on Eppendorf's Mastercycler® epGradientS Realplex^2, using KAPA SYBR® FAST qPCR Master Mix (2X) Universal according to the manufacturer's recommendations (KM4101, KAPA Biosystems, Wilmington, MA). Sequences of primers used are below. Expression of LC3B and p62 gene products were normalized to levels of PGK1, and plotted as induction over vehicle-treated samples. Primer sequences as follows: *mpgk1*_F2 GCTATCTTGGGAGGCCTAA; *mpgk1*_R2 AAAGGCCATTCCACCACCAA; *p62* (SQSTM1) forward 5'-GATGACATCTTCCGCATCTACA-3'; *p62* (SQSTM1) reverse 5'-TGCAACCATCACAGATCACA-3'; *LC3B* (Map1lc3b) forward 5'-

CGTCCTGGACAAGACCAAGT-3'; *LC3B* (Map1lc3b) reverse 5'-CCATTCACCAGGAGGAAGAA-3';
mATG5 FWD GATGGACAGCTGCACACACT; *mATG5* REV TTGGCTCTATCCCGTGAATC

pQCXI DsRED-LC3-II Retrovirus Production and Transduction

HEK 293T cells were plated at 2.5 x 10^6 cells per 6cm dish, and maintained in DMEM supplemented with 10% FBS and 100 IU/ml Penicillin. The next day, HEK 293T's were transfected using 8 µg pQCXI Puro DsRED-LC3-GFP plasmid (from Addgene#31182) and 4µg pCL10A (from Imgenex), 168 µL sterile water, 20 µL 2.5M $CaCl_2$, and 200 µL HBS. The following day, media was changed on transfected HEK 293T's to standard STHDH Q7/Q7 and Q111/Q111 cell media. Q7 and Q111 were also plated with 40,000/50,000 cells/mL, respectively into 6-well plates. 24 hours later, viral supernatant was collected from HEK293 cells, 0.45 µM sterile filtered, and 8 µg/mL final concentration of Hexadimethrine bromide was added – viral supernatant was incubated with Hexadimethrine bromide at room temperature for 5 minutes. Media was then removed from Q7 and Q111 cells and replaced with virus-containing media. Q7 and Q111 cells were transduced following this same procedure two more times over the next two days. After 3 total days/rounds of transduction, media was replaced with standard media and cells were given 24 hours to recover before selection with Puromycin at 1ug/mL for roughly 48 hours. The population was maintained in low dose Puromycin for expansion, then frozen down. For all LC3-II IF experiments (aside from severity score experiment), cells were thawed in normal media and immediately used. Though this plasmid should express LC3I in GFP and LC3II in dsRed, we found that the GFP signal after transduction was very weak and diffuse and did not offer quantificational benefit. However, as only LC3II is expressed in dsRed (not LC3I), this methodology allows for specific localization of LC3II which cannot be picked up via an LC3 antibody (as both forms are detected). Once these images were quantified, the images were decoded to reveal exposure conditions and averaged together for final values. For p62 immunofluorescence, cells were permeabilized in .2% triton in PBS for 20 minutes following fixation with 4% paraformaldehyde for 15 minutes. Cells were incubated overnight at 4°C in 1:100 primary antibody (Abcam #ab56416) in 5% normal donkey serum (Jackson Immunoresearch #3017-000-121) with .05% triton. The following day, cells were washed with .05% triton and incubated with anti-mouse-488 secondary for 3 hours. Cells were washed three more times and incubated with Hoecst (1:2000) for 10 minutes. Cells were washed three more times and imaged.   For LC3-II and p62 puncta quantification, Cell Profiler was used to detect the number of LC3-II puncta and cells per image.

For the LC3 severity score assay, STHdh Q7/Q7 and Q111/Q111 cells were transfected with the pQCXI Puro DsRED-LC3-GFP plasmid (Addgene#31182) using Mirus TransIT-LT transfection reagent

(Madison, WI) following manufacturer's protocol. Plasmid was transformed into DH5 alpha E.coli, colonies were picked and inoculated in LB broth, and plasmid DNA was isolated via Qiagen Maxi Prep kit. Cells were plated at 100,000 cells/mL 18-24hrs prior to transfection in a 6-well plate. 2.5 µg of plasmid and 7.5ul of TransIT-LT were combined in 250ul of serum-free Opti-MEM per well. This was added dropwise into the media in the well. 24 hours after transfection, cells were selected with 2.5µg/µL of puromycin for 3 days. These cells were plated at 50,000 cells/mL and 16-24 hours later, the cells were exposed with manganese or small molecules. Cells were then fixed with 4% paraformaldehyde for 15 minutes after 24 hours and nuclei were stained with Hoecst stain. Images were taken using a Zeiss ObserverZ1 Light microscope by an investigator blinded to the exposures. For LC3-II severity scores, a second, blinded individual designated each image with an arbitrary code name. A third person then blindly scored each cell by severity (none-low, mild, medium, high, or severe) using the representative scale in **Figure 4-12C**.

For lysotracker imaging, LC3-II expressing STHdh cells were exposed for 24hrs and then stained with 50nM lysotracker Deep Red (L12492, Invitrogen) and DAPI for 30 minutes. Cells were washed 3X with fresh media and immediately imaged. Cell profiler was used to detect the number of lysotracker puncta and cells (DAPI) per image.

Electron Microscopy

Electron microscopy was carried about by the Vanderbilt Cell Imaging Shared Resource (CISR). Samples were washed, fixed, and prepared as designated by the core. Methods are as follows: Samples for electron microscopy were rinsed in 0.1M cacodylate buffer, fixed in 2.5% glutaraldehyde in 0.1M cacodylate buffer and post-fixed in 1% osmium tetroxide. Following fixation, the samples were dehydrated through a graded series of alcohol and embedded in Embed 812 resin. Thin sections were cut and observed at 100 keV with a Tecnai 12 electron microscope (FEI/Thermo Fisher). TEM images were taken by a CISR technician who was uninformed of any hypotheses. Roughly 8-15 images were taken for each condition across two separate biological replicates, each with two separate sections. Autophagosome loading status (i.e. empty, partial, full) were assessed by a single blinded individual after all images were randomized by a separate individual. Empty<10% full, partial>10%,<90%, full>90% as assessed by eye.

GFP-HTT 72Q HEK293 cells

The exon-1-72Q-HTT-GFP-pCDNA3.1 plasmid was prepared in Dr. Vittorio Maglione's lab (Italy). Plasmid was transformed into DH5 alpha E.coli, and grown on ampicillin plates. Colonies were

picked and inoculated in LB broth, and plasmid DNA was isolated via Qiagen Midi Prep kit. HEK293 cells were transfected with 1µg/µl plasmid using Mirus LT. 24hrs after transfection cells were split. 48 hours after transfection, cells were assessed to confirm aggregate production and were frozen down so that a new vial could be used for each set of experiments. Cells were plated at 100,000 cells/mL and treated 16-24hrs after plating. Cells were treated for 24hrs with Mn and/or chloroquine and fixed with 4% paraformaldehyde for 15 minutes at room temperature. Cells were later stained with Hoecst stain prior to imaging. GFP-tagged HTT was visualized using a Zeiss ObserverZ1 Light Microscope. Cell Profiler was used to quantify the number of aggregates (GFP puncta) and cells (Hoecst) per image. Confocal imaging was performed on LSM 710 META Inverted microscope by a Vanderbilt Cell imaging Shared Resource (CISR) technician, and images were viewed using Ziess Zen Black Software. For confocal imaging of LC3 puncta, an LC3A/B antibody (Cell signaling 4108) was used which detects both LC3I and LC3II. This is different from the virally transduced pQCXI dsRED-LC3-II expressing STHdh which only express the lipidated LC3-II form under dsRED.

siRNA ATG5 knockdown

The transfection was conducted using Lipofectamine® RNAiMAX Transfection Reagent from ThermoFisher Scientific and ON-TARGETplus Mouse ATG5 siRNA (Cat# L-064838-00-0005) from Dharmacon, with the scrambled condition as Silencer™ Negative Control No. 1 siRNA (Cat# AM4611) (ThermoFisher Scientific). For each transfection, 9 µL RNAiMax and 15 µL of 5µM scrambled siRNA, or 15 µL of 5µM ATG5 siRNA, in a total volume of 250µL of TE buffer were used per well of a 6-well plate. Q7/Q7 STHdh ds-RED-LC3II Cells were plated at normal plating density into 6-well plates and grown for 16-24 hours prior to siRNA transfection. After transfection, cells were cultured for an additional 24hrs. The following day these cells were split once more for experiments into 6-well plates for western blot or 96-well plates for immunofluorescence. 16-24hrs later, cells were exposed with Mn and/or CQ/BafA for 24hrs. 72hrs after siRNA transfection, cells were then processed for western blot or immunofluorescence to detect LC3/p62 or LC3-II puncta, respectively.

Statistical analysis

For most statistical tests, GraphPad Prism v8.0.1 was used. Most data are shown as linear fold change versus vehicle controls to ease data interpretation. However, all data that was analyzed by ANOVA was converted to log values to better approximate a normal distribution prior to statistical analysis. For experiments in which data is graphed in comparison to a unitary value of a vehicle control (=1); raw, unnormalized data were first converted to log values and underwent ANOVA analysis. When

data sets were significant by ANOVA, post-hoc multiple comparisons tests were used to determine specific differences within data sets. For analyses between all possible treatment and genotype groups, Tukey's test was performed. For analyses comparing data back to a specific condition only, Dunnet's or Sidak's tests were performed. For the majority of data sets, paired analyses were used as all samples were collected as full sets. For a few data sets which two groups were specifically compared, a paired student's t-test was used. Microscopy data including LC3 puncta, lysotracker, and HEK293 72Q were all quantified using CellProfiler 3.0.0. Most representative sets of microscopy images were brightened so that they could be more easily interpreted by the reader, but these images were not adjusted prior to quantification. If this was performed, all images were equally brightened.

Authors' contributions:

MRB and ABB designed all experiments. MRB performed most data analyses on western blot and microscopy data. MRB, MO, KN, DR, RN, and MU carried out cell culture and experiments for all figures. AMF generated LC3-expressing STHdh cell lines and performed all qRT-PCR. PJ carried out hiPSC-derived cell culture and differentiations. AP and VM generated and shared the 72Q-GFP plasmid. ZZ and MA assisted in experimental design and interpretation. All authors read and approved the final manuscript.

Acknowledgments:

CHAPTER 5

FUTURE DIRECTIONS AND GLOBAL DISCUSSION

Introduction

In this chapter, I will review and discuss unpublished data which may provide future avenues of investigation. Additionally, in the global discussion, I will review limitations of this thesis' work and how to potentially remedy these. A primary focus will be how to determine which effects of Mn are most biologically relevant and translational for future studies.

Results

The effects of CRISPR-mediated HTT loss-of-function on Mn uptake and Mn-induced IGF signaling and autophagy

Mutant HTT likely causes both gain-of-function (GOF) and loss-of-function (LOF) phenotypes via gain of mutant toxicity and loss of WT function [394-396]. Recently, this has become even more important as many developing therapies, including anti-sense oligos, are aimed at reducing both WT and mutant alleles [397,398]. Recent studies examining the effects of loss of WT HTT function have revealed highly different results—revealing that, depending on the model and experimental context, loss of WT HTT function may improve some aspects of disease pathology while exacerbating others[399-403]. We wanted to examine whether the observed reduced Mn uptake and Mn induced p-AKT in HD cells is a GOF or LOF mutation. In order to assess this, we utilized the CRISPR-Cas9 system to target exon 2 of HTT with a single 18 bp gRNA sequence (**Fig 5-1B**) [404]. We transfected STHdh Q7/Q7 and Q111/Q111 cells with the PX459 plasmid encoding both Cas9 and our sgRNA. Transfected populations underwent puromycin selection and subsequently underwent single-cell sorting into 96 well plates. Clones were collected and sequenced for indel formation utilizing two separate primer sets (**Fig 5-1A, G**). Interestingly, more than 2 indels were observed in the clones isolated (**Fig 5-1G**). This is consistent with mostly-hypertetraploid phenotype detected in these cells[405]. We confirmed partial or complete loss of HTT protein expression by two separate HTT antibodies (MAB2166, CST5656) (**Fig 5-1D, E**). Interestingly, we observed HTT mRNA at exon 3, 12, and 55 was *increased* in those same clones which lack HTT protein expression. (**Fig 5-1F**). We hypothesize that the indels generated by our CRISPR construct do not result in non-sense mediated decay of HTT mRNA, but rather a decrease in translation or increase in degradation of the HTT protein itself.

We first assessed Mn uptake via CFMEA in the STHdh Q7/Q7 and Q111/Q111 and their KO counterparts. We found that loss of HTT restored Mn uptake to WT levels in Q111-KO. Furthermore,
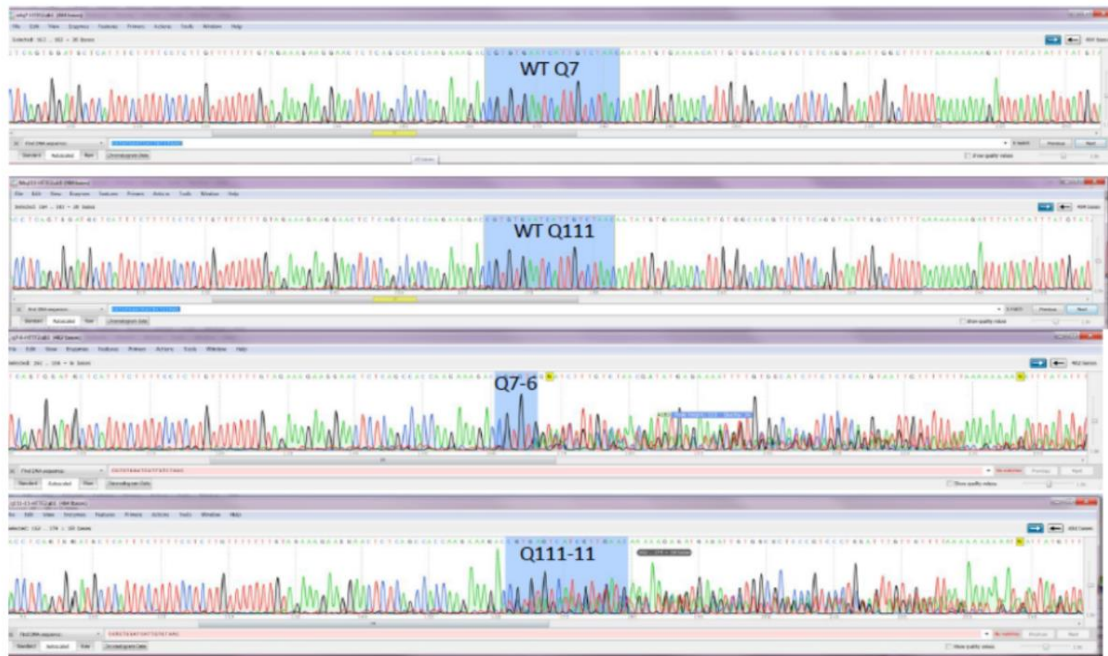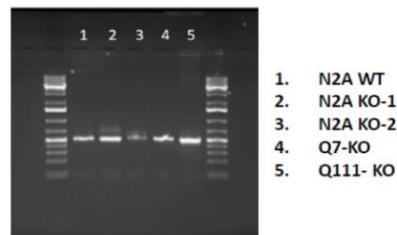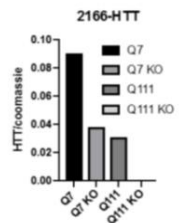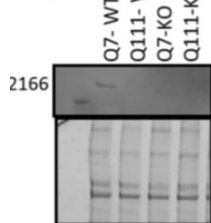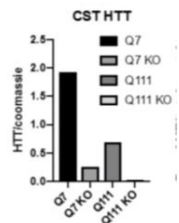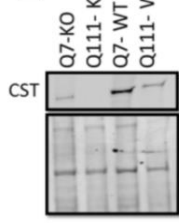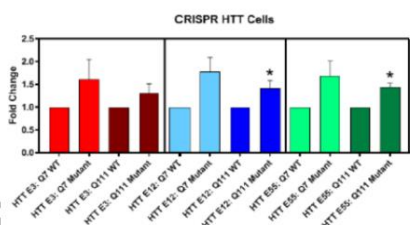
Figure 5-1: Validation of CRISPR-based HTT knockout cell lines. A) Sequences for WT and KO STHdh Q7/Q111, CRISPR sequence is highlighted. **B)** map of CRISPR cutsite within exon 2 of HTT. **C)** Representative PCR product flanking CRISPR cutsite. Western blot for HTT with **D)** (mAB 2166), **E)** CST (5656) in WT and CRISPR KO clones. **F)** Quantification of HTT mRNA in STHdh cells and KO lines. **G)** Quantification of relative indels and percentage of occurrence, respectively. ***Work done with the assistance of Daniel Rose and Rachana Nitin.***
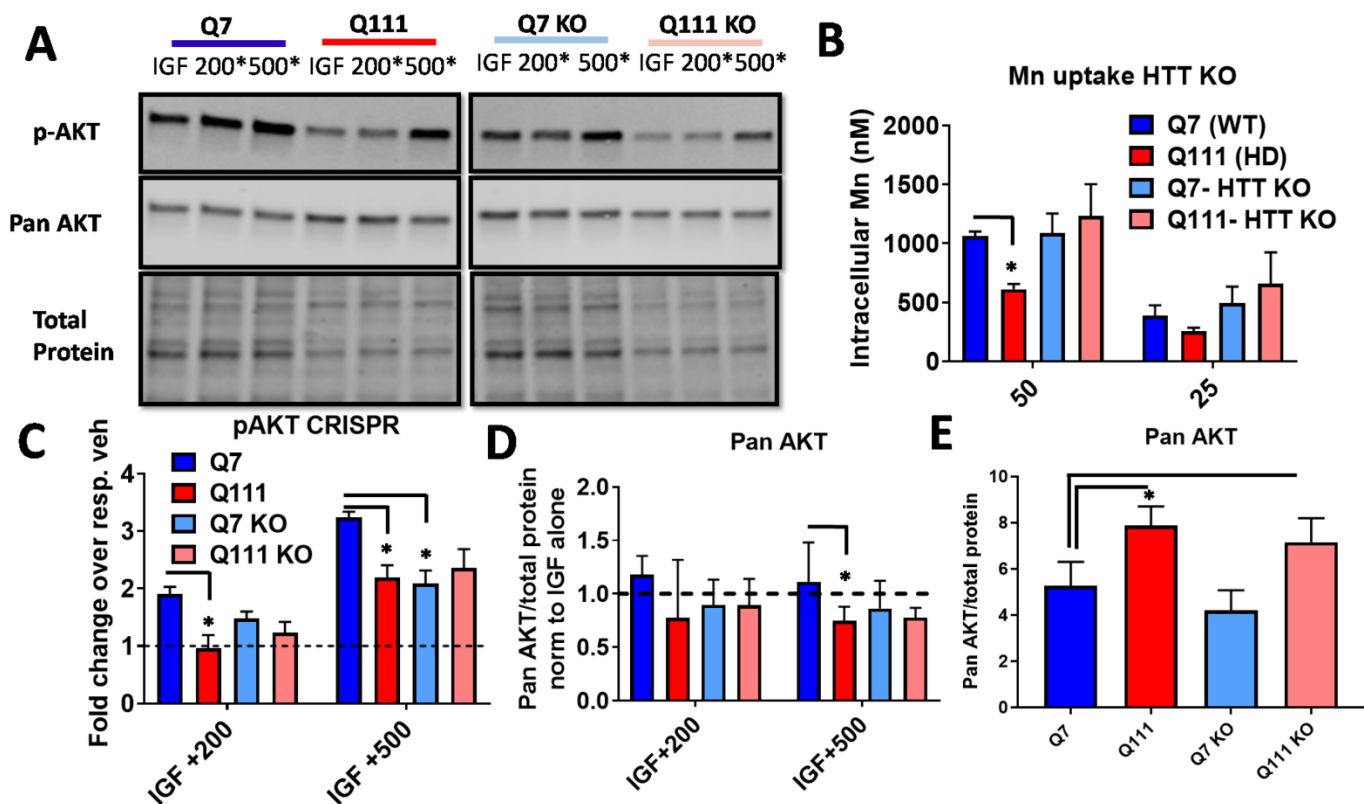
Figure 5-2: Assessing the effects of WT and mutant HTT in Mn-induced pAKT A) Representative blot of p-AKT expression in STHdh Q7/Q7, Q111/Q111, and their counterpart CRISPR KO clones. Cells were exposure for 3hrs in HBSS with 10nM IGF1 with 200/500uM Mn following a 1hr serum deprivation. **B)** Assessment of Mn uptake by CFMEA following 24hr exposure with 25/50uM Mn. **C)** Quantification of p-AKT expression from panel A. **D)** quantification of Mn/IGF-induced pan AKT. **E)** Quantification of basal pan AKT. Note: in panel A, both sections of the western blot are taken from a single western blot to exclude une N=4; All conditions normalized to respective vehicle treatment. Error bars= SEM *= significant difference compared to STHdh Q7/Q7 by student t-test. ***Work done with the assistance of Daniel Rose and Rachana Nitin.***
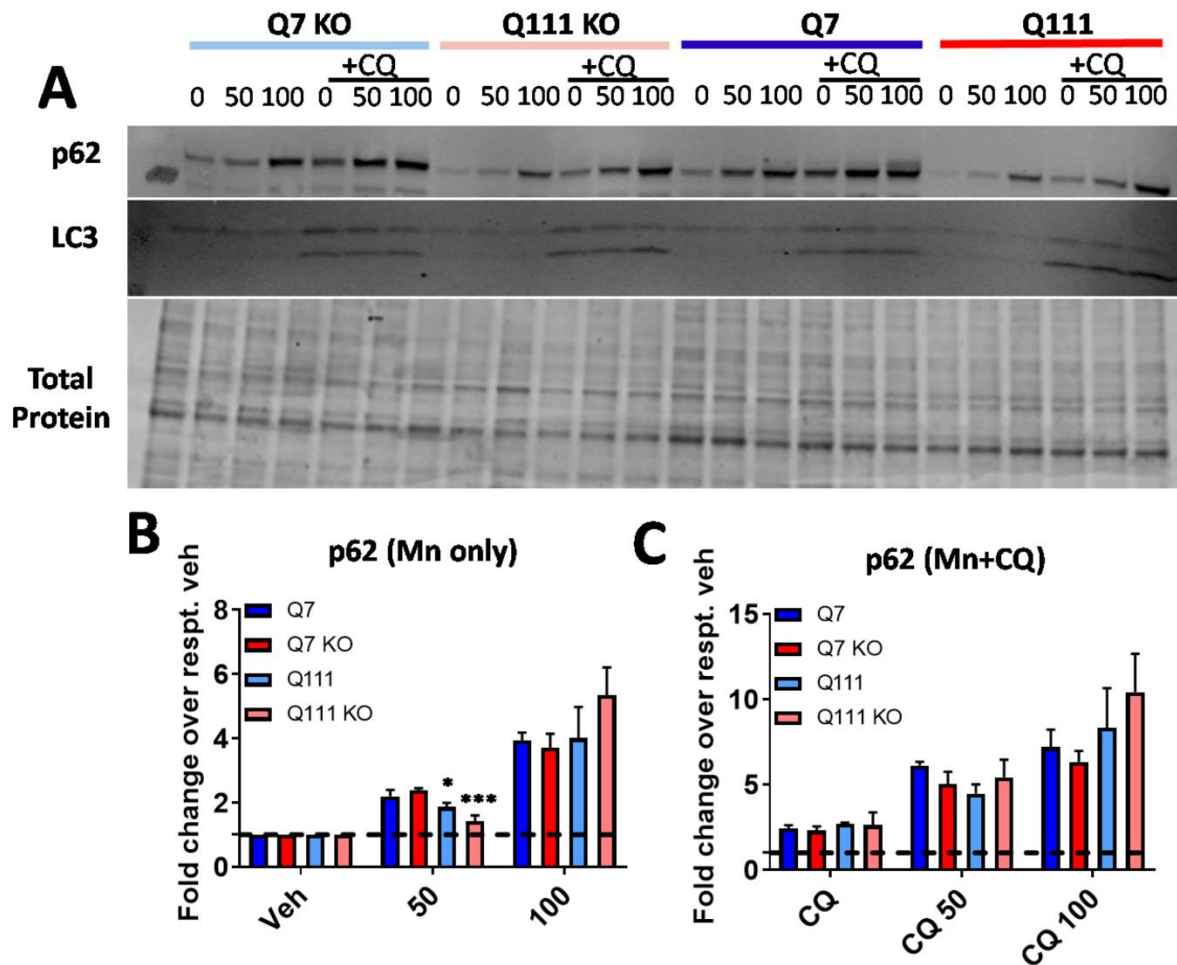
Figure 5-3: Mn-induced p62 defect persists in Q111/Q111 HTT KO. Quantification of p62 expression after 24hr Mn treatment in CRISPR-Cas9 HTT knockouts. A) Representative western blot of p62 in STHdh Q7/Q7 and Q111/Q111 and their KO counterparts **B**) Quantification of p62 after Mn treatment (50-100uM) **C**) p62 after Mn+CQ treatment **D**) quantification of intracellular Mn by CFMEA in STHdh cells and HTT KOs. N=3; Error bars= SEM; *= significant difference from Q7/Q7 by student t-test. ***Work done with the assistance of Daniel Rose.***

loss of HTT expression in Q7 cells did not increase net Mn uptake (**Fig 5-2B**). Additionally, loss of HTT expression in WT Neuro2A (clones 459-8 and HTT-1) cells did not affect Mn uptake (**data not shown**). This suggest 1) Mn uptake defect in the Q111 cells is due to a gain-of-function transport deficit and 2) WT HTT does not play a substantial role in Mn transport in these cells. We also assessed Mn-induced p-AKT after a 1hr serum deprivation followed by 3hr Mn+IGF exposure. Interestingly, Mn induced p-AKT was blunted equally in the Q111 and both Q7-KO and Q111-KO cells compared to Q7 (**Fig 5-2A, C**). Pan AKT was not changed by Mn exposure in any cell line, though basal levels of pan AKT were slightly higher in Q111 and Q111 KO. This provides evidence that Mn induced p-AKT is not entirely dependent on intracellular Mn levels and that loss of HTT function may cripple Mn induced cell signaling without affecting Mn uptake.

We then tested the hypotheses that knocking out HTT negatively effects autophagy, that Mn-induced autophagy is HTT dependent, and if knocking out HTT ameliorated Mn-induced autophagy in HD cells. We treated unmodified and CRISPR KO Q7 and Q111 cells with Mn and/or CQ for 24hrs and found that loss of mutHTT expression in Q111 cells restored Mn-induced p62 (50 µM Mn). Interestingly, Mn-induced p62 after 100 µM Mn was not different between cells lines which may be due to a ceiling effect (**Fig 5-3B**). This included the Q111 cell line which exhibits a Mn-induced p62 deficit at 50 µM. Similar to previous results, p62 expression after CQ or Mn+CQ was similar between all lines, even the HTT KOs (**Fig 5-3C**). These data suggest that loss of all HTT expression does not perturb Mn-induced autophagy in these cells. We did not investigate whether loss of mutHTT restored "cargo recognition failure" in Q111 cells, though this could provide a future follow-up study.

Together, these results suggest loss of WT HTT function may initiate a complex set of downstream events. First, we found that loss of WT HTT from the Q7/Q7 cells, did not affect Mn uptake, suggesting WT HTT does not play a significant role in normal Mn homeostasis in these cells. Second, while loss of mutant HTT in the Q111/Q111 cells (which do not express WT HTT), normalized Mn uptake and did not negatively impact basal expression of autophagy markers or Mn-induced autophagy, loss of WT HTT in the Q7/Q7 cells resulted in impaired Mn-induced p-AKT. Since Mn uptake is identical between Q7/Q7 WT cells and their HTT KO counterparts, but yet Mn-induced p-AKT is negatively affected in the KO cells, this may suggest that p-AKT induction by other stimuli (IGF/insulin, glucose, etc), may also be impacted as well. Future studies will have to examine if this is the case *in vitro*, and, if so, determine if this presents significant, biologically-relevant effects *in vivo. Lastly,* while decreased Mn bioavailablity has not yet been directly detected in human HD patients (only in hiPSC-derived neuroprogenitors), this data suggests, in the context of HTT-silencing ASOs, that loss of mutant HTT can normalize Mn bioavailabilty and potentially remedy Mn-centric phenotypes in HD. Follow-up studies

should examine whether loss of mutant HTT can normalize net Mn uptake and ameliorate *in vivo* Mn-dependent HD phenotypes such as arginase activity.

KB-R7943 likely functions as an autophagy inhibitor to increase net Mn uptake

Perhaps one of the most significant obstacles in examining Mn uptake in HD models is the fact that our only experimental procedure to increase net Mn uptake is to treat HD cells or mice with high-levels of exogenous Mn. However, these presents two major issues: 1) treatment with Mn is usually much higher than the concentrations present in normal brain tissue or CSF and 2) after treatment with Mn, we are no longer observing basal, biological Mn homeostasis. Thus, our lab and others have sought way to genetically or pharmacologically manipulate Mn uptake. We previously reported that a small molecule (KB-R7943), an inhibitor of NCX1/3, could increase Mn uptake in HD cells, ameliorating a Mn-induced p-p53 defect. We wanted to discern the mechanism by which KB-R7943 can increase Mn uptake. We compared Mn uptake after exposure with KB-R7943 (10uM) and SEA0400 (2nM), a more specific inhibitor of NCX1/3, for 3 and 24hrs. We found that SEA0400 did not increase Mn uptake, even after 24hr exposures **(Fig 5-4A, B)**. A previous study found that KB-R7943 can inhibit autophagy in prostate cancer cells[406]. We hypothesized that, similar to CQ and BafA, KB-R7943 increases Mn uptake by impinging on autophagic degradation. We exposed cells to combinations of Mn, CQ, and KB-R7943 and found that co-treatment of KB-R7943 and CQ doesn't increase Mn uptake more than KB-R7943 or CQ alone **(Fig 5-4C)**. This suggest a shared mechanism of increasing net Mn uptake by CQ and KB-R7943. Similar to CQ, KB-R7943-induced increases in Mn uptake were negated by co-treatment with the autophagy inhibitor 3-methyladenine (**Fig 5-4D**). Finally, we confirmed that KB-R7943, similar to CQ and BafA, increases LC3II/I and p62 expression **(Fig 5-4E,F)**. We also observed an increased in LC3-II puncta in ds-Red LC3-II expressing SThdh cells **(data not shown).** Together, this suggests manipulation of the autophagic processing in these cells may present a method to modulate Mn homeostasis pharmacologically. However, these experiments with KB-R7943 were done in the presence of exogenous, high levels of Mn, as detection of basal Mn concentrations is low-throughput and costly to perform. Future experiments should determine whether treatment with KB-R7943 and other autophagy inhibitors (CQ, BafA, 3-MA) can affect basal Mn homeostasis (without co-exposure with Mn) via use of GFAAS or ICP-MS. Since the HD SThdh cells also present with a basal Mn deficiency, one might hypothesize that autophagy inhibitors could ameliorate this basal difference. If this is the case, future experiments in hiPSC-derived neuroprogenitor and *in vivo* could confirm whether defects in autophagic processing may contribute (or even be a primary cause) of the net Mn uptake we have observed in multiple HD models.
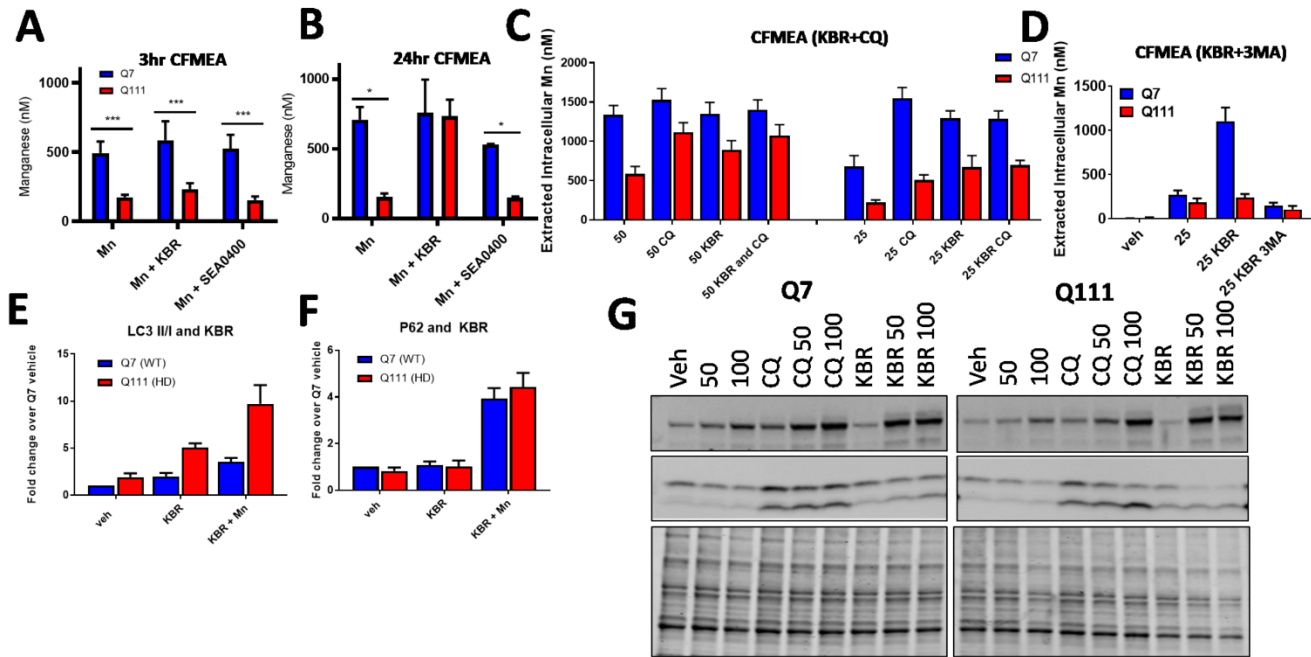
Figure 5-4: KB-R7943 increases Mn uptake via chloroquine-like properties, not via effects on NCX1/3. A, B) Mn uptake (CFMEA) in STHdh cells following treatment with 10uM KB-R7943 or 1uM SEA0400 (NCX1/3 inhibitor) after 3hrs (A) or 24hrs (B). **C)** Mn uptake (CFMEA) in STHdh cells after 24hrs with 25, 50uM MN and 10uM KB-R7943 or 10uM chloroquine. **D)** Mn uptake in STHdh cells after 24hr treatment with 25uM Mn with 10uM KB-R7943 and 5mM 3-methyladenine. **E, F)** LC3II/I (E) and p62 (F) expression in STHdh cells after 24hr treatment with 50uM Mn and 10uM KB-R7943. **G)** Representative western blot of STHdh cells after 24hr treatment with Mn (50-100uM) and CQ (10uM) or KB-R7943 (10uM). N=3, error= SEM. *= significant treatment difference by student t-test. *Work done with the assistance of Michael O'Brien.*

Patient-derived lymphoblasts are not an appropriate model system to examine Mn-induced IGF signaling or autophagic processing in HD

Our lab has detected Mn-dependent phenotypes in hiPSC-derived striatal neuroprogenitors, STHdh immortalized cells, HTT-inducible PC12 cells, and in YAC128 mice[81,82,315]. However, we wanted to explore whether patient-derived lymphoblasts could be a viable HD model in which we could cheaply and easily acquire a range of HD patients with various CAG repeats and disease pathology. Through HD-enroll, we acquired 30+ control and HD patient-derived lymphoblast (male/female, with non-pathogenic CAG repeats or 40, 50, 60, or 70+ CAG repeats). We assessed Mn-induced p-AKT and p-S6 in control and HD patient-derived lymphoblasts. For these experiments, we used two control lines (Conl3, Conl5) and three HD lines with 40, 50 or 70 CAG repeats (HD40, HD50, HD70). We did not observe a genotype difference in Mn-induced p-AKT or p-S6. However, consistent with our results in other cell lines, BMS-536924 was able to block Mn- induced p-AKT in WT cells (**Fig 5-5B, C**). However, we found high variability between cell lines (of the same genotype) and between replicates which could be a result of patient-to-patient differences and inconsistent growth patterns of lymphoblast culture **(Fig 5-5C, E)**. Additionally, we found that p-AKT and p-S6 in these cells was unresponsive to IGF treatment (either in normal-serum conditions or after IGF deprivation), suggesting a unique IGF physiology in these cultures which isn't present in any other cell lines tested (**data not shown**). This also excludes the possibility that the RPMI media (with 15% FBS) used for 24hr exposures is the reason these cells are unresponsive to IGF. Thus, these cells are likely a poor system to study IGF-based signaling. Next, we wanted to explore autophagy-centric HD phenotypes in these cells as HD lymphoblasts were one of the models used the study by Martinez-Vicente and colleagues to detect mutant HTT-dependent defective cargo recognition[131]. Similar to Figure 4-20, we carried out TEM on control and HD lymphoblasts to detect and quantify the number of "empty" autophagic vacuoles in these cells. Unlike the STHdh cells, we found that autophagosomes in HD lymphoblasts presented with highly variable size, number, and morphology. Most importantly, we observed a high number of empty autophagosomes in both control and HD lymphoblasts (though this varied drastically between cells) **(Fig 5-5F).** Presently, we do not understand the reasons autophagy in our lymphoblasts presented very differently from Martinez-Vicente and colleagues[131]. However, we found that maintaining uniformity between cell lines and replicates in lymphoblasts cultures was more difficult than STHdh cells. This is primarily because the grow in large, adhesive clumped suspension culture which could lead to vastly difference nutrient biology depending on cell growth and density of cellular "clumps." This may lead to perturbations in normal IGF/insulin signaling and autophagy in these cells. Future studies examining autophagy in
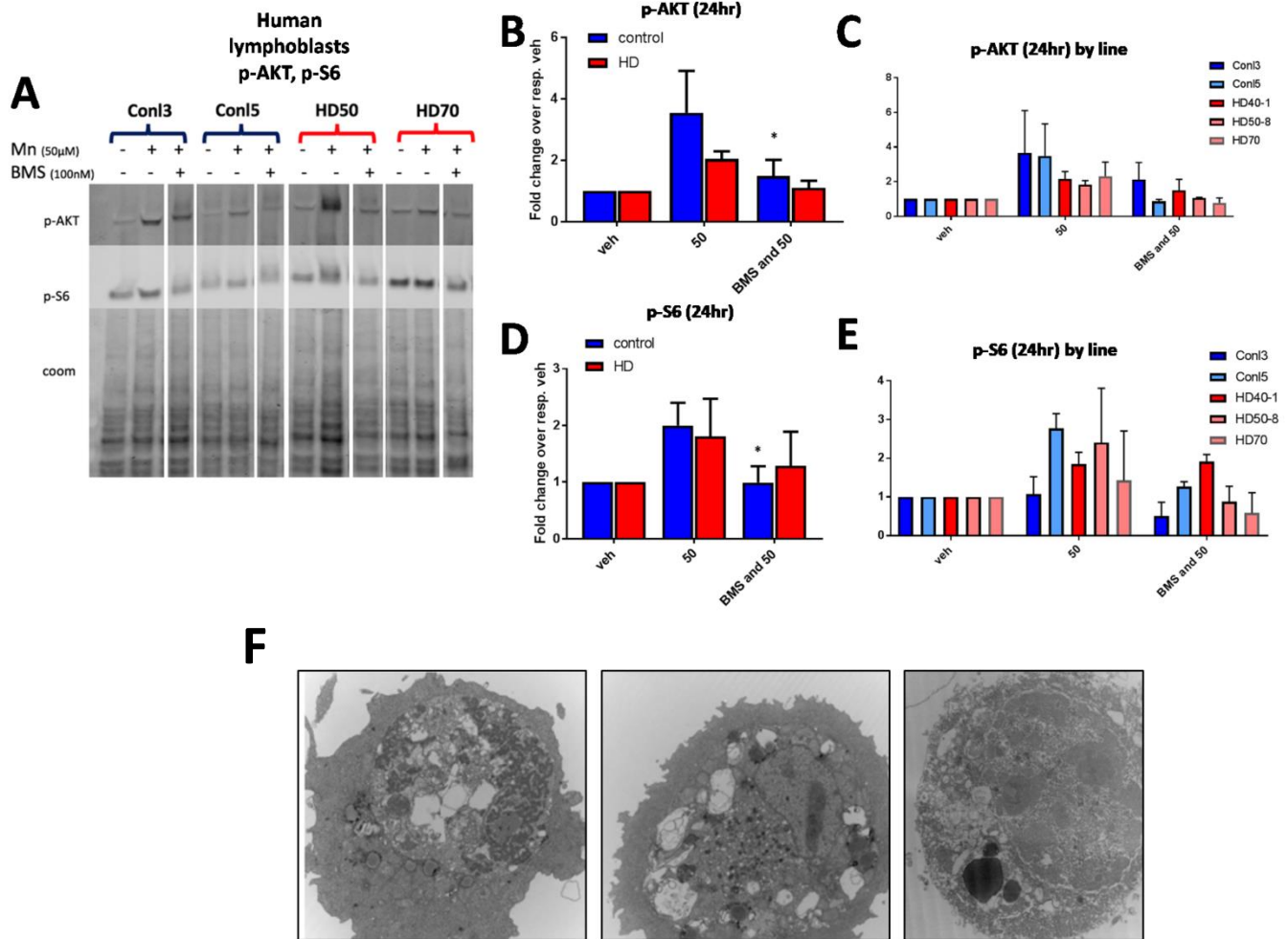
Figure 5-5: Representative western blots and quantification of lymphoblasts from control and HD patients probed with p-AKT, and p-S6. Quantification of p-AKT **(B, C)** or p-S6 **(D, E)** shown with all control and HD lines pooled (left) or separate (right). **F)** Representative TEM images of heavily disrupted autophagic-lysosomal processing in lymphoblasts. *= significant difference from 50uM Mn alone by student t-test. ***Work done with the assistance of Kristen Nordham.***

these cells will need to carefully determine ideal plating density, growth-rates, and trituration of these cells to establish rigorous, uniform cultures between cell lines and replicates if possible.

HD cells are more responsive to Mn-induced lipophagy (lipid autophagy)

After observing increased cargo-loading with 24hr Mn treatment, we wanted to investigate whether this affects specific autophagic cargo. Cuervo and colleagues previously found that defective cargo recognition resulted in accumulation of mitochondria and lipids [131]. We hypothesized that Mn treatment may correct this autophagy-related phenotype via increased lipid cargo loading and subsequent degradation. Consistent with this previous study, we found that HD cells exhibited significantly higher number of bodipy puncta than WT after vehicle treatment. Additionally, Mn treatment significantly increase bodipy puncta, though HD cells were surprisingly more sensitive. 100uM Mn treatment in WT cells increased bodipy puncta to HD levels. When co-exposed with CQ, Mn treatment increased bodipy puncta in HD cells only **(Fig 5-6).** These results are counter-intuitive given our existing data, but may suggest that Mn treatment differentially affects autophagy depending on genotype and type of cargo. Future studies should consider utilizing confocal imaging to count bodipy puncta across the entire depth of the cell, as our studies utilized single-plane light microscopy. This may provide a more accurate measurement of lipophagy.

Mn-induced toxicity is unaffected by pharmacological IGF receptor inhibition

There is great interest in determining novel avenues to counteract Mn-neurotoxicity. Mn-induced AKT activity has been correlated with Mn exposure and neurotoxicity for some time, though the exact mechanism how this occurs was unknown[42,49,85,301]. We found Mn-induced p-AKT is almost entirely dependent on insulin/IGF receptors. However, we wanted to assess if inhibition of Mn- induced p-AKT (by targeting IGFR/IR) was capable of preventing Mn-induced neurotoxicity as well. We assessed STHdh, 3T3, HEK293, Neuro2A, and SHSY-5Y cell viability after 24hrs using toxic Mn exposure with or without BMS-754807. We found that BMS-754807 neither prevented or exacerbated Mn-induced cytotoxicity (**Fig 5-7**). This suggests that Mn-induced p-AKT does not mediate Mn cytotoxicity under acute exposures in these cells and is likely not a viable target to counteract Mn neurotoxicity.

Mn-induces p62 and p-AKT in mouse kidney and liver tissues, but not cortex

Lastly, we investigated whether autophagy markers (p62, LC3, and beclin) were upregulated by *in vivo* Mn-treatment in acutely treated 13-week old or chronically treated 32-week old mice. For these experiments, we used YAC128Q mice expressing a transgene for full-length mutHTT with 128Q and WT littermates. We examined cortical tissue in the brain in addition to kidney and liver tissues (both of

which play a large role in sequestration and clearance of Mn after subcutaneous treatment). In acutely treated (1-week) mouse liver and kidney, we found that Mn was only able to significantly increase p-AKT in WT mice (**Fig 5-8**). We have not yet investigated whether HD liver or kidney (in addition to striatum) exhibit reduced Mn uptake, though this could explain the difference in Mn-induced p-AKT. Mn-induced p-IGFR/IR, p-S6, and p62 trended towards significant difference by treatment, and should be investigated with a higher number of replicates.

We also investigated the effect of Mn on chronically-treated (20-week treatment) mouse liver in kidney. In liver, we found that Mn was only able to significantly increase WT p62, but not p-IGFR/IR, p-AKT, or p-S6 (**Fig 5-9)**. Mn trended towards increasing p-AKT and decreasing p-S6, though additional replicates are needed. In kidney, Mn significantly increased p-AKT and p62 in WT mice and p-AKT and p-S6 in HD mice (**Fig 5-10**). Here, we did not observe a difference in Mn-induced p-AKT, which we did observe in acutely treated mouse kidney. Surprisingly, Mn increased p-S6 only in HD mice, suggesting HD kidney p-S6 may be *more* responsive to Mn. Similar to chronically treated mouse liver, we found Mn induced p62 only in WT mice, though HD mice trended very similarly. Overall, chronically-treated mouse kidney and liver were more responsive than acutely-treated.

We next investigated the effects of chronic (20-week) Mn treatment in mouse cortex (striatal tissue was not available). Mn did not upregulate p-AKT, p-S6, or p62 in mouse cortex (p-IGFR/IR was undetectable). We have previously shown that acutely Mn-treated cortex takes up ~33% less Mn than striata[81], though this may not be the case under chronic Mn injection. This may provide and explanation as to why we saw no effect on p-AKT, p-S6, or p62. In order to investigate this further, striatal tissue should be analyzed. Previous studies have observed Mn-induced p-AKT in post-natal treated rat striata[85]. If Mn also has no effect in the striatum, this may suggest that these proteins are only responsive to toxic Mn conditions (as our current injections do not cause overt cell death in the brain). Injections with higher concentrations of Mn under similar *in vivo* experimental paradigms may allow us to understand why IGF signaling/autophagy in the cortex (or the brain as a whole) is less responsive to Mn treatment than *in vitro* cell culture and chronically Mn-treated mouse liver and kidney. ICP-MS also allows us to determine true Mn uptake (nmol Mn/mg protein) and could directly compare Mn uptake in kidney, liver, cortex, striata, and cell culture. This may reveal the threshold Mn concentration which is necessary to trigger activation of these proteins.
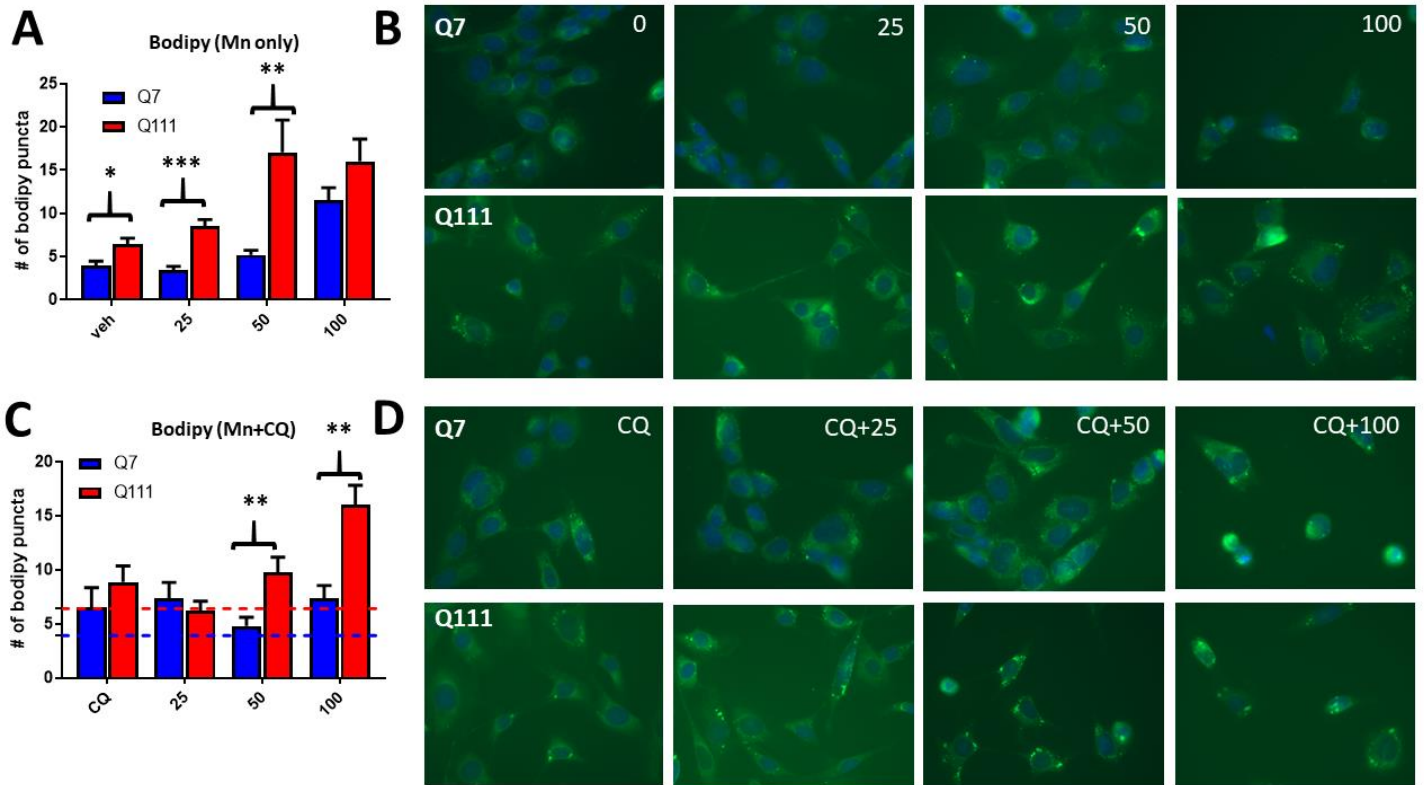
Figure 5-6: Mn induces bodipy puncta differently between Q7/Q7 and Q111/Q111. **A)** Quantification bodipy puncta in STHdh cells treated with 25-100uM Mn for 24hrs**. B)** Representative bodipy images of STHdh Q7/Q7 and Q111/Q111 cells after Mn treatment. **C)** Quantification bodipy puncta in STHdh cells treated with CQ and 25-100uM Mn for 24hrs. **D)** Representative bodipy images of STHdh Q7/Q7 and Q111/Q111 cells after CQ+Mn treatment. ***Work done with the assistance of Rachana Nitin.***
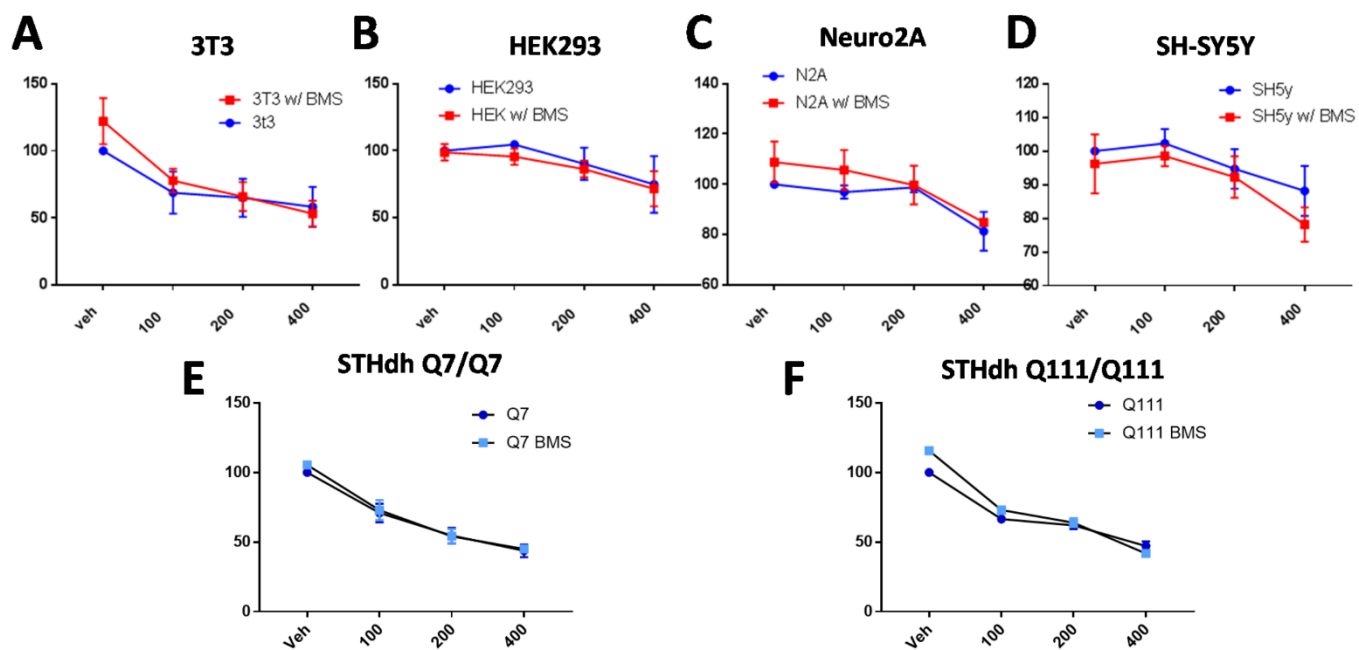
Figure 5-7: Mn-induced toxicity is not modulated by IGFR/IR inhibition. Quantification of cell survival following exposure with 100-400uM Mn with or without BMS754807 (2nM) for 24hrs in 3T3 (**A**), HEK293 (**B**), Neuro2A (**B**), SH-SY5Y (**D**), STHdh Q7/Q7 (**E**), STHdh Q111/Q111 (**F**). N=3; Error bars= SEM
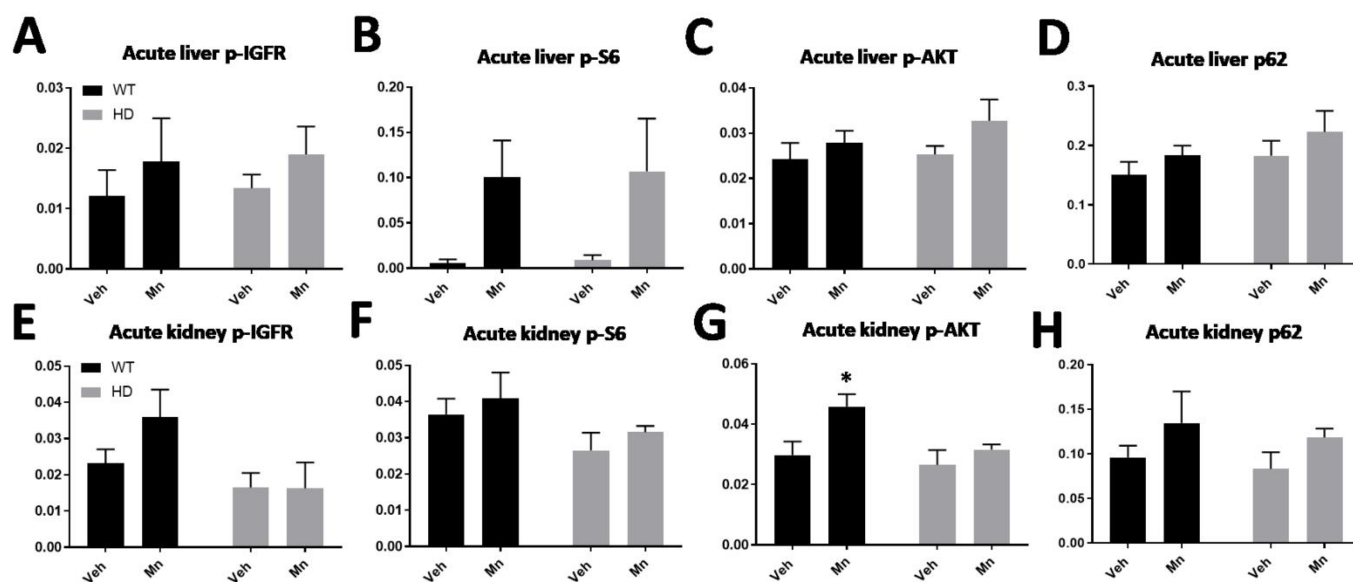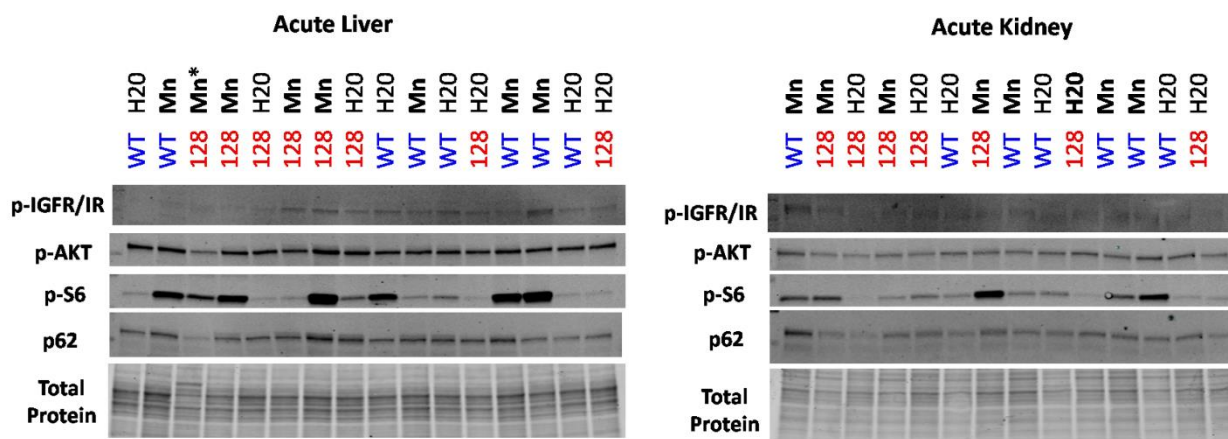
Figure 5-8: Mn increases p-AKT expression in mouse kidney after 1-week of subcutaneous injection. Western blot images and quantification for p-IGFR/IR, p-AKT, p-S6, and p62 in 13-week old mouse liver (**A-D**) and mouse kidney (**E-H**). N=3-4 per condition, per genotype. Both male and female mice were used. Quantified as signal/total protein for each lane. *= Significance treatment difference by student t-test. ***Mouse tissue dissected by Jordyn Wilcox and Anna Pfalzer.***
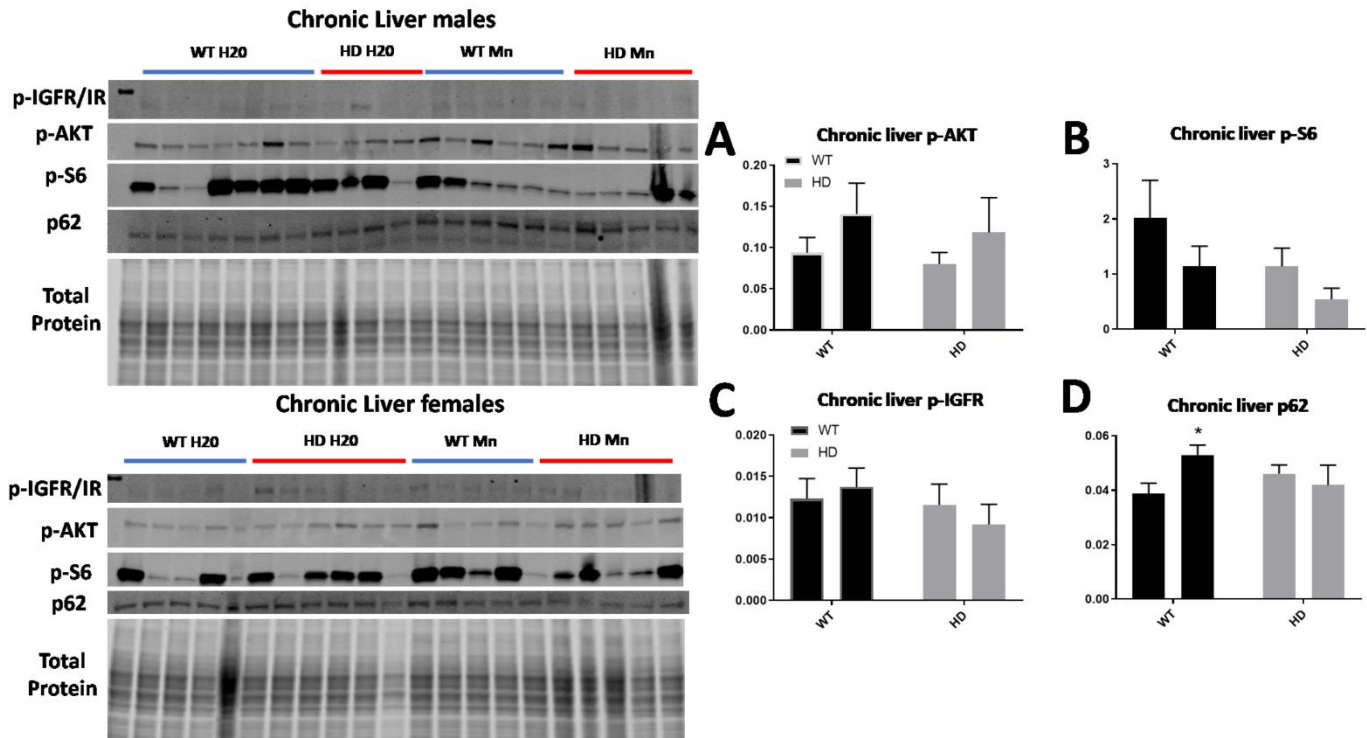
Figure 5-9: Mn increases p62 expression in mouse cortex following chronic 20-week chronic subcutaneous injection. Western blot images and quantification for p-AKT (**A**), p-S6 (**B**), p-IGFR/IR (**C**)and p62 (**D**) in 32-week old mouse cortex after chronic 20-week Mn injection. N=10-12 per treatment, per genotype. Males and females were used. Quantified as signal/total protein for each lane. *= Significance treatment difference by student t-test. *__Mouse tissue dissected by Jordyn Wilcox and Anna Pfalzer.__*
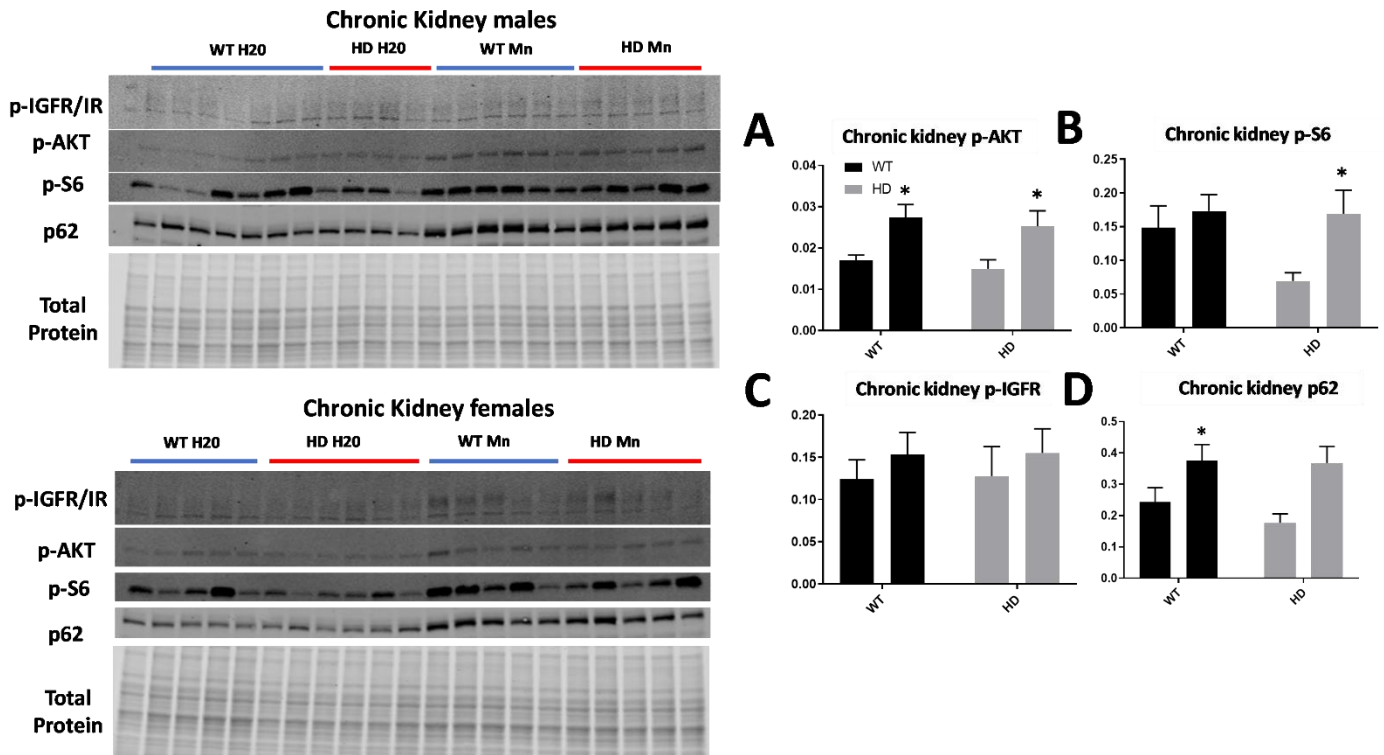
Figure 5-10: Mn increases p-AKT and p62 expression in mouse kidney following chronic 20-week chronic subcutaneous injection. Western blot images and quantification for p-AKT (**A**), p-S6 (**B**), p-IGFR/IR (**C**), and p62 (**D**) in 32-week old mouse cortex after chronic 20-week Mn injections N=10-12 per treatment, per genotype. Males and females were used. Quantified as signal/total protein for each lane. *= Significance treatment difference by student t-test. ***Mouse tissue dissected by Jordyn Wilcox and Anna Pfalzer.***
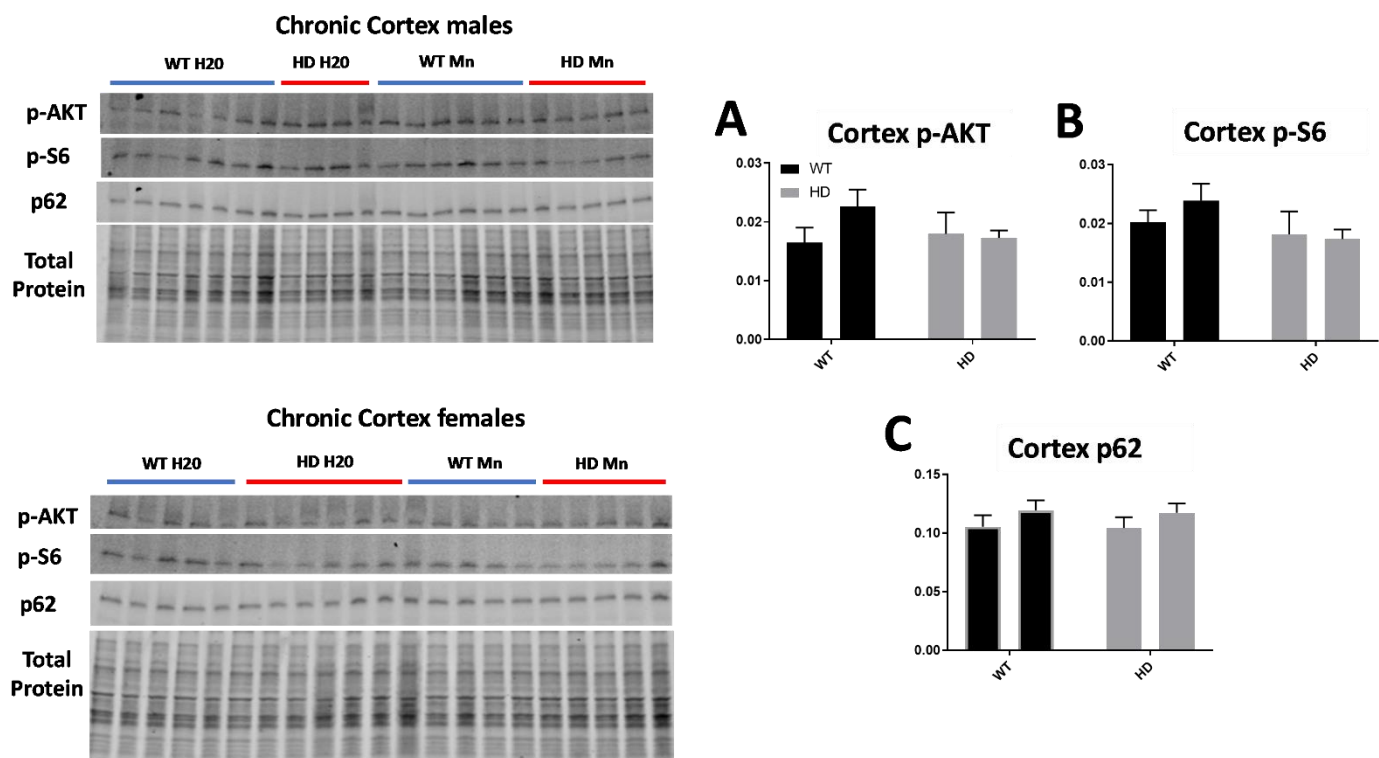
Figure 5-11: Mn does not increase p-AKT, p-S6, or p62 expression in mouse cortex following chronic 20-week chronic subcutaneous injection. Western blot images and quantification for p-AKT (**A**), p-S6 (**B**), and p62 (**C**) in 32-week old mouse cortex after chronic injection. N=10-12 per treatment, per genotype. Males and females were used. Quantified as signal/total protein for each lane. *Mouse tissue dissected by Jordyn Wilcox and Anna Pfalzer.*

Global Discussion

As a growing body of evidence supports a role for Mn in a wide-variety of kinase signaling, including IGFR/IR, it leads us to wonder: what is the full extent of the Mn-induced kinase signaling network and to what extent is this network perturbed under Mn toxicity or Mn deficiency? This work has shown that Mn can robustly activate p-AKT, p-S6, and p-IGFR/IR and also able to induce downstream processes such as glucose uptake and autophagy. However, the list of Mn-dependent enzymes (MnSOD, PP2A phosphatase, pyruvate carboxylase, ATM, LRRK2, members of MRE DNA-damage complex, glutamine synthetase, etc.) and Mn-responsive proteins (MAPK/ERK, JNK, NFKB, Nrf2, tyrosine hydroxylase, FOXO1/3, tau, etc.) is extremely vast and growing[32]. Since the vast majority of kinases are Mn or Mg-dependent, one would expect many other proteins to be Mn-dependent or responsive[340]. With the advent of RNA-seq and high-throughput protein expression platforms, future studies should examine how Mn exposure or deficiency modulate entire networks of signaling pathways. Given the extensive list of Mn-responsive proteins, there is likely complex co-regulation and feedback between these pathways which could be missed without analysis of whole signaling networks. Here, we provide evidence that autophagy and glucose uptake are both affected by Mn exposure and blunted in the context of Mn-deficiency (HD cells). This may provide two avenues by which Mn treatment may be efficacious in treating HD models- work that is currently being carried out in our lab. However, given the extensive network of proteins which can respond to Mn, other studies should examine which other biological processes are affected by Mn treatment. In particular, the field should carefully elucidate of processes which are most sensitive to Mn (near normal brain/CSF Mn concentration). Understanding which pathways are explicitly affected by normal vs toxic concentrations of Mn is an important avenue of investigation and could help justify treatment with Mn in HD.

Fortunately, numerous studies, including our own, have found several HD-relevant proteins and pathways which are responsive to Mn and could provide the foundation for future studies. Work from Tidball et al, suggest the DNA damage response may be another process which exquisitely tied to Mn homeostasis since several enzymes necessary for this process are Mn-dependent.[82] Furthermore, AKT and p53, two major proteins involved in inhibition or activation of apoptosis, respectively, (via interactions with MDM2), are Mn-responsive, suggesting a role for Mn in mediating apoptosis[407]. In Chapter 5, I present evidence that lipid biology (via interactions with autophagy) is also sensitive to Mn treatment. While a few studies have examined the effect of dietary Mn on lipid homeostasis, few have investigated this at the cellular level[408,409]. Mn toxicity has also been associated with increased accumulation of ROS via interactions with Nrf2, NFKB, and MnSOD (Nrf2 and NFKB are both also implicated in autophagy and interact with p62)[380,410-417]. Because of this, many studies have suggested

that Mn toxicity may begin via early accumulation and subsequently-associated decline in mitochondrial function though this hypothesis [52,266,280-283,355] has been under some contention. Contrarily, Mn homeostasis must maintain proper function of anti-oxidant proteins such as MnSOD which counteract ROS accumulation and subsequent mitochondrial failure[32,418]. Thus, studies must carefully determine the threshold of essentiality and toxicity on mitochondrial function. Furthermore, if Mn directly affects mitochondrial function (positively or negatively), what does this mean for downstream cellular energetics? Are processes such as oxygen consumption, ATP production, and glucose metabolism also affected and how this is differentially affected between Mn deficiency, normal Mn concentrations, and toxic Mn concentrations? Together, a comprehensive comparison between a variety of Mn-responsive biological processes, may provide valuable insight into processes which are most exquisitely tied to Mn homeostasis and provide the highest degree of meaningful, translational potential- in both the context of Mn deficiency (HD) and Mn toxicity.

Lastly, and perhaps most importantly, how do the effects of Mn on these processes then manifest themselves *in vivo,* particularly in the brain? For instance, does Mn increase glucose uptake or autophagic cargo recognition *in vivo.* Here, we find that micromolar concentrations of Mn are able to stimulate these processes, but this likely causes cellular accumulation of Mn which is several degrees higher than what would be observed in humans, even if sub-cytotoxic during our exposures. This led us to examine whether sub-toxic Mn supplementation could also upregulate IGF signaling and autophagy *in vivo.* In Figures 5-8, 5-9, 5-10, 5-11 we have shown that acute and chronic Mn treatment can incur significant changes in p-AKT and p62 in mouse liver and kidney, but not in cortical tissue (striatal tissue was not available). While the basal ganglia contain the highest concentrations of Mn in the brain, the liver and kidney play a large role in bodily Mn homeostasis and excretion[84,418]. With this in mind, we should 1) monitor potential peripheral, in addition to CNS, effects after in vivo Mn treatment and 2) put forth more effort into understanding why the brain is resistant to Mn-induced signaling. One reason for this may be the route of Mn delivery. As we treat mice with subcutaneous injection which must be processed by the periphery before transport to the brain, this may lead to increased peripheral effects with diminished effects in the CNS. Since Mn toxicity is most often caused by inhalation (and more easily transported across the blood-brain-barrier via the nasal passage), one must wonder if intranasal Mn delivery may be a more appropriate mode of delivery to incur the highest and most CNS specific Mn response. IGF treatment in HD models was performed via intranasal delivery for these same reasons[92]. Alternatively, our results likely also suggest *in vivo* models are capable of diminishing the effects of Mn on the CNS (via higher excretion through the periphery or decreasing net Mn uptake into the brain- cellularly or across the blood brain barrier). Together, future studies have multiple

avenues of investigation but should carefully interrogate which enzymes and pathways are most sensitive, most specific to the CNS, and result in biologically-relevant, *in vivo* responses.

There are several challenges to studying Mn biology in HD. First, Mn is more difficult and less throughput to quantify than other cell signaling modifiers (enzymes, ligands, etc). Currently, we can only measure Mn concentrations in lab via CFMEA after exogenous Mn exposure (CFMEA cannot measure basal Mn concentrations). While we have access to measure Mn by GFAAS and ICP-MS via collaborators, these methods are costly, low-throughput, and often highly variable. Our lab is actively working on other pharmacological methods to modulate and measure Mn homeostasis, but still lack the utility and sensitivity to robustly interrogate certain aspects of Mn-HD biology. As mentioned above, XANES spectrometry may offer a more sensitive and useful measurement of Mn (and other ions), but this technology is not widely available. Second, we currently can only test how exogenous Mn treatment can ameliorate HD phenotypes. While this is useful in determining whether Mn treatment may remedy HD phenotypes, it lacks some mechanistic utility. For instance, we can confidently state that Mn treatment normalizes arginase activity of HD mice *in vivo*[315], but we don't know if Mn deficiency causes defects in arginase activity in WT mice. In these studies, we find similar results with IGF signaling and autophagy. One of the primary reasons this is difficult to manipulate, is that Mn can be transported via dozens of other ion transporters (particularly at high concentrations), so genetic or pharmacological inhibition of specific transporters is often ineffective[32]. To our knowledge, there are not any specific Mn chelators or small molecule inhibitors which could provide a method to cause Mn deficiency and would allow us to determine if Mn deficiency causes HD- phenotypes. We are actively looking into methods to lower dietary Mn *in vivo*, create medias with low Mn concentrations to mimic the effects of Mn deficiency, and investigate Mn-specific small molecules which may provide other highly-mechanistic alternatives. Lastly, our studies are limited by the models currently available to us. While both the STHdh and hiPSC-derived neuroprogenitors are of striatal-like origin, they are very different from the mature MSNs which degenerate in HD. While our studies here suggest Mn treatment robustly activates IGF signaling and autophagy in neuroprogenitors, this may be very different in post-mitotic, electrically-active MSNs with drastically different signaling and cellular homeostasis (potentially including Mn uptake). If they are different, does this suggest only immature neuronal subtypes exhibit reduced Mn uptake? If so, this would drastically alter our understanding of this phenotype and should influence how future studies approach Mn supplementation. Future studies should search for more ideal models such as primary striatal culture from mice or iPSC-derived medium spiny neurons, and directly compare these to our present models. However, these are far less throughput, more difficult to culture, and more costly than our current models.

Concluding Remarks

Huntington's disease remains a disease without a cure. While incredibly promising therapies lay on the horizon, the field as a whole must continue to search for unique avenues to better understand and target this terrible disease. Our lab has now discovered a variety of HD phenotypes (both *in vitro* and *in vivo*) caused by reduced Mn bioavailability and several which can be rescued by Mn supplementation- two of which (autophagy and IGF signaling) our outlined in this thesis. Many of these, including defects in the urea cycle and in glucose metabolism, are detected very early in HD pathology (prior to neuronal loss and the advent of motor and cognitive dysfunction)[331,419,420]. Similarly, we observed reduced Mn uptake only in prodromal HD mice (prior to disease manifestation). This suggest that reduced striatal Mn may play a key role in early HD pathogenesis and eventually contribute to the motor and cognitive defects observed later in pathology. This may also indicate that early, low-dose Mn supplementation may promote a wide-variety of neuroprotective signaling events and processes (including, but certainly not limited, to IGF-AKT signaling and autophagy, in addition to others mentioned earlier). Thus, pursuit of *in vivo* justification of said neuroprotection should be the primary priority for future studies. With this said, future studies should diligently determine the most appropriate, and most biologically relevant, paradigms (when, how, how much, and how long) to administer Mn supplementation and rigorously examine the potential, wide array of therapeutic benefit on HD phenotypes. While my part of this story may be finished for now, I'm extremely honored to have been a part of this endeavor to find a new way to combat this disease. I'll be excitingly waiting to hear the progress of current and future Bowmanites—good luck!

Materials and Methods

Generation of HTT CRISPR knockout lines

pSpCas9(BB)-2A-Puro (PX459) Vector was a generous gift from Dr. Doug Mortlock. The listed top/bottom oligonucleotides were annealed to create an 18bp adapter sequence which encodes for the sgRNA. The PX459 vector was cut with bbsI and gel purified. Using the Quick Ligation Kit (NEB), adapter sequence was annealed into the PX458 vector. Plasmid was transformed into DH5alpha cells and plated onto a LB+AMP plate. Colonies were picked and Qiagen mini-prep was performed on several colonies. DNA was sequences for the U6F1 (primer sequence listed below) to confirm the adapter was inserted properly. Once insertion was confirmed, the colony was grown up and underwent

a midiprep to isolate the HTT Exon 2 CRISPR plasmid. The selected CRISPR cut site is located in exon 2 of mouse HTT. Cells were plated at 40,000 cells/mL for Q7/Q7 and 50,000 for Q111/Q111. The following day, cells were transfected with Mirus-LT with 1.25 µg PX458 DNA per mL of cells for 24 hours. After transfection, 7.5 µg/mL of puromycin was added for selection for 48 hours. Cells were then expanded and immediately frozen prior to single cell sorting.

The Vanderbilt Cell Imaging Shared Resource (CISR) was used to separate 0.5 million Q7-6 cells and 0.5 million Q111-11 cells to a single cell density on 96 well plates. When viable colonies were established in the well, they were transferred to a 24 well plate. When confluent, the cell lines on the 24-well plate were transferred to a 6 well plate and grown to ~80% confluency. From the 6 well plate, the cells were then split 1:2 and allowed to grown to ~80% confluency in both wells. For each clone, one well was extracted for DNA by aspirating off media, washing twice consecutively with 1mL of PBS, scraping the cells off the plate, and transferring 1mL of PBS and cells to a 1.5 mL micro tube. The other well was frozen down in media with 10% DMSO.

Using the DNeasy kit (Qiagen), DNA was isolated from each clone and underwent PCR targeting a region flanking the CRISPR cut site in exon 2 (Primers and cut sequences below). ThermoScientific DreamTaq Green PCR Master (Catalog ID: K1081) was used for all PCR reactions. PCR reaction: 95ºC/0:15 seconds, 56ºC/0:30 seconds (58ºC for R3 primers), and 72ºC/0:45 seconds for 35 cycles and held at 10 ºC. The PCR was run on 2% agarose gel to assure proper size and specificity (**Fig 5-1**). Products were then purified using Promega Wizard PCR purification kit and submitted for sequencing via Genewiz. These sequences were then entered directly into the TIDE online software for indel formation assessment (https://tide-calculator.nki.nl/). DNA from clones was sequenced for indels via two sets of primers (**Fig 5-1**). A wild-type sequence for each cell line was used for each analysis. Primer sequences are as follows: mHTT- exon 2 CRISPR site R: GTTAGACAATGATTCACA; mHTT- exon 2 CRISPR site F: TGTGAATCATTGTCTAAC; mHTT exon 2 Forward primer: TCTGTCGTCATCCCTTCCTC; mHTT exon 2 reverse primer: CCTCCTGAATGCCAGGTTAC; mHTT- exon2 R3 Forward primer: TGAGTGTCGTGTGAGGAAGC; mHTT- exon2 R3 Reverse primer: GGCTATCCCTGAACTCACCA; U6F1 primer: TACGATACAAGGCTGTTAGAGAG

KB-R7943 pharmacology

KB-R7943 was purchased from Tocris Biological (Cat# 1244) and diluted in DMSO to 10mM. For all experiments, KB-R7943 and chloroquine was used at 10uM. 3MA was used at 5mM. Mn-uptake (CFMEA), western blot, and LC3-II puncta analysis were done as described above in Chapter 3 materials and methods.

Lymphoblast culture

Lymphoblasts were acquired through HD-enroll. 10 control lines and 25 HD cell lines were acquired but only two control lines and three HD cell lines were used for experiments. For all experiments, cells were cultured in RPMI 1640 media with 2mM glutamax and 15% FBS at 37°C. Cell lines were brought up in T25 flask to maintain at 200,000-500,000 cells/mL. Flasks were cultured upright with vented caps with no more than 20mLs of media. Prior to experiments, cells were spun down at 300g for 5-10 minutes to pellet living cells and leave cellular debris in the supernatant. For experiments, cells were plated into T25 flasks at 200,000 cells/mL. During exposures, cells were moved to a 50mL conical and spun down at 200g for 5 minutes. Cells were then re-suspended in media containing Mn and/or BMS-536924 and moved to a T25 flasks. Cells were then incubated for 24hrs. Following this, cells were collected into 50mL conical tubes, spun down at 200g for 5 minutes, and lysed with RIPA containing protease and phosphatase inhibitors. Western blot procedure was carried out identical to methods outlined Chapters 1-3. For TEM, cells were treated with Mn and/or CQ for 24hrs. Following this, cells were prepared for TEM identical to methods outlined Chapter 3.

Bodipy staining

SThdh Q7/Q7 and Q111/Q111 were plated at 80,000 and 100,000 cells/mL, respectively, in Grenier mu-clear 96-well plates. 16- 24 hours after plating, cells were treated for 24hr with Mn(25-100uM) and/or CQ (10uM). 30 minutes before the end of the 24hrs, Bodipy 493/503 (Cat# D3922 Invitrogen) was diluted to 2uM in PBS. Cell media was removed from the 96-well plates and 100uL of PBS+bodipy was added to each well for 15 minutes at 33° C in the dark. After 15 minutes, cells were washed 3X with fresh PBS to rinse away dye and 100uL fresh media (without Mn or CQ) as added back onto the cells. Cells were then immediately imaged (5 images per condition, per cell line for 3 biological replicates). Bodipy puncta and number of DAPI (# of cells) were counted via Cell Profiler 3.0.0.

Cell titer Blue

Mouse striatal cells (STHdh$^{Q7/Q7}$ STHdh$^{Q111/Q1111}$), HEK293, 3T3, Neuro2A, and SH-SY5Y were grown on 96-well plates (33°C for STHdh, 37°C for all other cells). The day after replating, the cells were exposed to toxicants in the cell-type appropriate medium. After 22 hours of exposure with Mn (100-400uM) and/or BMS-754807 (2nM), 20 µL of CellTiterBlue reagent (Promega, Madison, WI) was added to each well. Prior to this addition, cell lysis buffer was added to several wells to provide an accurate fluorescence background for 0% viable cells. The plates were then incubated for 2 hours at

33°C or 37°C. Fluorescence was measured using excitation of 570 nm and emission of 600 nm on a microplate reader.

In vivo analysis of Mn-induced p-AKT, p-S6, and p62 in YAC128 mice

All animal experiments were approved by the Vanderbilt University Medical Center Institutional Animal Care and Use Committee and were designed to minimized pain. The FVB-Tg (YAC128)53Hay/J mouse was purchased from Jackson Laboratory. C57-YAC128Q mice were generated by crossing YAC128Q with WT C57Bl/6J animals followed by backcrossing >10 generations. Mice were maintained in their genetic backgrounds by crossing hemizygous transgenic animals with their WT littermates. Mice were genotypes by Transetyx for qPCR-based genotyping (Htt Wildtype Forward Primer: GAGAAAGAGAATGTTTAACTCTCCAAGAGA, Reverse Primer: CACATGCACTTTCTACAGCTAGGT, Reporter 1: AAGCAGCTCCAATATC; Htt mutant Forward Primer: CCACTTCCCTCTTCTAGTCTGAGA, Reverse Primer: CCACATCTCTCCAGCTCCAAA, Reporter 1: CCCCGCCTCCTCTCG). WT and transgenic littermates were used for experiments. For *in vivo* studies, mice were treated under two paradigms 1) acute injection or 2) chronic injection. Mice were injected with a 1% solution of $MnCl2 \times 4H2O$ in filtered MilliQ water at 50 mg/kg body weight, or with vehicle (filtered water). For acute injections, only males were used. For chronic injections, males and females were used. For acute injections, mice were treated at 12 weeks of age for 7 days (injected with 50mg/kg Mn on day 0, 3, and 6). On the seventh day, mice were sacrificed by cervical dislocation, kidney and liver tissues were dissected and collected, snap frozen in liquid nitrogen, and stored at -80 degrees. For chronic injections, mice were treated at 12 weeks with 50mg/kg of Mn (injected 2 times a week) until 32 weeks old. At the end of the 12-week treatment, mice were dissected and kidney, liver, and cortical tissues were collected, snap frozen in liquid nitrogen, and stored at -80 degrees Mouse tissues were lysed in RIPA with protease and phosphatase inhibitors and protein concentration was determined with BCA assay. Following this, western blot was carried out as described in methods section of Chapter 1-3.

Acknowledgments

REFERENCES

1   Greenwood, B. N. & Fleshner, M. Exercise, Learned Helplessness, and the Stress-Resistant Brain. *NeuroMolecular Medicine* **10**, 81-98, doi:10.1007/s12017-008-8029-y (2008).

2   Trejo, J. L., Llorens-Martín, M. V. & Torres-Alemán, I. The effects of exercise on spatial learning and anxiety-like behavior are mediated by an IGF-I-dependent mechanism related to hippocampal neurogenesis. *Molecular and cellular neurosciences* **37**, 402-411 (2007).

3   Xiang, Y., Ding, N., Xing, Z., Zhang, W., Liu, H. & Li, Z. Insulin-Like Growth Factor-1 Regulates Neurite Outgrowth and Neuronal Migration From Organotypic Cultured Dorsal Root Ganglion. *International Journal of Neuroscience* **121**, 101-106, doi:10.3109/00207454.2010.535935 (2010).

4   Xing, C., Yin, Y., Chang, R., Gong, X., He, X. & Xie, Z. Effects of insulin-like growth factor 1 on synaptic excitability in cultured rat hippocampal neurons. *Experimental neurology* **205**, 222-229 (2007).

5   Xing, C., Yin, Y., He, X. & Xie, Z. Effects of insulin-like growth factor 1 on voltage-gated ion channels in cultured rat hippocampal neurons. *Brain research* **1072**, 30-35 (2006).

6   Liou, J.-C., Tsai, F.-Z. & Ho, S.-Y. Potentiation of quantal secretion by insulin-like growth factor-1 at developing motoneurons in Xenopus cell culture. *The Journal of physiology* **553**, 719-728 (2003).

7   Ozdinler, H. P. & Macklis, J. D. IGF-I specifically enhances axon outgrowth of corticospinal motor neurons. *Nature neuroscience* **9**, 1371-1381 (2006).

8   Skeberdis, V. A., Lan, J., Zheng, X., Zukin, R. S. & Bennett, M. V. Insulin promotes rapid delivery of N-methyl-D-aspartate receptors to the cell surface by exocytosis. *Proceedings of the National Academy of Sciences of the United States of America* **98**, 3561-3566 (2001).

9   Sosa, L., Dupraz, S., Laurino, L., Bollati, F., Bisbal, M., Cáceres, A., Pfenninger, K. H. & Quiroga, S. IGF-1 receptor is essential for the establishment of hippocampal neuronal polarity. *Nature neuroscience* **9**, 993-995 (2006).

10   Liu, W., Ye, P., O'Kusky, J. R. & D'Ercole, J. A. Type 1 insulin-like growth factor receptor signaling is essential for the development of the hippocampal formation and dentate gyrus. *Journal of Neuroscience Research* **87**, 2821-2832, doi:10.1002/jnr.22129 (2009).

11   Dentremont, K. D., Ye, P., D'Ercole, A. J. & O'Kusky, J. R. Increased insulin-like growth factor-I (IGF-I) expression during early postnatal development differentially increases neuron number and growth in medullary nuclei of the mouse. *Brain research. Developmental brain research* **114**, 135-141 (1999).

12   O'Kusky, J. R., Ye, P. & D'Ercole, A. J. Insulin-like growth factor-I promotes neurogenesis and synaptogenesis in the hippocampal dentate gyrus during postnatal development. *The Journal of neuroscience : the official journal of the Society for Neuroscience* **20**, 8435-8442 (2000).

13   Hurtado-Chong, A., Yusta-Boyo, M. J., Vergaño-Vera, E., Bulfone, A., Pablo, F. & Vicario-Abejón, C. IGF-I promotes neuronal migration and positioning in the olfactory bulb and the exit of neuroblasts from the subventricular zone. *European Journal of Neuroscience* **30**, 742-755, doi:10.1111/j.1460-9568.2009.06870.x (2009).

14   Oishi, K., Watatani, K., Itoh, Y., Okano, H., Guillemot, F., Nakajima, K. & Gotoh, Y. Selective induction of neocortical GABAergic neurons by the PDK1-Akt pathway through activation of Mash1. *Proceedings of the National Academy of Sciences* **106**, 13064-13069, doi:10.1073/pnas.0808400106 (2009).

15   Chiu, S.-L., Chen, C.-M. & Cline, H. T. Insulin Receptor Signaling Regulates Synapse Number, Dendritic Plasticity, and Circuit Function In Vivo. *Neuron* **58**, 708-719, doi:10.1016/j.neuron.2008.04.014 (2008).

16   Ciucci, F., Putignano, E., Baroncelli, L., Landi, S., Berardi, N. & Maffei, L. Insulin-like growth factor 1 (IGF-1) mediates the effects of enriched environment (EE) on visual cortical development. *PloS one* **2** (2007).

17   Hodge, R. D., D'Ercole, J. A. & O'Kusky, J. R. Insulin-like growth factor-I accelerates the cell cycle by decreasing G1 phase length and increases cell cycle reentry in the embryonic cerebral cortex. *The Journal of neuroscience : the official journal of the Society for Neuroscience* **24**, 10201-10210 (2004).

18   D'Ercole, A. J., Ye, P., Calikoglu, A. S. & Gutierrez-Ospina, G. The role of the insulin-like growth factors in the central nervous system. *Molecular neurobiology* **13**, 227-255 (1996).

19   D'Ercole, J. A., Ye, P. & O'Kusky, J. R. Mutant mouse models of insulin-like growth factor actions in the central nervous system. *Neuropeptides* **36**, 209-220 (2002).

20   Root, C. M., Ko, K. I., Jafari, A. & Wang, J. W. Presynaptic Facilitation by Neuropeptide Signaling Mediates Odor-Driven Food Search. *Cell* **145**, 133-144, doi:10.1016/j.cell.2011.02.008 (2011).

21   Jiu, Y.-M., Yue, Y., Yang, S., Liu, L., Yu, J.-W., Wu, Z.-X. & Xu, T. Insulin-like signaling pathway functions in integrative response to an olfactory and a gustatory stimuli in Caenorhabditis elegans. *Protein & Cell* **1**, 75-81, doi:10.1007/s13238-010-0003-4 (2010).

22   Marks, D. R., Tucker, K., Cavallin, M. A., Mast, T. G. & Fadool, D. A. Awake Intranasal Insulin Delivery Modifies Protein Complexes and Alters Memory, Anxiety, and Olfactory Behaviors. *The Journal of Neuroscience* **29**, 6734-6751, doi:10.1523/jneurosci.1350-09.2009 (2009).

23   Haj-ali, V., Mohaddes, G. & Babri, S. H. Intracerebroventricular insulin improves spatial learning and memory in male Wistar rats. *Behavioral Neuroscience* **123**, 1309, doi:10.1037/a0017722 (2009).

24   Dhamoon, M. S., Noble, J. M. & Craft, S. INTRANASAL INSULIN IMPROVES COGNITION AND MODULATES - AMYLOID IN EARLY AD. *Neurology* **72**, 292-294, doi:10.1212/01.wnl.0000344246.91081.2c (2009).

25   Zhao, W., Chen, H., Xu, H., Moore, E., Meiri, N., Quon, M. J. & Alkon, D. L. Brain insulin receptors and spatial memory. Correlated changes in gene expression, tyrosine phosphorylation, and signaling molecules in the hippocampus of water maze trained rats. *The Journal of biological chemistry* **274**, 34893-34902 (1999).

26   Deijen, J. B., de Boer, H. & van der Veen, E. A. Cognitive changes during growth hormone replacement in adult men. *Psychoneuroendocrinology* **23**, 45-55 (1998).

27   Fernandez, A. M. & Torres-Alemán, I. The many faces of insulin-like peptide signalling in the brain. *Nature reviews. Neuroscience* **13**, 225-239, doi:10.1038/nrn3209 (2012).

28   Baxter, R. C. IGF binding proteins in cancer: mechanistic and clinical insights. *Nature reviews. Cancer* **14**, 329-341, doi:10.1038/nrc3720 (2014).

29   Clemmons, D. R., Busby, W. H., Arai, T., Nam, T. J., Clarke, J. B., Jones, J. I. & Ankrapp, D. K. Role of insulin-like growth factor binding proteins in the control of IGF actions. *Progress in growth factor research* **6**, 357-366 (1995).

30   Chan, D. W., Son, S. C., Block, W., Ye, R., Khanna, K. K., Wold, M. S., Douglas, P., Goodarzi, A. A., Pelley, J., Taya, Y. *et al.* Purification and characterization of ATM from human placenta. A manganese-dependent, wortmannin-sensitive serine/threonine protein kinase. *The Journal of biological chemistry* **275**, 7803-7810 (2000).

31   Sato, T., Nakashima, A., Guo, L. & Tamanoi, F. Specific Activation of mTORC1 by Rheb G-protein in Vitro Involves Enhanced Recruitment of Its Substrate Protein. *Journal of Biological Chemistry* **284**, 12783-12791, doi:10.1074/jbc.m809207200 (2009).

32   Horning, K. J., Caito, S. W., Tipps, K. G., Bowman, A. B. & Aschner, M. Manganese Is Essential for Neuronal Health. *Annual review of nutrition* **35**, 71-108, doi:10.1146/annurev-nutr-071714-034419 (2015).

33   Paull, T. T. & Gellert, M. The 3' to 5' exonuclease activity of Mre 11 facilitates repair of DNA double-strand breaks. *Molecular cell* **1**, 969-979 (1998).

34   Trujillo, K. M., Yuan, S. S., Lee, E. Y. & Sung, P. Nuclease activities in a complex of human recombination and DNA repair factors Rad50, Mre11, and p95. *The Journal of biological chemistry* **273**, 21447-21450 (1998).

35   D'Antonio, E. L., Hai, Y. & Christianson, D. W. Structure and function of non-native metal clusters in human arginase I. *Biochemistry* **51**, 8399-8409, doi:10.1021/bi301145n (2012).

36   Kanyo, Z. F., Scolnick, L. R., Ash, D. E. & Christianson, D. W. Structure of a unique binuclear manganese cluster in arginase. *Nature* **383**, 554-557 (1996).

37   Neulen, A., Blaudeck, N., Zittrich, S., Metzler, D., Pfitzer, G. & Stehle, R. Mn2+-dependent protein phosphatase 1 enhances protein kinase A-induced Ca2+ desensitisation in skinned murine myocardium. *Cardiovascular research* **74**, 124-132 (2007).

38   Woźniak-Celmer, E., Ołdziej, S. & Ciarkowski, J. Theoretical models of catalytic domains of protein phosphatases 1 and 2A with Zn2+ and Mn2+ metal dications and putative bioligands in their catalytic centers. *Acta biochimica Polonica* **48**, 35-52 (2001).

39   Maydan, M., McDonald, P. C., Sanghera, J., Yan, J., Rallis, C., Pinchin, S., Hannigan, G. E., Foster, L. J., Ish-Horowicz, D., Walsh, M. P. *et al.* Integrin-Linked Kinase Is a Functional Mn2+-Dependent Protein Kinase that Regulates Glycogen Synthase Kinase-3β (GSK-3β) Phosphorylation. *PLoS ONE* **5**, doi:10.1371/journal.pone.0012356 (2010).

40   Wedler, F. C. & Ley, B. W. Kinetic, ESR, and trapping evidence for in vivo binding of Mn(II) to glutamine synthetase in brain cells. *Neurochemical research* **19**, 139-144 (1994).

41   Dormond, O., Ponsonnet, L., Hasmim, M., Foletti, A. & Rüegg, C. Manganese-induced integrin affinity maturation promotes recruitment of alpha V beta 3 integrin to focal adhesions in endothelial cells: evidence for a role of phosphatidylinositol 3-kinase and Src. *Thrombosis and haemostasis* **92**, 151-161 (2004).

42   Bae, J.-H., Jang, B.-C., Suh, S.-I., Ha, E., Baik, H., Kim, S.-S., Lee, M.-y. & Shin, D.-H. Manganese induces inducible nitric oxide synthase (iNOS) expression via activation of both MAP kinase and PI3K/Akt pathways in BV2 microglial cells. *Neuroscience letters* **398**, 151-154, doi:10.1016/j.neulet.2005.12.067 (2006).

43   Cordova, F. M., Aguiar, A. S., Peres, T. V., Lopes, M. W., Gonçalves, F. M., Remor, A. P., Lopes, S. C., Pilati, C., Latini, A. S., Prediger, R. D. *et al.* In vivo manganese exposure modulates Erk, Akt and Darpp-32 in the striatum of developing rats, and impairs their motor function. *PloS one* **7**, doi:10.1371/journal.pone.0033057 (2012).

44   Crittenden, P. L. & Filipov, N. M. Manganese modulation of MAPK pathways: effects on upstream mitogen activated protein kinase kinases and mitogen activated kinase phosphatase-1 in microglial cells. *Journal of applied toxicology : JAT* **31**, 1-10, doi:10.1002/jat.1552 (2011).

45   Exil, V., Ping, L., Yu, Y., Chakraborty, S., Caito, S. W., Wells, K. S., Karki, P., Lee, E. & Aschner, M. Activation of MAPK and FoxO by manganese (Mn) in rat neonatal primary astrocyte cultures. *PloS one* **9**, doi:10.1371/journal.pone.0094753 (2014).

46   Jang, B.-C. C. Induction of COX-2 in human airway cells by manganese: role of PI3K/PKB, p38 MAPK, PKCs, Src, and glutathione depletion. *Toxicology in vitro : an international journal published in association with BIBRA* **23**, 120-126, doi:10.1016/j.tiv.2008.11.005 (2009).

47   Cordova, F. M., Aguiar, A. S., Peres, T. V., Lopes, M. W., Gonçalves, F. M., Pedro, D. Z., Lopes, S. C., Pilati, C., Prediger, R. D., Farina, M. *et al.* Manganese-exposed developing rats display motor deficits and striatal oxidative stress that are reversed by Trolox. *Archives of toxicology* **87**, 1231-1244, doi:10.1007/s00204-013-1017-5 (2013).

48   Dearth, R. K., Hiney, J. K., Srivastava, V. K., Hamilton, A. M. & Dees, W. L. Prepubertal exposure to elevated manganese results in estradiol regulated mammary gland ductal differentiation and hyperplasia in female rats. *Experimental Biology and Medicine* **239**, 871-882, doi:10.1177/1535370214531865 (2014).

49   Srivastava, V. K., Hiney, J. K. & Dees, W. L. Manganese stimulated Kisspeptin is mediated by the Insulin-like growth factor-1/Akt/ mammalian target of rapamycin pathway in the prepubertal female rat. *Endocrinology*, doi:10.1210/en.2016-1090 (2016).

50   Zhang, J., Cao, R., Cai, T., Aschner, M., Zhao, F., Yao, T., Chen, Y., Cao, Z., Luo, W. & Chen, J. The Role of Autophagy Dysregulation in Manganese-Induced Dopaminergic Neurodegeneration. *Neurotoxicity Research* **24**, 478-490, doi:10.1007/s12640-013-9392-5 (2013).

51   Hiney, J. K., Srivastava, V. K. & Dees, W. L. Manganese induces IGF-1 and cyclooxygenase-2 gene expressions in the basal hypothalamus during prepubertal female development. *Toxicological sciences : an official journal of the Society of Toxicology* **121**, 389-396, doi:10.1093/toxsci/kfr057 (2011).

52   Gunter, T. E., Gavin, C. E. & Gunter, K. K. The case for manganese interaction with mitochondria. *NeuroToxicology* **30**, 727-729, doi:10.1016/j.neuro.2009.05.003 (2009).

53   Kalia, K., Jiang, W. & Zheng, W. Manganese accumulates primarily in nuclei of cultured brain cells. *NeuroToxicology* **29**, 466-470, doi:10.1016/j.neuro.2008.02.012 (2008).

54   Morello, M., Canini, A., Mattioli, P., Sorge, R. P., Alimonti, A., Bocca, B., Forte, G., Martorana, A., Bernardi, G. & Sancesario, G. Sub-cellular localization of manganese in the basal ganglia of normal and manganese-treated rats An electron spectroscopy imaging and electron energy-loss spectroscopy study. *Neurotoxicology* **29**, 60-72, doi:10.1016/j.neuro.2007.09.001 (2008).

55   Chen, P., Chakraborty, S., Mukhopadhyay, S., Lee, E., Paoliello, M. M., Bowman, A. B. & Aschner, M. Manganese homeostasis in the nervous system. *Journal of neurochemistry* **134**, 601-610, doi:10.1111/jnc.13170 (2015).

56   DeWitt, M. R., Chen, P. & Aschner, M. Manganese efflux in Parkinsonism: Insights from newly characterized SLC30A10 mutations. *Biochemical and Biophysical Research Communications* **432**, 1-4, doi:10.1016/j.bbrc.2013.01.058 (2013).

57   Leyva-Illades, D., Chen, P., Zogzas, C. E., Hutchens, S., Mercado, J. M., Swaim, C. D., Morrisett, R. A., Bowman, A. B., Aschner, M. & Mukhopadhyay, S. SLC30A10 Is a Cell Surface-Localized Manganese Efflux Transporter, and

Parkinsonism-Causing Mutations Block Its Intracellular Trafficking and Efflux Activity. *The Journal of Neuroscience* **34**, 14079-14095, doi:10.1523/jneurosci.2329-14.2014 (2014).

58   Quadri, M., Federico, A., Zhao, T., Breedveld, G. J., Battisti, C., Delnooz, C., Severijnen, L.-A., Di Toro Mammarella, L., Mignarri, A., Monti, L. *et al.* Mutations in SLC30A10 Cause Parkinsonism and Dystonia with Hypermanganesemia, Polycythemia, and Chronic Liver Disease. *The American Journal of Human Genetics* **90**, 467-477, doi:10.1016/j.ajhg.2012.01.017 (2012).

59   Baly, D. L. Effect of Manganese Deficiency on Insulin Secretion and Carbohydrate Heomostasis in Rats. *J.Nutrition* (1984).

60   Baly, D. L., Keen, C. L. & Hurley, L. S. Effects of manganese deficiency on pyruvate carboxylase and phosphoenolpyruvate carboxykinase activity and carbohydrate homeostasis in adult rats. *Biological Trace Element Research* **11**, 201-212, doi:10.1007/bf02795535 (1986).

61   Baly, D. L., Lee, I. & Doshi, R. Mechanism of decreased insulinogenesis in manganese-deficient rats. Decreased insulin mRNA levels. *FEBS letters* **239**, 55-58 (1988).

62   Baly, D. L., Schneiderman, J. S. & Garcia-Welsh, A. L. Effect of manganese deficiency on insulin binding, glucose transport and metabolism in rat adipocytes. *The Journal of nutrition* **120**, 1075-1079 (1990).

63   Keen, C. L., Baly, D. L. & Lönnerdal, B. Metabolic effects of high doses of manganese in rats. *Biological Trace Element Research* **6**, 309-315, doi:10.1007/BF02989238 (1984).

64   Subasinghe, S., Greenbaum, A. L. & McLean, P. The insulin-mimetic action of Mn2+: involvement of cyclic nucleotides and insulin in the regulation of hepatic hexokinase and glucokinase. *Biochemical medicine* **34**, 83-92, doi:10.1016/0006-2944(85)90064-X (1985).

65   Clegg, M. S., Donovan, S. M., Monaco, M. H., Baly, D. L., Ensunsa, J. L. & Keen, C. L. The influence of manganese deficiency on serum IGF-1 and IGF binding proteins in the male rat. *Proceedings of the Society for Experimental Biology and Medicine. Society for Experimental Biology and Medicine (New York, N.Y.)* **219**, 41-47 (1998).

66   Lee, S.-H., Jouihan, H. A., Cooksey, R. C., Jones, D., Kim, H. J., Winge, D. R. & McClain, D. A. Manganese Supplementation Protects Against Diet-Induced Diabetes in Wild Type Mice by Enhancing Insulin Secretion. *Endocrinology* **154**, 1029-1038, doi:10.1210/en.2012-1445 (2013).

67   Ekmekcioglu, C., Prohaska, C., Pomazal, K., Steffan, I., Schernthaner, G. & Marktl, W. Concentrations of seven trace elements in different hematological matrices in patients with type 2 diabetes as compared to healthy controls. *Biological trace element research* **79**, 205-219, doi:10.1385/BTER:79:3:205 (2001).

68   Koh, E. S., Kim, S. J., Yoon, H. E., Chung, J. H., Chung, S., Park, C. W., Chang, Y. S. & Shin, S. J. Association of blood manganese level with diabetes and renal dysfunction: a cross-sectional study of the Korean general population. *BMC endocrine disorders* **14**, 24, doi:10.1186/1472-6823-14-24 (2014).

69   Rubenstein, A. H., Levin, N. W. & Elliott, G. A. Manganese-induced hypoglycaemia. *Lancet (London, England)* **2**, 1348-1351 (1962).

70   Srivastava, V. K., Hiney, J. K. & Dees, W. L. Early Life Manganese Exposure Upregulates Tumor-Associated Genes in the Hypothalamus of Female Rats: Relationship to Manganese-Induced Precocious Puberty. *Toxicological Sciences* **136**, 373-381, doi:10.1093/toxsci/kft195 (2013).

71   Lee, B., Hiney, J. K., Pine, M. D., Srivastava, V. K. & Dees, L. W. Manganese stimulates luteinizing hormone releasing hormone secretion in prepubertal female rats: hypothalamic site and mechanism of action. *The Journal of Physiology* **578**, 765-772, doi:10.1113/jphysiol.2006.123083 (2007).

72   Lee, B., Pine, M., Johnson, L., Rettori, V., Hiney, J. K. & Dees, L. W. Manganese acts centrally to activate reproductive hormone secretion and pubertal development in male rats. *Reproductive toxicology (Elmsford, N.Y.)* **22**, 580-585 (2006).

73   Srivastava, V. K., Hiney, J. K. & Dees, L. W. Prepubertal ethanol exposure alters hypothalamic transforming growth factor-α and erbB1 receptor signaling in the female rat. *Alcohol* **45**, 173-181, doi:10.1016/j.alcohol.2010.08.014 (2011).

74   Bates, G. P., Dorsey, R., Gusella, J. F., Hayden, M. R., Kay, C., Leavitt, B. R., Nance, M., Ross, C. A., Scahill, R. I., Wetzel, R. *et al.* Huntington disease. *Nature reviews. Disease primers* **1**, 15005, doi:10.1038/nrdp.2015.5 (2015).

75   Landles, C. & Bates, G. P. Huntingtin and the molecular pathogenesis of Huntington's disease. *EMBO reports* **5**, 958-963, doi:10.1038/sj.embor.7400250 (2004).

76 Kumar, A., Singh, S., Kumar, V., Kumar, D., Agarwal, S. & Rana, M. Huntington's disease: An update of therapeutic strategies. *Gene* **556**, 91-97, doi:10.1016/j.gene.2014.11.022 (2015).

77 Cattaneo, E., Zuccato, C. & Tartari, M. Normal huntingtin function: an alternative approach to Huntington's disease. *Nature reviews. Neuroscience* **6**, 919-930, doi:10.1038/nrn1806 (2005).

78 Gusella, J. F. & MacDonald, M. E. Huntington's disease: the case for genetic modifiers. *Genome Medicine* **1**, 80, doi:10.1186/gm80 (2009).

79 Prohaska, J. R. Functions of trace elements in brain metabolism. *Physiological reviews* **67**, 858-901 (1987).

80 Larsen, N. A., Pakkenberg, H., Damsgaard, E. & Heydorn, K. Topographical distribution of arsenic, manganese, and selenium in the normal human brain. *Journal of the Neurological Sciences* **42**, 407-416, doi:10.1016/0022-510X(79)90173-4 (1979).

81 Williams, B. B., Li, D., Wegrzynowicz, M., Vadodaria, B. K., Anderson, J. G., Kwakye, G. F., Aschner, M., Erikson, K. M. & Bowman, A. B. Disease-toxicant screen reveals a neuroprotective interaction between Huntington's disease and manganese exposure. *Journal of neurochemistry* **112**, 227-237, doi:10.1111/j.1471-4159.2009.06445.x (2010).

82 Tidball, A. M., Bryan, M. R., Uhouse, M. A., Kumar, K. K., Aboud, A. A., Feist, J. E., Ess, K. C., Neely, D. M., Aschner, M. & Bowman, A. B. A novel manganese-dependent ATM-p53 signaling pathway is selectively impaired in patient-based neuroprogenitor and murine striatal models of Huntington's disease. *Human Molecular Genetics* **24**, 1929-1944, doi:10.1093/hmg/ddu609 (2015).

83 Takeda, A. Manganese action in brain function. *Brain Research Reviews* **41**, 79-87, doi:10.1016/S0165-0173(02)00234-5 (2003).

84 Tidball, A. M., Bichell, T. & Bowman, A. B. Manganese in Health and Disease. *rsc*, 540-573, doi:10.1039/9781782622383-00540 (2015).

85 Cordova, F. M., Aguiar, A. S., Peres, T. V., Lopes, M. W., Gonçalves, F. M., Remor, A. P., Lopes, S. C., Pilati, C., Latini, A. S., Prediger, R. D. S. *et al.* In Vivo Manganese Exposure Modulates Erk, Akt and Darpp-32 in the Striatum of Developing Rats, and Impairs Their Motor Function. *PLoS ONE* **7**, doi:10.1371/journal.pone.0033057 (2012).

86 Guilarte, T. R. APLP1, Alzheimer's-like pathology and neurodegeneration in the frontal cortex of manganese-exposed non-human primates. *NeuroToxicology* **31**, 572-574, doi:10.1016/j.neuro.2010.02.004 (2010).

87 Lee, J. H., Tecedor, L., Chen, Y., Monteys, A., Sowada, M. J., Thompson, L. M. & Davidson, B. L. Reinstating aberrant mTORC1 activity in Huntington's disease mice improves disease phenotypes. *Neuron* **85**, 303-315, doi:10.1016/j.neuron.2014.12.019 (2014).

88 Humbert, S., Bryson, E. A., Cordelières, F. P., Connors, N. C., Datta, S. R., Finkbeiner, S., Greenberg, M. E. & Saudou, F. The IGF-1/Akt Pathway Is Neuroprotective in Huntington's Disease and Involves Huntingtin Phosphorylation by Akt. *Developmental Cell* **2**, 831-837, doi:10.1016/S1534-5807(02)00188-0 (2002).

89 Blázquez, C., Chiarlone, A., Bellocchio, L., Resel, E., Pruunsild, P., García-Rincón, D., Sendtner, M., Timmusk, T., Lutz, B., Galve-Roperh, I. *et al.* The CB₁ cannabinoid receptor signals striatal neuroprotection via a PI3K/Akt/mTORC1/BDNF pathway. *Cell death and differentiation* **22**, 1618-1629, doi:10.1038/cdd.2015.11 (2015).

90 Gines, S., Ivanova, E., Seong, I.-S., Saura, C. A. & MacDonald, M. E. Enhanced Akt Signaling Is an Early Pro-survival Response That Reflects N-Methyl-D-aspartate Receptor Activation in Huntington's Disease Knock-in Striatal Cells. *Journal of Biological Chemistry* **278**, 50514-50522, doi:10.1074/jbc.M309348200 (2003).

91 Humbert, S. & Saudou, F. Huntingtin phosphorylation and signaling pathways that regulate toxicity in Huntington's disease. *Clinical Neuroscience Research* **3**, 149-155, doi:10.1016/S1566-2772(03)00057-4 (2003).

92 Lopes, C., Ribeiro, M., Duarte, A. I., Humbert, S., Saudou, F., Pereira de Almeida, L., Hayden, M. & Rego, A. C. IGF-1 intranasal administration rescues Huntington's disease phenotypes in YAC128 mice. *Molecular neurobiology* **49**, 1126-1142, doi:10.1007/s12035-013-8585-5 (2014).

93 Ribeiro, M., Rosenstock, T. R., Oliveira, A. M., Oliveira, C. R. & Rego, A. C. Insulin and IGF-1 improve mitochondrial function in a PI-3K/Akt-dependent manner and reduce mitochondrial generation of reactive oxygen species in Huntington's disease knock-in striatal cells. *Free radical biology & medicine* **74**, 129-144, doi:10.1016/j.freeradbiomed.2014.06.023 (2014).

94   Saavedra, A., García-Martínez, J. M., Xifró, X., Giralt, A., Torres-Peraza, J. F., Canals, J. M., Díaz-Hernández, M., Lucas, J. J., Alberch, J. & Pérez-Navarro, E. PH domain leucine-rich repeat protein phosphatase 1 contributes to maintain the activation of the PI3K/Akt pro-survival pathway in Huntington's disease striatum. *Cell death and differentiation* **17**, 324-335, doi:10.1038/cdd.2009.127 (2009).

95   Zala, D., Colin, E., Rangone, H., Liot, G., Humbert, S. & Saudou, F. Phosphorylation of mutant huntingtin at S421 restores anterograde and retrograde transport in neurons. *Human Molecular Genetics* **17**, 3837-3846, doi:10.1093/hmg/ddn281 (2008).

96   Naia, L., Ferreira, I. L., Cunha-Oliveira, T., Duarte, A. I., Ribeiro, M., Rosenstock, T. R., Laço, M. N. N., Ribeiro, M. J., Oliveira, C. R., Saudou, F. *et al.* Activation of IGF-1 and insulin signaling pathways ameliorate mitochondrial function and energy metabolism in Huntington's Disease human lymphoblasts. *Molecular neurobiology* **51**, 331-348, doi:10.1007/s12035-014-8735-4 (2015).

97   Naia, L., Ribeiro, M., Rodrigues, J., Duarte, A. I., Lopes, C., Rosenstock, T. R., Hayden, M. R. & Rego, C. A. Insulin and IGF-1 regularize energy metabolites in neural cells expressing full-length mutant huntingtin. *Neuropeptides*, doi:10.1016/j.npep.2016.01.009 (2016).

98   Gauthier, L. R., Charrin, B. C., Borrell-Pagès, M., Dompierre, J. P., Rangone, H., Cordelières, F. P., Mey, J., MacDonald, M. E., Leßmann, V., Humbert, S. *et al.* Huntingtin Controls Neurotrophic Support and Survival of Neurons by Enhancing BDNF Vesicular Transport along Microtubules. *Cell* **118**, 127-138, doi:10.1016/j.cell.2004.06.018 (2004).

99   Stansfield, K. H., Bichell, T., Bowman, A. B. & Guilarte, T. R. BDNF and Huntingtin protein modifications by manganese: implications for striatal medium spiny neuron pathology in manganese neurotoxicity. *Journal of neurochemistry* **131**, 655-666, doi:10.1111/jnc.12926 (2014).

100   Pryor, W. M., Biagioli, M., Shahani, N., Swarnkar, S., Huang, W.-C., Page, D. T., MacDonald, M. E. & Subramaniam, S. Huntingtin promotes mTORC1 signaling in the pathogenesis of Huntington's disease. *Science signaling* **7**, doi:10.1126/scisignal.2005633 (2014).

101   Sarkar, S., Ravikumar, B., Floto, R. A. & Rubinsztein, D. C. Rapamycin and mTOR-independent autophagy inducers ameliorate toxicity of polyglutamine-expanded huntingtin and related proteinopathies. *Cell death and differentiation* **16**, 46-56, doi:10.1038/cdd.2008.110 (2008).

102   Pouladi, M. A., Xie, Y., Skotte, N. H., Ehrnhoefer, D. E., Graham, R. K., Kim, J. E., Bissada, N., Yang, X. W., Paganetti, P., Friedlander, R. M. *et al.* Full-length huntingtin levels modulate body weight by influencing insulin-like growth factor 1 expression. *Human molecular genetics* **19**, 1528-1538, doi:10.1093/hmg/ddq026 (2010).

103   Saleh, N., Moutereau, S., Azulay, J. P., Verny, C., Simonin, C., Tranchant, C., Hawajri, E. N., Bachoud-Lévi, A. C., Maison, P. & Group, H. High insulinlike growth factor I is associated with cognitive decline in Huntington disease. *Neurology* **75**, 57-63, doi:10.1212/WNL.0b013e3181e62076 (2010).

104   Yamamoto, A., Cremona, M. L. & Rothman, J. E. Autophagy-mediated clearance of huntingtin aggregates triggered by the insulin-signaling pathway. *The Journal of cell biology* **172**, 719-731, doi:10.1083/jcb.200510065 (2006).

105   Duarte, A. I., Petit, G. H., Ranganathan, S., Li, J. Y., Oliveira, C. R., Brundin, P., Björkqvist, M. & Rego, A. C. IGF-1 protects against diabetic features in an in vivo model of Huntington's disease. *Experimental Neurology* **231**, 314-319, doi:10.1016/j.expneurol.2011.06.016 (2011).

106   Alexi, T., Hughes, P. E., van Roon-Mom, W. M., Faull, R. L., Williams, C. E., Clark, R. G. & Gluckman, P. D. The IGF-I amino-terminal tripeptide glycine-proline-glutamate (GPE) is neuroprotective to striatum in the quinolinic acid lesion animal model of Huntington's disease. *Experimental neurology* **159**, 84-97 (1999).

107   Metzler, M., Gan, L., Mazarei, G., Graham, R. K., Liu, L., Bissada, N., Lu, G., Leavitt, B. R. & Hayden, M. R. Phosphorylation of Huntingtin at Ser421 in YAC128 Neurons Is Associated with Protection of YAC128 Neurons from NMDA-Mediated Excitotoxicity and Is Modulated by PP1 and PP2A. *The Journal of Neuroscience* **30**, 14318-14329, doi:10.1523/jneurosci.1589-10.2010 (2010).

108   Warby, S. C., Doty, C. N., Graham, R. K., Shively, J., Singaraja, R. R. & Hayden, M. R. Phosphorylation of huntingtin reduces the accumulation of its nuclear fragments. *Molecular and Cellular Neuroscience* **40**, 121-127, doi:10.1016/j.mcn.2008.09.007 (2009).

109   Quesada, A., Lee, B. Y. & Micevych, P. E. PI3 kinase/Akt activation mediates estrogen and IGF-1 nigral DA neuronal neuroprotection against a unilateral rat model of Parkinson's disease. *Developmental neurobiology* **68**, 632-644, doi:10.1002/dneu.20609 (2008).

110   Allodi, I., Comley, L., Nichterwitz, S., Nizzardo, M., Simone, C., Benitez, J. A., Cao, M., Corti, S. & Hedlund, E. Differential neuronal vulnerability identifies IGF-2 as a protective factor in ALS. *Scientific reports* **6**, 25960, doi:10.1038/srep25960 (2016).

111   Bassil, F., Fernagut, P.-O., Bezard, E. & Meissner, W. G. Insulin, IGF-1 and GLP-1 signaling in neurodegenerative disorders: Targets for disease modification? *Progress in Neurobiology* **118**, 1-18, doi:10.1016/j.pneurobio.2014.02.005 (2014).

112   Gasparini, L. & Xu, H. Potential roles of insulin and IGF-1 in Alzheimer's disease. *Trends in Neurosciences* **26**, 404-406, doi:10.1016/s0166-2236(03)00163-2 (2003).

113   Aleman, I. Insulin-Like Growth Factor-1 and Central Neurodegenerative Diseases. *Endocrinology and Metabolism Clinics of North America* **41**, 395-408, doi:10.1016/j.ecl.2012.04.016 (2012).

114   Homolak, J., Janeš, I. & Filipović, M. The role of IGF-1 in neurodegenerative diseases. *Gyrus* **3**, 162-167, doi:10.17486/gyr.3.1035 (2015).

115   Bernhard, F. P., Heinzel, S., Binder, G., Weber, K., Apel, A., Roeben, B., Deuschle, C., Maechtel, M., Heger, T., Nussbaum, S. *et al.* Insulin-Like Growth Factor 1 (IGF-1) in Parkinson's Disease: Potential as Trait-, Progression- and Prediction Marker and Confounding Factors. *PLOS ONE* **11**, doi:10.1371/journal.pone.0150552 (2016).

116   Reger, M. A., Watson, G. S., Green, P. S., Wilkinson, C. W., Baker, L. D., Cholerton, B., Fishel, M. A., Plymate, S. R., Breitner, J. C. S., DeGroodt, W. *et al.* Intranasal insulin improves cognition and modulates beta-amyloid in early AD. *Neurology* **70**, 440-448 (2007).

117   Truant, R., Atwal, R., Desmond, C., Munsie, L. & Tran, T. Huntington's disease: revisiting the aggregation hypothesis in polyglutamine neurodegenerative diseases. *The FEBS journal* **275**, 4252-4262, doi:10.1111/j.1742-4658.2008.06561.x (2008).

118   Arrasate, M. & Finkbeiner, S. Protein aggregates in Huntington's disease. *Experimental neurology* **238**, 1-11, doi:10.1016/j.expneurol.2011.12.013 (2011).

119   Bano, D., Zanetti, F., Mende, Y. & Nicotera, P. Neurodegenerative processes in Huntington's disease. *Cell Death & Disease* **2**, doi:10.1038/cddis.2011.112 (2011).

120   Lim, J. & Yue, Z. Neuronal Aggregates: Formation, Clearance, and Spreading. *Developmental Cell* **32**, 491-501, doi:10.1016/j.devcel.2015.02.002 (2015).

121   Cortes, C. J. & Spada, A. R. The many faces of autophagy dysfunction in Huntington's disease: from mechanism to therapy. *Drug discovery today* **19**, 963-971, doi:10.1016/j.drudis.2014.02.014 (2014).

122   Cuervo, A. & Zhang, S. Selective autophagy and Huntingtin: learning from disease. *Cell Cycle* **14**, doi:10.1080/15384101.2015.1039365 (2015).

123   Martin, D. D. O., Ladha, S., Ehrnhoefer, D. E. & Hayden, M. R. Autophagy in Huntington disease and huntingtin in autophagy. *Trends in neurosciences* **38**, 26-35, doi:10.1016/j.tins.2014.09.003 (2014).

124   Ravikumar, B. & Rubinsztein, D. C. Role of autophagy in the clearance of mutant huntingtin: a step towards therapy? *Molecular aspects of medicine* **27**, 520-527, doi:10.1016/j.mam.2006.08.008 (2006).

125   Sarkar, S. & Rubinsztein, D. C. Huntington's disease: degradation of mutant huntingtin by autophagy. *The FEBS journal* **275**, 4263-4270, doi:10.1111/j.1742-4658.2008.06562.x (2008).

126   Williams, A., Sarkar, S., Cuddon, P., Ttofi, E. K., Saiki, S., Siddiqi, F. H., Jahreiss, L., Fleming, A., Pask, D., Goldsmith, P. *et al.* Novel targets for Huntington's disease in an mTOR-independent autophagy pathway. *Nature Chemical Biology* **4**, 295-305, doi:10.1038/nchembio.79 (2008).

127   Rui, Y.-N. N., Xu, Z., Patel, B., Chen, Z., Chen, D., Tito, A., David, G., Sun, Y., Stimming, E. F., Bellen, H. J. *et al.* Huntingtin functions as a scaffold for selective macroautophagy. *Nature cell biology* **17**, doi:10.1038/ncb3101 (2015).

128   Gelman, A., Rawet-Slobodkin, M. & Elazar, Z. Huntingtin facilitates selective autophagy. *Nature cell biology* **17**, 214-215, doi:10.1038/ncb3125 (2015).

129   Ochaba, J., Lukacsovich, T., Csikos, G., Zheng, S., Margulis, J., Salazar, L., Mao, K., Lau, A. L., Yeung, S. Y., Humbert, S. *et al.* Potential function for the Huntingtin protein as a scaffold for selective autophagy. *Proceedings of the National Academy of Sciences* **111**, 16889-16894, doi:10.1073/pnas.1420103111 (2014).

130   Saudou, F. & Humbert, S. The Biology of Huntingtin. *Neuron* **89**, 910-926, doi:10.1016/j.neuron.2016.02.003 (2016).

131   Martinez-Vicente, M., Talloczy, Z., Wong, E., Tang, G., Koga, H., Kaushik, S., de Vries, R., Arias, E., Harris, S., Sulzer, D. *et al.* Cargo recognition failure is responsible for inefficient autophagy in Huntington's disease. *Nature neuroscience* **13**, 567-576, doi:10.1038/nn.2528 (2010).

132   Sasazawa, Y., Sato, N., Umezawa, K. & Simizu, S. Conophylline Protects Cells in Cellular Models of Neurodegenerative Diseases by Inducing Mammalian Target of Rapamycin (mTOR)-independent Autophagy. *Journal of Biological Chemistry* **290**, 6168-6178, doi:10.1074/jbc.m114.606293 (2015).

133   Gorojod, R. M., Alaimo, A., Porte Alcon, S., Pomilio, C., Saravia, F. & Kotler, M. L. The autophagic- lysosomal pathway determines the fate of glial cells under manganese- induced oxidative stress conditions. *Free radical biology & medicine* **87**, 237-251, doi:10.1016/j.freeradbiomed.2015.06.034 (2015).

134   Zhang, Z., Miah, M., Culbreth, M. & Aschner, M. Autophagy in Neurodegenerative Diseases and Metal Neurotoxicity. *Neurochemical research* **41**, 409-422, doi:10.1007/s11064-016-1844-x (2016).

135   Filosto, M., Scarpelli, M., Cotelli, M., Vielmi, V., Todeschini, A., Gregorelli, V., Tonin, P., Tomelleri, G. & Padovani, A. The role of mitochondria in neurodegenerative diseases. *Journal of Neurology* **258**, 1763-1774, doi:10.1007/s00415-011-6104-z (2011).

136   Johri, A. & Beal, F. M. Mitochondrial Dysfunction in Neurodegenerative Diseases. *Journal of Pharmacology and Experimental Therapeutics* **342**, 619-630, doi:10.1124/jpet.112.192138 (2012).

137   Martin, L. J. Chapter 11 Biology of Mitochondria in Neurodegenerative Diseases. *Progress in Molecular Biology and Translational Science* **107**, 355-415, doi:10.1016/b978-0-12-385883-2.00005-9 (2012).

138   Saleh, N., Moutereau, S., Durr, A., Krystkowiak, P., Azulay, J.-P., Tranchant, C., Broussolle, E., Morin, F., Bachoud-Lévi, A.-C. & Maison, P. Neuroendocrine Disturbances in Huntington's Disease. *PLoS ONE* **4**, doi:10.1371/journal.pone.0004962 (2009).

139   Farrer, L. A. Diabetes mellitus in Huntington disease. *Clinical genetics* **27**, 62-67 (1985).

140   Hurlbert, M. S., Zhou, W., Wasmeier, C., Kaddis, F. G., Hutton, J. C. & Freed, C. R. Mice transgenic for an expanded CAG repeat in the Huntington's disease gene develop diabetes. *Diabetes* **48**, 649-651, doi:10.2337/diabetes.48.3.649 (1999).

141   Lalić, N. M., Marić, J., Svetel, M., Jotić, A., Stefanova, E., Lalić, K., Dragašević, N., Miličić, T., Lukić, L. & Kostić, V. S. Glucose Homeostasis in Huntington Disease: Abnormalities in Insulin Sensitivity and Early-Phase Insulin Secretion. *Archives of Neurology* **65**, 476-480, doi:10.1001/archneur.65.4.476 (2008).

142   Podolsky, S., Leopold, N. & Sax, D. INCREASED FREQUENCY OF DIABETES MELLITUS IN PATIENTS WITH HUNTINGTON'S CHOREA. *The Lancet* **299**, 1356-1359, doi:10.1016/s0140-6736(72)91092-6 (1972).

143   Pouladi, M. A., Xie, Y., Skotte, N., Ehrnhoefer, D. E., Graham, R. K., Kim, J., Bissada, N., Yang, W. X., Paganetti, P., Friedlander, R. M. *et al.* Full-length huntingtin levels modulate body weight by influencing insulin-like growth factor 1 expression. *Human Molecular Genetics* **19**, 1528-1538, doi:10.1093/hmg/ddq026 (2010).

144   Mochel, F., Charles, P., Seguin, F., Barritault, J., Coussieu, C., Perin, L., Bouc, Y., Gervais, C., Carcelain, G., Vassault, A. *et al.* Early Energy Deficit in Huntington Disease: Identification of a Plasma Biomarker Traceable during Disease Progression. *PLoS ONE* **2**, doi:10.1371/journal.pone.0000647 (2007).

145   Goodman, A., Murgatroyd, P. R., Medina-Gomez, G., Wood, N. I., Finer, N., Vidal-Puig, A. J., Morton, J. A. & Barker, R. A. The metabolic profile of early Huntington's disease- a combined human and transgenic mouse study. *Experimental Neurology* **210**, 691-698, doi:10.1016/j.expneurol.2007.12.026 (2008).

146   Gaba, A. M., Zhang, K., Marder, K., Moskowitz, C. B., Werner, P. & Boozer, C. N. Energy balance in early-stage Huntington disease. *The American journal of clinical nutrition* **81**, 1335-1341 (2005).

147   Josefsen, K., Nielsen, M. D., Jørgensen, K. H., Bock, T., Nørremølle, A., Sørensen, S. A., Naver, B. & Hasholt, L. Impaired glucose tolerance in the R6/1 transgenic mouse model of Huntington's disease. *Journal of neuroendocrinology* **20**, 165-172 (2007).

148   Oláh, J., Klivényi, P., Gardián, G., Vécsei, L., Orosz, F., Kovacs, G. G., Westerhoff, H. V. & Ovádi, J. Increased glucose metabolism and ATP level in brain tissue of Huntington's disease transgenic mice. *FEBS Journal* **275**, 4740-4755, doi:10.1111/j.1742-4658.2008.06612.x (2008).

149   Ismailoglu, I., Chen, Q., Popowski, M., Yang, L., Gross, S. S. & Brivanlou, A. H. Huntingtin protein is essential for mitochondrial metabolism, bioenergetics and structure in murine embryonic stem cells. *Developmental Biology* **391**, 230-240, doi:10.1016/j.ydbio.2014.04.005 (2014).

150   Koroshetz, W. J., Jenkins, B. G., Rosen, B. R. & Beal, F. M. Energy metabolism defects in Huntington's disease and effects of coenzyme Q10. *Annals of Neurology* **41**, 160-165, doi:10.1002/ana.410410206 (1997).

151   Schilling, G., Coonfield, M. L., Ross, C. A. & Borchelt, D. R. Coenzyme Q10 and remacemide hydrochloride ameliorate motor deficits in a Huntington's disease transgenic mouse model. *Neuroscience letters* **315**, 149-153, doi:10.1016/S0304-3940(01)02326-6 (2001).

152   Andreassen, O. A., Dedeoglu, A., Ferrante, R. J., Jenkins, B. G., Ferrante, K. L., Thomas, M., Friedlich, A., Browne, S. E., Schilling, G., Borchelt, D. R. *et al.* Creatine increase survival and delays motor symptoms in a transgenic animal model of Huntington's disease. *Neurobiology of disease* **8**, 479-491 (2001).

153   Ferrante, R. J., Andreassen, O. A., Jenkins, B. G., Dedeoglu, A., Kuemmerle, S., Kubilus, J. K., Kaddurah-Daouk, R., Hersch, S. M. & Beal, M. F. Neuroprotective effects of creatine in a transgenic mouse model of Huntington's disease. *The Journal of neuroscience : the official journal of the Society for Neuroscience* **20**, 4389-4397 (2000).

154   Tabrizi, S. J., Blamire, A. M., Manners, D. N., Rajagopalan, B., Styles, P., Schapira, A. H. V. & Warner, T. T. Creatine therapy for Huntington's disease: clinical and MRS findings in a 1-year pilot study. *Neurology* **61**, 141-142 (2003).

155   Verbessem, P., Lemiere, J., Eijnde, B. O., Swinnen, S., Vanhees, L., Leemputte, V. M., Hespel, P. & Dom, R. Creatine supplementation in Huntington's disease: a placebo-controlled pilot trial. *Neurology* **61**, 925-930 (2003).

156   Ferrante, R. J., Andreassen, O. A., Dedeoglu, A., Ferrante, K. L., Jenkins, B. G., Hersch, S. M. & Beal, F. M. Therapeutic effects of coenzyme Q10 and remacemide in transgenic mouse models of Huntington's disease. *The Journal of neuroscience : the official journal of the Society for Neuroscience* **22**, 1592-1599 (2002).

157   Ferreira, I. L., Nascimento, M. V., Ribeiro, M., Almeida, S., Cardoso, S. M., Grazina, M., Pratas, J., Santos, M., Januário, C., Oliveira, C. R. *et al.* Mitochondrial-dependent apoptosis in Huntington's disease human cybrids. *Experimental Neurology* **222**, 243-255, doi:10.1016/j.expneurol.2010.01.002 (2010).

158   Damiano, M., Galvan, L., Déglon, N. & Brouillet, E. Mitochondria in Huntington's disease. *Biochimica et Biophysica Acta (BBA) - Molecular Basis of Disease* **1802**, 52-61, doi:10.1016/j.bbadis.2009.07.012 (2010).

159   Kim, J., Moody, J. P., Edgerly, C. K., Bordiuk, O. L., Cormier, K., Smith, K., Beal, F. M. & Ferrante, R. J. Mitochondrial loss, dysfunction and altered dynamics in Huntington's disease. *Human Molecular Genetics* **19**, 3919-3935, doi:10.1093/hmg/ddq306 (2010).

160   Reddy, H. P., Mao, P. & Manczak, M. Mitochondrial structural and functional dynamics in Huntington's disease. *Brain research reviews* **61**, 33-48, doi:10.1016/j.brainresrev.2009.04.001 (2009).

161   Martin, W. W. R., Wieler, M. & Hanstock, C. C. Is brain lactate increased in Huntington's disease? *Journal of the neurological sciences* **263**, 70-74 (2007).

162   Milakovic, T. & Johnson, G. V. W. Mitochondrial respiration and ATP production are significantly impaired in striatal cells expressing mutant huntingtin. *The Journal of biological chemistry* **280**, 30773-30782 (2005).

163   Weydt, P., Pineda, V. V., Torrence, A. E., Libby, R. T., Satterfield, T. F., Lazarowski, E. R., Gilbert, M. L., Morton, G. J., Bammler, T. K., Strand, A. D. *et al.* Thermoregulatory and metabolic defects in Huntington's disease transgenic mice implicate PGC-1α in Huntington's disease neurodegeneration. *Cell Metabolism* **4**, 349-362, doi:10.1016/j.cmet.2006.10.004 (2006).

164   Lou, S., Lepak, T., Eberly, L. E., Roth, B., Cui, W., Zhu, X.-H., Öz, G. & Dubinsky, J. M. Oxygen Consumption Deficit In Huntington Disease Mouse Brain Under Metabolic Stress. *Human molecular genetics* (2016).

165   Ferreira, L. I., Cunha-Oliveira, T., Nascimento, M. V., Ribeiro, M., Proença, T. M., Januário, C., Oliveira, C. R. & Rego, C. A. Bioenergetic dysfunction in Huntington's disease human cybrids. *Experimental Neurology* **231**, 127-134, doi:10.1016/j.expneurol.2011.05.024 (2011).

166   Gouarné, C., Tardif, G., Tracz, J., Latyszenok, V., Michaud, M., Clemens, L., Yu-Taeger, L., Nguyen, H., Bordet, T. & Pruss, R. M. Early Deficits in Glycolysis Are Specific to Striatal Neurons from a Rat Model of Huntington Disease. *PLoS ONE* **8**, doi:10.1371/journal.pone.0081528 (2013).

167   Nagano, I., Shiote, M., Murakami, T., Kamada, H., Hamakawa, Y., Matsubara, E., Yokoyama, M., Morita, K., Shoji, M. & Abe, K. Beneficial effects of intrathecal IGF-1 administration in patients with amyotrophic lateral sclerosis. *Neurological Research* **27**, 768-772, doi:10.1179/016164105x39860 (2013).

168   Sorenson, E. J., Windbank, A. J., Mandrekar, J. N., Bamlet, W. R., Appel, S. H., Armon, C., Barkhaus, P. E., Bosch, P., Boylan, K., David, W. S. *et al.* Subcutaneous IGF-1 is not beneficial in 2-year ALS trial. *Neurology* **71**, 1770-1775, doi:10.1212/01.wnl.0000335970.78664.36 (2008).

169   Hölscher, C. First clinical data of the neuroprotective effects of nasal insulin application in patients with Alzheimer's disease. *Alzheimer's & dementia : the journal of the Alzheimer's Association* **10**, 7, doi:10.1016/j.jalz.2013.12.006 (2014).

170   Rauskolb, S., Dombert, B. & Sendtner, M. Insulin-like growth factor 1 in diabetic neuropathy and amyotrophic lateral sclerosis. *Neurobiology of disease*, doi:10.1016/j.nbd.2016.04.007 (2016).

171   Sulzer, D. Multiple hit hypotheses for dopamine neuron loss in Parkinson's disease. *Trends in neurosciences* **30**, 244-250, doi:10.1016/j.tins.2007.03.009 (2007).

172   Guilarte, T. R. & Gonzales, K. K. Manganese-Induced Parkinsonism Is Not Idiopathic Parkinson's Disease: Environmental and Genetic Evidence. *Toxicological Sciences* **146**, 204-212, doi:10.1093/toxsci/kfv099 (2015).

173   Cersosimo, M. G. & Koller, W. C. The diagnosis of manganese-induced parkinsonism. *Neurotoxicology* **27**, 340-346, doi:10.1016/j.neuro.2005.10.006 (2005).

174   Kwakye, G. F., Paoliello, M. M., Mukhopadhyay, S., Bowman, A. B. & Aschner, M. Manganese-Induced Parkinsonism and Parkinson's Disease: Shared and Distinguishable Features. *International journal of environmental research and public health* **12**, 7519-7540, doi:10.3390/ijerph120707519 (2015).

175   Bowman, A. B., Kwakye, G. F., Hernández, E. & Aschner, M. Role of manganese in neurodegenerative diseases. *Journal of Trace Elements in Medicine and Biology* **25**, 191-203, doi:10.1016/j.jtemb.2011.08.144 (2011).

176   Aschner, M., Erikson, K. M., Hernández, E., Hernández, E. & Tjalkens, R. Manganese and its Role in Parkinson's Disease: From Transport to Neuropathology. *NeuroMolecular Medicine* **11**, 252-266, doi:10.1007/s12017-009-8083-0 (2009).

177   Guilarte, T. R. Manganese and Parkinson's Disease: A Critical Review and New Findings. *Environmental Health Perspectives* **118**, 1071-1080, doi:10.1289/ehp.0901748 (2010).

178   Zhang, D., Kanthasamy, A., Anantharam, V. & Kanthasamy, A. Effects of manganese on tyrosine hydroxylase (TH) activity and TH-phosphorylation in a dopaminergic neural cell line. *Toxicology and Applied Pharmacology* **254**, 65-71, doi:10.1016/j.taap.2010.03.023 (2011).

179   Tong, M., Dong, M. & de la Monte, S. M. Brain insulin-like growth factor and neurotrophin resistance in Parkinson's disease and dementia with Lewy bodies: potential role of manganese neurotoxicity. *Journal of Alzheimer's disease : JAD* **16**, 585-599, doi:10.3233/jad-2009-0995 (2009).

180   Harischandra, D. S., Jin, H., Anantharam, V., Kanthasamy, A. & Kanthasamy, A. G. α-Synuclein Protects Against Manganese Neurotoxic Insult During the Early Stages of Exposure in a Dopaminergic Cell Model of Parkinson's Disease. *Toxicological Sciences* **143**, 454-468, doi:10.1093/toxsci/kfu247 (2015).

181   Peres, T., Parmalee, N. L., Martinez-Finley, E. J. & Aschner, M. Untangling the Manganese-α-Synuclein Web. *Frontiers in Neuroscience* **10**, 364, doi:10.3389/fnins.2016.00364 (2016).

182   Ayadi, A. E., Zigmond, M. J. & Smith, A. D. IGF-1 protects dopamine neurons against oxidative stress: association with changes in phosphokinases. *Experimental brain research* **234**, 1863-1873, doi:10.1007/s00221-016-4572-1 (2016).

183   Offen, D., Shtaif, B., Hadad, D., Weizman, A., Melamed, E. & Gil-Ad, I. Protective effect of insulin-like-growth-factor-1 against dopamine-induced neurotoxicity in human and rodent neuronal cultures: possible implications for Parkinson's disease. *Neuroscience letters* **316**, 129-132 (2001).

184   Krishnamurthi, R., Stott, S., Maingay, M., Faull, R. L. M., McCarthy, D., Gluckman, P. & Guan, J. N-terminal tripeptide of IGF-1 improves functional deficits after 6-OHDA lesion in rats. *Neuroreport* **15**, 1601-1604 (2004).

185   Lee, J.-M., Wheeler, V. C., Chao, M. J., Vonsattel, J., Pinto, R., Lucente, D., Abu-Elneel, K., Ramos, E., Mysore, J., Gillis, T. *et al.* Identification of Genetic Factors that Modify Clinical Onset of Huntington's Disease. *Cell* **162**, 516-526, doi:10.1016/j.cell.2015.07.003 (2015).

186   Godau, J., Herfurth, M., Kattner, B., Gasser, T. & Berg, D. Increased serum insulin-like growth factor 1 in early idiopathic Parkinson's disease. *Journal of neurology, neurosurgery, and psychiatry* **81**, 536-538, doi:10.1136/jnnp.2009.175752 (2010).

187 Picillo, M., Erro, R., Santangelo, G., Pivonello, R., Longo, K., Pivonello, C., Vitale, C., Amboni, M., Moccia, M., Colao, A. *et al.* Insulin-like growth factor-1 and progression of motor symptoms in early, drug-naïve Parkinson's disease. *Journal of Neurology* **260**, 1724-1730, doi:10.1007/s00415-013-6851-0 (2013).

188 Gong, L., Zhang, Q. L., Zhang, N., Hua, W. Y., Huang, Y. X., Di, P. W., Huang, T., Xu, X. S., Liu, C. F., Hu, L. F. *et al.* Neuroprotection by urate on 6-OHDA-lesioned rat model of Parkinson's disease: linking to Akt/GSK3β signaling pathway. *Journal of Neurochemistry* **123**, 876-885, doi:10.1111/jnc.12038 (2012).

189 Nakaso, K., Ito, S. & Nakashima, K. Caffeine activates the PI3K/Akt pathway and prevents apoptotic cell death in a Parkinson's disease model of SH-SY5Y cells. *Neuroscience letters* **432** (2008).

190 Timmons, S., Coakley, M. F., Moloney, A. M. & Neill, C. Akt signal transduction dysfunction in Parkinson's disease. *Neuroscience Letters* **467**, 30-35, doi:10.1016/j.neulet.2009.09.055 (2009).

191 Xiromerisiou, G., Hadjigeorgiou, G. M., Papadimitriou, A., Katsarogiannis, E., Gourbali, V. & Singleton, A. B. Association between AKT1 gene and Parkinson's disease: a protective haplotype. *Neuroscience letters* **436** (2008).

192 Xu, Y., Liu, C., Chen, S., Ye, Y., Guo, M., Ren, Q., Liu, L., Zhang, H., Xu, C. & Zhou, Q. Activation of AMPK and inactivation of Akt result in suppression of mTOR-mediated S6K1 and 4E-BP1 pathways leading to neuronal cell death in in vitro models of Parkinson's disease. *Cellular signalling* **26** (2014).

193 Bandmann, O., Weiss, K. & Kaler, S. G. Wilson's disease and other neurological copper disorders. *The Lancet Neurology* **14**, 103-113, doi:10.1016/S1474-4422(14)70190-5 (2015).

194 Dieter, H. H., Bayer, T. A. & Multhaup, G. Environmental Copper and Manganese in the Pathophysiology of Neurologic Diseases (Alzheimer's Disease and Manganism). *Acta hydrochimica et hydrobiologica* **33**, 72-78, doi:10.1002/aheh.200400556 (2005).

195 Hare, D. J., Faux, N. G., Roberts, B. R., Volitakis, I., Martins, R. N. & Bush, A. I. Lead and manganese levels in serum and erythrocytes in Alzheimer's disease and mild cognitive impairment: results from the Australian Imaging, Biomarkers and Lifestyle Flagship Study of Ageing. *Metallomics* **8**, 628-632, doi:10.1039/c6mt00019c (2016).

196 Chui, D., Yang, H., Wang, H., Tuo, J. I., Yu, J., Zhang, S., Chen, Z. & Xiao, W. The dishomeostasis of metal ions plays an important role for the cognitive impartment. *Molecular Neurodegeneration* **8**, 1-1, doi:10.1186/1750-1326-8-s1-p13 (2013).

197 Suzanne, M. & Wands, J. R. Alzheimer's disease is type 3 diabetes—evidence reviewed. *Journal of diabetes science and technology* **2** (2008).

198 Schubert, M., Gautam, D., Surjo, D., Ueki, K., Baudler, S., Schubert, D., Kondo, T., Alber, J., Galldiks, N. & Küstermann, E. Role for neuronal insulin resistance in neurodegenerative diseases. *Proceedings of the National Academy of Sciences of the United States of America* **101** (2004).

199 Cohen, E., Du, D., Joyce, D., Kapernick, E. A., Volovik, Y., Kelly, J. W. & Dillin, A. Temporal requirements of insulin/IGF-1 signaling for proteotoxicity protection. *Aging Cell* **9**, 126-134, doi:10.1111/j.1474-9726.2009.00541.x (2010).

200 Cohen, E., Paulsson, J. F., Blinder, P., Burstyn-Cohen, T., Du, D., Estepa, G., Adame, A., Pham, H. M., Holzenberger, M., Kelly, J. W. *et al.* Reduced IGF-1 Signaling Delays Age-Associated Proteotoxicity in Mice. *Cell* **139**, 1157-1169, doi:10.1016/j.cell.2009.11.014 (2009).

201 Freude, S., Schilbach, K. & Schubert, M. The role of IGF-1 receptor and insulin receptor signaling for the pathogenesis of Alzheimer's disease: from model organisms to human disease. *Current Alzheimer research* **6**, 213-223 (2009).

202 Moloney, A. M., Griffin, R. J., Timmons, S., O'Connor, R., Ravid, R. & O'Neill, C. Defects in IGF-1 receptor, insulin receptor and IRS-1/2 in Alzheimer's disease indicate possible resistance to IGF-1 and insulin signalling. *Neurobiology of aging* **31** (2010).

203 Neill, C. PI3-kinase/Akt/mTOR signaling: impaired on/off switches in aging, cognitive decline and Alzheimer's disease. *Experimental gerontology* **48**, 647-653, doi:10.1016/j.exger.2013.02.025 (2013).

204 Torres-Aleman, I. Targeting insulin-like growth factor-1 to treat Alzheimer's disease. *Expert opinion on therapeutic targets* **11**, 1535-1542 (2007).

205 Craft, S. & Watson, G. S. Insulin and neurodegenerative disease: shared and specific mechanisms. *The Lancet. Neurology* **3**, 169-178, doi:10.1016/S1474-4422(04)00681-7 (2004).

206   de la Monte, S. M. & Wands, J. R. Review of insulin and insulin-like growth factor expression, signaling, and malfunction in the central nervous system: relevance to Alzheimer's disease. *Journal of Alzheimer's Disease* **7** (2005).

207   Rivera, E. J., Goldin, A., Fulmer, N., Tavares, R., Wands, J. R. & de la Monte, S. M. Insulin and insulin-like growth factor expression and function deteriorate with progression of Alzheimer's disease: link to brain reductions in acetylcholine. *Journal of Alzheimer's Disease* **8** (2005).

208   Steen, E., Terry, B. M., Rivera, E. J., Cannon, J. L., Neely, T. R., Tavares, R., Xu, J. X., Wands, J. R. & de la Monte, S. M. Impaired insulin and insulin-like growth factor expression and signaling mechanisms in Alzheimer's disease—is this type 3 diabetes? *Journal of Alzheimer's disease* **7** (2005).

209   Vidal, J.-S. S., Hanon, O., Funalot, B., Brunel, N., Viollet, C., Rigaud, A.-S. S., Seux, M.-L. L., le-Bouc, Y., Epelbaum, J. & Duron, E. Low Serum Insulin-Like Growth Factor-I Predicts Cognitive Decline in Alzheimer's Disease. *Journal of Alzheimer's disease : JAD* **52**, 641-649, doi:10.3233/JAD-151162 (2016).

210   Liu, Y., Liu, F., Grundke-Iqbal, I., Iqbal, K. & Gong, C. X. Deficient brain insulin signalling pathway in Alzheimer's disease and diabetes. *The Journal of Pathology* **225**, 54-62, doi:10.1002/path.2912 (2011).

211   Åberg, D., Johansson, P., Isgaard, J., Wallin, A., Johansson, J.-O., Andreasson, U., Blennow, K., Zetterberg, H., Åberg, D. N. & Svensson, J. Increased Cerebrospinal Fluid Level of Insulin-like Growth Factor-II in Male Patients with Alzheimer's Disease. *Journal of Alzheimer's disease : JAD* **48**, 637-646, doi:10.3233/jad-150351 (2015).

212   Johansson, P., Åberg, D., Johansson, J.-O., Mattsson, N., Hansson, O., Ahrén, B., Isgaard, J., Åberg, D. N., Blennow, K., Zetterberg, H. *et al.* Serum but not cerebrospinal fluid levels of insulin-like growth factor-I (IGF-I) and IGF-binding protein-3 (IGFBP-3) are increased in Alzheimer's disease. *Psychoneuroendocrinology* **38**, 1729-1737, doi:10.1016/j.psyneuen.2013.02.006 (2013).

213   Griffin, R. J., Moloney, A., Kelliher, M., Johnston, J. A., Ravid, R., Dockery, P., O'Connor, R. & O'Neill, C. Activation of Akt/PKB, increased phosphorylation of Akt substrates and loss and altered distribution of Akt and PTEN are features of Alzheimer's disease pathology. *Journal of Neurochemistry* **93**, 105-117, doi:10.1111/j.1471-4159.2004.02949.x (2005).

214   Rickle, A., Bogdanovic, N., Volkman, I., Winblad, B., Ravid, R. & Cowburn, R. F. Akt activity in Alzheimer's disease and other neurodegenerative disorders. *Neuroreport* **15**, 955-959 (2004).

215   Roos, P. M., Lierhagen, S., Flaten, T., Syversen, T., Vesterberg, O. & Nordberg, M. Manganese in cerebrospinal fluid and blood plasma of patients with amyotrophic lateral sclerosis. *Experimental Biology and Medicine* **237**, 803-810, doi:10.1258/ebm.2012.011396 (2012).

216   Peters, T. L., Beard, J. D., Umbach, D. M., Allen, K., Keller, J., Mariosa, D., Sandler, D. P., Schmidt, S., Fang, F., Ye, W. *et al.* Blood levels of trace metals and amyotrophic lateral sclerosis. *NeuroToxicology* **54**, 119-126, doi:10.1016/j.neuro.2016.03.022 (2016).

217   Miyata, S., Nakamura, S., Nagata, H. & Kameyama, M. Increased manganese level in spinal cords of amyotrophic lateral sclerosis determined by radiochemical neutron activation analysis. *Journal of the Neurological Sciences* **61**, 283-293, doi:10.1016/0022-510x(83)90012-6 (1983).

218   Nagata, H., Miyata, S., Nakamura, S., Kameyama, M. & Katsui, Y. Heavy metal concentrations in blood cells in patients with amyotrophic lateral sclerosis. *Journal of the Neurological Sciences* **67**, 173-178, doi:10.1016/0022-510x(85)90113-3 (1985).

219   Reyes, E. T., Perurena, O. H., Festoff, B. W., Jorgensen, R. & Moore, W. V. Insulin resistance in amyotrophic lateral sclerosis. *Journal of the neurological sciences* **63**, 317-324 (1984).

220   Adem, A., Ekblom, J., Gillberg, P. G., Jossan, S. S., Hoog, A., Winblad, B., Aquilonius, S. M., Wang, L. H. & Sara, V. Insulin-like growth factor-1 receptors in human spinal cord: changes in amyotrophic lateral sclerosis. *Journal of Neural Transmission* **97**, 73-84, doi:10.1007/bf01277964 (1994).

221   Bilic, E., Bilic, E., Rudan, I., Kusec, V., Zurak, N., Delimar, D. & Zagar, M. Comparison of the growth hormone, IGF-1 and insulin in cerebrospinal fluid and serum between patients with motor neuron disease and healthy controls. *European Journal of Neurology* **13**, 1340-1345, doi:10.1111/j.1468-1331.2006.01503.x (2006).

222   Nagano, I., Ilieva, H., Shiote, M., Murakami, T., Yokoyama, M., Shoji, M. & Abe, K. Therapeutic benefit of intrathecal injection of insulin-like growth factor-1 in a mouse model of amyotrophic lateral sclerosis. *Journal of the neurological sciences* **235** (2005).

223   Saccà, F., Quarantelli, M., Rinaldi, C., Tucci, T., Piro, R., Perrotta, G., Carotenuto, B., Marsili, A., Palma, V., Michele, G. *et al.* A randomized controlled clinical trial of growth hormone in amyotrophic lateral sclerosis: clinical, neuroimaging, and hormonal results. *Journal of Neurology* **259**, 132-138, doi:10.1007/s00415-011-6146-2 (2012).

224   Borasio, G. D., Robberecht, W., Leigh, P. N., Emile, J., Guiloff, R. J., Jerusalem, F., Silani, V., Vos, P. E., Wokke, J. H. & Dobbins, T. A placebo-controlled trial of insulin-like growth factor-I in amyotrophic lateral sclerosis. European ALS/IGF-I Study Group. *Neurology* **51**, 583-586 (1998).

225   Harris, H. & Rubinsztein, D. C. Control of autophagy as a therapy for neurodegenerative disease. *Nature reviews. Neurology* **8**, 108-117, doi:10.1038/nrneurol.2011.200 (2011).

226   Chinta, S. J., Mallajosyula, J. K., Rane, A. & Andersen, J. K. Mitochondrial α-synuclein accumulation impairs complex I function in dopaminergic neurons and results in increased mitophagy in vivo. *Neuroscience letters* **486**, 235-239, doi:10.1016/j.neulet.2010.09.061 (2010).

227   Deas, E., Wood, N. W. & Plun-Favreau, H. Mitophagy and Parkinson's disease: the PINK1-parkin link. *Biochimica et biophysica acta* **1813**, 623-633, doi:10.1016/j.bbamcr.2010.08.007 (2010).

228   Geisler, S., Holmström, K. M., Skujat, D., Fiesel, F. C., Rothfuss, O. C., Kahle, P. J. & Springer, W. PINK1/Parkin-mediated mitophagy is dependent on VDAC1 and p62/SQSTM1. *Nature cell biology* **12**, 119-131, doi:10.1038/ncb2012 (2010).

229   Michiorri, S., Gelmetti, V., Giarda, E., Lombardi, F., Romano, F., Marongiu, R., Nerini-Molteni, S., Sale, P., Vago, R., Arena, G. *et al.* The Parkinson-associated protein PINK1 interacts with Beclin1 and promotes autophagy. *Cell death and differentiation* **17**, 962-974, doi:10.1038/cdd.2009.200 (2010).

230   Narendra, D., Tanaka, A., Suen, D.-F. & Youle, R. J. Parkin-induced mitophagy in the pathogenesis of Parkinson disease. *Autophagy* **5**, 706-708, doi:10.4161/auto.5.5.8505 (2009).

231   Vives-Bauza, C. & Przedborski, S. Mitophagy: the latest problem for Parkinson's disease. *Trends in molecular medicine* **17**, 158-165, doi:10.1016/j.molmed.2010.11.002 (2010).

232   Wolfe, D. M., Lee, J. h., Kumar, A., Lee, S., Orenstein, S. J. & Nixon, R. A. Autophagy failure in Alzheimer's disease and the role of defective lysosomal acidification. *European Journal of Neuroscience* **37**, 1949-1961, doi:10.1111/ejn.12169 (2013).

233   Spilman, P., Podlutskaya, N., Hart, M. J., Debnath, J., Gorostiza, O., Bredesen, D., Richardson, A., Strong, R. & Galvan, V. Inhibition of mTOR by Rapamycin Abolishes Cognitive Deficits and Reduces Amyloid-β Levels in a Mouse Model of Alzheimer's Disease. *PLoS ONE* **5**, doi:10.1371/journal.pone.0009979 (2010).

234   Yang, D.-S., Stavrides, P., Mohan, P. S., Kaushik, S., Kumar, A., Ohno, M., Schmidt, S. D., Wesson, D., Bandyopadhyay, U., Jiang, Y. *et al.* Reversal of autophagy dysfunction in the TgCRND8 mouse model of Alzheimer's disease ameliorates amyloid pathologies and memory deficits. *Brain : a journal of neurology* **134**, 258-277, doi:10.1093/brain/awq341 (2011).

235   Yu, H. W., Cuervo, A., Kumar, A., Peterhoff, C. M., Schmidt, S. D., Lee, J.-H., Mohan, P. S., Mercken, M., Farmery, M. R. & Tjernberg, L. O. Macroautophagy—a novel β-amyloid peptide-generating pathway activated in Alzheimer's disease. *The Journal of cell biology* **171** (2005).

236   Gomes, C., Escrevente, C. & Costa, J. Mutant superoxide dismutase 1 overexpression in NSC-34 cells: Effect of trehalose on aggregation, TDP-43 localization and levels of co-expressed glycoproteins. *Neuroscience Letters* **475**, 145-149, doi:10.1016/j.neulet.2010.03.065 (2010).

237   Wang, X., Fan, H., Ying, Z., Li, B., Wang, H. & Wang, G. Degradation of TDP-43 and its pathogenic form by autophagy and the ubiquitin-proteasome system. *Neuroscience Letters* **469**, 112-116, doi:10.1016/j.neulet.2009.11.055 (2010).

238   Gal, J., Ström, A. L., Kwinter, D. M., Kilty, R., Zhang, J., Shi, P., Fu, W., Wooten, M. W. & Zhu, H. Sequestosome 1/p62 links familial ALS mutant SOD1 to LC3 via an ubiquitin-independent mechanism. *Journal of Neurochemistry* **111**, 1062-1073, doi:10.1111/j.1471-4159.2009.06388.x (2009).

239   Chen, S., Zhang, X., Song, L. & Le, W. Autophagy Dysregulation in Amyotrophic Lateral Sclerosis. *Brain Pathology* **22**, 110-116, doi:10.1111/j.1750-3639.2011.00546.x (2012).

240   Luo, X., Suzuki, M., Ghandhi, S. A., Amundson, S. A. & Boothman, D. A. ATM Regulates Insulin-Like Growth Factor 1-Secretory Clusterin (IGF-1-sCLU) Expression that Protects Cells against Senescence. *PLoS ONE* **9**, doi:10.1371/journal.pone.0099983 (2014).

241 Peretz, S., Jensen, R., Baserga, R. & Glazer, P. M. ATM-dependent expression of the insulin-like growth factor-I receptor in a pathway regulating radiation response. *Proceedings of the National Academy of Sciences* **98**, 1676-1681, doi:10.1073/pnas.98.4.1676 (2001).

242 Miles, P. D., Treuner, K., Latronica, M., Olefsky, J. M. & Barlow, C. Impaired insulin secretion in a mouse model of ataxia telangiectasia. *American journal of physiology. Endocrinology and metabolism* **293**, 4 (2007).

243 Zhou, T., Chou, J., Zhou, Y., Simpson, D. A., Cao, F., Bushel, P. R., Paules, R. S. & Kaufmann, W. K. Ataxia telangiectasia-mutated dependent DNA damage checkpoint functions regulate gene expression in human fibroblasts. *Molecular cancer research : MCR* **5**, 813-822 (2007).

244 Ehlayel, M., Soliman, A. & Sanctis, V. Linear growth and endocrine function in children with ataxia telangiectasia. *Indian Journal of Endocrinology and Metabolism* **18**, 93-96, doi:10.4103/2230-8210.145079 (2014).

245 Kieslich, M., Hoche, F., Reichenbach, J., Weidauer, S., Porto, L., Vlaho, S., Schubert, R. & Zielen, S. Extracerebellar MRI—Lesions in Ataxia Telangiectasia Go Along with Deficiency of the GH/IGF-1 Axis, Markedly Reduced Body Weight, High Ataxia Scores and Advanced Age. *The Cerebellum* **9**, 190-197, doi:10.1007/s12311-009-0138-0 (2010).

246 Nissenkorn, A., Levy-Shraga, Y., Banet-Levi, Y., Lahad, A., Sarouk, I. & Modan-Moses, D. Endocrine abnormalities in ataxia telangiectasia: findings from a national cohort. *Pediatric Research* **79**, 889-894, doi:10.1038/pr.2016.19 (2016).

247 Schubert, R., Reichenbach, J. & Zielen, S. Growth factor deficiency in patients with ataxia telangiectasia. *Clinical & Experimental Immunology* **140**, 517-519, doi:10.1111/j.1365-2249.2005.02782.x (2005).

248 Goetz, E. M., Shankar, B., Zou, Y., Morales, J. C., Luo, X., Araki, S., Bachoo, R., Mayo, L. D. & Boothman, D. A. ATM-dependent IGF-1 induction regulates secretory clusterin expression after DNA damage and in genetic instability. *Oncogene* **30**, 3745-3754, doi:10.1038/onc.2011.92 (2011).

249 Shahrabani-Gargir, L., Pandita, T. K. & Werner, H. Ataxia-telangiectasia mutated gene controls insulin-like growth factor I receptor gene expression in a deoxyribonucleic acid damage response pathway via mechanisms involving zinc-finger transcription factors Sp1 and WT1. *Endocrinology* **145**, 5679-5687 (2004).

250 Bhat, M. A., Rios, J. C., Lu, Y., Garcia-Fresco, G. P., Ching, W., Martin, M., Li, J., Einheber, S., Chesler, M., Rosenbluth, J. *et al.* Axon-Glia Interactions and the Domain Organization of Myelinated Axons Requires Neurexin IV/Caspr/Paranodin. *Neuron* **30**, 369-383, doi:10.1016/S0896-6273(01)00294-X (2001).

251 Ching, J., Luebbert, S. H., Zhang, Z., Marupudi, N., Banerjee, S., Hurd, R., Collins, I. V., Roy, L., Ralston, L. & Fisher, J. S. Ataxia telangiectasia mutated (ATM) is required in insulin-like growth factor-1 (IGF-1) signaling through the PI3K/Akt pathway. *The FASEB Journal* **23** (2009).

252 Chitnis, M. M., Lodhia, K. A., Aleksic, T., Gao, S., Protheroe, A. S. & Macaulay, V. M. IGF-1R inhibition enhances radiosensitivity and delays double-strand break repair by both non-homologous end-joining and homologous recombination. *Oncogene* **33**, 5262-5273, doi:10.1038/onc.2013.460 (2014).

253 Valenciano, A., Henríquez-Hernández, L., Moreno, M., Lloret, M. & Lara, P. Role of IGF-1 Receptor in Radiation Response. *Translational Oncology* **5**, 1-9, doi:10.1593/tlo.11265 (2014).

254 Halaby, M.-J., Hibma, J. C., He, J. & Yang, D.-Q. ATM protein kinase mediates full activation of Akt and regulates glucose transporter 4 translocation by insulin in muscle cells. *Cellular Signalling* **20**, 1555-1563, doi:10.1016/j.cellsig.2008.04.011 (2008).

255 Vara, J., Casado, E., de Castro, J., Cejas, P., Belda-Iniesta, C. & González-Barón, M. PI3K/Akt signalling pathway and cancer. *Cancer treatment reviews* **30**, 193-204, doi:10.1016/j.ctrv.2003.07.007 (2004).

256 The association between deficient manganese levels and breast cancer: a meta-analysis. *The association between deficient manganese levels and breast cancer: a meta-analysis*.

257 Behrend, L., Mohr, A., Dick, T. & Zwacka, R. M. Manganese superoxide dismutase induces p53-dependent senescence in colorectal cancer cells. *Molecular and cellular biology* **25**, 7758-7769 (2005).

258 Ho, C.-m. J., Zheng, S., Comhair, S. A., Farver, C. & Erzurum, S. C. Differential expression of manganese superoxide dismutase and catalase in lung cancer. *Cancer research* **61**, 8578-8585 (2001).

259 Hu, Y., Rosen, D. G., Zhou, Y., Feng, L., Yang, G., Liu, J. & Huang, P. Mitochondrial manganese-superoxide dismutase expression in ovarian cancer: role in cell proliferation and response to oxidative stress. *The Journal of biological chemistry* **280**, 39485-39492 (2005).

260   Weydert, C. J., Waugh, T. A., Ritchie, J. M., Iyer, K. S., Smith, J. L., Li, L., Spitz, D. R. & Oberley, L. W. Overexpression of manganese or copper-zinc superoxide dismutase inhibits breast cancer growth. *Free radical biology & medicine* **41**, 226-237 (2006).

261   Sørensen, A. S., Fenger, K. & Olsen, J. H. Significantly lower incidence of cancer among patients with Huntington disease. *Cancer* **86**, 1342-1346, doi:10.1002/(SICI)1097-0142(19991001)86:7<1342::AID-CNCR33>3.0.CO;2-3 (1999).

262   Kwakye, G. F., Li, D. & Bowman, A. B. Novel high-throughput assay to assess cellular manganese levels in a striatal cell line model of Huntington's disease confirms a deficit in manganese accumulation. *NeuroToxicology* **32**, 630-639, doi:10.1016/j.neuro.2011.01.002 (2011).

263   Williams, B. B., Kwakye, G. F., Wegrzynowicz, M., Li, D., Aschner, M., Erikson, K. M. & Bowman, A. B. Altered Manganese Homeostasis and Manganese Toxicity in a Huntington's Disease Striatal Cell Model Are Not Explained by Defects in the Iron Transport System. *Toxicological Sciences* **117**, 169-179, doi:10.1093/toxsci/kfq174 (2010).

264   Cordova, F. M., Aguiar, A. S., Peres, T. V., Lopes, M. W., Gonçalves, F. M., Pedro, D. Z., Lopes, S. C., Pilati, C., Prediger, R. D. S., Farina, M. *et al.* Manganese-exposed developing rats display motor deficits and striatal oxidative stress that are reversed by Trolox. *Archives of toxicology* **87**, 1231-1244, doi:10.1007/s00204-013-1017-5 (2013).

265   Ma, X., Han, J., Wu, Q., Liu, H., Shi, S., Wang, C., Wang, Y., Xiao, J., Zhao, J., Jiang, J. *et al.* Involvement of dysregulated Wip1 in manganese-induced p53 signaling and neuronal apoptosis. *Toxicology Letters* **235**, 17-27, doi:10.1016/j.toxlet.2014.12.019 (2015).

266   Wan, C., Ma, X., Shi, S., Zhao, J., Nie, X., Han, J., Xiao, J., Wang, X., Jiang, S. & Jiang, J. Pivotal roles of p53 transcription-dependent and -independent pathways in manganese-induced mitochondrial dysfunction and neuronal apoptosis. *Toxicology and Applied Pharmacology* **281**, 294-302, doi:10.1016/j.taap.2014.10.013 (2014).

267   Guilarte, T. R., Burton, N. C., Verina, T., Prabhu, V. V., Becker, K. G., Syversen, T. & Schneider, J. S. Increased APLP1 expression and neurodegeneration in the frontal cortex of manganese-exposed non-human primates. *Journal of Neurochemistry* **105**, 1948-1959, doi:10.1111/j.1471-4159.2008.05295.x (2008).

268   Golding, S. E., Rosenberg, E., Valerie, N., Hussaini, I., Frigerio, M., Cockcroft, X. F., Chong, W., Hummersone, M., Rigoreau, L., Menear, K. A. *et al.* Improved ATM kinase inhibitor KU-60019 radiosensitizes glioma cells, compromises insulin, AKT and ERK prosurvival signaling, and inhibits migration and invasion. *Molecular cancer therapeutics* **8**, 2894-2902, doi:10.1158/1535-7163.mct-09-0519 (2009).

269   Hickson, I., Zhao, Y., Richardson, C. J., Green, S. J., Martin, N. M., Orr, A. I., Reaper, P. M., Jackson, S. P., Curtin, N. J. & Smith, G. C. Identification and characterization of a novel and specific inhibitor of the ataxia-telangiectasia mutated kinase ATM. *Cancer research* **64**, 9152-9159, doi:10.1158/0008-5472.CAN-04-2727 (2004).

270   Leahy, J., Golding, B. T., Griffin, R. J., Hardcastle, I. R., Richardson, C., Rigoreau, L. & Smith, G. Identification of a highly potent and selective DNA-dependent protein kinase (DNA-PK) inhibitor (NU7441) by screening of chromenone libraries. *Bioorganic & Medicinal Chemistry Letters* **14**, 6083-6087, doi:10.1016/j.bmcl.2004.09.060 (2004).

271   Vlahos, C. J., Matter, W. F., Hui, K. Y. & Brown, R. F. A specific inhibitor of phosphatidylinositol 3-kinase, 2-(4-morpholinyl)-8-phenyl-4H-1-benzopyran-4-one (LY294002). *The Journal of biological chemistry* **269**, 5241-5248 (1994).

272   Bar, J., Lukaschuk, N., Zalcenstein, A., Wilder, S., Seger, R. & Oren, M. The PI3K inhibitor LY294002 prevents p53 induction by DNA damage and attenuates chemotherapy-induced apoptosis. *Cell Death & Differentiation* **12**, 1578-1587, doi:10.1038/sj.cdd.4401677 (2005).

273   Liu, Q., Xu, C., Kirubakaran, S., Zhang, X., Hur, W., Liu, Y., Kwiatkowski, N. P., Wang, J., Westover, K. D., Gao, P. *et al.* Characterization of Torin2, an ATP-Competitive Inhibitor of mTOR, ATM, and ATR. *Cancer Research* **73**, 2574-2586, doi:10.1158/0008-5472.can-12-1702 (2013).

274   Thoreen, C. C., Kang, S. A., Chang, J., Liu, Q., Zhang, J., Gao, Y., Reichling, L. J., Sim, T., Sabatini, D. M. & Gray, N. S. An ATP-competitive Mammalian Target of Rapamycin Inhibitor Reveals Rapamycin-resistant Functions of mTORC1. *Journal of Biological Chemistry* **284**, 8023-8032, doi:10.1074/jbc.m900301200 (2009).

275   Brunn, G. J., Williams, J., Sabers, C., Wiederrecht, G., Lawrence, J. C. & Abraham, R. T. Direct inhibition of the signaling functions of the mammalian target of rapamycin by the phosphoinositide 3-kinase inhibitors, wortmannin and LY294002. *The EMBO journal* **15**, 5256-5267 (1996).

276   Ballou, L. M., Selinger, E. S., Choi, J., Drueckhammer, D. G. & Lin, R. Z. Inhibition of mammalian target of rapamycin signaling by 2-(morpholin-1-yl)pyrimido[2,1-alpha]isoquinolin-4-one. *The Journal of biological chemistry* **282**, 24463-24470 (2007).

277   Brouillet, E. P., Shinobu, L., McGarvey, U., Hochberg, F. & Beal, M. F. Manganese Injection into the Rat Striatum Produces Excitotoxic Lesions by Impairing Energy Metabolism. *Experimental Neurology* **120**, 89-94, doi:10.1006/exnr.1993.1042 (1993).

278   Neal, A. P. & Guilarte, T. R. Mechanisms of lead and manganese neurotoxicity. *Toxicology Research* **2**, 99-114, doi:10.1039/c2tx20064c (2013).

279   An, M. C., Zhang, N., Scott, G., Montoro, D., Wittkop, T., Mooney, S., Melov, S. & Ellerby, L. M. Genetic correction of Huntington's disease phenotypes in induced pluripotent stem cells. *Cell stem cell* **11**, 253-263, doi:10.1016/j.stem.2012.04.026 (2012).

280   Zhang, S., Fu, J. & Zhou, Z. In vitro effect of manganese chloride exposure on reactive oxygen species generation and respiratory chain complexes activities of mitochondria isolated from rat brain. *Toxicology in Vitro* **18**, 71-77, doi:10.1016/j.tiv.2003.09.002 (2004).

281   Zhang, S., Zhou, Z. & Fu, J. Effect of manganese chloride exposure on liver and brain mitochondria function in rats. *Environmental Research* **93**, 149-157, doi:10.1016/s0013-9351(03)00109-9 (2003).

282   Gavin, C. E., Gunter, K. K. & Gunter, T. E. Manganese and calcium transport in mitochondria: implications for manganese toxicity. *Neurotoxicology* **20**, 445-453 (1999).

283   Malecki, E. A. Manganese toxicity is associated with mitochondrial dysfunction and DNA fragmentation in rat primary striatal neurons. *Brain Research Bulletin* **55**, 225-228, doi:10.1016/s0361-9230(01)00456-7 (2001).

284   Chauhan, V., Singh, S. S., Chauhan, A. & Brockerhoff, H. Phosphatidylinositol 3-kinase: Inhibition of intrinsic protein-serine kinase activity by phosphoinositides, and of lipid kinase activity by Mn2+. *Biochimica et Biophysica Acta (BBA) - Molecular Cell Research* **1267**, 139-144, doi:10.1016/0167-4889(95)00032-N (1995).

285   Cai, T., Che, H., Yao, T., Chen, Y., Huang, C., Zhang, W., Du, K., Zhang, J., Cao, Y., Chen, J. *et al.* Manganese Induces Tau Hyperphosphorylation through the Activation of ERK MAPK Pathway in PC12 Cells. *Toxicological Sciences* **119**, 169-177, doi:10.1093/toxsci/kfq308 (2011).

286   McDougall, S. A., Der-Ghazarian, T., Britt, C. E., Varela, F. A. & Crawford, C. A. Postnatal manganese exposure alters the expression of D2L and D2S receptor isoforms: relationship to PKA activity and Akt levels. *Synapse (New York, N.Y.)* **65**, 583-591, doi:10.1002/syn.20877 (2011).

287   Srivastava, V. K., Hiney, J. K. & Dees, W. L. Manganese-Stimulated Kisspeptin Is Mediated by the IGF-1/Akt/Mammalian Target of Rapamycin Pathway in the Prepubertal Female Rat. *Endocrinology* **157**, 3233-3241, doi:10.1210/en.2016-1090 (2016).

288   Hirata, Y., Adachi, K. & Kiuchi, K. Activation of JNK pathway and induction of apoptosis by manganese in PC12 cells. *Journal of neurochemistry* **71**, 1607-1615 (1998).

289   Hirata, Y., Adachi, K. & Kiuchi, K. Phosphorylation and activation of p70 S6 kinase by manganese in PC12 cells. *Neuroreport* **9**, 3037-3040 (1998).

290   Tai, Y., Chew, K. C. M., Tan, B. W. Q., Lim, K.-L. & Soong, T. Iron mitigates DMT1-mediated manganese cytotoxicity via the ASK1-JNK signaling axis: Implications of iron supplementation for manganese toxicity. *Scientific Reports* **6**, 21113, doi:10.1038/srep21113 (2016).

291   Moreno, J. A., Streifel, K. M., Sullivan, K. A., Hanneman, W. H. & Tjalkens, R. B. Manganese-Induced NF-κB Activation and Nitrosative Stress Is Decreased by Estrogen in Juvenile Mice. *Toxicological Sciences* **122**, 121-133, doi:10.1093/toxsci/kfr091 (2011).

292   Wang, L., Fu, H., Liu, B., Liu, X., Chen, W. & Yu, X. The effect of postnatal manganese exposure on the NMDA receptor signaling pathway in rat hippocampus. *Journal of Biochemical and Molecular Toxicology* **31**, doi:10.1002/jbt.21969 (2017).

293   Perl, D. P. & Olanow, W. C. The Neuropathology of Manganese-Induced Parkinsonism. *Journal of Neuropathology & Experimental Neurology* **66**, 675-682, doi:10.1097/nen.0b013e31812503cf (2007).

294   Kwakye, G. F., Paoliello, M., Mukhopadhyay, S., Bowman, A. B. & Aschner, M. Manganese-Induced Parkinsonism and Parkinson's Disease: Shared and Distinguishable Features. *International Journal of Environmental Research and Public Health* **12**, 7519-7540, doi:10.3390/ijerph120707519 (2015).

295   Olanow, C. W. Manganese-Induced Parkinsonism and Parkinson's Disease. *Annals of the New York Academy of Sciences* **1012**, 209-223, doi:10.1196/annals.1306.018 (2004).

296   Park, R. M. Neurobehavioral Deficits and Parkinsonism in Occupations with Manganese Exposure: A Review of Methodological Issues in the Epidemiological Literature. *Safety and Health at Work* **4**, 123-135, doi:10.1016/j.shaw.2013.07.003 (2013).

297   Nagatomo, S., Umehara, F., Hanada, K., Nobuhara, Takenaga, S., Arimura, K. & Osame, M. Manganese intoxication during total parenteral nutrition: report of two cases and review of the literature. *Journal of the Neurological Sciences* **162**, 102-105, doi:10.1016/s0022-510x(98)00289-5 (1999).

298   Lucchini, R. G., Guazzetti, S., Zoni, S., Donna, F., Peter, S., Zacco, A., Salmistraro, M., Bontempi, E., Zimmerman, N. J. & Smith, D. R. Tremor, olfactory and motor changes in Italian adolescents exposed to historical ferro-manganese emission. *NeuroToxicology* **33**, 687-696, doi:10.1016/j.neuro.2012.01.005 (2012).

299   McDougall, S. A., Der-Ghazarian, T., Britt, C. E., Varela, F. A. & Crawford, C. A. Postnatal manganese exposure alters the expression of D2L and D2S receptor isoforms: Relationship to PKA activity and Akt levels. *Synapse* **65**, 583-591, doi:10.1002/syn.20877 (2011).

300   Bryan, M. R., Uhouse, M. A., Nordham, K. D., Joshi, P., Rose, D., O'Brien, M. T., Aschner, M. & Bowman, A. B. Phosphatidylinositol 3 kinase (PI3K) modulates manganese homeostasis and manganese-induced cell signaling in a murine striatal cell line. *NeuroToxicology*, doi:10.1016/j.neuro.2017.07.026 (2017).

301   Cheng, H., Xia, B., Su, C., Chen, K., Chen, X., Chen, P., Zou, Y. & Yang, X. PI3K/Akt signaling pathway and Hsp70 activate in hippocampus of rats with chronic manganese sulfate exposure. *Journal of Trace Elements in Medicine and Biology*, doi:10.1016/j.jtemb.2018.07.019 (2018).

302   Acevedo-Torres, K., Berríos, L., Rosario, N., Dufault, V., Skatchkov, S., Eaton, M. J., Torres-Ramos, C. A. & Ayala-Torres, S. Mitochondrial DNA damage is a hallmark of chemically induced and the R6/2 transgenic model of Huntington's disease. *DNA Repair* **8**, 126-136, doi:10.1016/j.dnarep.2008.09.004 (2009).

303   Guan, J., Krishnamurthi, R., Waldvogel, H. J., Faull, R. L., Clark, R. & Gluckman, P. N-terminal tripeptide of IGF-1 (GPE) prevents the loss of TH positive neurons after 6-OHDA induced nigral lesion in rats. *Brain research* **859**, 286-292 (2000).

304   Ebert, A. D., Beres, A. J., Barber, A. E. & Svendsen, C. N. Human neural progenitor cells over-expressing IGF-1 protect dopamine neurons and restore function in a rat model of Parkinson's disease. *Experimental neurology* **209**, 213-223 (2007).

305   Pellecchia, M. T., Santangelo, G., Picillo, M., Pivonello, R., Longo, K., Pivonello, C., Vitale, C., Amboni, M., Rosa, A., Moccia, M. *et al.* Insulin-like growth factor-1 predicts cognitive functions at 2-year follow-up in early, drug-naïve Parkinson's disease. *European Journal of Neurology* **21**, 802-807, doi:10.1111/ene.12137 (2014).

306   Busiguina, S., Fernandez, A. M., Barrios, V., Clark, R., Tolbert, D. L., Berciano, J. & Torres-Aleman, I. Neurodegeneration is associated to changes in serum insulin-like growth factors. *Neurobiology of disease* **7**, 657-665, doi:10.1006/nbdi.2000.0311 (2000).

307   Morrison, B. D., Feltz, S. M. & Pessin, J. E. Polylysine specifically activates the insulin-dependent insulin receptor protein kinase. *The Journal of biological chemistry* **264**, 9994-10001 (1989).

308   Ueda, M., Robinson, F. W., Smith, M. M. & Kono, T. Effects of divalent cations on the regulation of insulin-sensitive glucose transport and cAMP phosphodiesterase in adipocytes. Insulin-like effects of divalent cations. *The Journal of biological chemistry* **259**, 9520-9525 (1984).

309   Mooney, R. A. & Green, D. A. Insulin receptor dephosphorylation in permeabilized adipocytes is inhibitable by manganese and independent of receptor kinase activity. *Biochemical and Biophysical Research Communications* **162**, 1200-1206, doi:10.1016/0006-291x(89)90801-2 (1989).

310   Xu, B., Bird, V. G. & Miller, W. T. Substrate specificities of the insulin and insulin-like growth factor 1 receptor tyrosine kinase catalytic domains. *The Journal of biological chemistry* **270**, 29825-29830 (1995).

311   Singh, T. J. Activation of a manganese-dependent membrane protein kinase by serine and tyrosine phosphorylation. *Biochemical and biophysical research communications* **171**, 75-83 (1990).

312   Lopes, C., Ribeiro, M., Duarte, A. I., Humbert, S., Saudou, F., de Almeida, L., Hayden, M. & Rego, A. C. IGF-1 intranasal administration rescues Huntington's disease phenotypes in YAC128 mice. *Molecular neurobiology* **49**, 1126-1142, doi:10.1007/s12035-013-8585-5 (2014).

313   Williams, B. B., Kwakye, G. F., Wegrzynowicz, M., Li, D., Aschner, M., Erikson, K. M. & Bowman, A. B. Altered manganese homeostasis and manganese toxicity in a Huntington's disease striatal cell model are not explained by defects in the iron transport system. *Toxicological sciences : an official journal of the Society of Toxicology* **117**, 169-179, doi:10.1093/toxsci/kfq174 (2010).

314   Madison, J. L., Wegrzynowicz, M., Aschner, M. & Bowman, A. B. Disease-toxicant interactions in manganese exposed Huntington disease mice: early changes in striatal neuron morphology and dopamine metabolism. *PloS one* **7**, doi:10.1371/journal.pone.0031024 (2012).

315   Bichell, T. V., Wegrzynowicz, M., Tipps, G. K., Bradley, E. M., Uhouse, M. A., Bryan, M., Horning, K., Fisher, N., Dudek, K., Halbesma, T. *et al.* Reduced bioavailable manganese causes striatal urea cycle pathology in Huntington's disease mouse model. *Biochimica et Biophysica Acta (BBA) - Molecular Basis of Disease* **1863**, 1596-1604, doi:10.1016/j.bbadis.2017.02.013 (2017).

316   Pfalzer, A. C., Wages, P. A., Porter, N. A. & Bowman, A. B. Striatal Cholesterol Precursors Are Altered with Age in Female Huntington's Disease Model Mice. *Journal of Huntington's disease*, doi:10.3233/JHD-180321 (2019).

317   Talbot, K., Wang, H.-Y., Kazi, H., Han, L.-Y., Bakshi, K. P., Stucky, A., Fuino, R. L., Kawaguchi, K. R., Samoyedny, A. J. & Wilson, R. S. Demonstrated brain insulin resistance in Alzheimer's disease patients is associated with IGF-1 resistance, IRS-1 dysregulation, and cognitive decline. *The Journal of clinical investigation* **122** (2012).

318   Bowman, A. B. & Aschner, M. Considerations on manganese (Mn) treatments for in vitro studies. *NeuroToxicology* **41**, 141-142, doi:10.1016/j.neuro.2014.01.010 (2014).

319   Colin, E., Régulier, E., Perrin, V., Dürr, A., Brice, A., Aebischer, P., Déglon, N., Humbert, S. & Saudou, F. Akt is altered in an animal model of Huntington's disease and in patients. *The European journal of neuroscience* **21**, 1478-1488, doi:10.1111/j.1460-9568.2005.03985.x (2005).

320   Boucher, J., Tseng, Y.-H. & Kahn, R. C. Insulin and Insulin-like Growth Factor-1 Receptors Act as Ligand-specific Amplitude Modulators of a Common Pathway Regulating Gene Transcription. *Journal of Biological Chemistry* **285**, 17235-17245, doi:10.1074/jbc.m110.118620 (2010).

321   Boucher, J., Kleinridders, A. & Kahn, R. C. Insulin Receptor Signaling in Normal and Insulin-Resistant States. *Cold Spring Harbor Perspectives in Biology* **6**, doi:10.1101/cshperspect.a009191 (2014).

322   Wittman, M., Carboni, J., Attar, R., Balasubramanian, B., Balimane, P., Brassil, P., Beaulieu, F., Chang, C., Clarke, W., Dell, J. *et al.* Discovery of a (1H-benzoimidazol-2-yl)-1H-pyridin-2-one (BMS-536924) inhibitor of insulin-like growth factor I receptor kinase with in vivo antitumor activity. *Journal of medicinal chemistry* **48**, 5639-5643, doi:10.1021/jm050392q (2005).

323   Wittman, M. D., Carboni, J. M., Yang, Z., Lee, F. Y., Antman, M., Attar, R., Balimane, P., Chang, C., Chen, C., Discenza, L. *et al.* Discovery of a 2,4-disubstituted pyrrolo[1,2-f][1,2,4]triazine inhibitor (BMS-754807) of insulin-like growth factor receptor (IGF-1R) kinase in clinical development. *Journal of medicinal chemistry* **52**, 7360-7363, doi:10.1021/jm900786r (2009).

324   Mulvihill, M. J., Cooke, A., Rosenfeld-Franklin, M., Buck, E., Foreman, K., Landfair, D., O'Connor, M., Pirritt, C., Sun, Y., Yao, Y. *et al.* Discovery of OSI-906: a selective and orally efficacious dual inhibitor of the IGF-1 receptor and insulin receptor. *Future Medicinal Chemistry* **1**, 1153-1171, doi:10.4155/fmc.09.89 (2009).

325   García-Echeverría, C., Pearson, M. A., Marti, A., Meyer, T., Mestan, J., Zimmermann, J., Gao, J., Brueggen, J., Capraro, H.-G., Cozens, R. *et al.* In vivo antitumor activity of NVP-AEW541—A novel, potent, and selective inhibitor of the IGF-IR kinase. *Cancer Cell* **5**, 231-239, doi:10.1016/s1535-6108(04)00051-0 (2004).

326   Manning, B. D. & Cantley, L. C. AKT/PKB signaling: navigating downstream. *Cell* **129**, 1261-1274, doi:10.1016/j.cell.2007.06.009 (2007).

327   Acuña, A. I., Esparza, M., Kramm, C., Beltrán, F. A., Parra, A. V., Cepeda, C., Toro, C. A., Vidal, R. L., Hetz, C., Concha, I. I. *et al.* A failure in energy metabolism and antioxidant uptake precede symptoms of Huntington's disease in mice. *Nature Communications* **4**, 2917, doi:10.1038/ncomms3917 (2013).

328   Mochel, F. & Haller, R. G. Energy deficit in Huntington disease: why it matters. *Journal of Clinical Investigation* **121**, 493-499, doi:10.1172/jci45691 (2011).

329   Morea, V., Bidollari, E., Colotti, G., Fiorillo, A., Rosati, J., Filippis, L., Squitieri, F. & Ilari, A. Glucose transportation in the brain and its impairment in Huntington disease: one more shade of the energetic metabolism failure? *Amino Acids* **49**, 1147-1157, doi:10.1007/s00726-017-2417-2 (2017).

330   Browne, S. E. & Beal, F. M. The Energetics of Huntington's Disease. *Neurochemical Research* **29**, 531-546, doi:10.1023/b:nere.0000014824.04728.dd (2004).

331   Ciarmiello, A., Giovacchini, G., Orobello, S., Bruselli, L., Elifani, F. & Squitieri, F. 18F-FDG PET uptake in the pre-Huntington disease caudate affects the time-to-onset independently of CAG expansion size. *European Journal of Nuclear Medicine and Molecular Imaging* **39**, 1030-1036, doi:10.1007/s00259-012-2114-z (2012).

332   Yan, H., Mitschelen, M., Bixler, G. V., Brucklacher, R. M., Farley, J. A., Han, S., Freeman, W. M. & Sonntag, W. E. Circulating IGF1 regulates hippocampal IGF1 levels and brain gene expression during adolescence. *Journal of Endocrinology* **211**, 27-37, doi:10.1530/joe-11-0200 (2011).

333   Milatovic, D., Yin, Z., Gupta, R. C., Sidoryk, M., Albrecht, J., Aschner, J. L. & Aschner, M. Manganese Induces Oxidative Impairment in Cultured Rat Astrocytes. *Toxicological Sciences* **98**, 198-205, doi:10.1093/toxsci/kfm095 (2007).

334   Milatovic, D., Zaja-Milatovic, S., Gupta, R. C., Yu, Y. & Aschner, M. Oxidative damage and neurodegeneration in manganese-induced neurotoxicity. *Toxicology and Applied Pharmacology* **240**, 219-225, doi:10.1016/j.taap.2009.07.004 (2009).

335   Pan, J., Chang, Q., Wang, X., Son, Y., Zhang, Z., Chen, G., Luo, J., Bi, Y., Chen, F. & Shi, X. Reactive Oxygen Species-Activated Akt/ASK1/p38 Signaling Pathway in Nickel Compound-Induced Apoptosis in BEAS 2B Cells. *Chemical Research in Toxicology* **23**, 568-577, doi:10.1021/tx9003193 (2010).

336   Li, J., Davidson, G., Huang, Y., Jiang, B.-H., Shi, X., Costa, M. & Huang, C. Nickel Compounds Act through Phosphatidylinositol-3-kinase/Akt-Dependent, p70S6k-Independent Pathway to Induce Hypoxia Inducible Factor Transactivation and Cap43 Expression in Mouse Epidermal Cl41 Cells. *Cancer Research* **64**, 94-101, doi:10.1158/0008-5472.can-03-0737 (2004).

337   Ostrakhovitch, E. A., Lordnejad, M., Schliess, F., Sies, H. & Klotz, L.-O. Copper Ions Strongly Activate the Phosphoinositide-3-Kinase/Akt Pathway Independent of the Generation of Reactive Oxygen Species. *Archives of Biochemistry and Biophysics* **397**, 232-239, doi:10.1006/abbi.2001.2559 (2002).

338   Barthel, A., Ostrakhovitch, E. A., Walter, P. L., Kampkötter, A. & Klotz, L.-O. Stimulation of phosphoinositide 3-kinase/Akt signaling by copper and zinc ions: Mechanisms and consequences. *Archives of Biochemistry and Biophysics* **463**, 175-182, doi:10.1016/j.abb.2007.04.015 (2007).

339   Tang, X. & Shay, N. F. Zinc has an insulin-like effect on glucose transport mediated by phosphoinositol-3-kinase and Akt in 3T3-L1 fibroblasts and adipocytes. *The Journal of nutrition* **131**, 1414-1420, doi:10.1093/jn/131.5.1414 (2001).

340   Bidlack, W. R. The Biological Chemistry of Magnesium Edited by J. A. Cowan (The Ohio State University). VCH Publishers, Inc.: New York. 1995. xvi + 254 pp. $59.95. ISBN 1-56081-627-9. *Journal of the American Chemical Society* **118**, 6-7, doi:10.1021/ja9552398 (1996).

341   Lovitt, B., Vanderporten, E. C., Sheng, Z., Zhu, H., Drummond, J. & Liu, Y. Differential effects of divalent manganese and magnesium on the kinase activity of leucine-rich repeat kinase 2 (LRRK2). *Biochemistry* **49**, 3092-3100, doi:10.1021/bi901726c (2010).

342   Aberg, D. N., Brywe, K. & Isgaard, J. Aspects of growth hormone and insulin-like growth factor-I related to neuroprotection, regeneration, and functional plasticity in the adult brain. *TheScientificWorldJournal* **6**, 53-80 (2006).

343   Fang, X.-X., Jiang, X.-L., Han, X.-H., Peng, Y.-P. & Qiu, Y.-H. Neuroprotection of Interleukin-6 Against NMDA-induced Neurotoxicity is Mediated by JAK/STAT3, MAPK/ERK, and PI3K/AKT Signaling Pathways. *Cellular and Molecular Neurobiology* **33**, 241-251, doi:10.1007/s10571-012-9891-6 (2013).

344   Zhao, Q., Ye, J., Wei, N., Fong, C. & Dong, X. Protection against MPP+-induced neurotoxicity in SH-SY5Y cells by tormentic acid via the activation of PI3-K/Akt/GSK3β pathway. *Neurochemistry International* **97**, 117-123, doi:10.1016/j.neuint.2016.03.010 (2016).

345   Whiteman, E. L., Cho, H. & Birnbaum, M. J. Role of Akt/protein kinase B in metabolism. *Trends in Endocrinology & Metabolism* **13**, 444-451, doi:10.1016/S1043-2760(02)00662-8 (2002).

346   Duarte, A. I., Proença, T., Oliveira, C. R., Santos, M. S. & Rego, A. C. Insulin restores metabolic function in cultured cortical neurons subjected to oxidative stress. *Diabetes* **55**, 2863-2870, doi:10.2337/db06-0030 (2006).

347   Culbreth, M., Zhang, Z. & Neurotoxicology, A.-M. Methylmercury augments Nrf2 activity by downregulation of the Src family kinase Fyn. *Neurotoxicology* (2017).

348   Allen, J. W., Mutkus, L. A. & Aschner, M. Isolation of neonatal rat cortical astrocytes for primary cultures. *Current protocols in toxicology* **4** (2000).

349   Bates, G., Tabrizi, S. & Jones, L. Huntington's disease. *Huntington's disease* (2014).

350   Floto, A. R., Sarkar, S., Perlstein, E. O., Kampmann, B., Schreiber, S. L. & Rubinsztein, D. C. Small molecule enhancers of rapamycin-induced TOR inhibition promote autophagy, reduce toxicity in Huntington's disease models and enhance killing of mycobacteria by macrophages. *Autophagy* **3**, 620-622, doi:10.4161/auto.4898 (2007).

351   Sarkar, S., Perlstein, E. O., Imarisio, S., Pineau, S., Cordenier, A., Maglathlin, R. L., Webster, J. A., Lewis, T. A., O'Kane, C. J., Schreiber, S. L. *et al.* Small molecules enhance autophagy and reduce toxicity in Huntington's disease models. *Nature chemical biology* **3**, 331-338, doi:10.1038/nchembio883 (2007).

352   Zhang, L., Yu, J., Pan, H., Hu, P., Hao, Y., Cai, W., Zhu, H., Yu, A. D., Xie, X., Ma, D. *et al.* Small molecule regulators of autophagy identified by an image-based high-throughput screen. *Proceedings of the National Academy of Sciences* **104**, 19023-19028, doi:10.1073/pnas.0709695104 (2007).

353   King, M. A., Hands, S., Hafiz, F., Mizushima, N., Tolkovsky, A. M. & Wyttenbach, A. Rapamycin Inhibits Polyglutamine Aggregation Independently of Autophagy by Reducing Protein Synthesis. *Molecular Pharmacology* **73**, 1052-1063, doi:10.1124/mol.107.043398 (2008).

354   Fox, J. H., Connor, T., Chopra, V., Dorsey, K., Kama, J. A., Bleckmann, D., Betschart, C., Hoyer, D., Frentzel, S., DiFiglia, M. *et al.* The mTOR kinase inhibitor Everolimus decreases S6 kinase phosphorylation but fails to reduce mutant huntingtin levels in brain and is not neuroprotective in the R6/2 mouse model of Huntington's disease. *Molecular Neurodegeneration* **5**, 1-12, doi:10.1186/1750-1326-5-26 (2010).

355   Ngwa, H., Kanthasamy, A., Gu, Y., Fang, N., Anantharam, V. & Kanthasamy, A. G. Manganese nanoparticle activates mitochondrial dependent apoptotic signaling and autophagy in dopaminergic neuronal cells. *Toxicology and Applied Pharmacology* **256**, 227-240, doi:10.1016/j.taap.2011.07.018 (2011).

356   Wang, D., Zhang, J., Jiang, W., Cao, Z., Zhao, F., Cai, T., Aschner, M. & Luo, W. The role of NLRP3-CASP1 in inflammasome-mediated neuroinflammation and autophagy dysfunction in manganese-induced, hippocampal-dependent impairment of learning and memory ability. *Autophagy*, doi:10.1080/15548627.2017.1293766 (2017).

357   Zhou, Q., Fu, X., Wang, X., Wu, Q., Lu, Y., Shi, J., Klaunig, J. E. & Zhou, S. Autophagy plays a protective role in Mn-induced toxicity in PC12 cells. *Toxicology* **394**, 45-53, doi:10.1016/j.tox.2017.12.001 (2018).

358   Ma, Z., Wang, C., Liu, C., Yan, D. Y., Deng, Y., Liu, W., Yang, T. Y., Xu, Z. F. & Xu, B. The role S-nitrosylation in manganese-induced autophagy dysregulation in SH-SY5Y cells. *Environmental Toxicology* **32**, 2428-2439, doi:10.1002/tox.22457 (2017).

359   Kanninen, K. M., Grubman, A., Meyerowitz, J., Duncan, C., Tan, J.-L., Parker, S. J., Crouch, P. J., Paterson, B. M., Hickey, J. L., Donnelly, P. S. *et al.* Increased Zinc and Manganese in Parallel with Neurodegeneration, Synaptic Protein Changes and Activation of Akt/GSK3 Signaling in Ovine CLN6 Neuronal Ceroid Lipofuscinosis. *PLoS ONE* **8**, doi:10.1371/journal.pone.0058644 (2013).

360   Wong, V., Wu, A., Wang, J., Liu, L. & Law, B. Neferine attenuates the protein level and toxicity of mutant huntingtin in PC-12 cells via induction of autophagy. *Molecules (Basel, Switzerland)* **20**, 3496-3514, doi:10.3390/molecules20033496 (2015).

361   Yu, L., Shang, Z.-F., Hsu, F.-M., Zhang, Z., Tumati, V., Lin, Y.-F., Chen, B. P. C. & Saha, D. NSCLC cells demonstrate differential mode of cell death in response to the combined treatment of radiation and a DNA-PKcs inhibitor. *Oncotarget* **6**, 3848-3860, doi:10.18632/oncotarget.2975 (2014).

362   Leahy, J. J. J., Golding, B. T., Griffin, R. J., Hardcastle, I. R., Richardson, C., Rigoreau, L. & Smith, G. C. M. Identification of a highly potent and selective DNA-dependent protein kinase (DNA-PK) inhibitor (NU7441) by screening of chromenone libraries. *Bioorganic & medicinal chemistry letters* **14**, 6083-6087, doi:10.1016/j.bmcl.2004.09.060 (2004).

363   Waguri, S. & Komatsu, M. Methods in Enzymology. *Methods in enzymology* **453**, 181-196, doi:10.1016/s0076-6879(08)04009-3 (2009).

364   Klionsky, D. J., Abdelmohsen, K., Abe, A., Abedin, M. J., Abeliovich, H., Acevedo Arozena, A., Adachi, H., Adams, C. M., Adams, P. D., Adeli, K. *et al.* Guidelines for the use and interpretation of assays for monitoring autophagy (3rd edition). *Autophagy* **12**, 1-222, doi:10.1080/15548627.2015.1100356 (2016).

365   Mauthe, M., Orhon, I., Rocchi, C., Zhou, X., Luhr, M., Hijlkema, K.-J., Coppes, R. P., Engedal, N., Mari, M. & Reggiori, F. Chloroquine inhibits autophagic flux by decreasing autophagosome-lysosome fusion. *Autophagy*, 1-21, doi:10.1080/15548627.2018.1474314 (2018).

366   Yoshimori, T., Yamamoto, A., Moriyama, Y., Futai, M. & Tashiro, Y. Bafilomycin A1, a specific inhibitor of vacuolar-type H(+)-ATPase, inhibits acidification and protein degradation in lysosomes of cultured cells. *The Journal of biological chemistry* **266**, 17707-17712 (1991).

367   Klionsky, D. J., Elazar, Z., Seglen, P. O. & Rubinsztein, D. C. Does bafilomycin A1 block the fusion of autophagosomes with lysosomes? *Does bafilomycin A1 block the fusion of autophagosomes with lysosomes?*, doi:10.4161/auto.6845 (2008).

368   Fung, F. K. C., Law, B. Y. K. & Lo, A. C. Y. Lutein Attenuates Both Apoptosis and Autophagy upon Cobalt (II) Chloride-Induced Hypoxia in Rat Műller Cells. *PLOS ONE* **11**, doi:10.1371/journal.pone.0167828 (2016).

369   Chen, R., Jiang, T., She, Y., Xu, J., Li, C., Zhou, S., Shen, H., Shi, H. & Liu, S. Effects of Cobalt Chloride, a Hypoxia-Mimetic Agent, on Autophagy and Atrophy in Skeletal C2C12 Myotubes. *BioMed Research International* **2017**, 7097580, doi:10.1155/2017/7097580 (2017).

370   Lee, S.-J. & Koh, J.-Y. Roles of zinc and metallothionein-3 in oxidative stress-induced lysosomal dysfunction, cell death, and autophagy in neurons and astrocytes. *Molecular Brain* **3**, 30, doi:10.1186/1756-6606-3-30 (2010).

371   Trejo-Solís, C., Jimenez-Farfan, D., Rodriguez-Enriquez, S., Fernandez-Valverde, F., Cruz-Salgado, A., Ruiz-Azuara, L. & Sotelo, J. Copper compound induces autophagy and apoptosis of glioma cells by reactive oxygen species and jnk activation. *BMC Cancer* **12**, 156, doi:10.1186/1471-2407-12-156 (2012).

372   Pircs, K., Petri, R., Madsen, S., Brattås, P., Vuono, R., Ottosson, D. R., St-Amour, I., Hersbach, B. A., Matusiak-Brückner, M., Lundh, S. *et al.* Huntingtin Aggregation Impairs Autophagy, Leading to Argonaute-2 Accumulation and Global MicroRNA Dysregulation. *Cell Reports* **24**, 1397-1406, doi:10.1016/j.celrep.2018.07.017 (2018).

373   Bjørkøy, G., Lamark, T., Brech, A., Outzen, H., Perander, M., Øvervatn, A., Stenmark, H. & Johansen, T. p62/SQSTM1 forms protein aggregates degraded by autophagy and has a protective effect on huntingtin-induced cell death. *The Journal of Cell Biology* **171**, 603-614, doi:10.1083/jcb.200507002 (2005).

374   Shibata, M., Lu, T., Furuya, T., Degterev, A., Mizushima, N., Yoshimori, T., MacDonald, M., Yankner, B. & Yuan, J. Regulation of Intracellular Accumulation of Mutant Huntingtin by Beclin 1. *Journal of Biological Chemistry* **281**, 14474-14485, doi:10.1074/jbc.m600364200 (2006).

375   Ravikumar, B., Duden, R. & Rubinsztein, D. C. Aggregate-prone proteins with polyglutamine and polyalanine expansions are degraded by autophagy. *Human Molecular Genetics* **11**, 1107-1117, doi:10.1093/hmg/11.9.1107 (2002).

376   Yamamoto, A., Tagawa, Y., Yoshimori, T., Moriyama, Y., Masaki, R. & Tashiro, Y. Bafilomycin A1 Prevents Maturation of Autophagic Vacuoles by Inhibiting Fusion between Autophagosomes and Lysosomes in Rat Hepatoma Cell Line, H-4-II-E Cells. *Cell Structure and Function* **23**, 33-42, doi:10.1247/csf.23.33 (1998).

377   Seglen, P. O. & Gordon, P. B. 3-Methyladenine: Specific inhibitor of autophagic/lysosomal protein degradation in isolated rat hepatocytes. *Proceedings of the National Academy of Sciences* **79**, 1889-1892, doi:10.1073/pnas.79.6.1889 (1982).

378   Puissant, A., Fenouille, N. & Auberger, P. When autophagy meets cancer through p62/SQSTM1. *American journal of cancer research* **2**, 397-413 (2012).

379   Liu, W., Ye, L., Huang, W., Guo, L., Xu, Z., Wu, H., Yang, C. & Liu, H. p62 links the autophagy pathway and the ubiqutin–proteasome system upon ubiquitinated protein degradation. *Cellular & Molecular Biology Letters* **21**, 29, doi:10.1186/s11658-016-0031-z (2016).

380   Jiang, T., Harder, B., de la Vega, M., Wong, P. K., Chapman, E. & Zhang, D. D. p62 links autophagy and Nrf2 signaling. *Free Radical Biology and Medicine* **88**, 199-204, doi:10.1016/j.freeradbiomed.2015.06.014 (2015).

381   Krauß, S., Griesche, N., Jastrzebska, E. & Nature …, C.-C. Translation of HTT mRNA with expanded CAG repeats is regulated by the MID1–PP2A protein complex. *Nature …* (2013).

382 Jain, A., Lamark, T., Sjøttem, E., Larsen, K., Awuh, J., Øvervatn, A., McMahon, M., Hayes, J. D. & Johansen, T. p62/SQSTM1 Is a Target Gene for Transcription Factor NRF2 and Creates a Positive Feedback Loop by Inducing Antioxidant Response Element-driven Gene Transcription. *Journal of Biological Chemistry* **285**, 22576-22591, doi:10.1074/jbc.m110.118976 (2010).

383 Neisch, A. L., Neufeld, T. P. & Biol, H.-T. S. J. A STRIPAK complex mediates axonal transport of autophagosomes and dense core vesicles through PP2A regulation. *J Cell Biol*, doi:10.1083/jcb.201606082 (2017).

384 Suzuki, H., Wada, O., Inoue, K., Tosaka, H. & Ono, T. Role of brain lysosomes in the development of manganese toxicity in mice. *Toxicology and Applied Pharmacology* **71**, 422-429, doi:10.1016/0041-008x(83)90030-3 (1983).

385 Okamoto, Y., Oshima, R., Inagaki, K., Aita, S., Nisioka, H., Kondo, Y., Ishizuka, H., Takada, J. & Nishida, M. The Presence of A manganese-rich particle in lysosome of rat pancreas due to excess manganese treatment. *IUBMB Life* **41**, 389-394, doi:10.1080/15216549700201401 (1997).

386 Fan, X., Luo, G., Yang, D., Ming, M., Liu, H., Pu, P. & Le, W. Critical role of lysosome and its associated protein cathepsin D in manganese-induced toxicity in cultured midbrain astrocyte. *Neurochemistry International* **56**, 291-300, doi:10.1016/j.neuint.2009.11.001 (2010).

387 Filimonenko, M., Isakson, P., Finley, K. D., Anderson, M., Jeong, H., Melia, T. J., Bartlett, B. J., Myers, K. M., Birkeland, H., Lamark, T. *et al.* The Selective Macroautophagic Degradation of Aggregated Proteins Requires the PI3P-Binding Protein Alfy. *Molecular Cell* **38**, 265-279, doi:10.1016/j.molcel.2010.04.007 (2010).

388 Isakson, P., Holland, P. & Simonsen, A. The role of ALFY in selective autophagy. *Cell Death & Differentiation* **20**, 12-20, doi:10.1038/cdd.2012.66 (2012).

389 Harischandra, D. S., Ghaisas, S., Rokad, D., Zamanian, M., Jin, H., Anantharam, V., Kimber, M., Kanthasamy, A. & Kanthasamy, A. G. Environmental neurotoxicant manganese regulates exosome-mediated extracellular miRNAs in cell culture model of Parkinson's disease: Relevance to α-synuclein misfolding in metal neurotoxicity. *NeuroToxicology* **64**, doi:10.1016/j.neuro.2017.04.007 (2018).

390 Sarkar, S., Davies, J. E., Huang, Z., Tunnacliffe, A. & Rubinsztein, D. C. Trehalose, a Novel mTOR-independent Autophagy Enhancer, Accelerates the Clearance of Mutant Huntingtin and α-Synuclein. *Journal of Biological Chemistry* **282**, 5641-5652, doi:10.1074/jbc.m609532200 (2007).

391 Ehrnhoefer, D. E., Martin, D. D. O., Schmidt, M. E., Qiu, X., Ladha, S., Caron, N. S., Skotte, N. H., Nguyen, Y. T. N., Vaid, K., Southwell, A. L. *et al.* Preventing mutant huntingtin proteolysis and intermittent fasting promote autophagy in models of Huntington disease. *Acta Neuropathologica Communications* **6**, 16, doi:10.1186/s40478-018-0518-0 (2018).

392 Walter, C., Clemens, L. E., Müller, A. J., Fallier-Becker, P., Proikas-Cezanne, T., Riess, O., Metzger, S. & Nguyen, H. P. Activation of AMPK-induced autophagy ameliorates Huntington disease pathology in vitro. *Neuropharmacology* **108**, 24-38, doi:10.1016/j.neuropharm.2016.04.041 (2016).

393 Vázquez-Manrique, R. P., Farina, F., Cambon, K., Sequedo, M., Parker, A. J., Millán, J., Weiss, A., Déglon, N. & Neri, C. AMPK activation protects from neuronal dysfunction and vulnerability across nematode, cellular and mouse models of Huntington's disease. *Human Molecular Genetics* **25**, 1043-1058, doi:10.1093/hmg/ddv513 (2016).

394 Feero, G. W. & Hoffman, E. P. Huntington's Disease: Their loss is our gain? *Current Biology* **5**, 1229-1231, doi:10.1016/s0960-9822(95)00244-2 (1995).

395 Schulte, J. & Littleton, T. J. The biological function of the Huntingtin protein and its relevance to Huntington's Disease pathology. *Current trends in neurology* **5**, 65-78 (2011).

396 Paine, H. Does loss of the normal protein function contribute to the pathogenesis of Huntington's disease? *Bioscience Horizons: The International Journal of Student Research* **8**, doi:10.1093/biohorizons/hzv005 (2015).

397 Kordasiewicz, H. B., Stanek, L. M., Wancewicz, E. V., Mazur, C., McAlonis, M. M., Pytel, K. A., Artates, J. W., Weiss, A., Cheng, S. H., Shihabuddin, L. S. *et al.* Sustained Therapeutic Reversal of Huntington's Disease by Transient Repression of Huntingtin Synthesis. *Neuron* **74**, 1031-1044, doi:10.1016/j.neuron.2012.05.009 (2012).

398 Lu, X.-H. & Yang, W. X. "Huntingtin Holiday": Progress toward an Antisense Therapy for Huntington's Disease. *Neuron* **74**, 964-966, doi:10.1016/j.neuron.2012.06.001 (2012).

399 Raamsdonk, J. M., Pearson, J., Rogers, D. A., Bissada, N., Vogl, W. A., Hayden, M. R. & Leavitt, B. R. Loss of wild-type huntingtin influences motor dysfunction and survival in the YAC128 mouse model of Huntington disease. *Human Molecular Genetics* **14**, 1379-1392, doi:10.1093/hmg/ddi147 (2005).

400   Reiner, A., Dragatsis, I., Zeitlin, S. & Goldowitz, D. Wild-type huntingtin plays a role in brain development and neuronal survival. *Molecular Neurobiology* **28**, 259-275, doi:10.1385/mn:28:3:259 (2003).

401   Dietrich, P., Johnson, I., Alli, S. & Dragatsis, I. Elimination of huntingtin in the adult mouse leads to progressive behavioral deficits, bilateral thalamic calcification, and altered brain iron homeostasis. *PLOS Genetics* **13**, doi:10.1371/journal.pgen.1006846 (2017).

402   Leavitt, B. R., Guttman, J. A., Hodgson, G. J., Kimel, G. H., Singaraja, R., Vogl, W. A. & Hayden, M. R. Wild-Type Huntingtin Reduces the Cellular Toxicity of Mutant Huntingtin In Vivo. *The American Journal of Human Genetics* **68**, 313-324, doi:10.1086/318207 (2001).

403   Kuhn, A., Goldstein, D. R., Hodges, A., Strand, A. D., Sengstag, T., Kooperberg, C., Becanovic, K., Pouladi, M. A., Sathasivam, K., Cha, J.-H. J. *et al.* Mutant huntingtin's effects on striatal gene expression in mice recapitulate changes observed in human Huntington's disease brain and do not differ with mutant huntingtin length or wild-type huntingtin dosage. *Human Molecular Genetics* **16**, 1845-1861, doi:10.1093/hmg/ddm133 (2007).

404   Popp, M. W. & Maquat, L. E. Leveraging Rules of Nonsense-Mediated mRNA Decay for Genome Engineering and Personalized Medicine. *Cell* **165**, 1319-1322, doi:10.1016/j.cell.2016.05.053 (2016).

405   Singer, E., Walter, C., Weber, J. J., Krahl, A.-C., Mau-Holzmann, U. A., Rischert, N., Riess, O., Clemensson, L. E. & Nguyen, H. P. Reduced cell size, chromosomal aberration and altered proliferation rates are characteristics and confounding factors in the STHdh cell model of Huntington disease. *Scientific Reports* **7**, 16880, doi:10.1038/s41598-017-17275-4 (2017).

406   Long, Z., Chen, B., Liu, Q., Zhao, J., Yang, Z., Dong, X., Xia, L., Huang, S., Hu, X., Song, B. *et al.* The reverse-mode NCX1 activity inhibitor KB-R7943 promotes prostate cancer cell death by activating the JNK pathway and blocking autophagic flux. *Oncotarget* **7**, 42059-42070, doi:10.18632/oncotarget.9806 (2016).

407   Ogawara, Y., Kishishita, S., Obata, T., Isazawa, Y., Suzuki, T., Tanaka, K., Masuyama, N. & Gotoh, Y. Akt Enhances Mdm2-mediated Ubiquitination and Degradation of p53. *Journal of Biological Chemistry* **277**, 21843-21850, doi:10.1074/jbc.m109745200 (2002).

408   Jenkins, K. J. & Kramer, J. K. G. Effect of Excess Dietary Manganese on Lipid Composition of Calf Blood Plasma, Heart, and Liver1. *Journal of Dairy Science* **74**, 3944-3948, doi:10.3168/jds.s0022-0302(91)78588-3 (1991).

409   Klimis-Tavantzis, D. J., Leach, R. M. & Kris-Etherton, P. M. The Effect of Dietary Manganese Deficiency on Cholesterol and Lipid Metabolism in the Wistar Rat and in the Genetically Hypercholesterolemic RICO Rat. *The Journal of Nutrition* **113**, 328-336, doi:10.1093/jn/113.2.328 (1983).

410   Casalino, E., Calzaretti, G., Landriscina, M., Sblano, C., Fabiano, A. & Landriscina, C. The Nrf2 transcription factor contributes to the induction of alpha-class GST isoenzymes in liver of acute cadmium or manganese intoxicated rats: Comparison with the toxic effect on NAD(P)H:quinone reductase. *Toxicology* **237**, 24-34, doi:10.1016/j.tox.2007.04.020 (2007).

411   Bahar, E., Kim, J.-Y. & Yoon, H. Quercetin Attenuates Manganese-Induced Neuroinflammation by Alleviating Oxidative Stress through Regulation of Apoptosis, iNOS/NF-κB and HO-1/Nrf2 Pathways. *International Journal of Molecular Sciences* **18**, 1989, doi:10.3390/ijms18091989 (2017).

412   Li, H., Wu, S., Shi, N., Lian, S. & Lin, W. Nrf2/HO-1 pathway activation by manganese is associated with reactive oxygen species and ubiquitin–proteasome pathway, not MAPKs signaling. *Journal of Applied Toxicology* **31**, 690-697, doi:10.1002/jat.1654 (2011).

413   Prabhakaran, K., Ghosh, D., Chapman, G. D. & Gunasekar, P. G. Molecular mechanism of manganese exposure-induced dopaminergic toxicity. *Brain Research Bulletin* **76**, 361-367, doi:10.1016/j.brainresbull.2008.03.004 (2008).

414   Ramesh, G. T., Ghosh, D. & Gunasekar, P. G. Activation of early signaling transcription factor, NF-κB following low-level manganese exposure. *Toxicology Letters* **136**, 151-158, doi:10.1016/s0378-4274(02)00332-6 (2002).

415   Prabhakaran, K., Chapman, G. D. & Gunasekar, P. G. α-Synuclein overexpression enhances manganese-induced neurotoxicity through the NF-κB-mediated pathway. *Toxicology Mechanisms and Methods* **21**, 435-443, doi:10.3109/15376516.2011.560210 (2011).

416   Wei, H., Wang, C., Croce, C. M. & Guan, J.-L. p62/SQSTM1 synergizes with autophagy for tumor growth in vivo. *Genes & Development* **28**, 1204-1216, doi:10.1101/gad.237354.113 (2014).

417   Duran, A., Linares, J. F., Galvez, A. S., Wikenheiser, K., Flores, J. M., Diaz-Meco, M. T. & Moscat, J. The Signaling Adaptor p62 Is an Important NF-κB Mediator in Tumorigenesis. *Cancer Cell* **13**, 343-354, doi:10.1016/j.ccr.2008.02.001 (2008).

418   Aschner, J. L. & Aschner, M. Nutritional aspects of manganese homeostasis. *Molecular Aspects of Medicine* **26**, 353-362, doi:10.1016/j.mam.2005.07.003 (2005).

419   Hayden, M. R., Martin, W. R. W., Stoessl, A. J., Clark, C., Hollenberg, S., Adam, M. J., Ammann, W., Harrop, R., Rogers, J., Ruth, T. *et al.* Positron emission tomography in the early diagnosis of Huntington's disease. *Neurology* **36**, 888-888, doi:10.1212/wnl.36.7.888 (1986).

420   Handley, R. R., Reid, S. J., Brauning, R., Maclean, P., Mears, E. R., Fourie, I., Patassini, S., Cooper, G. J. S., Rudiger, S. R., McLaughlan, C. J. *et al.* Brain urea increase is an early Huntington's disease pathogenic event observed in a prodromal transgenic sheep model and HD cases. *Proceedings of the National Academy of Sciences* **114**, doi:10.1073/pnas.1711243115 (2017).